Examining Aβ Isoform Interactions in Human-derived Astrocytes in Alzheimer's Disease

By

Hollie Elizabeth Wareing

University of Sheffield

Sheffield Institute for Translational Neuroscience

A thesis submitted for the degree
of Doctor of Philosophy (PhD)

September 2025

Abstract

Background: One hallmark characteristic of Alzheimer's Disease (AD) is the gradual build-up of amyloid-β (Aβ) plaques in the brain, with Aβ40 and Aβ42 being the most prevalent forms of Aβ. Despite Aβ40 being nearly ten-twenty times more prevalent than Aβ42 in healthy brains, most plaques in AD consist of Aβ42. The mechanisms governing the interplay between Aβ42 and Aβ40 and the preferential build-up of Aβ42 remain unclear. In AD, the function of astrocytes, which play a role in Aβ clearance and inflammation, is disrupted. This project aimed to explore the interactions between different Aβ isoforms and astrocytes, shedding light on Aβ clearance and their role in inducing pro-inflammatory markers.

Methods: Direct conversion of fibroblast to induced Neuronal Progenitor Cells to generate iAstrocytes from three individuals with AD and healthy controls were used. Directly-converted iAstrocytes retain a cellular ageing phenotype, enabling the investigation of Aβ-Astrocyte interactions within the AD context. Aβ aggregation was performed to make oligomers and fibrils using Aβ40 and Aβ42 in ratios representing both physiological and pathological conditions. The extent of Aβ uptake by iAstrocytes and an inflammatory marker screening were investigated to explore the link between Aβ aggregation and neurotoxic pathways.

Results: This study established a model system for preparing different Aβ aggregates and measured their uptake by iAstrocytes. The results demonstrate a selective uptake of specific Aβ oligomeric isoforms but not fibrils in control and AD iAstrocytes. However, there is significantly increased secretion of pro-inflammatory cytokines and chemokines, TNF-α, IL-1β, MCP1, and IL6, in both AD and control iAstrocytes. The prolonged treatment of cytokines significantly reduces the uptake of Aβ in AD astrocytes but not in controls.

Conclusion: The outcomes of this work enhance our knowledge of astrocyte internalisation of Aβ isoforms and activation of related inflammatory pathways, which is vital for understanding AD pathology.

Declaration

I, Hollie Wareing, confirm that this thesis is my own work. I am aware of the University's Guidance on the Use of Unfair Means (www.sheffield.ac.uk/ssid/unfair-means). I confirm that I shall abide by the University of Sheffield's regulations on plagiarism and that all written work shall be my own and will not have been plagiarised from other paper-based or electronic sources. Where used, material gathered from other sources will be clearly cited in the text. This work has not been previously been presented for an award at this, or any other, university.

Date: 08/08/2025

Name (Print): Hollie Elizabeth Wareing

Acknowledgment of Collaborative Work Within the Thesis

I, Hollie Wareing, confirm that the work submitted is their own, except where work that has formed part of jointly authored publications has been included. The contribution of the candidate and the other authors to this work has been explicitly indicated below. The candidate confirms that appropriate credit has been given within the thesis where reference has been made to the work of others.

Published Work

1. Co-author of publication. In the publication I, completed cell culture work and carried out experiments of which feature in the chapter three of this thesis as part of the Chapter 3, section 3.5. As part of the contribution of this work, I was listed as second author; 10.1038/s41380-024-02746-8. No other results of this publication are included in this thesis.

Non-Published Work

1. Appendix: S1. The following figure was taken with permission from thesis submitted by Chris Ryan Ratnathurai in fulfilment of for the degree of Master of Science in Translational Neuroscience, the University of Sheffield. Supervisor of project Dr Simon Bell, who was the project manager and academic supervisor. As part of this project, I acted as co-supervisor in the laboratory, carrying out the ICC staining protocol, image and data analysis alongside Ryan. The data used from Ryan's thesis into this thesis has been used as a proof on concept to support discussion argument in Chapter four, section 4.4.3.

2. Cytokine and Chemokine Screening. The ELISAs for the cytokine and chemokine release were carried out in a blind manner at the Dementia Research institute at The University of Cambridge. The assay, data plotting, and analysis was subsequently completed by the author of this thesis.

Publications, Presentations, and Conferences

Publications

Bell, S. M., **Wareing, H.**, Capriglia, F., Hughes, R., Barnes, K., Hamshaw, A., Adair, L., Shaw, A., Olejnik, A., De, S., New, E., Shaw, P. J., De Marco, M., Venneri, A., Blackburn, D. J., Ferraiuolo, L., & Mortiboys, H. (2024). Increasing hexokinase 1 expression improves mitochondrial and glycolytic functional deficits seen in sporadic Alzheimer's disease astrocytes. *Molecular psychiatry*, https://doi.org/10.1038/s41380-024-02746-8.

Xia, Z., Prescott, E. E., Urbanek, A., **Wareing, H. E.**, King, M. C., Olerinyova, A., Dakin, H., Leah, T., Barnes, K. A., Matuszyk, M. M., Dimou, E., Hidari, E., Zhang, Y. P., Lam, J. Y. L., Danial, J. S. H., Strickland, M. R., Jiang, H., Thornton, P., Crowther, D. C., Ohtonen, S., … De, S. (2024). Co-aggregation with Apolipoprotein E modulates the function of Amyloid-β in Alzheimer's disease. *Nature communications*, *15*(1), 4695. https://doi.org/10.1038/s41467-024-49028-z.

Urbanek, A., Garland, E. F., Prescott, E. E., King, M. C., Olerinyova, A., **Wareing, H. E.**, Georgieva, N., Bradshaw, E. L., Tzokov, S. B., Knight, A., Tartakovskii, A. I., Malm, T., Highley, J. R., & De, S. (2025). Molecular Determinants of Protein Pathogenicity at the Single-Aggregate Level. *Advanced science (Weinheim, Baden-Wurttemberg, Germany)*, *12*(9), e2410229. https://doi.org/10.1002/advs.202410229

Presentations and Conferences

- Poster presentation – Alzheimer's Association Advancements: Modernizing Diagnosis (Tokyo, Japan)- 2024
- Poster presentation - Alzheimer's Research UK Conference (Liverpool, UK) - 2024
- Poster presentation – Alzheimer's Research UK Conference (Aberdeen, UK) - 2023
- Internal Oral Presentation – The Sheffield Institute for Translational Neuroscience – 2022, 2023, and 2024
- Oral presentation at Dementia Futures - The Sheffield Institute for Translational Neuroscience - 2024

Acknowledgements

The research presented in this thesis would not have been possible without the guidance, support, feedback and expertise of my supervisors; Dr Suman De and Professor Stephen B Wharton. I am highly indebted to the enthusiasm and inspiration of Dr Suman De, who has encouraged and believed in me as a scientist. I would also like to thank my supervisors for supporting and aiding the development of both technical and interpersonal skills. I would also like the thank the other members of the De lab group; Dr Agnieszka Urbanek, Dr Emily Prescott, and Dr Emma Garland. Next, I would like to make an acknowledgment to Dr Simon Bell, who has shown me countless levels of support throughout my PhD. I would also like to thank Dr Adrian Higginbottom and Professor Heather Mortiboys for offering guidance and feedback during my PhD. Also, to Dr Matthew Livesey and Dr Clare Howarth for being my academic advisors, and Dr Scott Allen and Dr Janet Kumita for being viva examiners. Thank you all for showing me so much patience. I would also not have been able to complete my thesis without my colleagues and friends at SITraN, the lunchtime sofa carried me through many times.

To all my closest friends; Taylor, Katie, Samantha, Molly, Emma S, Teo, and Emma C. I wish to acknowledge all of you for being the most amazing people, and keeping my sane during this crazy journey. To my partner, Luke, I am profoundly grateful for you being my number one supporter. To mine and Luke's family, I am not sure what I would have done without you all looking after me. Additionally, to my Pomeranian, Alfie, who is blissfully unaware of the impact he has had on my journey.

I would also like to thank my funding body, Engineering and Physical Sciences Research Council and to the cell donors, and their families, without whom this research would not have been possible to complete.

Dedication

I wish to dedicate this thesis to my parents. From the very first day that I remember, you both have supported me in everything I have done and picked me back up when things haven't gone to plan. Without you both, I would never have been able to submit a thesis for a PhD in Neuroscience. As a first-generation university student, I hope I have made you proud. I would also like to dedicate this thesis to my nain, taid, and grandad – who I am sure have looked down on me during this process. Finally, to the cell donors, their families, and all those affected by Alzheimer's Disease.

Table of Contents

Abstract 1

Declaration 2

Acknowledgment of Collaborative Work Within the Thesis 3

Publications, Presentations, and Conferences 4

Acknowledgements 5

Dedication 6

Table of Contents 7

List of Figures 13

List of Tables 25

Abbreviations 26

Chapter 1. Introduction 28

1.1. Introduction to Alzheimer's Disease 28

1.2. The Amyloid Cascade Hypothesis 29

1.3. Aβ Production 32

1.4. Aβ Misfolding and Aggregation 33

1.5. Aβ Degradation and Clearance 37

1.5.1. Systemic Clearance of Aβ 37

1.5.2. Cell-mediated Degradation of Aβ 37

1.5.3. Glia-mediated Clearance 38

1.6. Astrocytes 39

1.6.1. The Role of Astrocytes in the Brain 39

1.6.2. The Role of Astrocytes in Alzheimer's Disease 40

1.7. Inflammation 42

1.7.1. Inflammation in the CNS....42
1.7.2. Inflammation in Alzheimer's Disease....43
1.8. Systems for Modelling AD....44
1.8.2. induced Pluripotent Stem Cells....45
1.8.3. induced Neuronal Progenitor Cells....46
1.9. Rational of this Project....48
1.10. Project Hypothesis....49
1.11. Aims and Objectives....49
1.11.1. Project Aim:....49
1.11.2. Overall Objectives....49
Chapter 2. Materials and Methods....50
2.1. Materials....50
2.1.1. Tissue Culture Media Constituents....50
2.1.2. Immunocytochemistry Constituents....51
2.1.3. Single Molecule Pull Down Constituents....52
2.2. Methods....54
2.2.1. Ethics Statement....54
2.2.2. Summary of Experimental Design for Thesis....54
2.2.3. Reprogramming of human-derived fibroblasts to iAstrocytes....55
2.2.3.2. General Tissue Culture....56
2.2.4. Reprogramming of human-derived fibroblasts to iAstrocytes....56
2.2.5. Differentiation of induced Neuronal Progenitor Cells into iAstrocytes....57
2.2.6. Immunocytochemistry....58
2.2.7. Thioflavin T Stock Preparation....59
2.2.8. Amyloid-β Stock Preparation....59
2.2.9. Amyloid-β Aggregate Preparation and Treatment....59

2.2.10. Cytokine and Chemokine Release post Amyloid-β Treatment Assay 60
2.2.11. Cytokine Exposure Assay 62
2.2.12. Total Internal Reflection Fluorescent Microscopy 62
2.2.13. Labelled Amyloid-β for Co-aggregate Single Molecule Imaging 62
2.2.14. Single-molecule PullDown Imaging 63
2.3. Data Analysis 65
2.3.1. Image Analysis 65
2.3.2. Image Analysis of Immunocytochemistry Staining 65
2.3.3. Image Analysis of Counting Amyloid-β Spots 67
2.4. Statistical Analysis 69
Chapter 3. Characterisation of Human-Derived iAstrocytes as a Model for Alzheimer's Disease 70
3.1. Chapter Overview 70
3.2. Introduction 70
3.3. The need for characterisation of human-derived cell models 72
3.4. Aims and Objectives 73
3.5. Results 74
3.5.1. Brightfield Imaging 74
3.5.2. iNPC characterisation 76
3.5.3. iAstrocyte Characterisation 79
3.6. Discussion 83
3.6.1. Discussion Overview 83
3.6.2. Immunocytochemistry confirms iNPC populations 83
3.6.3. Immunocytochemistry confirms iAstrocytes populations 84
3.6.4. Limitations and Future Work 85
3.7. Conclusion 87

3.8. Additional Chapter Information....87
Chapter 4. Evaluating the Uptake of Aβ Isoforms in iAstrocytes....89
4.1. Chapter Introduction....89
4.2. Hypothesis, Aims, and Objectives....91
4.2.1. Hypothesis....91
4.2.2. Aims....91
4.2.3. Objectives....91
4.3. Results....92
4.3.1. Thioflavin T based Aβ Aggregation and Characterisation of Species at the Single-aggregate Level....92
4.3.2. Uptake of Aβ in iAstrocytes....95
4.3.2.1. The Uptake of Aβ in Control iAstrocytes....97
4.3.2.2. The Uptake of Aβ in AD iAstrocytes....100
4.4. Discussion....103
4.4.1. Establishing a system for mimicking Aβ Uptake....103
4.4.2. The Uptake of Aβ in iAstrocytes....108
4.4.3. Clearance and Degradation of Aβ by Astrocytes....110
4.5. Conclusions....112
Chapter 5. The Induction of Pro-inflammatory Markers in iAstrocytes after Aβ Treatment....114
5.1. Chapter Overview....114
5.2. Introduction....114
5.2.1. Cytokines and Chemokines as Pro-inflammatory Markers....115
5.2. Hypothesis, Aims, and Objectives....116
5.2.1 Hypothesis....116
5.2.2. Aims....116

5.2.3. Objectives 116
5.3. Results 118
5.3.1. The Induction of Pro-Inflammatory Markers 118
5.3.2. Expression of GFAP, Vimentin, and CD44 Post Aβ Treatment 147
5.4. Discussion 158
5.4.1. Overview 158
5.4.2. Astrocytes derived from individuals with AD have an amplified induction of pro-inflammatory markers after the treatment of Aβ 158
5.4.3. iAstrocytes have a selective response to the induction of pro-inflammatory markers after the treatment of Aβ 160
5.4.4. Dual Role of Inflammation in AD and Associated Neurodegeneration 162
5.4.5. Aβ42 is a Key Driver of the Induction of Pro-inflammatory Markers in iAstrocytes 163
5.4.6. Expression of GFAP, Vimentin, and CD44 in Astrocytes post Aβ Treatment 165
5.5. Conclusions 165
Chapter 6. Chronic Inflammation and Aβ Uptake in iAstrocytes 167
6. Chapter Overview 167
6.1. Introduction 167
6.2. Hypothesis, Aims, and Objectives 169
6.2.1. Hypothesis 169
6.2.2. Aims 169
6.2.3. Objectives 169
6.3. Results 170
6.3.1. Uptake of Aβ in Control iAstrocytes after Prolonged Cytokine Treatment 170
6.3.2. Uptake of Aβ in AD iAstrocytes after Prolonged Cytokine Treatment 176
6.4. Discussion 181

6.4.2. Prolonged Treatment of Cytokines Reduces Aβ Uptake in iAstrocytes 182

6.5. Conclusions 184

Chapter 7. Main Discussions and Conclusions 185

7.1. Overview 185

7.2. Astrocytes Contribute to a Positive-Inflammatory Feedback Loop Associated to Alzheimer's Disease 185

7.3. Different Aβ40 and Aβ42 Isoforms Influence Aggregation and Subsequent Pro-Inflammatory Response in iAstrocytes 190

7.4. Overall Conclusions 193

Appendix: Supplementary Data 194

List of Figures

Figure 1. A. APP processing during the non-amyloidogenic and amyloidogenic pathway. Non-amyloidogenic APP processing uses α-secretase to produce secreted amyloid precursor protein alpha (sAPPα) and CTAα (C83). Next, CTAα is cleaved by γ-secretases to produce intracellular APP intracellular domain (AICD) and extracellular peptide P3. During amyloidogenic APP processing, APP is cleaved by β-secretase to secrete secreted amyloid precursor protein beta (sAPPβ) and CTFβ (C99). A fragment of CTFβ remains bound to the membrane and is cleaved by γ-secretase to produce AICD Aβ monomers. Extracellular monomeric Aβ aggregates in a process involving the transition into Aβ aggregate species (oligomers, protofibrils, fibrils), and ultimately plaques. **B. Aβ Aggregation Mechanisms**. Several aggregation mechanisms have been proposed, starting with primary nucleation and elongation, which is followed by secondary nucleation processes such as surface catalysation and fragmentation.....36

Figure 2. Illustrative diagram summarising the normal physiological functions of astrocyte (green) on the left. On the right, it highlights how they are affected by, or aid neuronal (pink) dysfunction associated to Alzheimer's Disease. Image created with BioRender.com. 41

Figure 3. A schematic summarising direct reprogramming to non-direct reprogramming. In direct programming fibroblasts are directly converted into induced Neuronal Progenitor Cells (iNPCs) then iAstrocytes (left). In non-direct reprogramming, fibroblasts are converted to induced Pluripotent Stem Cells (iPSCs) before being converted to iNPCs and iAstrocytes (right). Image created with BioRender.com. 47

Figure 4. Summary of experimental design for thesis. Image created with BioRender.com. 54

Figure 5. Key stages of reprogramming fibroblasts to iAstrocytes. Fibroblasts from donors obtained via skin biopsy before being reprogrammed into induced Neuronal Progenitor Cells (iNPCs) in a 18-24-day protocol. iNPCs are then differentiated into iAstrocytes in a 7-day protocol. Reprogramming factors for iNPCs (OCT3, SOX2, and KLF4) are highlighted. 58

Figure 6. Schematic showing Aβ treatment assay. On day 7 of differentiation, iAstrocytes were treated for 1 hour with Aβ (2.5 μM) isoforms. The culture medium was collected, centrifuged (1000 RPM), and snap frozen in liquid nitrogen before being stored at -80°C. The 96-well plates were fixed with 3.7 % PFA for immunocytochemistry.....61

Figure 7. **Image analysis of immunocytochemistry staining. A.** Input image for analysis; Vimentin (647) and Hoechst (blue). Example image shows Control 1 cell line Vimentin staining. **B.** Cell nuclei were identified by masking individual nucleus' using the Hoechst channel. **C.** Nuclei selected (green) or deselected (red) based on proximity to the image border. **D.** Dependent on the primary antibody being used the corresponding secondary antibody-channel was used to mask the cells. **E / F.** Negative staining populations were distinguished by setting an intensity threshold, and staining intensities below this threshold were excluded. **G / H.** Cells with intensity above the threshold were classified as positive. Scale bar: 50 μM. 66
Figure 8. **Image Analysis of Counting Amyloid- β Spots. A / B / C.** Input images for analysis; A. CD44 (568; yellow) and Hoechst (blue), B. Aβ (647; red) and Hoechst (blue), and C. Aβ (647; red). **D.** Cell nuclei were identified by masking individual nucleus' using the Hoechst channel. **E.** Nuclei selected (green) or deselected (red) based on proximity to the image border. **F.** Cells were masked using the 568 channel. **G.** Smoothing filter (gaussian) over the 647 channel to mask spots **H.** The find spots command was then used to detect all 647-spots within the cell region. **I.** Negative staining populations were distinguished by setting an intensity threshold, and staining intensities below this threshold were excluded. **J.** Any spots above the threshold was a selected population and referred to as a positive population for analysis. Scale bar: 50 μM.....68
Figure 9. Brightfield Images of Control and AD iNPCs (A-F) and iAstrocytes (G-L). Scale bar, 50 μM. 75
Figure 10. **Illustrations and quantification of induced Neuronal Progenitor Cells marker: Nestin, in control and AD cell lines. A-F**. Representative images of Nestin (red) and Hoechst (blue) in Control (A-C) and AD (D-F) iNPCs. Scale bar (50 μm). **G-H.** Control and AD iNPCs quantification showing the percentage of cells with positive staining for Nestin. Biological repeats (n=3) per cell line were averaged from 2 technical repeats.....76
Figure 11. Illustrations and quantification of induced Neuronal Progenitor Cells marker; PAX6 in control lines. A-F. Representative images of PAX6 (A-C; yellow) and PAX6/Hoechst (D-F; yellow/blue) in Control iNPCs. Scale bar (50 μm). **G.** Control iNPCs quantification showing the percentage of cells with positive staining for PAX6. Biological repeats (n=3) per cell line were averaged from 2 technical repeats.....77

Figure 12. Illustrations and quantification of induced Neuronal Progenitor Cells marker; PAX6 in AD lines. A-F. Representative images of PAX6 only (A-C; yellow) and PAX6/Hoechst (D-F; yellow/blue) in AD iNPCs. Scale bar (50 μm). **G.** AD iNPCs quantification showing the percentage of cells with positive staining for PAX6. Biological repeats (n=3) per cell line were averaged from 2 technical repeats. 78
Figure 13. Illustrations and quantification of CD44 in control and AD cell lines. A-F. Representative images of CD44 (yellow) and Hoechst (blue) in Control (A-C) and AD (D-F) iAstrocytes on day 7 of differentiation. Scale bar (50 μm). **G-H.** Control and AD iNPCs quantification showing the percentage of cells with positive staining for CD44. Biological repeats (n=3) per cell line were averaged from 2 technical repeats. 79
Figure 14. Illustrations and quantification of Vimentin in control and AD cell lines. A-F. Representative images of vimentin (red) and Hoechst (blue) in Control (A-C) and AD (D-F) iAstrocytes on day 7 of differentiation. Scale bar (50 μm). **G-H.** Control and AD iNPCs quantification showing the percentage of cells with positive staining for vimentin. Biological repeats (n=3) per cell line were averaged from 2 technical repeats. 80
Figure 15. Illustrations and quantification of EAAT2 in control and AD cell lines. A-F. Representative images of EAAT2 (yellow) and Hoechst (blue) in Control (A-C) and AD (D-F) iAstrocytes on day 7 of differentiation. Scale bar (50 μm). **G-H.** Control and AD iNPCs quantification showing the percentage of cells with positive staining for EAAT2. Biological repeats (n=3) per cell line were averaged from 2 technical repeats. 81
Figure 16. **Illustrations and quantification of GFAP in control and AD cell lines. A-F**. Representative images of GFAP (yellow) and Hoechst (blue) in Control (A-C) and AD (D-F) iAstrocytes on day 7 of differentiation. Scale bar (50 μm). **G-H.** Control and AD iNPCs quantification showing the percentage of cells with positive staining for GFAP. Biological repeats (n=3) per cell line were averaged from 2 technical repeats. 82
Figure 17. Thioflavin T (ThT) based Aβ aggregation curve. The aggregation of Aβ40 (10:0) (black), Aβ40: Aβ42 (9:1) (pink), Aβ40: Aβ42 (7:3) (green), and Aβ42 (0:10) (purple) (50 μM diluted in PBS, 37°C). Aggregation monitored by ThT intensity (A.U.) against Time (minutes), ThT = excitation; 450 nm, emission; 482 nm. Each aggregation curve represents the average of 3 repeats. 93
Figure 18. Total Internal Reflection Fluorescence (TIRF) microscopy images of Aβ species. A. representative TIRF images of oligomeric Aβ (2.5 μM) aggregates; Aβ40 (10:0), Aβ40:

Aβ42 (9:1), Aβ40: Aβ42 (7:3), and Aβ42 (0:10) (6E10-647 nm)**. B.** Representative TIRF images of fibrillar Aβ aggregates; Aβ40 (10:0), Aβ40: Aβ42 (9:1), Aβ40: Aβ42 (7:3), and Aβ42 (0:10) (6E10-647 nm)**. C.** Aβ40 and Aβ42 co-aggregate during fibril formation. Aβ40 (Anti-40-488 nm), Aβ42 (Anti-42-637 nm) and merged. 94

Figure 19. Illustrations of iAstrocytes after Aβ (2.5 μM) treatment using immunocytochemistry. A. Representative images of no Aβ treatment**. B.** Representative images of Aβ40 and Aβ42 after 1 hour's treatment. **C.** Representative images of Aβ40 and Aβ42 after 24 hours treatment **D.** Representative images of Aβ40 and Aβ42 after 48 hours treatment. Images show Aβ stained with 6E10-Alexa 647 nm (red), Astrocytes stained with CD44 (yellow), and Hoechst (blue). Scale bar (50μm). 96

Figure 20. The uptake of Aβ in control iAstrocytes after 1-hour (2.5 μM) treatment. (A) Aβ42 oligomers are taken up more than Aβ40 and Aβ40: Aβ42 (9:1) but not Aβ40: Aβ42 (7:3) in control iAstrocytes. (**B**) Aβ fibrils are not specifically taken up in control iAstrocytes. For iAstrocytes, each data point represents 3 technical repeats averaged into 1 biological repeat per line (total cell lines = 3). Data is visualised as mean ± S.D. Statistical analysis was completed using Kruskal-Wallis (**A**: H = 17.32, p-value = 0.0006) and **B**: H = 5.539, p-value = 0.1364). For oligomer post hoc analysis a Dunn's multiple comparisons test was performed. Post hoc analysis was not completed for fibrils due to overall Kruskal-Wallis displaying as non-significant. Where there are no statistical lines = non-significant (ns), * p-value = <0.05, ** p-value = <0.01, *** p-value = <0.001, and **** p-value = <0.0001. 97

Figure 21. Illustrations of control iAstrocytes after Aβ (2.5 μM) oligomers treatment using immunocytochemistry. CD44 (yellow), Hoechst (blue), and Aβ (6E10-Alexa 647 nm, red). Scale bar (50 μm). 98

Figure 22. Illustrations of control iAstrocytes after Aβ (2.5 μM) fibrils treatment using immunocytochemistry. CD44 (yellow), Hoechst (blue), and Aβ (6E10-Alexa 647 nm, red). Scale bar (50 μm). 99

Figure 23. The uptake of Aβ in AD iAstrocytes after 1-hour (2.5 μM) treatment. A. Aβ42 oligomers are up-taken more than Aβ40: Aβ42 (9:1 and 7:3), and no treatment but not Aβ40 (10:0). **B.** Aβ fibrils are not specifically up-taken in control iAstrocytes. For iAstrocytes, each data point represents 3 technical repeats averaged into 1 biological repeat per line (total cell lines = 3). Data is visualised as mean ± S.D. Statistical analysis was completed using ANOVA

(**A**; F= 8.214, p-value = 0.0003). For oligomer post hoc analysis a Tukey's multiple comparison test was performed. Post hoc analysis was not completed for fibrils due to overall Kruskal-Wallis displaying as non-significant. Where there are no statistical lines = non-significant (ns), * p-value = <0.05, ** p-value = <0.01, *** p-value = <0.001, and **** p-value = <0.0001.....100

Figure 24. Illustrations of AD iAstrocytes after Aβ (2.5 μM) oligomers treatment using immunocytochemistry. CD44 (yellow), Hoechst (blue), and Aβ (6E10-Alexa 647 nm, red). Scale bar (50 μm). 101

Figure 25. Illustrations of AD iAstrocytes after Aβ (2.5 μM) fibrils treatment using immunocytochemistry. CD44 (yellow), Hoechst (blue), and Aβ (6E10-Alexa 647 nm, red). Scale bar (50 μm). 102

Figure 26. In vitro kinetic model of Aβ aggregation visual explanation using Aβ42. The rate of Aβ is modelled kinetically in a sigmoidal reaction course in three distinct phases: lag, exponential, and stationary using Thioflavin T (ThT) intensity (A.U.) (excitation = 450 nm, emission = 482nm). **A**. Lag phase where monomeric Aβ peptides begin to accumulate for stability. As oligomeric species begin to form, indicated by detectable β-sheets at the end of the lag phase into the elongation phase, the intensity of ThT begins to increase (T1) **B.** The elongation phase is represented by a depletion of monomeric species and an increased concentration of oligomers, protofibrils and fibrillar species. **C**. The intensity of ThT begins to plateau, indicating the rate of the reaction declining as a result of the decline in soluble species and the formation of insoluble fibrils (T2). Aβ42 (0:10) (50 μM) aggregation curve is shown in this figure. Sample points for oligomers (T1) and fibrils (T2) sampling are shown. 105

Figure 27. The induction of TNF-α in control iAstrocytes after treatment with Aβ. Aβ oligomers (**A**) and Fibrils (**B**) result in the induction of TNF-α in control iAstrocytes, and isoform-specific differences in Aβ. For iAstrocytes, each data point represents 3 technical repeats averaged into 1 biological repeat per line (total cell lines = 3 per group). Data is visualised as mean ± S.D. Statistical analysis was completed using ANOVA (A; F = 167.6, p-value = <0.0001 and B; F = 56.12, p-value = <0.0001). Post-hoc analyses were completed using Tukey's multiple comparison and can be found in Tables 11 and 12. Where there are

no statistical lines = non-significant (ns), * p-value = <0.05, ** p-value = <0.01, *** p-value = <0.001, and **** p-value = <0.0001.....119
Figure 28. The induction of TNF-α in AD iAstrocytes after treatment with Aβ oligomers (**A**) and Fibrils **(B**) see the secretion of TNF-α in control iAstrocytes, and isoform-specific differences in Aβ in oligomers and fibrils. For iAstrocytes, each data point represents 3 technical repeats averaged into 1 biological repeat per line (total cell lines = 3 per group). Data is visualised as mean ± S.D. Statistical analysis was completed using Welch's ANOVA (A; W= F = 187.5, p-value = <0.0001 and B; W = 64.66, p-value = <0.0001). Post-hoc analyses were completed using Dunnett's T3 multiple comparisons test comparison and can be found in Tables 13 and 14. Where there are no statistical lines = non-significant (ns), * p-value = <0.05, ** p-value = <0.01, *** p-value = <0.001, and **** p-value = <0.0001. 121
Figure 29. The induction of TNF-α in control and AD iAstrocytes after treatment with Aβ. No treatment (**A**), Aβ oligomers (**B-E**) and Fibrils (**F-I**). For iAstrocytes, each data point represents 3 technical repeats averaged into 1 biological repeat per line (total cell lines = 3 per group). Data is visualised as mean ± S.D. Statistical analysis was completed using parametric unpaired t test, or non-parametric Mann-Whitney U test dependent on Shapiro-Wilk normality. Where there are no statistical lines = non-significant (ns), * p-value = <0.05, ** p-value = <0.01, *** p-value = <0.001, and **** p-value = <0.0001. 123
Figure 30. The induction of MCP1 in control iAstrocytes after treatment with Aβ. Aβ oligomers (**A**) and Fibrils (**B**) result in the induction of MCP1 in control iAstrocytes, and isoform-specific differences in Aβ. For iAstrocytes, each data point represents 3 technical repeats averaged into 1 biological repeat per line (total cell lines = 3 per group). Data is visualised as mean ± S.D. Statistical analysis was completed using One-way ANOVA (**A**; W = 171.9, p-value = <0.0001) and Welch's ANOVA (**B**; W = 90.55, p-value = 0.0001). Post-hoc analyses were completed using Tukey's multiple comparison and Dunnett's T3 multiple comparisons test comparison, and can be found in Tables 11 and 12. Where there are no statistical lines = non-significant (ns), * p-value = <0.05, ** p-value = <0.01, *** p-value = <0.001, and **** p-value = <0.0001.....125
Figure 31. The induction of MCP1 in AD iAstrocytes after treatment with Aβ. Aβ oligomers (**A**) and Fibrils (**B**) result in the induction of MCP1 in AD iAstrocytes, and isoform specific differences in Aβ. For iAstrocytes, each data point represents 3 technical repeats averaged into 1 biological repeat per line (total cell lines = 3 per group). Data is visualised as mean ±

S.D. Statistical analysis was completed using Welch's ANOVA (A; W = 139.5, p-value = <0.0001 and B; W = 64.66, p-value = <0.0001). Post-hoc analyses were completed using Dunnett's T3 multiple comparisons test comparison, and can be found in Tables 13 and 14. Where there are no statistical lines = non-significant (ns), * p-value = <0.05, ** p-value = <0.01, *** p-value = <0.001, and **** p-value = <0.0001. 127
Figure 32. The induction of MCP1 in control and AD iAstrocytes after treatment with Aβ. No treatment (**A**), Aβ oligomers (**B-E**) and Fibrils (**F-I**). For iAstrocytes, each data point represents 3 technical repeats averaged into 1 biological repeat per line (total cell lines = 3 per group). Data is visualised as mean ± S.D. Statistical analysis was completed using unpaired t-test or Mann-Whitney Test dependent on Shapiro-Wilk normality. Where there are no statistical lines = non-significant (ns), * p-value = <0.05, ** p-value = <0.01, *** p-value = <0.001, and **** p-value = <0.0001. 129
Figure 33. The induction of IL6 in control iAstrocytes after treatment with Aβ. Aβ oligomers (**A**) and Fibrils (**B**) result in the induction of IL6 in Control iAstrocytes, and isoform-specific differences in Aβ. For iAstrocytes, each data point represents 3 technical repeats averaged into 1 biological repeat per line (total cell lines = 3 per group). Data is visualised as mean ± S.D. Statistical analysis was completed using One-way ANOVA (A; F = 158.6, p-value = <0.0001) and Welch's ANOVA (B; F= 87.69, p-value = 0.0001). Post-hoc analyses were completed using Tukey's multiple comparison or Dunnett's T3 multiple comparisons test comparison and can be found in Tables 11 and 12. Where there are no statistical lines = non-significant (ns), * p-value = <0.05, ** p-value = <0.01, *** p-value = <0.001, and **** p-value = <0.0001. 131
Figure 34. The induction of IL6 in AD iAstrocytes after treatment with Aβ. Aβ oligomers (**A**) and Fibrils (**B**) result in the induction of IL6 in AD iAstrocytes, and isoform-specific differences in Aβ. For iAstrocytes, each data point represents 3 technical repeats averaged into 1 biological repeat per line (total cell lines = 3 per group). Data is visualised as mean ± S.D. Statistical analysis was completed using Welch's ANOVA (**A**; W = 203.0, p-value = <0.0001 and **B**; W = 87.79, p-value = <0.0001). Post-hoc analyses were completed using or Dunnett's T3 multiple comparisons test and can be found in Tables 13 and 14. Where there are no statistical lines = non-significant (ns), * p-value = <0.05, ** p-value = <0.01, *** p-value = <0.001, and **** p-value = <0.0001. 133

Figure 35. The induction of IL6 in control and AD iAstrocytes after treatment with Aβ. No treatment (**A**), Aβ oligomers (**B-E**) and Fibrils (**F-I**). For iAstrocytes, each data point represents 3 technical repeats averaged into 1 biological repeat per line (total cell lines = 3 per group). Data is visualised as mean ± S.D. Statistical analysis was completed using unpaired t-test or Mann-Whitney Test dependent on Shapiro-Wilk normality. Where there are no statistical lines = non-significant (ns), * p-value = <0.05, ** p-value = <0.01, *** p-value = <0.001, and **** p-value = <0.0001. 135
Figure 36. The induction of IL-1β in control iAstrocytes after treatment with Aβ. Aβ oligomers (**A**) and Fibrils (**B**) result in the induction of IL-1β in Control iAstrocytes, and isoform-specific differences in Aβ). For iAstrocytes, each data point represents 3 technical repeats averaged into 1 biological repeat per line (total cell lines = 3 per group). Data is visualised as mean ± S.D. Statistical analysis was completed using ANOVA (**A**; F= 138.5, p-value = <0.0001 and **B**; F= 46.12, p-value = <0.0001). Post-hoc analyses were completed using Tukey's multiple comparison and can be found in Tables 11 and 12. Where there are no statistical lines = non-significant (ns), * p-value = <0.05, ** p-value = <0.01, *** p-value = <0.001, and **** p-value = <0.0001.....137
Figure 37. The Induction of IL-1β in AD iAstrocytes after Treatment with Aβ. Aβ oligomers (**A**) and Fibrils (**B**) result in the induction of IL-1β in AD iAstrocytes, and isoform-specific differences in Aβ. For iAstrocytes, each data point represents 3 technical repeats averaged into 1 biological repeat per line (total cell lines = 3 per group). Data is visualised as mean ± S.D. Statistical analysis was completed using Welch's ANOVA (**A**; W = 179.7, p-value = <0.0001 and **B**; W = 61.80, p-value = 0.0001). Post-hoc analyses were completed using Dunnett's T3 multiple comparisons test and can be found in Tables 13 and 14. Where there are no statistical lines = non-significant (ns), * p-value = <0.05, ** p-value = <0.01, *** p-value = <0.001, and **** p-value = <0.0001. 139
Figure 38. The induction of IL-1β in control and AD iAstrocytes after treatment with Aβ. No treatment (**A**), Aβ oligomers (**B-E**) and Fibrils (**F-I**). For iAstrocytes, each data point represents 3 technical repeats averaged into 1 biological repeat per line (total cell lines = 3 per group). Data is visualised as mean ± S.D. Statistical analysis was completed using unpaired t-test or Mann-Whitney Test dependent on Shapiro-Wilk normality. Where there are no statistical lines = non-significant (ns), * p-value = <0.05, ** p-value = <0.01, *** p-value = <0.001, and **** p-value = <0.0001. 141

Figure 39. **Illustrations of control iAstrocytes after Aβ (2.5 μM) treatment using immunocytochemistry. A.** Representative GFAP (**A**), Vimentin (**B**), and CD44 (**C**) after no treatment, Aβ40 oligomers, Aβ42 oligomers, Aβ40 fibrils, and Aβ42 fibrils. Scale bar (50 μm). 150

Figure 40. Quantification of GFAP, Vimentin and CD44 expression in control iAstrocytes. The percentage of cells with positive staining for GFAP (**A**), Vimentin (**B**), and CD44 (**C**) after treatment with Aβ. **D.** Aβ species do not cause a significant difference in GFAP intensity (F= 2.558, p-value = 0.8996). **E.** Aβ species do not cause a significant difference in Vimentin intensity (F= 0.3190, p-value = 0.8590). **F.** Aβ species do not cause a significant difference in CD44 intensity (F= 0.3923, p-value = 0.8097). **G.** Aβ species do not cause a significant difference in the GFAP+ area (F= 0.5305, p-value = 0.7165). **H.** Aβ species do not cause a significant difference in the Vimentin+ area. F= 1.339, p-value = 0.3212). **I.** Aβ species do not cause a significant difference in the Vimentin+ area (F= 0.7037, p-value = 0.6072). All statistical analyses were completed using one-way ANOVA. Post-hoc analysis was not completed because the overall ANOVAs were displayed as non-significant. Data is visualised as mean ± S.D. Biological repeats (n=3) of one control line (control 2) were averaged from 3 technical repeats. For intensity after Aβ treatment, results were normalised total intensity/cell area/total cell count to create an intensity ratio. For intensity after Aβ treatment, results were normalised total area/total cell count. 151

Figure 41. **Illustrations of AD iAstrocytes after Aβ (2.5 μM) treatment using immunocytochemistry. A.** Representative GFAP (**A**), Vimentin (**B**), and CD44 (**C**) after no treatment, Aβ40 oligomers, Aβ42 oligomers, Aβ40 fibrils, and Aβ42 fibrils. Scale bar (50 μm). 155

Figure 42. Quantification of GFAP, Vimentin and CD44 expression in AD iAstrocytes. The percentage of cells with positive staining for GFAP (preliminary) (**A**), Vimentin (**B**), and CD44 (**C**) after treatment with Aβ. Preliminary GFAP intensity (**D**) and GFAP area (**G**). Statistical analysis was not completed (n=1). **E.** Aβ species do not cause a significant difference in Vimentin intensity (F= F= 0.3969, p-value = 0.8065). **F.** Aβ species do not cause a significant difference in CD44 intensity (F= 1.707, p-value = 0.2245). **H.** Aβ species do not cause a significant difference in the Vimentin+ area (F= 0.05522, p-value = 0.9934). **I.** Aβ species do not cause a significant difference in CD44+ area (F= 0.0032, p-value = 0.9978). All statistical analyses were completed using one-way ANOVA. Post-hoc analysis was not completed

because the overall ANOVAs were displayed as non-significant. Data is visualised as mean ± S.D. Biological repeats (n=3) of one AD line (AD 2) were averaged from 3 technical repeats for Vimentin and CD44. For intensity after Aβ treatment, results were normalised total intensity/cell area/total cell count to create an intensity ratio. For intensity after Aβ treatment, results were normalised total area/total cell count. 156

Figure 43. The uptake of Aβ in control iAstrocytes after 24-hour cytokine treatment and 1-hour Aβ (2.5 μM) treatment. A. The uptake of Aβ40 oligomers is not significantly reduced after cytokine treatment (F = 0.8442, p-value = 0.4753). **B.** The uptake of Aβ42 oligomers is not significantly reduced after cytokine treatment (F = 1.176, p-value = 0.3709). **C.** The uptake of Aβ40 fibrils is not significantly reduced after cytokine treatment (F = 1.305, p-value = 0.336) **D.** The uptake of Aβ42 fibrils is not significantly reduced after cytokine treatment (F = 2.655, p-value = 0.149). LD = low dose (10 ng/mL). HD = high dose (100 ng/mL). For iAstrocytes (n=1), each data point represents 3 technical repeats averaged into 1 biological repeat of one cell line. Data is visualised as mean ± S.D. All statistical analysis was completed using one-way ANOVA. Post hoc analysis was not completed due to overall ANOVA displaying as non-significant. Where there are no statistical lines = non-significant (ns), * p-value = <0.05, ** p-value = <0.01, *** p-value = <0.001, and **** p-value = <0.0001. **E.** Average mean percentage in decrease of Aβ40 oligomers. **F.** Average mean percentage in decrease of Aβ42 oligomers. **G.** Average mean percentage in decrease of Aβ40 fibrils. **H.** Average mean percentage in decrease of Aβ42 fibrils. 171

Figure 44. Illustrations of control iAstrocytes after Aβ40 (2.5 μM) oligomers treatment using immunocytochemistry. A. No dose cytokines **B.** Low dose cytokines (10 ng/mL). **C.** High dose cytokines (100 ng/mL). **D.** No treatment. CD44 (yellow), Hoechst (blue), and Aβ (6E10-647 nm, red). Scale bar (50 μm). 172

Figure 45. Illustrations of control iAstrocytes after Aβ42 (2.5 μM) oligomers treatment using immunocytochemistry. A. No dose cytokines **B.** Low dose cytokines (10 ng/mL). **C.** High dose cytokines (100 ng/ mL). **D.** No treatment. CD44 (yellow), Hoechst (blue), and Aβ (6E10-647 nm, red). Scale bar (50 μm). 173

Figure 46. **Illustrations of control iAstrocytes after Aβ40 (2.5 μM) fibrils treatment using immunocytochemistry. A.** No dose cytokines **B.** Low dose cytokines (10 ng/mL). **C.** High

dose cytokines (100 ng/ mL). **D.** No treatment. CD44 (yellow), Hoechst (blue), and Aβ (6E10-647 nm, red). Scale bar (50 μm). 174

Figure 47. Illustrations of control iAstrocytes after Aβ40 (2.5 μM) fibrils treatment using immunocytochemistry. A. No dose cytokines **B.** Low dose cytokines (10 ng/mL). **C.** High dose cytokines (100 ng/ mL). **D.** No treatment. CD44 (yellow), Hoechst (blue), and Aβ (6E10-647 nm, red). Scale bar (50 μm). 175

Figure 48. The uptake of Aβ in AD iAstrocytes after 24-hour cytokine treatment and 1-hour Aβ (2.5 μM) treatment. A. The uptake of Aβ40 oligomers is significantly reduced after cytokine treatment at both high and low dose, but not between cytokine groups (ANOVA, F = 8.683, p-value = 0.0169). **B.** The uptake of Aβ42 oligomers is significantly reduced after cytokine treatment at both high and low dose, but not between cytokine groups (ANOVA, F = 32.53, p-value = 0.0006). **C.** The uptake of Aβ40 fibrils is significantly reduced after cytokine treatment at both high and low dose, but not between cytokine groups (ANOVA, F = 6.931, p-value = 0.0276). **D.** The uptake of Aβ42 fibrils is significantly reduced after cytokine treatment at both high and low dose, but not between cytokine groups (ANOVA, F = 9.648, p-value = 0.0133). LD = low dose (10 ng/mL). HD = high dose (100 ng/mL). For iAstrocytes (n=1), each data point represents 3 technical repeats averaged into 1 biological repeat of one cell line. Data is visualised as mean ± S.D. Statistical analysis was completed using ANOVA. Post-hoc analyses were completed using Tukey's multiple comparison and can be found in S9. Where there are no statistical lines = non-significant (ns), * p-value = <0.05, ** p-value = <0.01, *** p-value = <0.001, and **** p-value = <0.0001. **E.** Average mean percentage in decrease of Aβ40 oligomers. **F.** Average mean percentage in decrease of Aβ42 oligomers. **G.** Average mean percentage in decrease of Aβ40 fibrils. **H.** Average mean percentage in decrease of Aβ42 fibrils. 177

Figure 49. Illustrations of AD iAstrocytes after Aβ40 (2.5 μM) oligomers treatment using immunocytochemistry. A. No dose cytokines **B.** Low dose cytokines (10 ng/mL). **C.** High dose cytokines (100 ng/mL). **D.** No treatment. CD44 (yellow), Hoechst (blue), and Aβ (6E10-647 nm, red). Scale bar (50 μm). 178

Figure 50. **Illustrations of AD iAstrocytes after Aβ42 (2.5 μM) oligomers treatment using immunocytochemistry. A.** No dose cytokines **B.** Low dose cytokines (10 ng/mL). **C.** High

dose cytokines (100 ng/mL). **D.** No treatment. CD44 (yellow), Hoechst (blue), and Aβ (6E10-647 nm, red). Scale bar (50 μm). 179

Figure 51. Illustrations of AD iAstrocytes after Aβ40 (2.5 μM) fibrils treatment using immunocytochemistry. A. No dose cytokines **B.** Low dose cytokines (10 ng/mL). **C.** High dose cytokines (100 ng/ mL). **D.** No treatment. CD44 (yellow), Hoechst (blue), and Aβ (6E10-647 nm, red). Scale bar (50 μm). 180

Figure 52. Illustrations of AD iAstrocytes after Aβ42 (2.5 μM) fibrils treatment using immunocytochemistry. A. No dose cytokines **B.** Low dose cytokines (10 ng/mL). **C.** High dose cytokines (100 ng/ mL). **D.** No treatment. CD44 (yellow), Hoechst (blue), and Aβ (6E10-647 nm, red). Scale bar (50 μm). 181

Figure 53. Illustrative diagram summarising the feedback loop. In the healthy brain Aβ clearance is maintained by activated astrocytes to keep a physiological Aβ40: Aβ42 deposition. In AD, chronic inflammatory states shift astrocytes from an Aβ-clearing phenotype to one with less clearance. Less clearance further activates astrocytes, creating a higher inflammatory environment and inducing downstream neuronal dysregulation and degeneration. Leading to a harmful cycle where less clearance increases Aβ production and aggregation, inducing further activation of astrocytes, increasing the release of pro-inflammatory markers, reduced clearance and further neurodegeneration.....189

List of Tables

Table 1. induced Neuronal Progenitor Cell (iNPC) Media Constituents. Supplements, concentration/volume, source; supplier and lot number are shown. 50

Table 2. iAstrocyte Media Constituents. Supplements, concentration/volume, source; supplier and lot number are shown. 50

Table 3. Primary Antibodies used for Immunocytochemistry. Antibody specificity, dilution (in 0.2% TritonTM (v/v) + 5% (v/v) horse serum/PBS), source; supplier and lot number, and species are shown. 51

Table 4. Secondary Antibodies for Immunocytochemistry. Antibody specificity, dilution (in 5% (v/v) horse serum/PBS), source; supplier and lot number are shown. 51

Table 5. Constituents for Immunocytochemistry. Constituents specificity, volume/concentration (v/v), source; supplier and lot number are shown. 52

Table 6. Single Molecule Pull Down (SiMPull) Constituents. Constituents specificity, concentration, source; supplier and lot number are shown. 52

Table 7. Antibodies for Single Molecule Pull Down and Co-aggregation Imaging. Antibody specificity, concentration (diluted in 0.1mg/mL (v/v) BSA/PBS), source; supplier and lot number. 53

Table 8. Cell Line Demographics. Cell line, Diagnosis, Gender, and Age are shown. 55

Table 9. Cell Lines and Fibronectin Dilution Factor. Control and AD iNPCs and iAstrocytes fibronectin dilution factor (40 ng (w/v) in 0.1% bovine serum albumin (BSA). 56

Table 10. Amyloid-β Aggregates. Isoforms, Aggregate Species, and Time Point. 60

Table 11. Summary TNF-α, MCP1, IL6, and IL-1β release after Aβ oligomers treatment in control iAstrocytes. 142

Table 12. Summary TNF-α, MCP1, IL6, and IL-1β release after Aβ fibrils treatment in control iAstrocytes. 143

Table 13. Summary TNF-α, MCP1, IL6, and IL-1β release after Aβ oligomers treatment in AD iAstrocytes. 144

Table 14. Summary TNF-α, MCP1, IL6, and IL-1β release after Aβ fibrils treatment in AD iAstrocytes. 145

Table 15. Summary TNF-α, MCP1, IL6, and IL-1β release for AD vs Control iAstrocytes. 146

Abbreviations

Abbreviation	Definition
AD	Alzheimer's Disease
ALS	Amyotrophic Lateral Sclerosis
APOE	Apolipoprotein E
APP	Aβ Precursor Protein
Aβ	Amyloid-β
CNS	Central Nervous System
CSF	Cerebrospinal Fluid
EAAT2	Excitatory Amino Acid Transporter-2
GFAP	Glial Fibrillary Acidic Protein
HD	Huntington's Disease
iAstrocytes	induced Astrocytes
ICC	Immunocytochemistry
IL-1β	Interleukin-1-β
IL6	Interleukin-6
iNPCs	induced Neuronal Progenitor Cells
iPSCs	induced Pluripotent Stem Cells
LRP1	Low-density Lipoprotein Receptor-related Protein-1
MAPK	Mitogen-Activated Protein Kinase
MCP1	Monocyte Chemoattractant Protein-1
NF-kB	Nuclear Factor-kappa B
NFTs	Neurofibrillary Tangles
PAX6	Paired Box 6
PD	Parkinson's Disease
PET	Positron Emission Tomography
PQC	Protein Quality Control (PQC) System
PSEN-1	Presenilin-1
PSEN-2	Presenilin-2

RT	Room Temperature
SiMPull	Single-molecule PullDown Imaging
ThT	Thioflavin T
TIRF	Total Internal Reflection Fluorescent
TNF-α	Tumor Necrosis Factor-a
TREM2	Triggering Receptor Expressed on Myeloid Cells 2

Chapter 1. Introduction

1.1. Introduction to Alzheimer's Disease

Alzheimer's Disease (AD) is the leading cause of dementia worldwide, with an estimated 55 million individuals currently living with dementia (Alzheimer's Society, 2025). It is predicted that the global number will rise to 139 million by 2050. Dementia is a major neurodegenerative disorder that is not specific to a disease but is an umbrella term used to describe a range of conditions. Dementia includes AD, Vascular dementia, Dementia with Lewy bodies, Frontotemporal dementia, Parkinson's dementia, and Mixed dementia (Alzheimer's Research UK, 2025). An estimated 60-70% of all dementia cases are AD, and in the UK alone, it has a prevalence of 944,000 in 2024, and was the leading cause of death in both 2022 and 2023 (Alzheimer's Society, 2025; Office for National Statistics, 2024).

Clinical representation shows that 90-95% of individuals develop AD sporadically with a later onset after ~65 years of age (Rabbito et al., 2020). The remaining 5-10% of AD cases are hereditary (familial), with an earlier onset before 60 years of age, with some patients having symptoms as early as 40 years old (Bali et al., 2012). Familial AD is linked to genetic mutations in the Aβ Precursor Protein (*APP*), presenilin-1 (*PSEN-1*), and presenilin-2 (*PSEN-2*) genes (Baranello et al., 2015). Instead, sporadic AD has been associated with genetic risk factors such as Apolipoprotein E (*APOE*) and the triggering receptor expressed on myeloid cells (*TREM2*) (Baranello et al., 2015). Longitudinal community-based cohort studies have shown that the strongest risk factors for AD are age and carriers of the APOE ε4 allele (van der Lee et al., 2018). Others have indicated that 66% of individuals with AD-type dementia have *APOEε4* (Mattsson et al., 2018). Besides genetic susceptibility, age is the main associated risk factor for AD (Liu et al., 2024b). It is also linked to a range of non-modifiable risk factors driven by environmental and lifestyle factors (Zhang et al., 2021). However, there is no known definitive cause of AD, and the underlying aetiology remains unknown (Breijyeh and Karaman, 2020; Livingston et al., 2020). Phenotypically, sporadic and familial AD are similar, resulting in progressive and irreversible cognitive decline, including aphasia, apraxia, behavioral changes, cognitive impairment, memory loss, and brain atrophy (Breijyeh and Karaman, 2020). Pathologically, AD is part of a larger group of neurodegenerative diseases characterised by the accumulation of positive lesions driven by

species of abnormally aggregated protein deposits (Kovacs, 2019). In this context, the histopathological hallmarks of AD are the deposition of extracellular Aβ senile plaques and intracellular neurofibrillary tangles (NFTs) which consist of phosphorylated microtubule-binding protein Tau. Due to Aβ and Tau being pathological hallmarks, they are routinely used in the diagnosis of AD, as part of the combination of several stages of testing. Firstly, a series of cognitive, functional, and behavioural tests assess the mental ability of the individual (NHS UK, 2024). Next, brain imaging such as magnetic resonance imaging and computed tomography are used to measure brain atrophy (Plant et al., 2010).

Furthermore, cerebrospinal fluid (CSF) biomarkers of Aβ and Tau by lumbar puncture or spinal tap are increasingly being used in the diagnosis of AD (Liu et al., 2024a; Jack et al., 2024; Paterson et al., 2018). Next, the density of the Aβ plaques and NFTs, coupled with Thal Phase and Tau Braak staging, which measures Aβ and Tau deposition, respectively (Wharton et al., 2019). In order to do this, positron emission tomography (PET) is used, and from such measures, it is now known that there is a neuroanatomical hierarchy of progression throughout brain regions affected during AD, though these proteins are pathologically different (Wharton et al., 2019). Although both NFTs and Aβ are characteristics of AD, Aβ plaques are more commonly found in brain regions that are impaired in AD and have long been proposed as one of the main drivers of AD. The hypothesis of Aβ plaques toxicity forms the central component of the amyloid cascade hypothesis.

1.2. The Amyloid Cascade Hypothesis

The amyloid cascade hypothesis was proposed in 1992 by Hardy and Higgins, which postulates that Aβ plaques drive the neurodegeneration associated with AD. Aβ plaques progressively build up around neurones, the most commonly affected cell type in AD, and the primary driver of clinical symptoms. For example, memory loss as a result of the loss of neurones in the hippocampus or difficulty reasoning due to damage in the prefrontal cortex (Wang et al., 2017). The amyloid cascade is strengthened by genetic evidence of autosomal dominant genes, e.g., *APP, PSEN-1,* and *PSEN-2,* which are associated with the production of Aβ, and pathological evidence highlighting that Aβ plaques are one of the probable causes of AD for familial AD (Barage and Sonawane, 2015). It is the association of the build-up of

plaques in the brain and genetic discoveries linked back to the production of Aβ that drove the original hypothesis.

However, clinical data have shown that Aβ deposition alone does not consistently correlate with cognitive decline or neuronal loss, the defining features of AD pathology (Ricciarelli and Fedele, 2017; Villemagne et al., 2011). Furthermore, the accumulation of Aβ plaques is also observed in those classed as cognitively normal (Mormino and Papp, 2018). An estimated 1/3 of the population over 70 has Aβ plaque deposition but do not go on to develop AD (Jansen et al., 2022). Indicating that the neuropathological component may not be the amount of neuritic plaque deposits (Nelson et al., 2012). Furthermore, despite decades of research for the early-onset mechanism and effective treatment focusing on plaques, there is still a lack of a cure for AD (Rabbito et al., 2020). For example, Aducanumab (Aduhelm) was the first FDA-approved drug to treat AD by removing the build-up of Aβ in the brain in 2021 (Mukhopadhyay and Banerjee, 2021). However, in November 2024, it was discontinued due to concerns about high cost and efficacy (Ashique et al., 2024). Despite this, other emerging disease-modifying treatments which focus on Aβ deposit clearance include Lecanemab (Leqembi) and Donanemab (Kisunla), which are currently approved by both the FDA and UK MHRA, though they are not currently provided through the NHS. Although there are recent breakthroughs in disease-modifying treatments, the lack of effective drugs, along with other evidence discussed, has cast doubt on the role of Aβ, as a core pathological cause of AD.

It has been argued that the timing of these treatments is one main driver for the lack of successful clinical trials. Firstly, a complete diagnosis of AD is primarily restricted to late prodromal or clinical stages of the disease. Clinically, the prodromal stages of AD, otherwise known as mild cognitive impairment (MCI), often include episodes of forgetfulness and disorientation (Creese et al., 2019). However, this is associated with the concept of normal ageing, and it is estimated that individuals do not present to the clinic for 3-4 years after the onset of mild symptoms (Creese et al., 2019). For patients to be diagnosed with AD, individuals need to meet the criteria for later-stage MCI, which includes being implicated with significant cognitive dysfunction or neurobehavioral symptoms (Chen et al., 2021). At this point in the disease, it has been hypothesised that the cellular death which causes symptoms has already happened and is irreversible. As a result, preceding the hierarchal progression of deposits throughout brain regions affected during AD (Wharton et al., 2019).

Additionally, it is now widely accepted that Aβ plaques are not deposited in their physiological form (Uddin et al., 2020). This has led to an updated view on the cascade that Aβ induces pathological effects at an earlier timepoint. Supporting this changes in Aβ deposition have been detected in CSF in AD patients before the onset of clinical symptoms (Ross and Dodel, 2025; Jia et al., 2024; Cai et al., 2023a; Bouwman et al., 2022; Niemantsverdriet et al., 2017). These include CSF; Aβ 42/40, and CSF p-tau 181/Aβ42, CSF t-tau/Aβ42 (Jack et al., 2024), highlighting that Aβ does still have a significant role in the development of AD. Moreover, the recent advances in blood-based biomarkers which detect Aβ are consistent with brain pathology (Strelnikova et al., 2025). It has also been shown that Aβ deposition occurs before tau dysfunctions and is one of the earliest pathological changes. These early changes in Aβ deposition have been shown to occur ~15-20 years before the onset of clinical symptoms in both sporadic and familial AD patients (Bateman et al., 2012; Caballero et al., 2020). Additionally, both Aβ CSF and PET precede measures of neurodegeneration, CSF tau, structural brain MRI, and cognitive dysfunction (Jack et al., 2024; Hampel et al., 2021). As a result, it is important to understand how the earlier stages of Aβ deposition contribute to AD dysfunction.

In recent years, the amyloid cascade hypothesis has also been adapted due to a better understanding of the progression of AD in the context of the cellular phase in the preclinical stage before Aβ plaques (Scheltens et al., 2021). Dysfunction of several cell types within the central nervous system, including neurones, oligodendrocytes, and glial cells; microglia and astrocytes, are all affected in AD (Zheng and Wang, 2025; Zhu et al., 2024). This is particular important when considering emerging treatment options for AD, and how it may affect different cell types. For example, current therapeutics and clinical trials have focussed on managing and slowing down symptoms through neuronal modulation via transmitter levels, excitability and regeneration (Mei et al., 2024). Alternatively, the removal of plaques in the brain through the increased clearance of Aβ. In the brain, glial cells have an essential role in the clearance of Aβ (see section 1.5.) and therefore treatments that reduce Aβ may directly or indirectly influence glial function to clear or reduce Aβ toxicity. Aβ dysfunction includes, in a largely multifactorial and unknown way, the spread of tau pathology by Aβ, neuroinflammation, oxidative stress, mitochondria damage, membrane permeabilization, and calcium dysregulation (De Strooper and Karran, 2016; Long and Holtzman, 2019). At present, little is known about the intermediate stages of Aβ, and how this affects different

downstream biochemical and cellular neurotoxic pathways. In order to unravel pathology-relevant aspects of AD, significant efforts have been made to understand the production and aggregation of Aβ, which ultimately produces senile plaques.

1.3. Aβ Production

Aβ is an extracellular peptide derived from proteolytic processing and hydrolysis of the membrane-bound APP (Huang and Liu, 2020). APP is highly conserved and ubiquitously expressed in neurons, microglia, and astrocytes, which play a central role in the pathology associated with AD (Chen et al., 2017). APP is a type I integral membrane protein consisting of three domains: A long extracellular N-terminal, a transmembrane endothelial segment, and a short cytoplasmic C-terminal fragment. There are two APP processing pathways in humans: non-amyloidogenic and amyloidogenic (Figure 1). The non-amyloidogenic pathway makes up to 90% of APP processing, starting with cleavage by the membrane-bound α-secretase to produce the extracellular N-terminal secreted amyloid precursor protein alpha (sAPPα) and membrane-bound CTAα (C83) (Uddin et al., 2020). Next, CTAα is subsequently cleaved by γ-secretases to produce the APP intracellular domain (AICD) and the extracellular peptide P3 (3 kDa) (Figure 1). Earlier studies have highlighted that P3 is considered pathologically irrelevant (Nhan et al., 2015). However, recent studies have shown that P3 can increase the aggregation of Aβ fibrils and disrupt membrane ion interactions in HEK293 cells (Tian et al., 2025). Highlighting the complex nature of APP processing to produce Aβ peptides.

In the classical amyloidogenic pathway, APP is cleaved by β-secretase to secrete sAPPβ and CTFβ (C99) (Figure 1). In neurons, microglia, and astrocytes, BACE1 is the major β-secretase to produce Aβ (Frost and Li, 2017). A fragment of CTFβ remains bound to the membrane and is cleaved by γ-secretase to produce Aβ (~4.3-4.5 kDa) peptides and AICD (Nhan et al., 2015). The γ-secretase complex consists of several subunits: nicastrin, anterior pharynx defective 1, PSEN-1, and PSEN-2. Non-specific cleavage by γ-secretase results in a heterogenous population of Aβ peptides of several lengths ranging from 38 to 43 amino acids long (Baek and Lee, 2024). Amongst the Aβ isoforms, Aβ40 and Aβ42 are the most abundant (Murphy and LeVine, 2010). Among them, Aβ40 is the more abundant isoform in the human brain and is found at levels ~10 times higher than Aβ42 in the healthy brain

(Dorey et al., 2015). However, despite its lower concentration, Aβ42 is the predominant component of amyloid plaques. Throughout disease progression, the Aβ42: Aβ40 ratio in the CSF decreases, reflecting the selective deposition of Aβ42 into plaques in the brain, a well-established pathological hallmark of AD pathology (Hansson et al., 2019). The mechanisms behind this remain largely unknown. However, the newly synthesised Aβ can remain associated with the cellular membrane or be released into the extracellular space, where it is prone to misfolding and aggregation (Chen et al., 2017).

1.4. Aβ Misfolding and Aggregation

Once released into the extracellular space, Aβ peptides are prone to misfolding and aggregation. Protein misfolding can be driven and modulated by several factors, including but not limited to somatic or genetic mutations, translational or post-translational errors, and structural modification through cellular environmental stress (Kumar et al., 2016; Yadav et al., 2019). Membrane-associated Aβ has little tendency to misfold and aggregate compared to non-membrane-bound Aβ (Ross and Poirier, 2004). Aβ peptides are intrinsically disordered and inherently unstable and so undergo conformational changes to attain stability and form aggregates even without stress conditions (Almeida et al., 2025). In particular, Aβ42 is more prone to aggregation than Aβ40 (Lin et al., 2019). The aggregation of Aβ is a complex process that involves the transition into oligomers, which aggregate further into protofibrils and fibrils, and ultimately plaques (Chen et al., 2017) (Figure 1, A). Several aggregation mechanisms have been proposed, starting with primary nucleation and elongation, which is followed by secondary nucleation processes such as surface catalysation and fragmentation (Figure 1, B) (Cohen et al., 2013). Primary nucleation is believed to initiate the formation of self-assembled nuclei from a pool of monomeric species, which is eventually followed by an elongation stage to produce fibrillar species (Knowles et al., 2014). It is associated with two or more monomers aggregating together (Ashe, 2020). Primary nucleation stages represent the lag phase between the initiation of aggregation and the formation of aggregates with detectable β-sheets (Kundel et al., 2018). Following primary nucleation, initial aggregates grow through elongation (Flagmeier et al., 2020). Next, secondary nucleation is often classed as the catalyst for aggregation, representing the exponential stages of aggregation from previously formed fibrils that

facilitate the binding of additional monomers (Sami et al., 2017; Ashe, 2020). Other secondary processes include monomer-independent processes such as fragmentation or monomer-dependent surface catalysation (Cremades and Dobson, 2018). During surface catalysation, existing preformed fibrils act as catalytic sites for the nucleation of new aggregates by attaching monomers to their surface (Habchi et al., 2018). During aggregation, the transition of monomers to oligomers involves the formation of β-sheet-rich structures (Azargoonjahromi, 2024). Like monomers, oligomeric species are metastable, transient and soluble (Sengupta et al., 2016). Aβ oligomers are highly heterogeneous and can have a molecular weight range of up to ~ 100 kDa (Cline et al., 2018). They can also adopt various structures including but not limited to dimers, trimers, pentamers, and heptamers, making them difficult to study (Zukowska et al., 2024). In recent years, Aβ oligomers have become an interesting point in AD pathology. Studies have shown that indivdiuals with AD patients have a higher concentration of Aβ oligomers in CSF than those without AD (Mroczko et al., 2018).

Furthermore, healthy individuals with high senile plaque loads have low-plaque associated Aβ oligomers, indicating that plaques may be sequestering Aβ oligomers rather than being toxic (Mroczko et al., 2018). Structurally, Aβ fibrils contain multiple cross-β sheet motifs, which aggregate into long unbranched and elongated structures (Baek and Lee, 2024). Fibrils form more stable structures due to the hydrogen bonds between the nitrogen and carbonyl groups between each β-sheet motif (Baek and Lee, 2024). Increased aggregation of fibrils results in the assembly of plaques (Prado and Baron, 2012). The dominant mechanisms of Aβ aggregate formation and how the formation of oligomers and fibrils determines the structure and, thus, the function of Aβ during normal physiological conditions and disease progression in humans are still not understood.

Aβ has been shown to have key physiological functions such as suppressing microbial infections, aiding synaptic plasticity, antioxidant properties, binding to neurotoxins, and regulating angiogenesis (Bishop and Robinson, 2004; Cai et al., 2023b; Jeong et al., 2022). As a result, the cleavage of APP to produce Aβ may not be fundamentally pathogenic, but instead, the misfolding and aggregation of the Aβ peptides (Johansson et al., 2024). This is supported by overwhelming evidence that the formation and accumulation of Aβ aggregates are associated with the cascade of downstream effects: neuronal dysfunction and death, glial activation, mitochondrial dysfunction, oxidative stress, membrane

permeabilisation, calcium dysregulation, tau hyperphosphorylation, neuroinflammation, DNA damage, and many more pathological events (Almeida et al., 2025; Zukowska et al., 2024; Azargoonjahromi, 2024; Hampel et al., 2021; Chen et al., 2017). Due to the neurotoxic pathways associated with accumulation, efficient degradation and clearance of Aβ is crucial for maintaining healthy brain function.

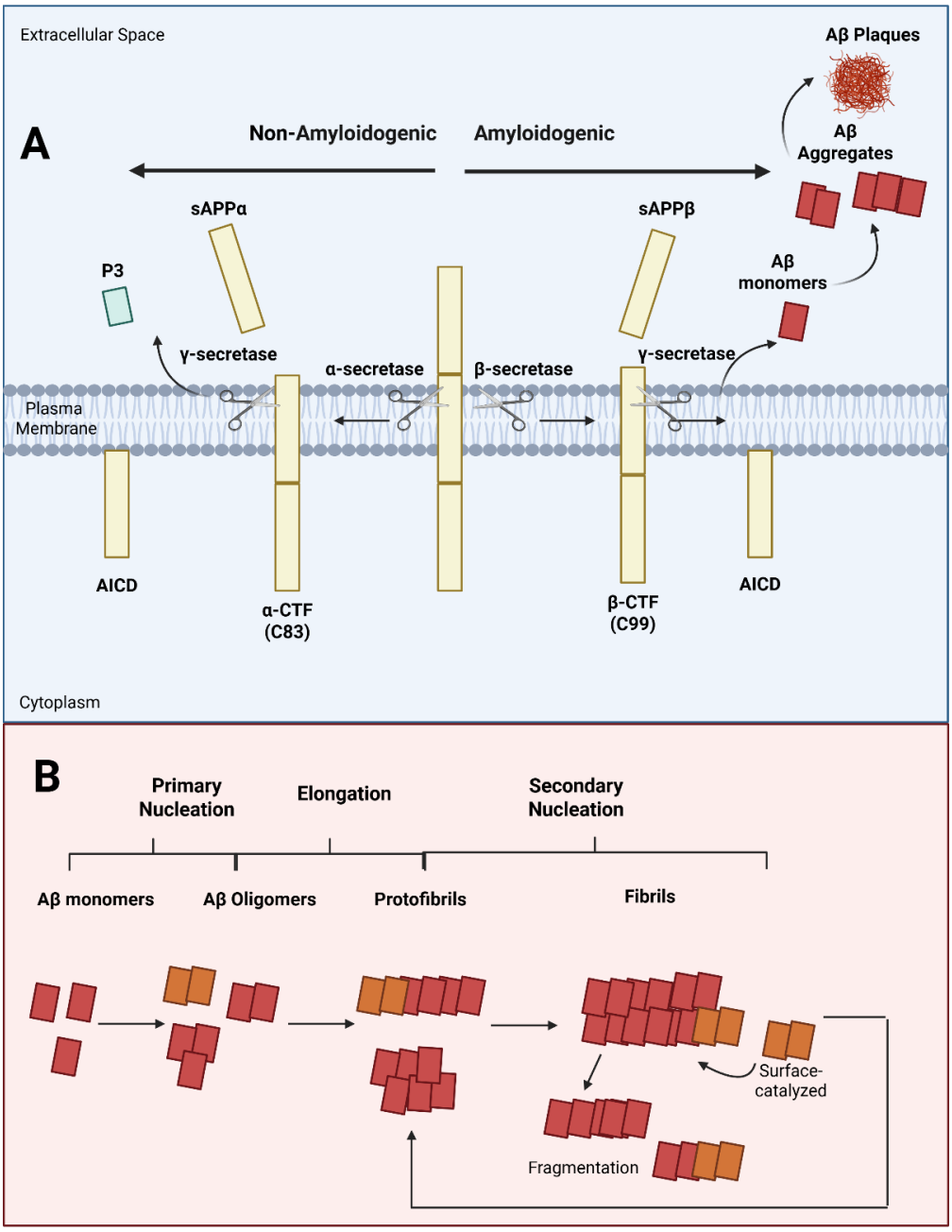

Figure 1. A. APP processing during the non-amyloidogenic and amyloidogenic pathways. *Non-amyloidogenic APP processing uses α-secretase to produce secreted amyloid precursor protein alpha (sAPPα) and CTAα (C83). Next, CTAα is cleaved by γ-secretases to produce the intracellular APP intracellular domain (AICD) and the extracellular peptide P3. During amyloidogenic APP processing, APP is cleaved by β-secretase to secrete secreted amyloid precursor protein beta (sAPPβ) and CTFβ (C99). A fragment of CTFβ remains bound to the membrane and is cleaved by γ-secretase to produce AICD Aβ monomers. Extracellular monomeric Aβ aggregates in a process involving the transition into Aβ aggregate species (oligomers, protofibrils, fibrils), and ultimately plaques.* ***B. Aβ Aggregation Mechanisms****. Several aggregation mechanisms have been proposed, starting with primary nucleation and elongation, which is followed by secondary nucleation processes such as surface catalysation and fragmentation.*

1.5. Aβ Degradation and Clearance

In the brain, Aβ is produced and removed continuously, and it is hypothesised that an imbalance between production and clearance leads to the pathology associated with AD (Saido and Leissring, 2012; Tarasoff-Conway et al., 2015a). Therefore, understanding the mechanisms behind the clearance of Aβ is crucial.

1.5.1. Systemic Clearance of Aβ

The removal of soluble extracellular Aβ from the brain is complex. It can be mediated through several systems, including the transport across the blood-brain barrier, CSF absorption, interstitial fluid (ISF) bulk flow drainage via intramural peri-arterial (IPAD) or lymphatic/glymphatic systems (Ullah and Lee, 2023; Xin et al., 2018). Systemic clearance of Aβ has been shown to overlap during clearance and is defined by the system from which it was cleared and directed. For example, Aβ can be absorbed into the CSF, which is drained into the lymphatic system and goes into the blood circulation (reviewed in Tarasoff-Conway et al., 2015). Alternatively, ISF bulk flow clearance can transport Aβ directly into blood or into the CSF sink, where it then can be drained to the lymphatic/glymphatic systems, or removed by the CSF from transportation to the blood-CSF barrier (reviewed in Tarasoff-Conway et al., 2015). Furthermore, the IPAD pathway clears ISF and solutes/debris, such as Aβ, along the basement membranes of capillaries and cerebral arteries from the brain (Weller et al., 2008). Failure of IPAD is associated with cerebral amyloid angiopathy, where Aβ deposits build up on the walls of blood vessels in the spinal cord and brain (Cozza et al., 2023).

1.5.2. Cell-mediated Degradation of Aβ

Alternatively, cell-mediated clearance is a core mechanism for the degradation and removal of Aβ. Though Aβ is predominantly an extracellular peptide, it can be recognised and internalised into cells via mechanisms such as phagocytosis and receptor-mediated endocytosis (Zhang et al., 2023a; Nazere et al., 2022; Bharadwaj et al., 2018). Once taken up it can be targeted by an extensive network known as the protein quality control (PQC) system. The PQC system consists of molecular chaperones, proteases, lysosomes, and

endosomes, which degrade and remove proteins (Pilla et al., 2017). Alternatively, Aβ can be degraded through enzymes via the ubiquitin-proteasome or autophagy-lysosome systems (Xin et al., 2018). Furthermore, Aβ can be degraded by cell surface proteases and enzymes, including zinc metalloendopeptidase, serine, and cysteine proteases (Saido and Leissring, 2012). The most commonly associated degrading enzymes include Neprillysin, Insulin degrading enzymes, angiotensin-converting enzymes, and cathepsin B (Kato et al., 2022). In the brain, endothelial cells, pericytes, neurones, and glial cells have all been shown to play a role in cell-mediated clearance (Ullah and Lee, 2023). However, glial cells (microglia and astrocytes) are the primary cellular source of clearance of Aβ (Wu and Eisel, 2023).

1.5.3. Glia-mediated Clearance

There are three major types of glial cells in the central nervous system (CNS): oligodendrocytes, microglia, and astrocytes. Oligodendrocytes are essential for the production of myelin formation, which protects and aids in the action potential function of neurones (Bradl and Lassmann, 2010). However, in the context of Aβ, research has highlighted that oligodendrocytes do not aid in clearing Aβ but are a source of Aβ production (Rajani et al., 2024). Instead, microglia and astrocytes are a major source of clearance of Aβ in the brain. Both cell types are involved in the clearance of Aβ through the BBB, ISF bulk flow, CSF absorption, and lymphatic/glymphatic drainage (Ries and Sastre, 2016a). Microglial and astrocytes express receptors such as LRP1, APOE, a2M, RAGE, and ABCB1, which aid in the clearance of Aβ across the blood brain barrier (Yoon and Jo, 2012). LRP1 promotes the efflux of Aβ across the BBB (Li et al., 2025). While, APOE is a cholesterol transporter that competes with Aβ for receptors on microglia and astrocytes. In the context of AD, LRP1 is a major receptor for APOE, a protein that regulates cholesterol and fats. The *APOE* gene has several alleles, including *APOE2*, *APOE3*, and *APOE4*, with *APOE4* being one of the most substantial genetic risk factors for AD (Shinohara et al., 2017). Besides their role in systemic removal of Aβ, one main mechanism by microglia and astrocytes is phagocytosis, which leads to the clearance of Aβ (Ries and Sastre, 2016a). Phagocytosis facilitates either the full engulfment of Aβ into the cells or the secretion of other degradation machinery before being removed (Deng et al., 2024). In microglia and astrocytes, phagocytosis is promoted through the activation of cell surface receptors that interact with extracellular Aβ.

This includes toll-like receptors, scavenger receptors, transmembrane proteins, advanced glycation end products, lipoprotein receptors related-proteins, and proteoglycans (Kim et al., 2024; Cai et al., 2023c; Jones et al., 2013). Impaired clearance mechanisms in microglia and astrocytes have been linked to the progression of AD (Yousif Saleh et al., 2024; Li et al., 2024; Giusti et al., 2024; Gabande-Rodriguez et al., 2020; Wildsmith et al., 2013). For example, the triggering receptor expressed on myeloid cells 2 (TREM2) is predominantly expressed in microglia but also in astrocytes. Dysfunction of TREM2 prevents the phagocytosis of Aβ by microglia and astrocytes, and increases neuronal damage (Huang et al., 2023). It has been described that loss-of-function gene variants in TREM2 are another associated risk factor for AD (Kiianitsa et al., 2024). Therefore, understanding the cellular-mediated uptake of Aβ is crucial. In particular, astrocytes are the most abundant type of glial cell and account for ~40% of all cell types within the brain, and as the most common cell type, they raise questions about how they contribute to the Aβ load in both healthy and AD brains (Khakh and Sofroniew, 2015). Besides the clearance of Aβ, astrocytes also have a crucial role in several other mechanisms in the brain and other AD-related pathologies.

1.6. Astrocytes

1.6.1. The Role of Astrocytes in the Brain

During development, astrocytes are core regulators of neural networks and in the mammalian brain, neuronal circuits are formatted within the network of astrocytes (Khakh and Sofroniew, 2015). In brain development, astrocytes aid in the development and maturation of neuronal synapses (Khakh and Sofroniew, 2015). In the adult brain, astrocytes have an overall role in and are essential for maintaining homeostasis (Figure 2). They are characterised by their “star-like” morphology, defined by branching processes which interact directly with neighbouring cells and blood vessels (Zhou et al., 2019). Next, astrocytes provide structural support to neurones using branching, which makes direct contact with them (Gradisnik and Velnar, 2023). They are also key regulators of cell-to-cell signalling via the recycling and uptake of neurotransmitters such as glutamate, ATP, and GABA to support synaptic plasticity and function as part of the tripartite synapse (Purushotham and Buskila, 2023). Astrocytes regulate the expression of ions such as

calcium, potassium, and sodium and signalling pathways (Akdemir et al., 2020). Furthermore, the metabolism of nutrients such as glucose and lactate, which are primarily exported to neurones for energy use, is regulated by astrocytes (Brandebura et al., 2023). Other functions include maintenance of the BBB, formation of matrix proteins and adhesion molecules, and a role in the immune response to infections (reviewed in Gradisnik and Velnar, 2023). Finally, astrocytes have a core role in the inflammatory response (Kaur et al., 2019). Due to astrocytes having a key role in many functions in the brain, they have also been implicated in many neurodegenerative conditions, including Parkinson's Disease (PD), Amyotrophic Lateral Sclerosis (ALS), Huntington's Disease (HD), and Alzheimer's Disease (Phatnani and Maniatis, 2015).

1.6.2. The Role of Astrocytes in Alzheimer's Disease

The increased number of senescent astrocytes is seen in both ageing and AD brains (Turnquist et al., 2016; Bhat et al., 2012). The normal physiological function of astrocytes is disrupted in AD and is an established biomarker of the disease (Zheng and Wang, 2025) (Figure 2). Signalling disruption leads to either a decrease in ion/neurotransmitter uptake or recycling, leading to hyperexcitability, less synaptic function, and dysregulated communication with neurones (Monterey et al., 2021). Others have shown that there is less maintenance of the blood-brain barrier and reduced waste/toxin clearance mechanisms (Giovannoni and Quintana, 2020). As astrocytes become dysfunctional, there is reduced clearance and degradation of debris such as Aβ aggregates, leading to plaque formation (Cavieres-Lepe and Stuardo, 2021). Finally, evidence has highlighted that inflammation is a pivotal mechanism implicated in AD (Botella Lucena and Heneka, 2024; Liu et al., 2023; Tansey et al., 2022; Singh, 2022; Zhou et al., 2019).

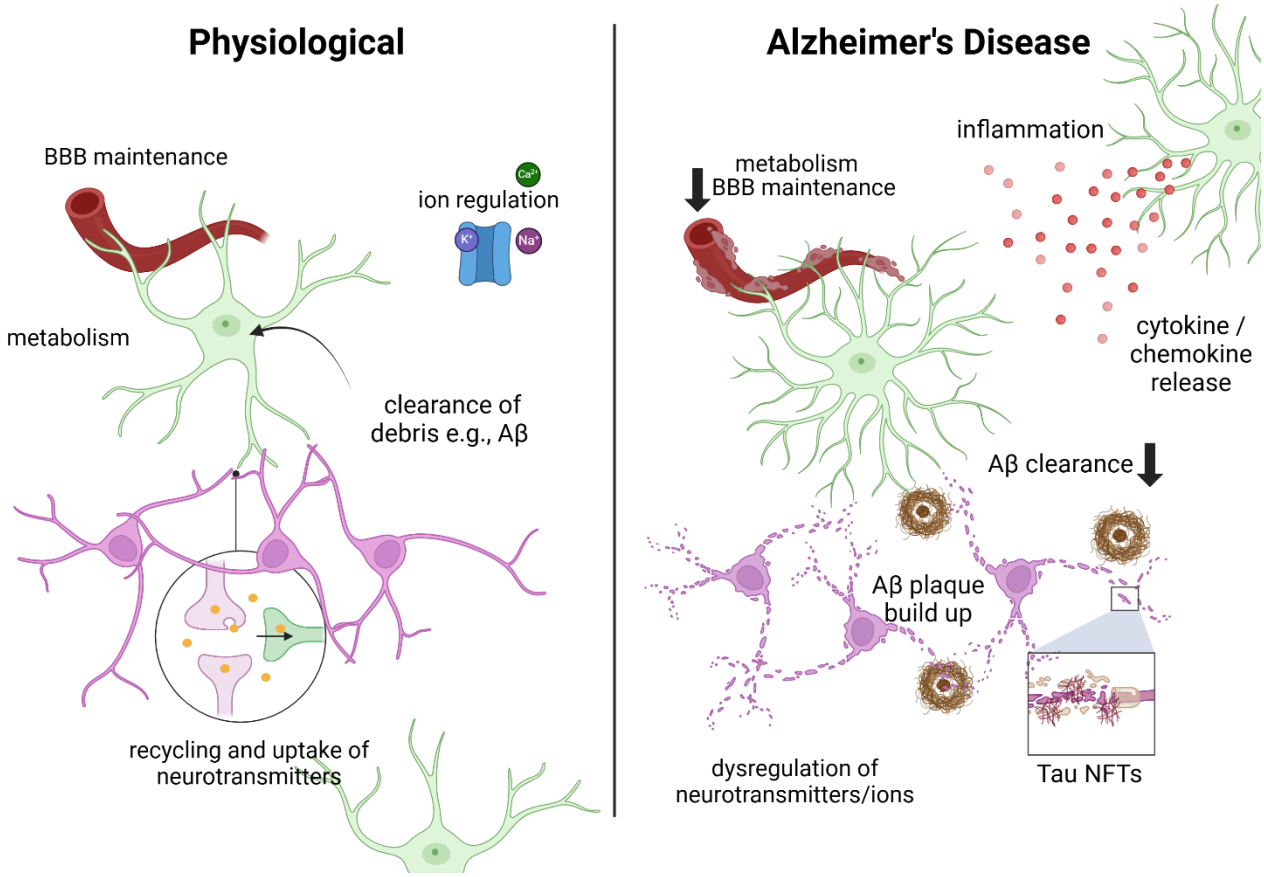

***Figure 2**. Illustrative diagram summarising the normal physiological functions of astrocyte (green) on the left. On the right, it highlights how they are affected by, or aid neuronal (pink) dysfunction associated to Alzheimer's Disease. Image created with BioRender.com.*

1.7. Inflammation

1.7.1. Inflammation in the CNS

In the human body, inflammation is a natural defence mechanism in the peripheral and CNS. Various stimuli, including injury, illness, and stress, activate it. The overall function of inflammation is to facilitate repair and remove pathogens, debris, and toxins as part of a protective response (Meraz-Rios et al., 2013). The inflammatory response involves several cell types, including innate immune cells, macrophages, neutrophils, T cells, and NK cells (DiSabato et al., 2016). Additionally, it encompasses non-immune cells: neurones, oligodendrocytes, microglia, and astrocytes (Costantini et al., 2018). As previously mentioned, a core function of astrocytes is their role in inflammation. Astrocytes undergo various structural, molecular, and functional changes and are referred to as reactive astrocytes (Singh, 2022). One core hallmark of reactivity in astrocytes is the change in cell morphology, which includes an increased size and elongation of the cell body (Kumar et al., 2023).

Furthermore, astrocytes' primary branches and end-feet can extend to increase their contact with neighbouring microglia and neurones (Cheng et al., 2019). It has been hypothesised that this can have a protective mechanism by forming a dense network around damaged tissue and cells (Cheng et al., 2019). Morphological changes in astrocytes are accompanied by the increased expression of core intermediate filament proteins such as GFAP and Vimentin, common markers of reactive astrocytes (Konstantinidis et al., 2023b; Smit et al., 2021). Astrocytes can induce the upregulation of anti-inflammatory cytokines and neurotrophic factors to promote cell survival, often referred to as A2 reactive astrocytes (Khodadadei et al., 2022). Cytokines and chemokines act as signaling molecules for cell-to-cell communication and activation.

On the other hand, astrocytes can produce pro-inflammatory cytokines and chemokines, which, when secreted, can activate downstream pathways associated with toxicity and death (Chen et al., 2024). These astrocytes are often referred to as A1 reactive astrocytes (Khodadadei et al., 2022). The inflammatory response is a protective mechanism and is believed to be self-limited (Zhao et al., 2021). However, during prolonged stimuli, the mechanisms of inflammation become overstimulated, resulting in chronic inflammation

(Zhang et al., 2023b). The chronic activation of astrocytes has been shown to amplify the inflammatory response by the prolonged production of chemokines, cytokines, reactive oxygen species, and nitric oxide to induce cellular death (Zhang et al., 2023b). As a result, it has been associated with a cycle of inflammation, whereby long-term activation leads to increased cytokines, exacerbating further inflammatory responses (Yuan and Ofengeim, 2024).

1.7.2. Inflammation in Alzheimer's Disease

Although different neurodegenerative diseases such as AD, PD, ALS, and HD have diverging pathogenic mechanisms, extensive evidence highlights that chronic inflammation is a hallmark of the disease (Mayne et al., 2020). In AD, earlier studies showed that individuals who took prolonged nonsteroidal anti-inflammatory drugs had up to ~50% reduction in the risk of developing AD (Kinney et al., 2018) —highlighting an important association between AD and inflammation. The occurrence of heightened chronic pro-inflammatory markers is detected in both the early and late stages of AD, highlighting their critical role in disease progression (Deng et al., 2024; Wang et al., 2023; Chai et al., 2023).

In particular, Tumor Necrosis Factor-α, Interleukin-1-β, Interleukin 6, and Monocyte chemoattractant protein-1 are closely associated with AD (Liu et al., 2023). Alongside this, astrocyte reactivity is an early biomarker of AD and, in some studies, precedes the histopathological and pathological features that can be detected in the brain (Botella Lucena and Heneka, 2024). Next, reactive astrocytes, which have pro-inflammatory markers, are closely correlated with Aβ plaques in APPswePS1dE9 mouse models of AD (Smit et al., 2021). Previously, protein deposition in the brain was believed to induce inflammation. However, the activation of astrocytes has been linked to promoting Tau hyperphosphorylation to lead to the formation of NFTs in neurones through the induction of cytokines (Chen and Yu, 2023). Furthermore, several mice studies have indicated that in addition to protein deposition of Tau, inflammation can also trigger the aggregation and deposition of Aβ, even in the earlier stages of the disease (Sosna et al., 2018; Hong et al., 2016). While studies have shown that astrocytes become reactive and adopt a pro-inflammatory phenotype, it remains incompletely understood how different Aβ isoforms and aggregates affect astrocyte inflammatory responses.

1.8. Systems for Modelling AD

Most of our knowledge about Aβ and inflammatory dysfunctions in familial and sporadic AD has been derived from post-mortem studies, allowing for the identification of major cellular and pathological components (Hammond et al., 2019). However, post-mortem studies only provide a snapshot of their role at the end stages of the disease, along with limited tissue availability (Drummond and Wisniewski, 2017). Next, animal models have aided the discovery of whole system mechanisms that underpin disease development, which are difficult to observe in the human brain (McKean et al., 2021). Animal models of AD utilise transgenic mice, rats, zebrafish, drosophila melanogaster, and caenorhabditis elegans (Akhtar et al., 2022). The most common animal model system for AD is transgenic mice, with more than 200 models since being created in 1995 (McKean et al., 2021). However, transgenic mice focus on the overexpression genes (e.g., Tg2576, 5xFAD, APPswe/PSEN1dE9, or 3xTg), which are based on familial mutations of AD (Yokoyama et al., 2022). Other models require the knockdown of specific genes, which disrupt pathways (Hammond et al., 2019). As a result, it is argued that they do not encompass sporadic AD, which accounts for ~95 % of cases. Modelling sporadic AD in complex, this is attributed by the multifactorial mechanisms which are involved in its pathogenicity and no clear genetic link. Some studies have explored methods to model sporadic AD by combining known familial genetic factors (e.g., APP) and environmental risk factors (Gotz et al., 2018; Iqbal et al., 2013). However, though these studies have described symptoms associated with AD such as cognitive decline, it has been argued that this does not reflect sporadic disease conditions and animal models do not mimic disease progression similar to humans (Gotz et al., 2018). Finally, the lack of translational application from animals to humans in clinical trials highlights the need for both human-derived and sporadic models of AD (McKean et al., 2021; Drummond and Wisniewski, 2017). Human-derived cellular models such as induced pluripotent stem cells have begun to address this limitation.

1.8.2. induced Pluripotent Stem Cells

The introduction of induced Pluripotent Stem Cells (iPSCs) by Shinya Yamanaka and Kazutoshi Takahashi almost two decades ago has revolutionised and reshaped stem cell biology and research. iPSCs were developed through the reprogramming of adult mouse fibroblasts into embryonic-like stem cells by four specific genes: *Myc, Oct3/4, Sox2, and Klf4*, known as the Yamanaka factors (Takahashi and Yamanaka, 2006). The Yamanaka factors were found to contain transcription factors encoding the conversion of somatic cells into iPSCs (Takahashi and Yamanaka, 2006). The following year, adult fibroblasts were used to generate human-derived iPSCs (hiPSCs) using the same reprogramming method (Takahashi et al., 2007). In the same year, another reprogramming method with lentivirus used four factors: *OCT4, SOX2, NANOG, and LIN28* to generate undifferentiated embryonic-like stem cells (Yu et al., 2007). These major breakthroughs have allowed for the development and expansion of cell culture research to model human disease mechanisms and progression.

By using donor fibroblast, blood mononuclear cells and epithelial cells, iPSCs have been generated into neural cells from individuals with AD both familial and sporadic AD (McKinney, 2017; Drummond and Wisniewski, 2017). iPSCs have enabled novel drug discovery through screening, evaluating drug toxicity, and developing regenerative/personalised medicine (Shi et al., 2017). By bridging the gap between preclinical and clinical studies, iPSCs have aided in overcoming limitations which animal model studies pose, such as ethical concerns and lack of resemblance to human disease states (Omole and Fakoya, 2018). Human-derived iPSC cellular models reveal phenotypes that are not manifested in animal models and are an important tool for complementing animal studies (Cerneckis et al., 2024). This has been particularly important in the production and differentiation of iPSCs to model neurodegenerative conditions such as Alzheimer's Disease. Due to the inaccessibility of harvesting human adult stem cells located in the brain, the *in vitro* generation of neural stem/progenitor cells to create brain cell types affected in AD is pivotal.

iPSC technologies offer the ability to make neuronal and glial cell types from somatic cells with self-renewal and multiple lineage differentiation potentials (reviewed in Cerneckis et al., 2024). However, studies have shown that cellular models can exhibit genetic instability such as DNA damage, chromosomal abnormalities and nucleotide variants (Vaz et al., 2021).

These events were primarily associated with iPSCs compared to embryonic stem cells, highlighting the link between iPSCs and tumorigenicity (Zhong et al., 2022; Romanazzo et al., 2020). One practical limitation of iPSC-derived cellular models is the high cost and time-intensive protocols, which make them less practical for large-scale studies. To overcome some of these limitations, this thesis employs a direct reprogramming approach to generate astrocytes (iAstrocytes) from induced Neuronal Progenitor Cells.

1.8.3. induced Neuronal Progenitor Cells

This cellular model involves the direct conversion of fibroblasts to iAstrocytes via induced Neuronal Progenitor Cells, which bypasses the intermediate pluripotent cell state or clonal isolation during somatic cell conversion (Figure 3). In this model, iNPCs to iAstrocytes is a 7-day differentiation protocol, making it a more time-efficient and faster method of producing human-derived astrocytes. For example, a 7-day differentiation protocol compared to 28- or 180-day protocols used during non-direct methods (Zhang et al., 2019; Krencik et al., 2011). Next, astrocytes derived by the same protocol used in this thesis exhibit disease-related toxic phenotypes in other neurodegenerative diseases such as Amyotrophic Lateral Sclerosis and Parkinson's Disease (Au et al., 2024; Schwartzentruber et al., 2020; Ferraiuolo et al., 2016; Meyer et al., 2014). Thus, highlighting the importance of utilising this model as a tool for investigating disease-related phenotypes and toxicity associated with AD. A key study demonstrated that directly converted astrocytes retain the ageing features of the donor fibroblasts (Gatto et al., 2021). Astrocytes exhibited DNA damage and oxidative stress, core cellular hallmarks of human ageing (Lemoine, 2021; Gatto et al., 2021). The retaining age-relate phenotype in astrocytes is important as AD incidence increases with age and is a key risk factor for developing the disease (Liu et al., 2024b). Therefore, the retention of the age phenotype is a unique and valuable aspect of the model.

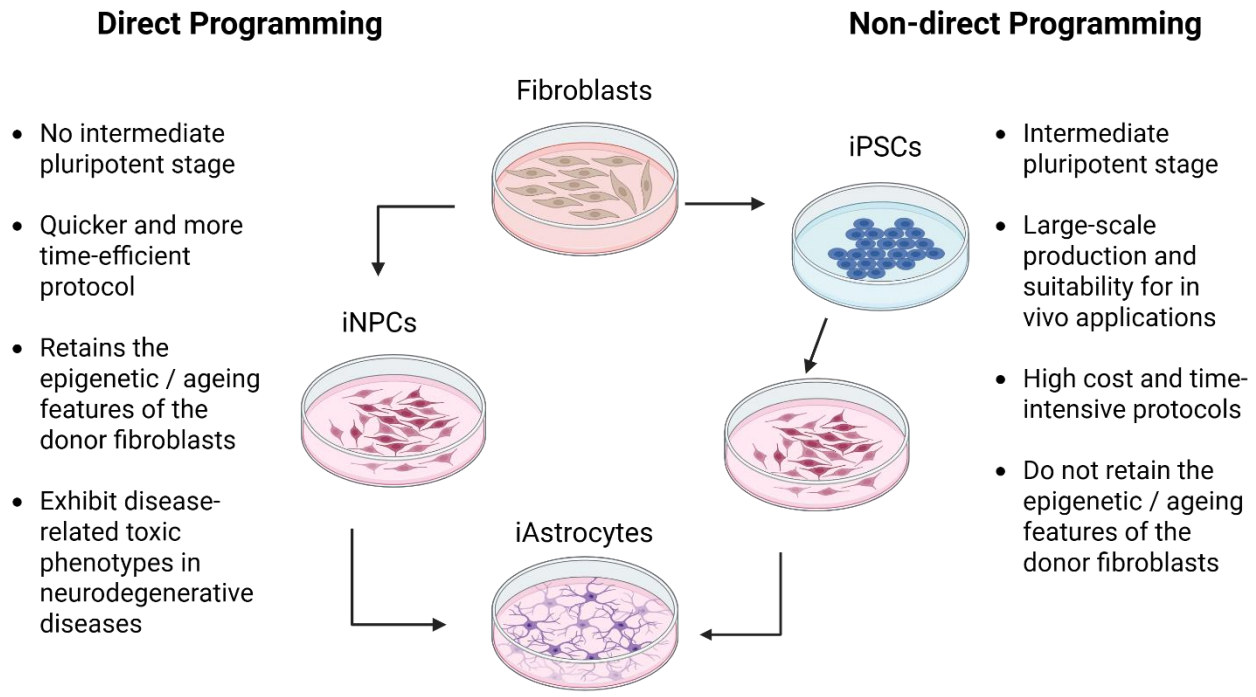

Figure 3. A schematic summarising direct reprogramming to non-direct reprogramming. *In direct programming fibroblasts are directly converted into induced Neuronal Progenitor Cells (iNPCs) then iAstrocytes (left). In non-direct reprogramming, fibroblasts are converted to induced Pluripotent Stem Cells (iPSCs) before being converted to iNPCs and iAstrocytes (right). Image created with BioRender.com.*

1.9. Rational of this Project

AD is characterised by the accumulation of Aβ plaques in the brain. The two most common isoforms of Aβ, Aβ40 and Aβ42, differ in their aggregation properties and roles in disease progression. In a healthy brain, Aβ40 is 10 - 20 times more abundant than Aβ42. However, in AD, plaques are primarily composed of Aβ42. This preferential deposition is attributed to a faster aggregation rate of Aβ42 and an increased tendency to form deposits. However, the overall burden of Aβ plaques in the brain does not correlate well with either disease severity or progression. This suggests that factors beyond total plaque accumulation - such as intermediate aggregates formed during the deposition process, inflammatory responses triggered by aggregates, and cellular dysfunction - may play a more significant role in driving neurodegeneration in AD. In this regard, impaired clearance is a key factor contributing to Aβ aggregation and toxicity. In a healthy brain, Aβ production, aggregation, and removal are tightly regulated to maintain balance. In AD, this balance is disrupted, leading to excessive Aβ accumulation and plaque formation. Astrocytes, the most abundant cell type in the human brain, play a crucial role in clearing Aβ.

In post-mortem AD brain tissue, reactive astrocytes are often found surrounding Aβ plaques, correlating with areas of increased inflammation. However, the precise relationship between Aβ deposition, the interactions between Aβ40 and Aβ42, astrocyte-mediated uptake, clearance, and neuroinflammation remains poorly understood. This project aims to systematically investigate these pathways by examining how astrocytes uptake Aβ species and how different species influence inflammation. Inflammation may alter Aβ uptake, potentially creating a feedback loop that exacerbates disease progression. A key question is whether specific Aβ isoforms or aggregation states contribute to pathological changes in astrocyte function, leading to impaired clearance and increased neurotoxicity. Additionally, this project will explore whether these processes differ between patient-derived astrocytes and those from healthy controls, providing insight into how astrocyte dysfunction contributes to AD pathology. By elucidating these processes, this project aims to gain critical insights into the interplay between Aβ aggregation, astrocyte function, and neuroinflammation in AD. Understanding these mechanisms could pave the way for novel therapeutic strategies targeting astrocyte-mediated uptake and neuroinflammatory responses to mitigate disease progression.

1.10. Project Hypothesis

Distinct species arising during Aβ aggregation and deposition possess unique functionalities, exhibit varying rates of uptake by astrocytes, and are associated with specific downstream inflammatory pathways.

1.11. Aims and Objectives

1.11.1. Project Aim:

Using directly converted iAstrocytes from both healthy and AD individuals, this project aimed to gain an understanding of the complex interplay between astrocytes and Aβ aggregates during uptake and inflammation.

1.11.2. Overall Objectives

- Characterise the direct differentiation of astrocytes from iNPCs in control and AD patient lines and characterise them.
- Establish a system to mimic Aβ aggregate uptake by astrocytes, including in vitro Aβ aggregate preparation, characterisation of their identity using single-aggregate imaging, and quantification of iAstrocyte-induced uptake.
- Quantify the uptake of Aβ in iAstrocytes, comparing Aβ40 and Aβ42 isoforms and ratios, as well as oligomeric and fibrillar forms, to evaluate potential differences in uptake efficiency.
- Measure the secretion and differences of pro-inflammatory markers, TNF-α, IL-1β, IL6, and MCP1 after treatment with Aβ aggregates of varying species and ratios in control and AD lines.
- Determine whether chronic cytokine exposure differentially affects Aβ uptake in iAstrocytes, evaluating if AD-derived iAstrocytes are more vulnerable to prolonged inflammatory conditions.

Chapter 2. Materials and Methods

2.1. Materials

2.1.1. Tissue Culture Media Constituents

Table 1. induced Neuronal Progenitor Cell (iNPC) Media Constituents. *Supplements, concentration/volume, source; supplier and lot number are shown.*

iNPC Media	Concentration/Volume	Supplier	Lot Number
DMEM| (F-12 (1:1) 1X) + GlutaMax	500 mL	Thermofisher	2581976
Human FGF-basic	40 ng/mL	PreproTECH (154 a.a)	102208
B-27 Supplement	5 mL per 500 mL (1% v/v)	Gibco	2389227
N-2 Supplement	5 mL per 500 mL (1% v/v)	Gibco	2372205

Table 2. iAstrocyte Media Constituents. *Supplements, concentration/volume, source; supplier and lot number are shown.*

iAstrocyte Media	Concentration/Volume	Supplier	Lot Number
Dulbecco's Modified Eagles Medium - High Glucose	500 mL	Sigma-Aldrich	RNBE7920
N-2 Supplement	1 mL per 500 mL (0.2% v/v)	Gibco	2372205
Penicillin Streptomycin Solution	50 U/mL	Corning	30001143
Foetal Bovine Solution - Heat Inactivated (BR)	50 mL in 500 mL (10% v/v)	LSP - Life Science Production	A41220HI

2.1.2. Immunocytochemistry Constituents

Table 3. Primary Antibodies used for Immunocytochemistry. *Antibody specificity, dilution (in 0.2% TritonTM (v/v) + 5% (v/v) horse serum/PBS), source; supplier and lot number, and species are shown.*

Antibody Used	Dilution	Supplier	Lot Number	Species
CD44	1:300	abcam	1024529-2	Rabbit
Vimentin	1:1000	antibodies.com	34196	Chicken
EAAT2	1:200	Abcam	AB41621	Rabbit
GFAP	1:200	Dako	Z0334	Rabbit
Nestin	1:200	Abcam	AB18102	Mouse
PAX6	1:200	Abcam	AB5790	Rabbit
LRP1	1:100	Abcam	EPR3724	Rabbit
TREM2	15 μg/mL	Bio-techne	MAB17291	Rabbit
CD10	1:500	Santa Cruz	sc-46656	Mouse

Table 4. Secondary Antibodies for Immunocytochemistry. *Antibody specificity, dilution (in 5% (v/v) horse serum/PBS), source; supplier and lot number are shown.*

Antibody Used	Dilution	Supplier	Lot Number
Alexa Fluor 568 goat anti-rabbit	1:1000	invitrogen	2379475
Alexa Fluor 647 goat anti-chicken	1:1000	invitrogen	23335730
Alexa Fluor 647 anti- β-Amyloid, 1-16 Mouse IgG1 6E10	0.5 mg/mL	Biolegend	B335859
Phalloidin-iFluor 488	1:1000	Abcam	AB176753 / 1034827-11
Alexa Fluor 488 goat anti-rabbit	1:1000	invitrogen	2551357
Hoechst 33342	1:5000	ThermoFisher	H1399
Alexa Fluor™ 488 goat anti-mouse	1:1000	Invitrogen	A-11008

Table 5. Constituents for Immunocytochemistry. *Constituents specificity, volume/concentration (v/v), source; supplier and lot number are shown.*

Immunocytochemistry Constituents	Volume/Concentration	Supplier	Lot Number
Phosphate Buffer (PBS) Solution			
Formaldehyde Solution	3.7% Formaldehyde Solution (stock: 37%) in PBS Solution	Fisher Scientific	2108424
Tween 20 Solution	0.2% in PBS Solution	Sigma-Aldrich	102493757
Triton X-100 Solution	0.2% in PBS Solution	Sigma-Aldrich	SLBM1396V
Antibody Buffer	5% horse serum and PBS	Horse Serum: Gibco™	Horse Serum: 16050122
Blocking Solution	5% horse serum, 0.2% Triton x-100 and PBS	Horse Serum: Gibco™	Horse Serum: 16050122

2.1.3. Single Molecule Pull Down Constituents

Table 6. Single Molecule Pull Down (SiMPull) Constituents*. Constituents specificity, concentration, source; supplier and lot number are shown.*

SiMPull Constituents	Concentration	Supplier	Lot Number
Potassium Hydroxide Solution (KOH)	1M in deionised water	Sigma-Aldrich	MB1977533138
3-Amonopropyltriethoxysilane (APTES): Acetic acid: Methanol Solution	Ratio; 1.5: 2.5: 50	APTES: thermo scientific Acetic Acid: sigma-aldrich Methanol: sigma-aldrich	APTES: XE351454 Acetic Acid: 2211009 Methanol: STBL0420
mPEG-SVA (methoxy PEG-succinimidyl valerate)	110 mg/mL in deionised water	174-130	Layson bio Inc
Biotin-PEG-Succinimidyl Valerate (Biotin-PEG-SVA)	100 mg/mL in deionised water	173-182	Layson bio Inc
mPEG-NHS and Biotin-PEG solution	Ratio; 99: 1	-	-
MS(peg)4 Methyl-PEG4-NHS	10 mg/mL in deionised water	Thermo Scientific	WK336766

Sodium bicarbonate, ACS reagent Solution (NaHCO3)	Molecular weight: 84 per mL	Thermo Scientific	A0435015
PBST (Tween20 and PBS) Solution	PBS and 0.05% Tween20	-	-
NeutrAvidin Solution	0.2 mg/mL in PBST	Thermo Scientific	wb318432
PBS-Bovine Serum Albumin (BSA) Solution	0.1 mg/mL BSA in PBS	Thermo scientific	01330548

Table 7. Antibodies for Single Molecule Pull Down and Co-aggregation Imaging. *Antibody specificity, concentration (diluted in 0.1mg/mL (v/v) BSA/PBS), source; supplier and lot number.*

Antibody Used	Concentration	Supplier	Lot Number:
Biotin (azide-free) anti-β-Amyloid, 1-16 6E10	1 mg/mL	Biolegend	B336279
Alexa Fluor 647 anti- β-Amyloid, 1-16 Mouse IgG1 6E10	0.5 mg/mL	Biolegend	B335859
Beta-Amyloid (1-40), HiLyte™ Fluor 488-labeled	0.1 mg/mL	AnaSpec	AS-60491-01
Beta-Amyloid (1-42), HiLyte™ Fluor 647-labeled	0.1 mg/mL	AnaSpec	AS-64161

2.2. Methods

2.2.1. Ethics Statement

All work carried out in this thesis was in accordance with the University of Sheffield policy on good research and innovation practice: https://www.sheffield.ac.uk/rpi/ethics-integrity/policy. Fibroblast collection and differentiation were carried out in accordance with the Yorkshire and Humber Research and Ethics Committee (Reference code: 16/YH/0155).

2.2.2. Summary of Experimental Design for Thesis

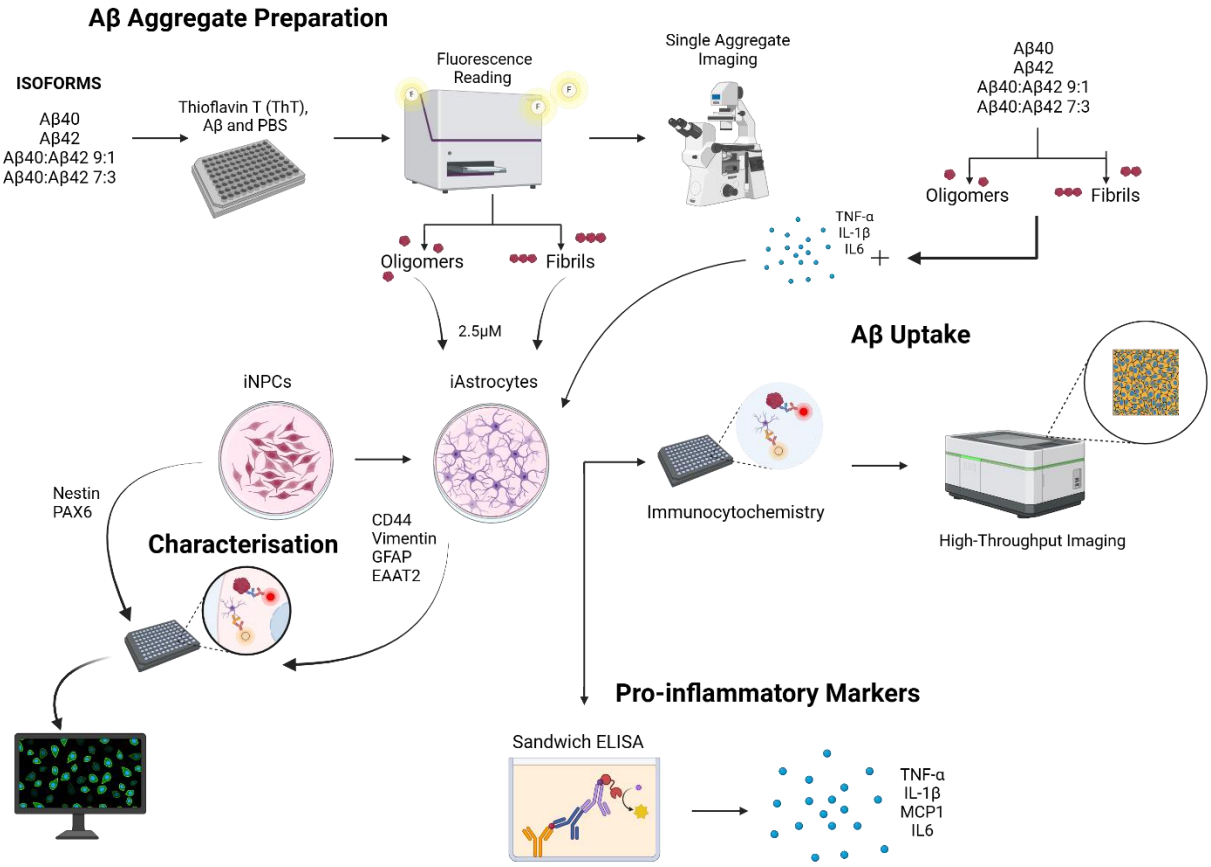

Figure 4. *Summary of experimental design for thesis. Image created with BioRender.com.*

2.2.3. Reprogramming of human-derived fibroblasts to iAstrocytes

2.2.3.1 Cell Line Demographics

For this project, fibroblasts from individuals with sporadic Alzheimer's Disease (AD) and matched controls (Section 2.2.3.1, Table 8) were obtained from biopsy as part of the MODEL-AD study (Yorkshire and Humber Research and Ethics Committee number: 16/YH/0155) (Bell et al., 2024). For the sporadic group, a diagnosis of Alzheimer's was made based on clinical guidelines set by the National Institute on Aging and the Alzheimer's Association (McKhann et al., 2011). At the time of sampling, information on Mini-Mental State Examination (MMSE), years in education, and AD treatment was provided (Bell et al., 2024).

Table 8. Cell Line Demographics. *Cell line, Diagnosis, Gender, and Age are shown.*

Cell Line	Gender	Age
Control (1)	F	100
Control (2)	M	56
Control (3)	F	72
AD (1)	F	77
AD (2)	M	59
AD (3)	F	62

Control lines: mean age = 76, Std. Deviation = 22.27.

AD lines: mean age = 66, Std. Deviation = 9.644.

2.2.3.2. General Tissue Culture

All tissue culture work was carried out in an Airstream® Gen 3 Class II BSC- G hood and cells were kept in a PHCbi Cell Culture Incubator at 37˚C, 5% CO2. Before thawing, culturing, and experimental plating 10cm dishes (Thermo Scientific) and 96-well plates (Phenoplate, PerkinElmer) were coated in hFibronectin (R&D Systems, Lot: MQC2723041) at a dilution (Table 9) in 5 mL PBS for at least 30 min. Fibroblasts were cultured using established protocols (Bell et al., 2018; Allen et al., 2014), and generated by Dr Simon Bell at The Sheffield Institute for Translational Neuroscience. In this project, cells were obtained and maintained at the induced Neuronal Progenitor Cell (iNPCs) level before reprogramming into iAstrocytes. iNPCs were differentiated into iAstrocytes as previously described by (Gatto et al., 2021; Meyer et al., 2014).

Table 9. Cell Lines and Fibronectin Dilution Factor. *Control and AD iNPCs and iAstrocytes fibronectin dilution factor (40 ng (w/v) in 0.1% bovine serum albumin (BSA).*

Cell Line	Fibronectin Dilution
iNPC Control 1	1:400
iNPC Control 2	1:400
iNPC Control 3	1:400
iNPC Sporadic 1	1:200
iNPC Sporadic 2	1:400
iNPC Sporadic 3	1:200
iAstrocyte Control 1	1:800
iAstrocyte Control 2	1:800
iAstrocyte Control 3	1:800
iAstrocyte Sporadic 1	1:400
iAstrocyte Sporadic 2	1:400
iAstrocyte Sporadic 3	1:400

2.2.4. Reprogramming of human-derived fibroblasts to iAstrocytes

2.2.4.1 Thawing induced Neuronal Progenitor Cells

All the cell lines were thawed from -80°C into 10cm dishes with 10mL iNPC media (DMEM| GlutaMax supplemented with 1% (v/v) N2, 1% (v/v) B27, and 40 ng/mL FGF-b; Section 2.1.1, Table 1) and placed into incubation overnight. The following day the iNPC media is changed to remove the DMSO from the freezing down process as described in section 2.2.4.3.

2.2.4.2 Culturing of induced Neuronal Progenitor Cells

iNPCs were maintained in iNPC media, and culture media was changed every 2 days and cells were split every 3-4 days dependent on the confluency (~90%) of the dish. To split the iNPCs, culture media was removed from the dish and adhered cells were lifted using 1 mL accutase (Sigma-Aldrich, #A6964-500mL) for 4 min at 37°C. The cells were then re-suspended with iNPC media to quench the accutase before being centrifuged (Eppendorf 5804) at 200RPM for 4 min at room temperature (RT). The supernatant was discarded and the cells were resuspended and re-plated in a suitable ratio to encourage recovery into 10 mL fresh iNPC media.

2.2.4.3 Cryopreservation of induced Neuronal Progenitor Cells

At confluency, the iNPCs were lifted as previously described in section 2.2.4.2. Cells were cryopreserved in 1 mL freezing medium (iNPC media supplemented with 10% (v/v) Dimethyl Sulfoxide (DMSO; Sigma Life Science, Lot: RNBK9369). For storage, 1 mL of cell resuspension were added to cryopure vials (sarstedt, Inc.) before being placed into a CoolCell™ Cell Freezing Container (Biocision) and stored at -80°C overnight. For long term storage, cells are kept in liquid nitrogen dewars.

2.2.5. Differentiation of induced Neuronal Progenitor Cells into iAstrocytes

The iNPCs were seeded in iAstrocyte media (DMEM – high glucose supplemented with 10% (v/v) FBS, 50 U/mL PenStrep, 0.2% (v/v) N2 in a 7-day differentiation protocol (Figure 5). Cells were cultured for four days in this media before removing and adding fresh iAstrocyte media. On day five, cells were lifted and split for experimental plating. To split iAstrocytes, cells were washed twice with PBS and lifted using accutase for 4 min at 37°C. The cells were then resuspended in iAstrocyte media before being centrifuged at 200RPM for 4 min at RT. The supernatant was discarded, and the cells were then resuspended and re-plated in a 1:2 split into 10 mL fresh iAstrocyte media.

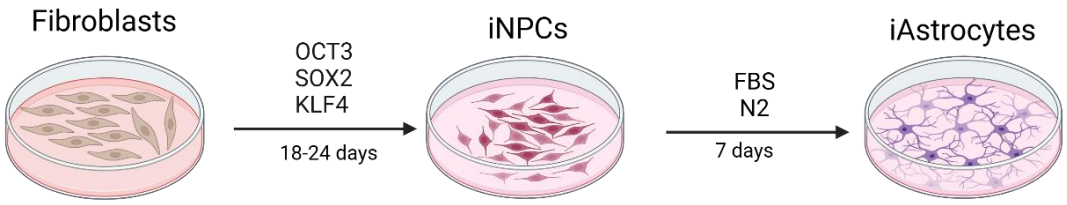

Figure 5. Key stages of reprogramming fibroblasts to iAstrocytes. *Fibroblasts from donors obtained via skin biopsy before being reprogrammed into induced Neuronal Progenitor Cells (iNPCs) in an 18-24-day protocol. iNPCs are then differentiated into iAstrocytes in a 7-day protocol. Reprogramming factors for iNPCs (OCT3, SOX2, and KLF4) are highlighted.*

2.2.6. Immunocytochemistry

Cells were seeded in black 96-well plates (Phenoplate, PerkinElmer) at a density of 4500 cells/well in 200 µl culture medium. After 24 hours, iNPCs were fixed with paraformaldehyde (3.7% (v/v) PFA/PBS) for 10 min. On day 7 of differentiation (Figure 5), iAstrocytes were fixed with PFA for 10 min. Cells were washed 3 times with PBS. Cells were permeabilised and blocked using 0.2 % Triton™ X-100 and 5% horse serum (+PBS) for 1 hour at RT. Primary antibodies (Section 2.1.2, table 3) diluted in antibody buffer (5% horse serum and PBS; Section 2.1.2, table 5) were incubated overnight at 4°C. There was no wash step in between blocking and primary antibody incubation. Cells were washed in 0.2% Tween^{20} in PBS for 5 min once, and twice with PBS for 5 min. Secondary antibodies (Section 2.1.2, table 4) diluted in antibody buffer were incubated for 1 hour at RT in the dark. Hoechst (10 mg/mL in PBS) was used to visualise nuclei for 5 min at RT in the dark. Cells were washed in 0.2% Tween^{20} in PBS for 5 min once, and twice with PBS for 5 min. Cells were then ready to image on the Opera Phenix high content imaging system (Perkin Elmer). For long term storage, 96-well plates were sealed with parafilm at kept 4˚C.

2.2.7. Thioflavin T Stock Preparation

Thioflavin T (ThT; AAT Bioquest, CAS 2390-54-7, #098033) was dissolved in DMSO. Dissolved ThT was diluted in PBS. The working concentration of ThT was calculated using the NanoDrop spectrophotometer using the equation below.

To calculate mM of ThT:

$$A = \in . \mathrm{C} . I$$

A = Absorbance (412 nm)

$\in$ = Molar Extinction Coefficient (36,000 $M^{-1}cm^{-1}$)

C = Concentration

I =Path Length (nanodrop 1 cm)

The absorbance (A) was determined by the average of 3 repeated absorbance measurements. Between each measurement, PBS was used as zero blanking solution to ensure accuracy of the absorbance reading and remove background noise. The ThT (796 μM) stock was then stored at -80°C.

2.2.8. Amyloid-β Stock Preparation

Aβ40 (1 mg, LOT #07062240NH) and Aβ42 (1 mg, LOT #07092142H) were resuspended in 1% NH_4OH (1 mg/mL) and diluted in 0.2 μM filtered PBS to a concentration of 200 μM per 50 μl in Protein LoBind tubes (Lot: M2123901). Stocks were snap frozen in liquid nitrogen and stored at -80 °C for long term storage.

2.2.9. Amyloid-β Aggregate Preparation and Treatment

For Aβ treatment to iAstrocytes, distinct populations of aggregate isoforms were generated *in vitro*; Oligomers (Aβ40, Aβ42, Aβ40: Aβ42 (9:1), Aβ40: Aβ42 (7:3)), and Fibrils (Aβ40, Aβ42, Aβ40: Aβ42 (9:1), Aβ40: Aβ42 (7:3)). Monomeric Aβ40, Aβ42, and their mixtures (50 μM) were added to a Corning Assay 96-well Plate (Non-binding surface, #00522028) diluted

in PBS. The assay plate was sealed with nunc aluminium tape (LNNI182F) and placed in the plate reader (CLARIO starplus, BMG LABTECH) at 37°C. In order to obtain different aggregate species (see table 10), Aβ40 and Aβ42 proteins were taken at different timepoints based on *in vitro* ThT kinetics (Soto and Pritzkow, 2018; Xue et al., 2017). To further confirm isoforms, aggregate species were taken for further analysis using Total Internal Reflection Fluorescent (TIRF) microscopy (2.2.13.). On day 7 of differentiation, iAstrocytes were treated with Aβ isoforms (2.5 μM) for 1 hour before being fixed for immunocytochemistry as previously described in section 2.2.6. For measurement of cytokine and chemokine release (section 2.2.10) post Aβ treatment culture medium was collected from each well, centrifuged at 1000 RPM, and snap frozen in liquid nitrogen. For long term storage, samples were kept at -80°C.

Table 10. Amyloid-β Aggregates*. Isoforms, Aggregate Species, and Time Point.*

Isoforms	Aggregate Species	Time Point
10:0 (Aβ40: Aβ42)	Oligomers	6 hours 30 min
10:0 (Aβ40: Aβ42)	Fibrils	30 hours
9:1 (Aβ40: Aβ42)	Oligomers	4 hours
9:1 (Aβ40: Aβ42)	Fibrils	20 hours
7:3 (Aβ40: Aβ42)	Oligomers	1 hour 30 min
7:3 (Aβ40: Aβ42)	Fibrils	10 hours
0:10 (Aβ40: Aβ42)	Oligomers	30 min
0:10 (Aβ40: Aβ42)	Fibrils	4 hours

2.2.10. Cytokine and Chemokine Release post Amyloid-β Treatment Assay

After treatment with Aβ aggregates, iAstrocyte media was collected and then centrifuged (1000 RPM; Sorvall Micro 17R) and snap frozen in liquid nitrogen and stored at -80°C (Figure 6). MCP-1, IL-1β, IL6, and TNF-α from the cell culture media were measured using the Duoset® enzyme-linked immunosorbent assay (ELISA Cat. No DY279, DY201, DY206, DY210) development system (R&D Systems, Abingdon, UK), according to the manufacturer's instructions. Measurements were taken on the Clariostar plate reader. The ELISA for the

cytokine and chemokine release were carried out in a blind manner at the Dementia Research Institute at The University of Cambridge.

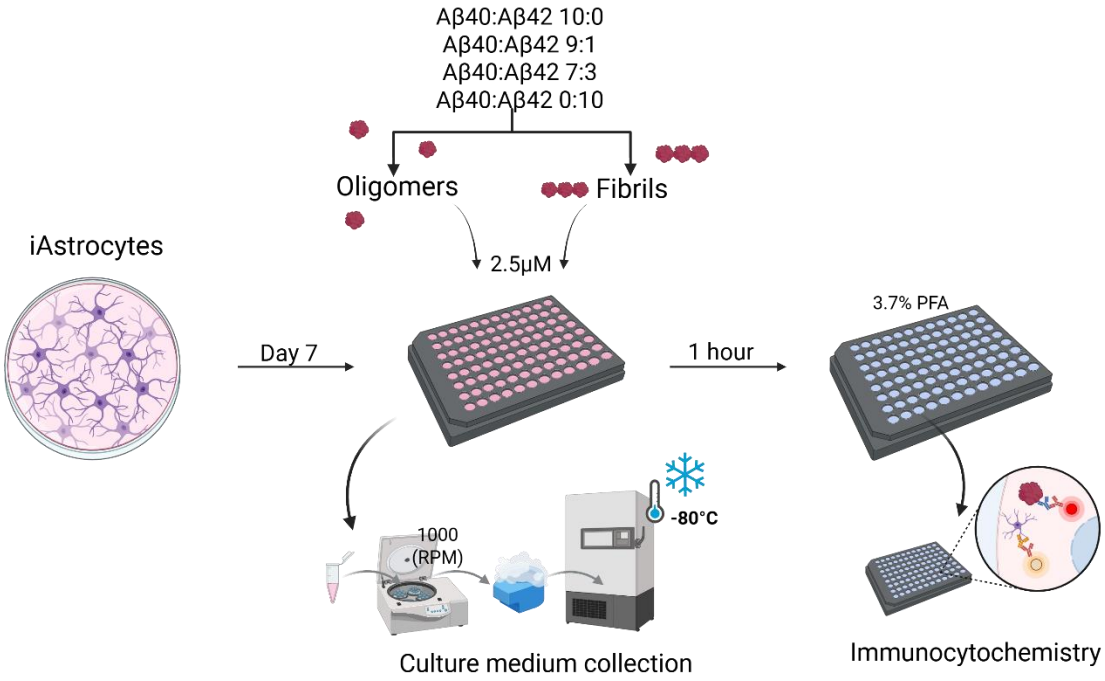

Figure 6. Schematic showing Aβ treatment assay. *On day 7 of differentiation, iAstrocytes were treated for 1 hour with Aβ (2.5 μM) isoforms. The culture medium was collected, centrifuged (1000 RPM), and snap frozen in liquid nitrogen before being stored at -80°C. The 96-well plates were fixed with 3.7 % PFA for immunocytochemistry.*

μ2.2.11. Cytokine Exposure Assay

On day 5 of differentiation, iAstrocytes were plated into 96-well plates and left for 24 hours to allow adhesion to the plate. On day 6, iAstrocytes were treated with Recombinant human TNF-αlpha (Animal-Free Recombinant Protein, PeproTech catalogue # AF-300-01A-50UG), IL-1β, and IL6 at a low dose (10 ng/mL) + PBS or high dose (100 ng/mL) + PBS for 24 hours. On day 7, iAstrocytes were treated with cytokines with Aβ present in the mixture (as described in section 2.2.9).

2.2.12. Total Internal Reflection Fluorescent Microscopy

For Total Internal Reflection Fluorescent Microscopy (TIRF), a Nikon Eclipse Ti2 microscope equipped with a Nikon PRIME 95B sCMOS camera was used. Micro-manager (version 2.0.120220224) was used to set up acquisition, 50 stacks at 50ms exposure time. ImageJ Fiji was used to visualise and present the images.

2.2.13. Labelled Amyloid-β for Co-aggregate Single Molecule Imaging

Fluorescently labelled peptides alongside unlabelled proteins were used to visualise the aggregates formed at the co-aggregation of Aβ40 and Aβ42. HiLyte 647-labelled Aβ42 and HiLyte 488-labelled Aβ40 were used at a 5% labelling ratio, with the remaining 95% unlabelled to minimise any impact of dye labelling on aggregation behaviour. For sample preparation, glass coverslips were plasma-cleaned (Diener Zepto) for 30 min to remove contaminants and improve surface adhesion. After this, coverslips were treated with poly-L-lysine for 30 min to enhance sample attachment. Excess poly-L-lysine was removed by washing the coverslips three times with PBS. Aβ40 and Aβ42 co-aggregates (1 μM) were incubated on the coated coverslips for 15 min at RT to allow attachment before imaging. TIRF microscopy was used to image the co-aggregates. The sample was illuminated using 488 nm and 647 nm excitation lasers to detect the respective fluorescently labelled Aβ species. Images were acquired in each channel separately and then merged to produce a composite image, allowing visualisation of co-aggregated species.

2.2.14. Single-molecule PullDown Imaging

2.2.14.1. Cover Slide Preparation for PEG assembly

Single-molecule Pull Down (SiMPull) methods were based on protocols previously described by Jain et al., 2012. Microscope slides were placed in a slide chamber facing the same order for the whole preparation. This was to ensure that the correct side of the cover slide was prepared equally and kept functional. Slides were sonicated in Milli-Q Water (MQ), Acetone, and Methanol, respectively, for 10 min. Next, slides were sonicated in KOH solution (Section 2.1.3, Table 6) for 20 min for etching, before being rinsed with MQ and methanol and dried with Nitrogen (N2) flow. Once dried, slides were placed in a plasma cleaner (Diener Zepto) for 30 min. Under foil, slides were sonicated in 3-Amonopropyltriethoxysilane (APTES): Acetic acid: Methanol Solution (Section 2.1.3, Table 6) for 1 min, rested for 10 min, and repeated. Sides were rinsed with methanol and MQ twice, and methanol once more before being dried with N_2 flow for PEG assembly.

2.2.14.2. Cover Slide PEG assembly

A CultureWell™ (Grace Bio-Labs, Lot: 1221100) chamber coverglass on the surface of the prepared cover slide before incubating mPEG-NHS and Biotin-PEG solution (Table 6) at 9 µl per well. After the mPEG-NHS and Biotin-PEG solution was made up, it was used within 10 min to ensure PEG dissolution to cover slide. At this stage, 1 µl of $NaHCO_3$ (Table 6) was added to each well to speed up the reaction. The slides were incubated overnight at 4˚C before being dried with N_2 flow. Next, slides were incubated with 9 ul MS (peg)4 Methyl-PEG4-NHS (Table 6) with 1 µl $NaHCO_3$ overnight at 4°C before being dried with N_2 flow. For long term storage, slides were placed into a vacuumed container and kept at -20˚C.

2.2.14.3. Aβ Aggregate Imaging

All buffers (PBS) were filtered to 0.1 µM to decrease impurities at the single-molecule level. Slides were left at RT for 1 hour before being added to the plasma cleaner (Diener Zepto) for 30 min. To each well, 10 µl NeutrAvidin Solution (Table 6) was added for 5 min and washed

twice with PBST (0.05 %) and once with PBST (1 %). Capture antibody (Table 7) was diluted at 10nM in PBS-BSA, and 10 μl added to each well for 5 min. The PBST (0.05 %) and PBST (1 %) wash step was then repeated. Sample was then added at 10 μl per well and incubated at RT for 1 hour. The PBST (0.05 %) and PBST (1 %) wash step was then repeated. Add to 10 μl of imaging antibody (Table 7) diluted in PBS-BSA for 30 min. Wash twice with PBST (0.05 %). An extra CultureWell™ (Grace Bio-Labs, Lot: 1221100) chamber was integrated on top of the cover slide. Once integrated, 5 μl of PBS was added to each well before being sealed with a coverslip ready for TIRF imaging.

2.3. Data Analysis

2.3.1. Image Analysis

All immunocytochemistry 96-well plates (Section 2.2.6.) and brightfield imaging were imaged on the Opera Phenix high content imaging system (Perkin Elmer; Instrument Serial Number: 1400L16100) at x40 magnification on NipKow-Confocal water objective unless stated otherwise. Image resolution (z) was set to 0.5uM with 5 z-stacks. Channels used: HOESCHT 333342 (excitation: 405, emission: 435-480), Alexa 488 (excitation: 488, emission: 500-550), Alexa 568 (excitation: 561, emission: 570-630), Alexa 647 (excitation: 640, emission: 650-760). Image analysis was performed on Harmony Engine (Acapella, Version; 5.2.2180.259).

2.3.2. Image Analysis of Immunocytochemistry Staining

Input images for building the analysis sequence were set to basic flatfield correction, and stack processing set to maximum projection to include all z-stacks. In order to locate cells, the Hoechst channel was used to mask individual nuclei which were then selected (green) or deselected (red) if touching the border of the image (Figure 7, B and C). Dependent on the primary antibody being used, the corresponding secondary antibody-channel was used to mask the cells (Figure 7, D). For CD44, PAX6, EAAT2, GFAP, LRP1, and TREM2 this was the 568 channel. The 647 channel was used to for Vimentin, Nestin, and Neprilysin. In order to distinguish between positive and negative staining, an intensity threshold was determined. To do this, each experiment consisted on a secondary antibody only control well whereby the maximum intensity was used as a threshold staining intensity. Once the threshold intensity was set, this excluded all staining below the threshold level to create a negative population of staining (Figure 7, E and F). Any cells which contained intensity above the threshold was a selected population and referred to as a positive population. (Figure 7, G and H). In order to calculate % of positive cells, the number of total selected nuclei was compared against the number of positively selected nuclei. The analysis blocks also allowed for information on cell region areas and wavelength intensities. This analysis was used for % cells, intensity of wavelength, and area of cell region.

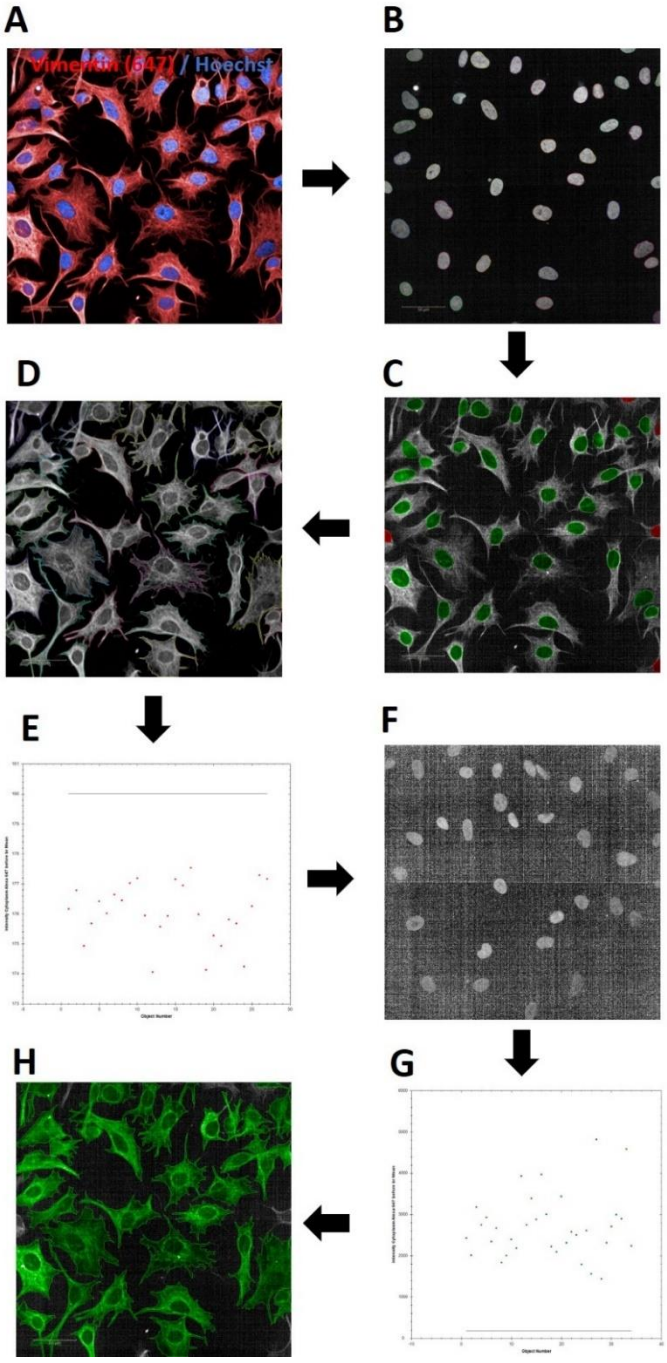

***Figure 7**. **Image analysis of immunocytochemistry staining. A.** Input image for analysis: Vimentin (647) and Hoechst (blue). Example image shows Control 1 cell line Vimentin staining. **B.** Cell nuclei were identified by masking individual nuclei using the Hoechst channel. **C.** Nuclei selected (green) or deselected (red) based on proximity to the image border. **D.** Dependent on the primary antibody being used, the corresponding secondary antibody-channel was used to mask the cells. **E / F.** Negative staining populations were distinguished by setting an intensity threshold, and staining intensities below this threshold were excluded. **G / H.** Cells with intensity above the threshold were classified as positive. Scale bar: 50 μM.*

2.3.3. Image Analysis of Counting Amyloid-β Spots

Firstly, cells were masked by using the method described in section 2.3.2. Next, a smoothing filter (Gaussian) over the 647 channel (6E10) was used, as a preparatory step to reduce noise and background by maximising 647-object intensity to mask spots (Figure 8, G). The find spots command was then used to detect all 647-spots within the cell region (Figure 8, H). To distinguish between positive and negative staining, an intensity threshold was determined. (Figure 8, I). To do this, the maximum intensity of the no treatment Aβ condition was used to set the threshold intensity. Any spots above the threshold were a selected population and referred to as a positive population for analysis (Figure 8, J). The analysis sequencing enabled the quantification of the total number of spots per well. The analysis blocks also allowed for information on cell region areas and wavelength intensities. This analysis was used for intensity of the wavelength (568) and the area of cell region.

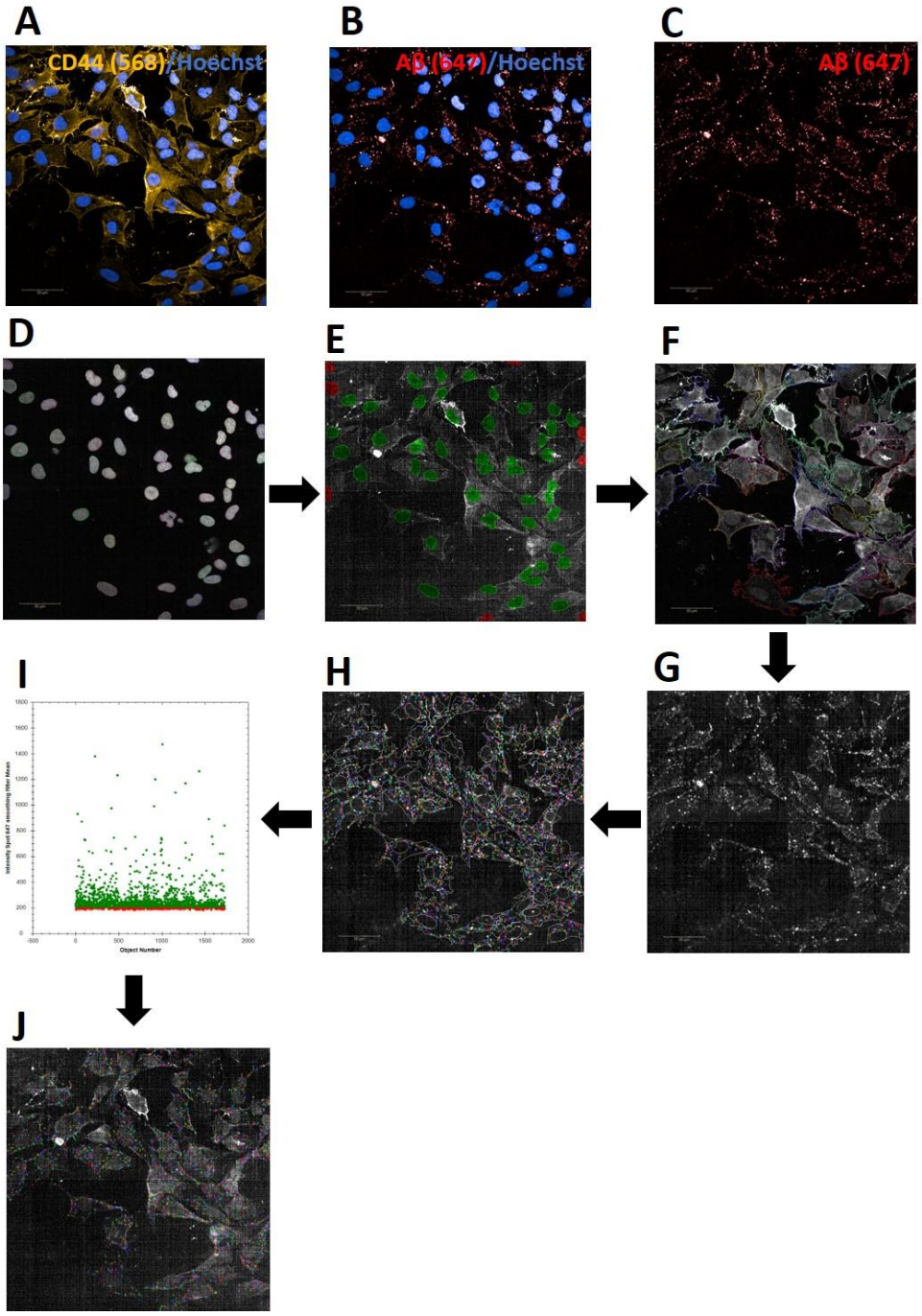

Figure 8. ***Image Analysis of Counting Amyloid- β Spots. A / B / C.*** *Input images for analysis; A. CD44 (568; yellow) and Hoechst (blue), B. Aβ (647; red) and Hoechst (blue), and C. Aβ (647; red).* ***D.*** *Cell nuclei were identified by masking individual nuclei using the Hoechst channel.* ***E.*** *Nuclei selected (green) or deselected (red) based on proximity to the image border.* ***F.*** *Cells were masked using the 568 channel.* ***G.*** *Smoothing filter (gaussian) over the 647 channel to mask spots* ***H.*** *The find spots command was then used to detect all 647-spots within the cell region.* ***I.*** *Negative staining populations were distinguished by setting an intensity threshold, and staining intensities below this threshold were excluded.* ***J.*** *Any spots above the threshold was a selected population and referred to as a positive population for analysis. Scale bar: 50 μM.*

2.4. Statistical Analysis

All experiments had three biological repeats per line, repeated into 3 technical repeats unless stated otherwise. A technical repeat was classified as a repeated condition within the same experimental plate and cell line split. After each cell line split into a different passage and differentiation, assays were repeated and this was classed as a biological repeat. Cell lines were split into separate analyses and the data compared the following groups; Control, AD, Control vs AD. Statistical analysis was completed on GraphPad Prism (10.4.1). All bar charts showed the mean ± SD. A Shapiro-Wilk test was used to test normality amongst the data sets. If the value > 0.05, the data was classed as parametric/normal. If < 0.05, the data was classed as not having a non-parametric/normal distribution. Data comparing two variables parametric independent *t* test, or non-parametric Mann-Whitney U Test were performed. Data comparing three or more variables parametric One-Way ANOVA, Welch's ANOVA, or Kruskal-Wallis Test were performed. In the case that one group in the data set failed the Shapiro-Wilk test for normality, a Welch's ANOVA test was performed. Significance threshold was set to 0.05. Non-significant data was denoted ns. Significant p values were denoted as the following; $p<0.05$ (*), $p<0.01$ (**), $p<0.001$ (***), and $p<0.0001$ (****).

Chapter 3. Characterisation of Human-Derived iAstrocytes as a Model for Alzheimer's Disease

3.1. Chapter Overview

The overall aim of this thesis is to gain an understanding of the complex interplay between astrocytes and amyloid-β (Aβ) aggregates during uptake and inflammation. To complete this aim, human-derived astrocytes from individuals with sporadic Alzheimer's Disease (AD) and healthy controls (Section 2.2.3.1, Table 8) by direct conversion were used. This chapter discusses the methodology of direct conversion and the use of directly converted cells as a model for AD. The first step in the thesis was to characterise the generation of iAstrocytes by immunostaining, along with the limitations and future work.

3.2. Introduction

Neuronal dysfunction and synaptic loss are some of the earliest and established characteristics of AD. However, increased evidence highlights that astrocytes are essential in the early development and progression of AD (Serrano-Pozo et al., 2024; Deng et al., 2024; Bellaver et al., 2023; Habib et al., 2020; Chun et al., 2020; Sollvander et al., 2016). Astrocytes are the most common cell type in the human brain, accounting for ~40% of all cell types (Khakh and Sofroniew, 2015). Briefly, in the brain, astrocytes are crucial for preserving homeostasis by providing metabolic, structural, and protection of neighbouring neurones (Patani et al., 2023). In addition, they are an important component of the tripartite synapse, which aids in regulating neurotransmitters/ions, allowing for communication between neurones and glial cells, synaptic transmission, and plasticity (Farhy-Tselnicker and Allen, 2018). Furthermore, they are involved in the regulation of the blood-brain barrier as a component of the neurovascular unit (Akdemir et al., 2020). Although astrocytes perform essential functions in the brain, they have been associated with contributing factors to AD pathology. This has been hypothesised through a loss of homeostatic function or gain of toxic function contributing to neuronal loss and degeneration (Deng et al., 2024). In particular, astrocytes have been shown to have a key role in the uptake and clearance of Aβ (Preman et al., 2021) and have raised questions about how they contribute to the Aβ load in both healthy and AD brains.

Aβ dysfunction is one of the earliest pathological events in AD. However, most of our knowledge about Aβ dysfunctions has been derived from post-mortem studies, which only provide a snapshot of the disease at the terminal stage. Biomarker studies indicate that Aβ dysfunction begins 10 to 20 years before the onset of clinical symptoms, yet the precise mechanisms driving this early dysfunction remain poorly understood (Jack et al., 2018; Bateman et al., 2012). Consequently, current therapeutic strategies predominantly target Aβ deposition in the later stages of the disease—by which point significant neuronal loss, memory impairment, and cognitive decline have already occurred. Given this, the limited success of Aβ-targeting therapies is not unexpected (Zhang et al., 2023d). Understanding how Aβ dysfunction arises at the cellular level is crucial to developing more effective earlier interventions for AD. Using patient-derived cellular models enables the ability to investigate earlier Aβ aggregate species, providing insights that post-mortem studies cannot.

Aβ production, aggregation, and clearance are finely balanced in the healthy brain. In AD, this equilibrium is disrupted, leading to excessive Aβ accumulation. Impaired clearance is a major contributor to this accumulation, which is thought to play a critical role in disease progression (Yousif Saleh et al., 2024). Astrocytes and microglia are key cellular players in the clearance of aggregated and potentially toxic Aβ (Ries and Sastre, 2016a). In this study, human astrocytes were generated by direct conversion of fibroblasts from three individuals with AD and matched controls (section 2.2.3.1, Table 8) to investigate their role in Aβ uptake and associated processes. Specifically, fibroblasts were directly converted into induced Neuronal Progenitor Cells (iNPCs), which were subsequently differentiated into astrocytes. Briefly, fibroblasts taken by skin biopsy from individuals with AD and healthy controls were directly converted using transduction of retroviral vectors for OCT3, Sox2, and KLF4 to iNPCs (Bell et al., 2024; Gatto et al., 2021; Akdemir et al., 2020; Meyer et al., 2014). The conversion of iNPCs was induced by growth factors: fibroblast growth factor 2 and epidermal growth factor (Bell et al., 2024). For iAstrocyte differentiation, iNPCs were seeded into a culture medium containing N2 and Foetal Bovine Serum (Meyer et al., 2014). Directly reprogrammed cells retain the donor's ageing phenotype and epigenetics, bypassing the pluripotent stage in iPSC modelling (Gatto et al., 2021). Allowing for a more time-efficient and cost-effective alternative than iPSCs. Furthermore, the retention of an ageing phenotype is an important aspect of the model, as AD incidences increase with age, with age being one of the largest risk factors of AD (Liu et al., 2024b). Therefore, the retention of

the age phenotype is a unique and valuable aspect of the model. Finally, astrocytes derived by the same protocol used in this thesis exhibit disease-related toxic phenotypes in other neurodegenerative diseases such as Amyotrophic Lateral Sclerosis and Parkinson's Disease (Au et al., 2024; Schwartzentruber et al., 2020; Ferraiuolo et al., 2016; Meyer et al., 2014). Therefore, using direct conversion could aid in the identification of disease-relevant phenotypes in AD.

3.3. The need for characterisation of human-derived cell models

Characterising human-derived cell models is essential to confirm their identity, functionality, and relevance to disease modelling. Since reprogramming involves transitioning through multiple cellular states, validating each stage— such as iNPCs and induced Astrocytes (iAstrocytes)—is crucial to ensure that the cells exhibit the expected molecular and functional properties rather than retaining characteristics of their original somatic state. One of the primary reasons for characterisation is to ensure accurate cell lineage specification. Reprogramming methods often yield heterogeneous populations, including neurons or other glial cells, and incomplete or misdirected reprogramming could lead to misleading experimental results. Immunohistochemical staining using cell type-specific markers allows for the confirmation and quantification of cell identity. For example, iAstrocytes can be characterised using astrocytic markers such as Vimentin, EAAT2, GFAP, and CD44, while iNPCs can be characterised using progenitor markers such as Nestin and PAX6. Validating cell types during differentiation ensures the exclusion of other cell types (e.g., neurones and other glial cells) and improves the reliability of results in this thesis.

Additionally, human-derived cells often undergo epigenetic and transcriptomic shifts during reprogramming, which may influence their phenotype and functionality (Basu and Tiwari, 2021). The characterisation is particularly critical when studying sporadic AD, where patient-derived models capture individual variability in disease mechanisms to compare staining patterns and expressions from different donors. Without characterisation, discrepancies in cell identity could obscure disease-relevant phenotypes. Therefore, establishing a characterisation framework for human-derived cell models ensures reproducibility, reliability, and relevance in neurodegenerative disease research (Basu and Tiwari, 2021).

3.4. Aims and Objectives

The overall aim of this chapter was to confirm the direct conversion of fibroblasts to iAstrocytes from three control individuals and individuals living with AD - highlighting the relevancy of using direct conversion to generate human-derived astrocytes to study Aβ-astrocyte interactions.

Objectives:

1. Confirm iNPC populations with Nestin and PAX6 by immunocytochemistry.

2. Confirm iAstrocyte populations with CD44, Vimentin, Excitatory Amino Acid Transporter-2, and Glial Fibrillary Acidic Protein by immunocytochemistry.

3.5. Results

3.5.1. Brightfield Imaging

The first step to characterising the direct-reprogramming from iNPCs the iAstrocytes was to visualise the differences in cell morphology between cell types using brightfield imaging (Figure 9). Both control and AD cells exhibit smaller sphere/rosette-like structures typical of that for undifferentiated iNPCs (Figure 9, A-F) (Fu et al., 2025; Meyer et al., 2014). After 7 days of differentiation, cells exhibit larger rounded/star-like morphologies with multiple elongated processes extending from the cell bodies (Gatto et al., 2021), highlighting a morphological difference in cell type between iNPCs and iAstrocytes.

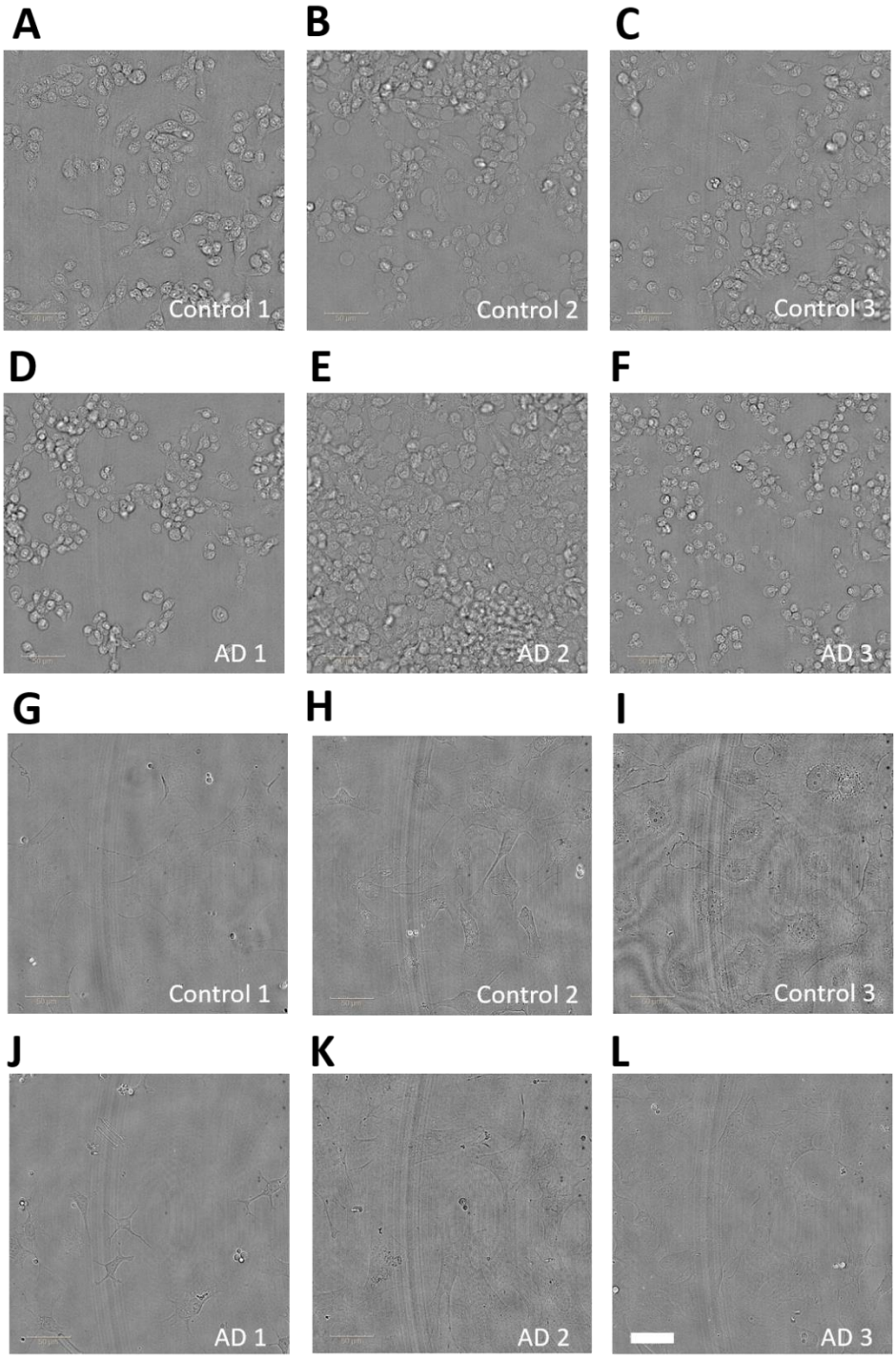

Figure 9. *Brightfield Images of Control and AD iNPCs (A-F) and iAstrocytes (G-L). Scale bar, 50 μM.*

3.5.2. iNPC characterisation

3.5.2.1 Nestin

Nestin, an intermediate filament protein, was visualised and quantified in cells to confirm iNPC populations in cell culture (Figure 10) by immunocytochemistry. Immunocytochemical analysis of the % of positive cells revealed a high proportion and consistent Nestin expression in all iNPC lines localised to the cytoplasm (Figure 10; G and H). The percentage of Nestin^{+} cells was high in all six lines with Control 1, Control 2, and Control 3 showing a mean percentage (n=3, biological repeats per cell line were averaged from 2 technical repeats) of 99.8%, 99.6%, and 99.7%, respectively. Furthermore, AD 1, AD 2, and AD 3 showed 97.2%, 96.3%, and 99.3%, respectively, indicating a positive population of Nestin^{+} iNPCs.

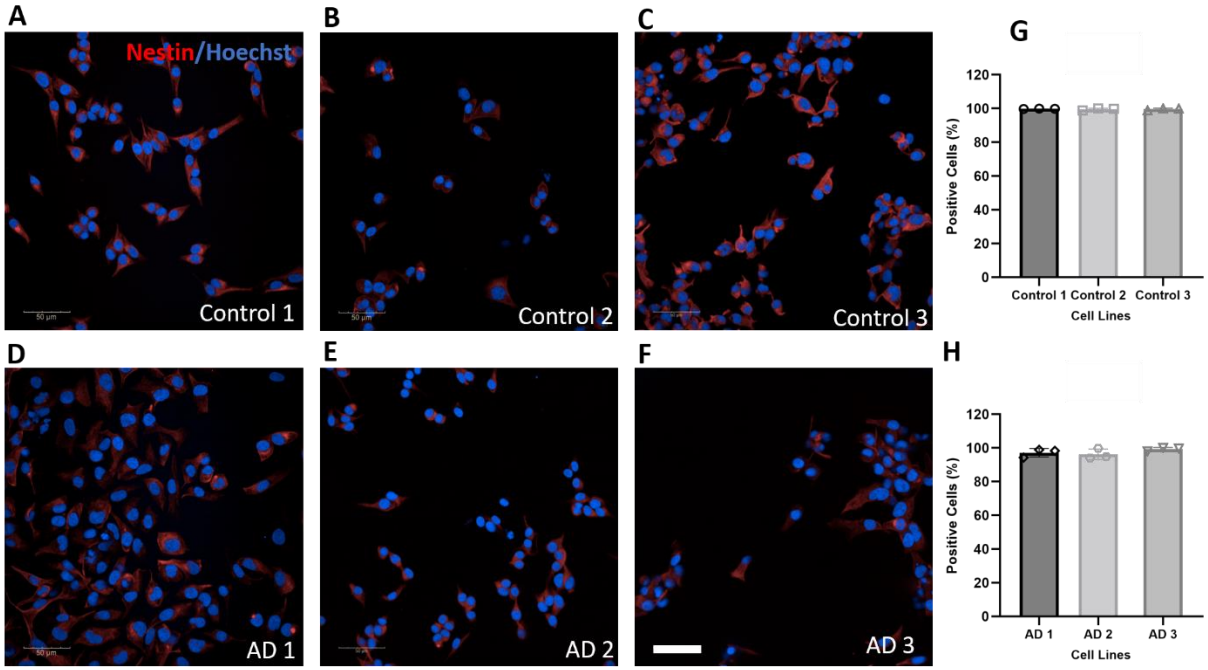

Figure 10. Illustrations and quantification of induced Neuronal Progenitor Cells marker: Nestin, in control and AD cell lines. ***A-F****. Representative images of Nestin (red) and Hoechst (blue) in Control (A-C) and AD (D-F) iNPCs. Scale bar (50 µm).* ***G-H.*** *Control and AD iNPCs quantification showing the percentage of cells with positive staining for Nestin. Biological repeats (n=3) per cell line were averaged from 2 technical repeats.*

.

3.5.2.2. Paired Box 6

Paired Box 6 (PAX6), a neural progenitor cell transcription factor, was visualised and quantified in cells to confirm iNPC populations in Control lines (Figure 11) and AD lines (Figure 12) by immunocytochemistry. Immunocytochemical analysis of the % of positive cells revealed a high proportion and consistent PAX6 expression in all iNPC lines (Figure 11; G and Figure 12; G). The percentage of $PAX6^{+}$ cells was high in all six lines with Control 1, Control 2, and Control 3 showing a mean percentage (n=3, biological repeats per cell line were averaged from 2 technical repeats) of 100%, 100%, and 100%, respectively. Furthermore, AD 1, AD 2, and AD 3 (n=3) show 88.7%, 97.9%, and 99.9%, respectively, indicating a positive population of $PAX6^{+}$ iNPCs.

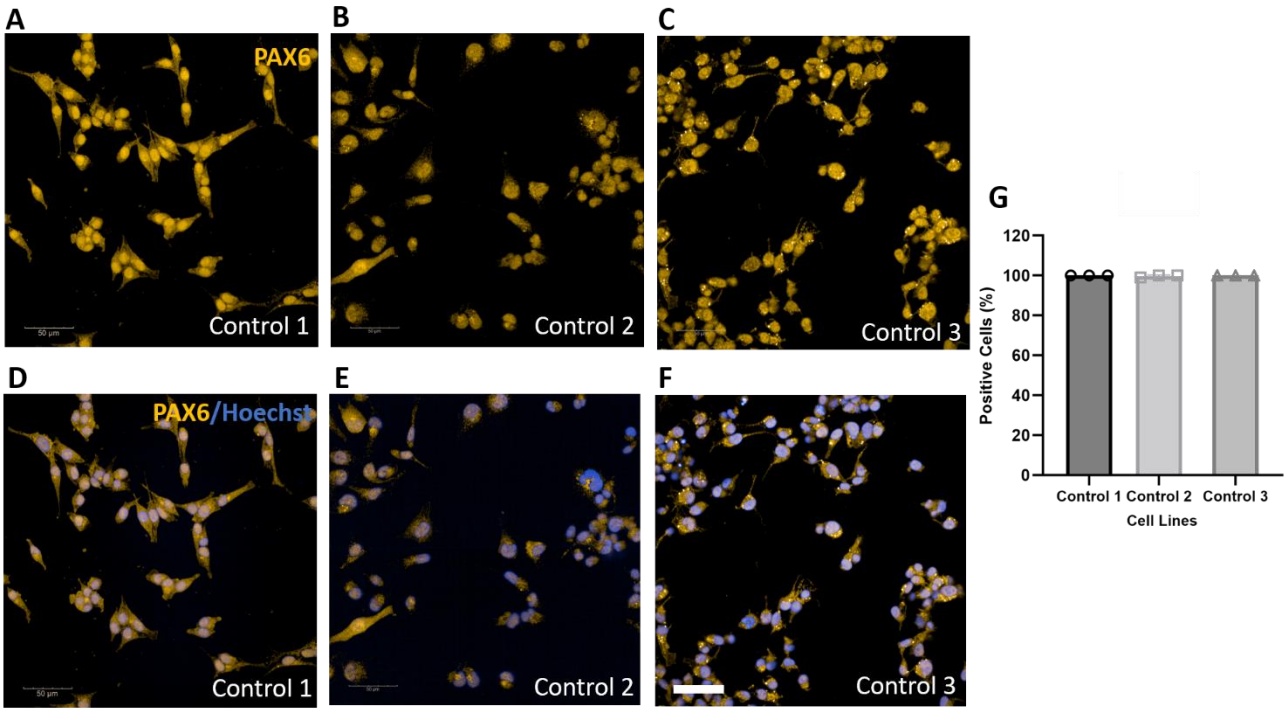

Figure 11. Illustrations and quantification of induced Neuronal Progenitor Cells marker; PAX6 in control lines. A-F*. Representative images of PAX6 (A-C; yellow) and PAX6/Hoechst (D-F; yellow/blue) in Control iNPCs. Scale bar (50 µm).* ***G.*** *Control iNPCs quantification showing the percentage of cells with positive staining for PAX6. Biological repeats (n=3) per cell line were averaged from 2 technical repeats.*

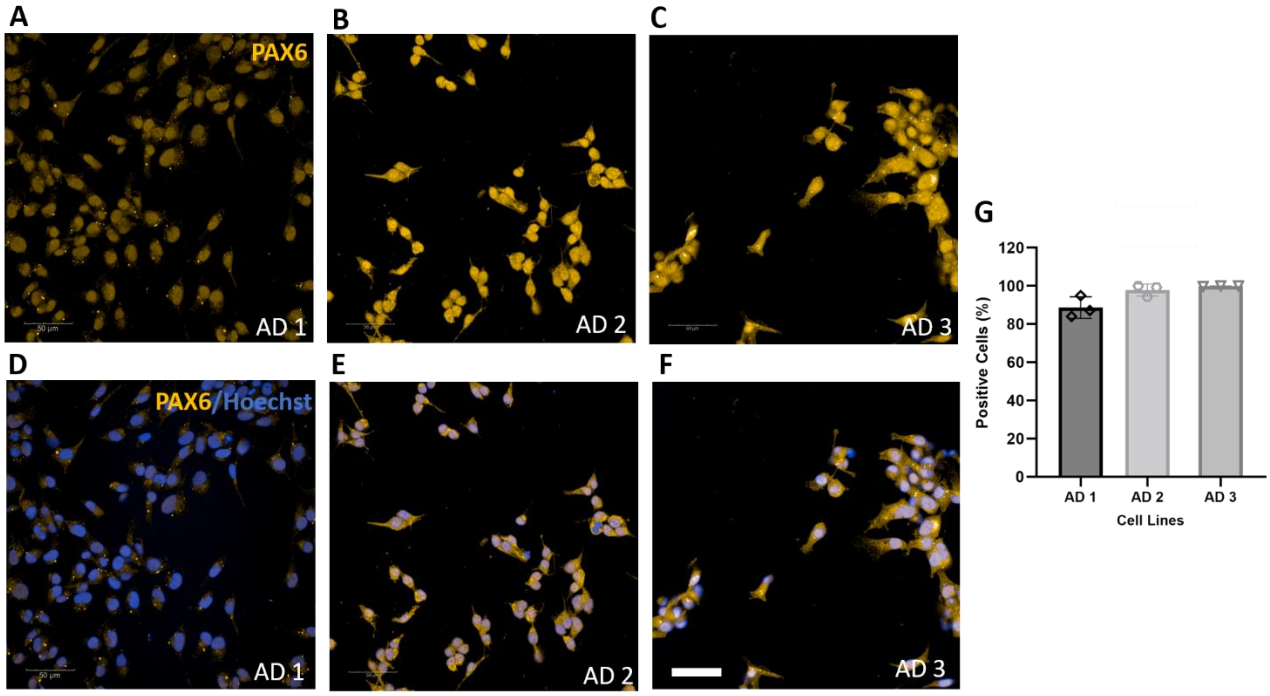

Figure 12. Illustrations and quantification of induced Neuronal Progenitor Cells marker; PAX6 in AD lines. A-F*. Representative images of PAX6 only (A-C; yellow) and PAX6/Hoechst (D-F; yellow/blue) in AD iNPCs. Scale bar (50 µm).* ***G.*** *AD iNPCs quantification showing the percentage of cells with positive staining for PAX6. Biological repeats (n=3) per cell line were averaged from 2 technical repeats.*

3.5.3. iAstrocyte Characterisation

3.5.3.1. CD44

CD44, a cell adhesion molecule responsible for maintenance of astrocyte structure, was visualised and quantified in cells to confirm iAstrocyte populations in cell culture (Figure 13) by immunocytochemistry. Immunocytochemical analysis of the % of positive cells revealed a high proportion and consistent CD44 expression in all iAstrocyte lines (Figure 13; G and H). The mean percentage of $CD44^+$ cells was high in all six lines with Control 1, Control 2, and Control 3 showing a mean percentage (n=3, biological repeats per cell line were averaged from 2 technical repeats) of 99.5%, 99.8%, and 95.3%, respectively. Furthermore, AD 1, AD 2, and AD 3 (n=3) show 99.6%, 98.1%, and 98.4%, respectively, indicating a positive population of $CD44^+$ iAstrocytes.

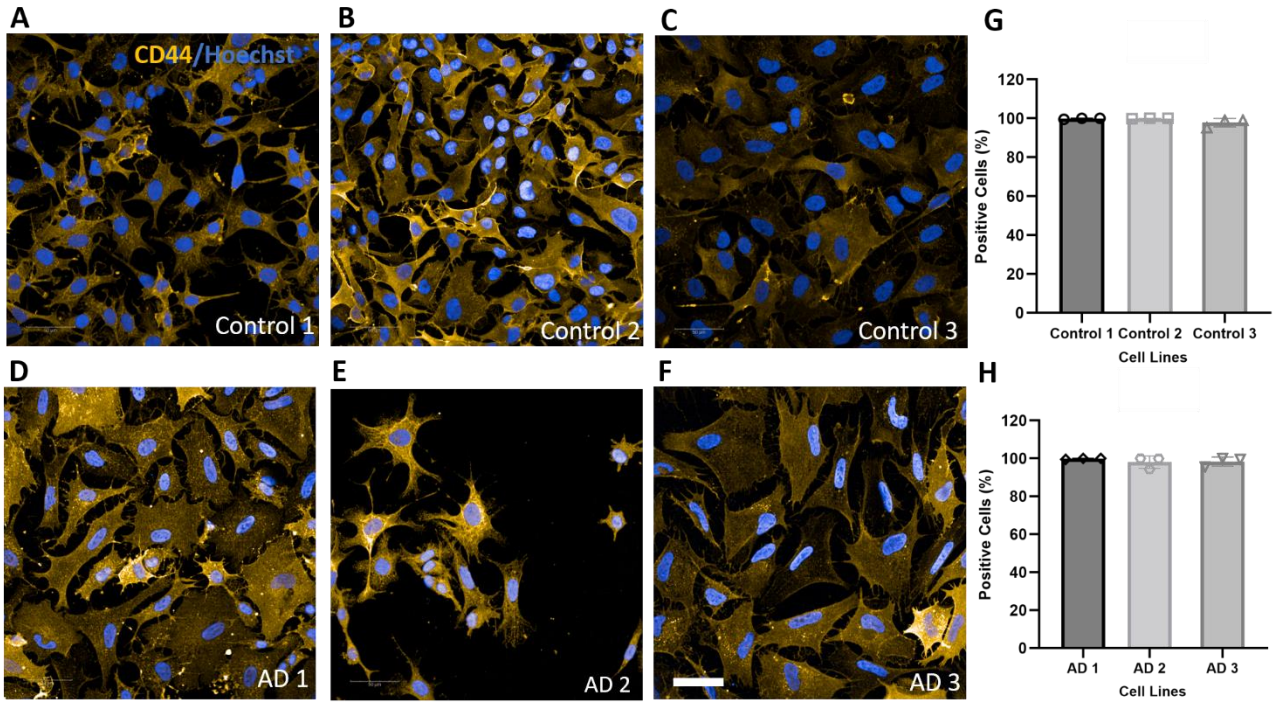

Figure 13. Illustrations and quantification of CD44 in control and AD cell lines. A-F. *Representative images of CD44 (yellow) and Hoechst (blue) in Control (A-C) and AD (D-F) iAstrocytes on day 7 of differentiation. Scale bar (50 µm).* ***G-H.*** *Control and AD iNPCs quantification showing the percentage of cells with positive staining for CD44. Biological repeats (n=3) per cell line were averaged from 2 technical repeats.*

3.5.3.2. Vimentin

Vimentin, an intermediate filament protein, was visualised and quantified in cells to confirm iAstrocyte populations in cell culture (Figure 14) by immunocytochemistry. Analysis of the % of positive cells revealed a high proportion and consistent vimentin expression in all iAstrocyte lines (Figure 14; G and H). The percentage of Vimentin^{+} cells was high in all six lines with Control 1, Control 2, and Control 3 showing a mean percentage (n=3, biological repeats per cell line were averaged from 2 technical repeats) of 100%, 100%, and 100%, respectively. Furthermore, AD 1, AD 2, and AD 3 (n=3) show 100%, 100%, and 99.1%, respectively, indicating a positive population of Vimentin^{+} iAstrocytes.

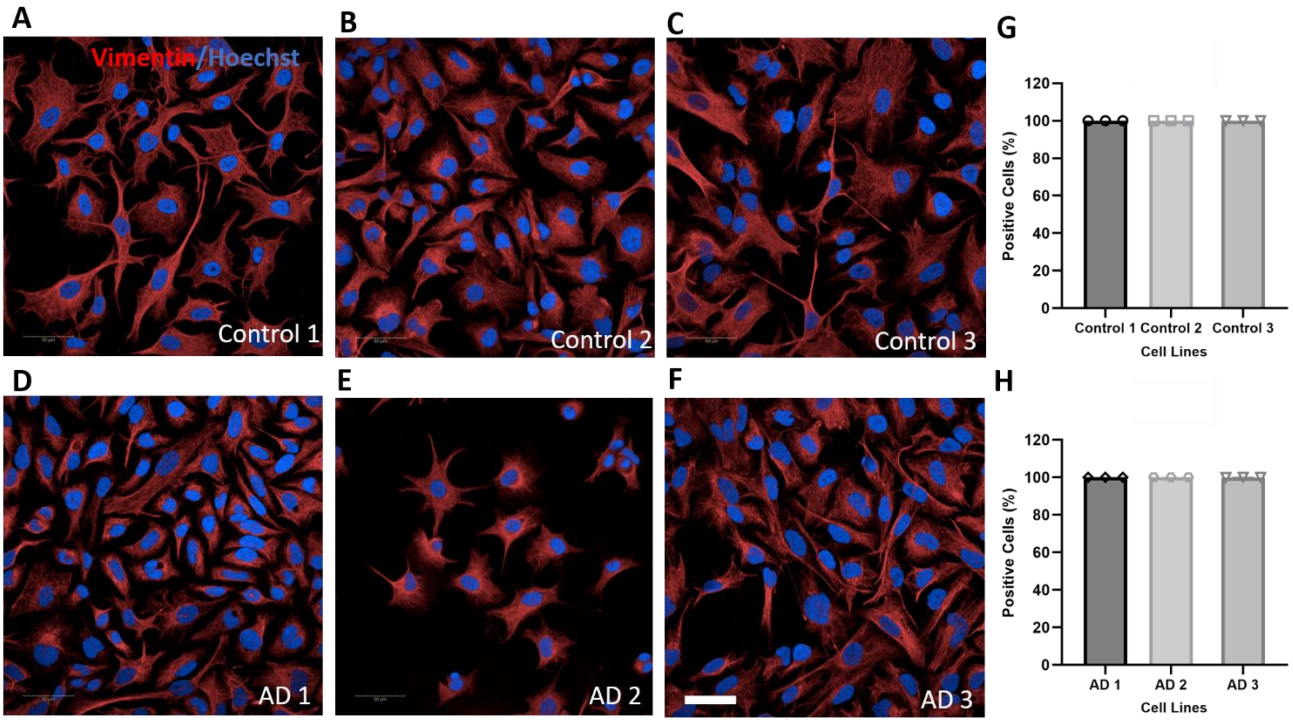

Figure 14. Illustrations and quantification of Vimentin in control and AD cell lines. A-F. *Representative images of vimentin (red) and Hoechst (blue) in Control (A-C) and AD (D-F) iAstrocytes on day 7 of differentiation. Scale bar (50 µm).* ***G-H.*** *Control and AD iNPCs quantification showing the percentage of cells with positive staining for vimentin. Biological repeats (n=3) per cell line were averaged from 2 technical repeats.*

3.5.3.3. Excitatory Amino Acid Transporter-2

Excitatory Amino Acid Transporter-2 (EAAT2), a glutamate transporter protein, was visualised and quantified in cells to confirm iAstrocyte populations in cell culture (Figure 15) by immunocytochemistry. Immunocytochemical analysis of the % of positive cells revealed a high proportion and consistent EAAT2 expression in all iAstrocyte lines (Figure 15; G and H). The percentage of EAAT2^{+} cells was high in all six lines with Control 1, Control 2, and Control 3 showing a mean percentage (n=3, biological repeats per cell line were averaged from 2 technical repeats) of 98.9%, 97.6%, and 98.1%, respectively. Furthermore, AD 1, AD 2, and AD 3 (n=3) showing 96.7%, 97.2%, and 98.6%, respectively, indicating a positive population of EAAT2^{+} iAstrocytes.

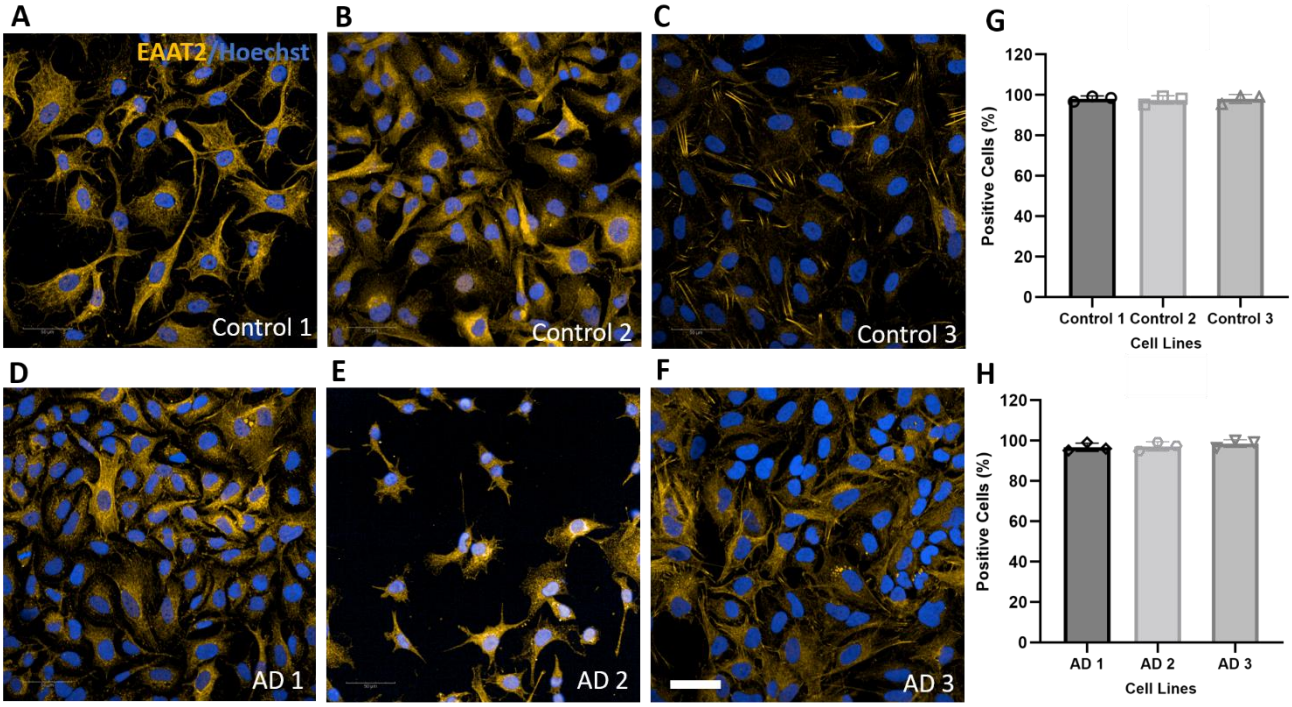

Figure 15. Illustrations and quantification of EAAT2 in control and AD cell lines. A-F. *Representative images of EAAT2 (yellow) and Hoechst (blue) in Control (A-C) and AD (D-F) iAstrocytes on day 7 of differentiation. Scale bar (50 µm).* ***G-H.*** *Control and AD iNPCs quantification showing the percentage of cells with positive staining for EAAT2. Biological repeats (n=3) per cell line were averaged from 2 technical repeats.*

3.5.3.4. Glial Fibrillary Acidic Protein

Glial fibrillary acidic protein (GFAP), a scaffold protein for structural support in astrocytes, was visualised and quantified in cell culture (Figure 16) by immunocytochemistry. Immunocytochemical analysis of the % of positive cells revealed a high proportion and consistent GFAP expression in all iAstrocyte lines (Figure 16; G and H). The percentage of $GFAP^+$ cells was high in all six lines with Control 1, Control 2, and Control 3 showing a mean percentage (n=3, biological repeats per cell line were averaged from 2 technical repeats) of 100%, 100%, and 100%, respectively. Furthermore, AD 1, AD 2, and AD 3 (n=3) show 99.7%, 99.8%, and 99.9%, respectively, indicating a positive population of $GFAP^+$ iAstrocytes.

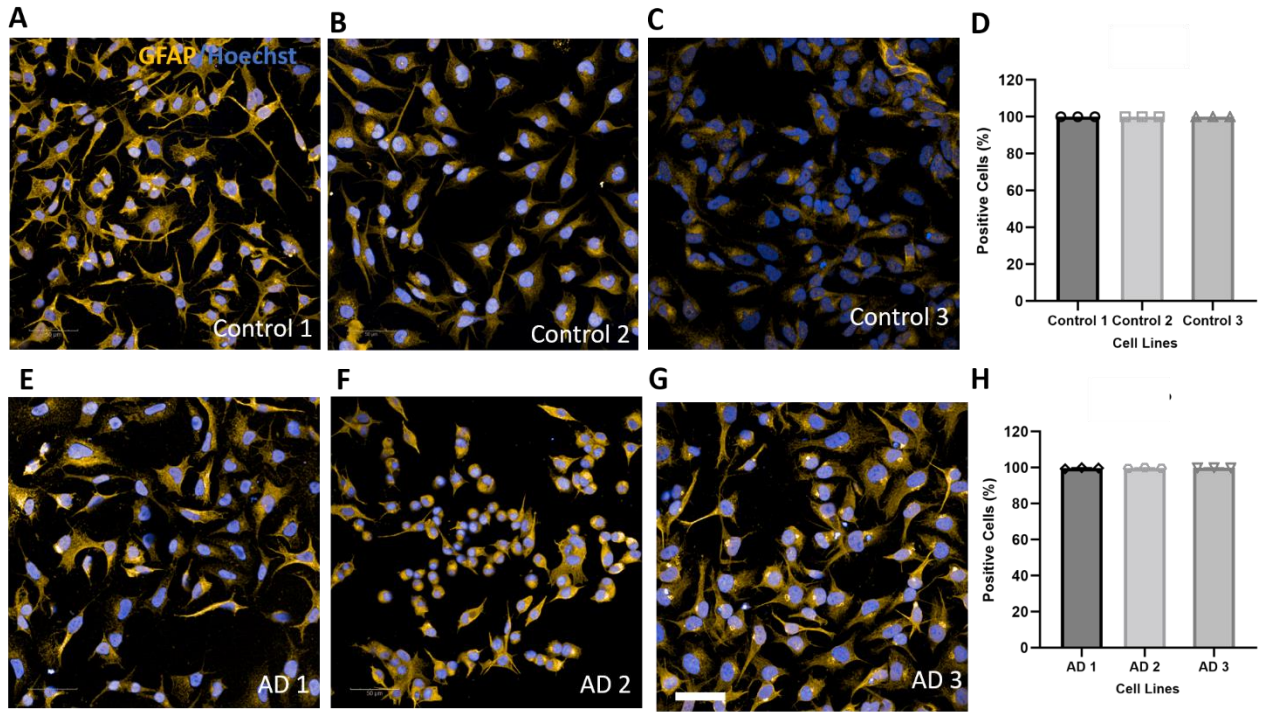

***Figure 16**. **Illustrations and quantification of GFAP in control and AD cell lines. A-F**. Representative images of GFAP (yellow) and Hoechst (blue) in Control (A-C) and AD (D-F) iAstrocytes on day 7 of differentiation. Scale bar (50 µm). **G-H.** Control and AD iNPCs quantification showing the percentage of cells with positive staining for GFAP. Biological repeats (n=3) per cell line were averaged from 2 technical repeats.*

3.6. Discussion

3.6.1. Discussion Overview

The first step in this thesis was to characterise human-derived astrocytes generated from individuals with AD and healthy controls through direct reprogramming of fibroblasts to iAstrocytes. It was important to do this as a model to use iAstrocytes to investigate Amyloid-β-Astrocyte interaction within the context of uptake and inflammation.

3.6.2. Immunocytochemistry confirms iNPC populations

Firstly, iNPC populations were confirmed using Nestin (Figure 10). Nestin is a cytoskeletal type VI intermediate filament protein in neural stem/progenitor cells (Bernal and Arranz, 2018). It functions for cell self-renewal, proliferation, and protection from cellular stress (Bernal and Arranz, 2018). Nestin is an established marker of undifferentiated central nervous system cells and is localised in the cytoplasm of NPCs (Suzuki et al., 2010). In conjunction with Nestin, iNPCs were also stained for PAX6 (Figures 11 and 12).

PAX6 is a highly conserved vertebrate transcription factor that regulates the expression of neuroectoderm genes (Thakurela et al., 2016). PAX6 is predominantly localised to the nucleus, though its expression has also been found in the cytoplasm of cells due to its active nucleo-cytoplasmic shuttling during gene expression regulation (Zhang et al., 2018; Xu et al., 2018; Parisi and Collinson, 2012). By targeting the promoters of the neuroectoderm and repressing non-neuronal lineages, PAX6 has a key role in neuroectoderm differentiation (Thakurela et al., 2016). Unlike microglia, which arise from the mesoderm, cells from the neuroectoderm are neurones, oligodendrocytes, and astrocytes (Araki et al., 2021). Furthermore, in both human-derived NPCs and rodents, PAX6 can be used to predict the differentiation into astrocytes (Zhou et al., 2016; Sakurai and Osumi, 2008). Highlighting the importance of using PAX6 to stain the iNPCs in this project. Positive staining for Nestin and PAX6 in the cell lines confirms iNPCs populations in both the control and AD lines.

3.6.3. Immunocytochemistry confirms iAstrocytes populations

Post differentiation, iAstrocyte cultures were stained using CD44, vimentin, EAAT2, and GFAP (Figures 13, 14, 15, and 16). CD44 and vimentin are established prototypic markers of astrocytes (Jurga et al., 2021). CD44 is a cell surface, adhesion, and signalling glycoprotein commonly linked to cell-cell and cell-matrix interactions. Early immunofluorescence has shown that 95% of adult astrocytes express CD44 (Moretto et al., 1993). Vimentin is a cytoskeletal intermediate filament protein that aids in maintaining cell structure and regulating cell signalling pathways. CD44 and vimentin are linked to astrocyte reactivity and morphology changes in several neurodegenerative diseases, including Parkinson's disease (Wang et al., 2022; Kano et al., 2020), ALS (Bradford et al., 2024; Zhou et al., 2015), and AD (Dai et al., 2023; Pinner et al., 2017). CD44 and vimentin expression have been used to measure Aβ-induced pro-inflammatory reactivity in astrocytes (LaRocca et al., 2021b; Kamphuis et al., 2015). Highlighting Vimentin and CD44 as not only a markers for astrocytes, but also as a markers of reactivity associated with Aβ and inflammation.

Next, the iAstrocytes were stained for functional markers EAAT2 and GFAP (Figures 15 and 16). EAAT2, also known as glutamate transporter 1 (GLT-1) or solute carrier family-1 member 2 (SLC1A2), is a glutamate transporter receptor predominantly expressed in astrocytes. As part of their role in maintaining homeostasis, astrocytes have a key role in regulating glutamate levels in the brain. Glutamate is the most common excitatory neurotransmitter essential for learning, memory, and cognition. Glutamate is released from the presynaptic terminals of neurones, where it diffuses into the synaptic cleft to bind to the glutamate receptors on the postsynaptic neurone. Astrocytes actively uptake excess glutamate in the synaptic cleft to maintain neurotransmitter balance (Takahashi et al., 2015). Although there are five isoforms of EAAT glutamate receptors in the CNS, EAAT2 is responsible for ~90% of all glutamate reuptake (Rao et al., 2015). In astrocytes, the primary function of EAAT2 is to detect and remove excess glutamate from the synapses. As glutamate is an excitatory neurotransmitter, excess can lead to prolonged activation of glutamate receptors and continuous neuronal excitation (Todd and Hardingham, 2020). Therefore, regulating glutamate through EAAT2 plays an essential role in neuronal synaptic activity by preventing excitotoxicity, leading to synaptic loss (Rao et al., 2015).

Furthermore, dysfunction or loss of EAAT2 is linked to neurological conditions such as epilepsy and neurodegenerative diseases, ALS, PD, and AD (Todd and Hardingham, 2020).

Finally, GFAP is a type III intermediate filament protein, and like other intermediate filament proteins such as Vimentin, GFAP aids in maintaining the shape and structure of astrocytes (Middeldorp and Hol, 2011). GFAP is closely linked to astrocyte's role in maintaining homeostasis and part of hypertrophic reactivity, particularly in response to injury in the CNS (Burda and Sofroniew, 2014). Upregulation of GFAP levels can be detected in the blood during several neurological disorders including, but not limited to stroke, intracerebral haemorrhages, and traumatic brain injuries (Yang and Wang, 2015). Furthermore, it is used to identify and predict the prognosis of multiple sclerosis and brain tumours such as glioblastoma multiforme (Yang and Wang, 2015). In recent years, there has been increasing evidence of dysregulation of GFAP-astrocyte function and its potential to be a screening tool to identify early changes in AD (Ozcelikay-Akyildiz et al., 2024). For example, in individuals with Aβ pathology (determined by Aβ-PET), GFAP concentration in the CSF was significantly higher than in individuals without Aβ pathology (Pereira et al., 2021). Interestingly, using GFAP levels with Aβ-PET, the different stages of AD were readily detectable but not Tau (Pereira et al., 2021). Highlighting the correlation of GFAP with Aβ pathology, one of the earliest dysfunctions in AD.

3.6.4. Limitations and Future Work

Studies have reported that in the healthy human brain, the levels of GFAP expressed in astrocytes are relatively low and are upregulated during reactivity (Yang and Wang, 2015). The results from this study show that all lines have a high population of GFAP-positive iAstrocytes despite being stained from quiescent conditions with no external stressors (Figure 16). Studies have indicated that a resting low GFAP expression indicates a healthy brain environment, and in AD is distinctly higher (Kim et al., 2023b). The results in this chapter show the mean percentage of cells which were positive for GFAP, and although confirms the expression of GFAP it does not give information on the levels of expression in the individual lines. As a result, future avenues could evaluate the intensity of the GFAP staining between control and AD cell lines. Additionally, this limitation is relevant for the other markers used in this study. For example, EAAT2 expression has been shown to be reduced in sporadic AD brains, whilst CD44 has been highlighted to be increased in the

hippocampus in AD compared to healthy individuals (Nguyen et al., 2024; Sharma et al., 2019). Therefore, investigation of the expression of markers rather than just the number of cells expressing each marker would have been an interesting avenue for further characterisation of the cell lines used in this study. Furthermore, a main limitation of this body of work is the lack of comparison of markers between the fibroblasts, iNPCs, and iAstrocytes. As the overall aim of this chapter was to confirm the direct conversion of fibroblasts to iAstrocytes, using cell type specific markers on each different cell type to confirm the negative staining would have been a valuable extension to this chapter. Next, though CD44 has a strong association as an astrocyte marker, it is also shown to be expressed in microglia and oligodendrocytes (Bradford et al., 2024; Moretto et al., 1993). Vimentin is a pan-glial marker found in other glial subtypes, including microglia and ependymal cells (Vidovic et al., 2018; Jiang et al., 2012). However, in the context of the direct conversion model used in this thesis, the iNPCs are tripotent (Meyer et al., 2014). As a result, the iNPCs can be differentiated into three major neuronal lineages: astrocytes, oligodendrocytes, and neurones. Further work could characterise the astrocytes differentiated in this protocol further by staining for other astrocyte markers, including s100 calcium-binding protein B (S100β), Aquaporin 4 (AQP4), and Aldehyde dehydrogenase 1A1 (*ALDH1A1*) (Bhalla et al., 2025; Huang et al., 2023; Meyer et al., 2014). Alternatively, staining for neurone-specific markers, b-III tubulin (Tuj1) and Microtubule-associated protein 2 (MAP2), or oligodendrocytes specific markers, oligodendrocyte transcription factor 2 (OLIG2) and Myelin regulatory factor (MYRF). After differentiation, this staining could confirm negative neuronal and oligodendrocyte populations in cell culture. Furthermore, electrophysiology could be used to determine the resting potential to test the astrocytes' functionality further. Unlike neurones, which have a resting potential between -50 and -70 s (mV), astrocytes have a resting potential of ~80 (mV) (McNeill et al., 2021). This highlights the diversity of other cell types to further confirm the astrocyte population in culture. Astrocytes are also key regulators of voltage channels sodium, potassium, and calcium signalling, giving rise to the potential to test the function of the differentiated astrocytes in this capacity (McNeill et al., 2021).

Finally, as previously mentioned, the retention of an ageing phenotype is an important aspect of the model. Previous studies have shown that when comparing young and old iNPCs from the same direct conversion method used in this thesis, there were 80%

transcriptional differences, highlighting distinct profiles between old and young donors (Gatto et al., 2021). Next, it has been shown that age-related transcripts are preserved from the fibroblasts to both directly converted astrocytes and neurones (Gatto et al., 2021; Mertens et al., 2015). In particular, RAN binding protein 17 (*RANBP17*), laminin subunit alpha 3A (*LAMA3A*), and telomeric repeat-binding factor 2 (TERF2) have been shown to decrease with age, but are preserved from their fibroblast origin (Gatto et al., 2021) . However, in this study these transcriptional changes were not explored from the donor cell lines in comparison to young donors, and as a result to confirm the ageing phenotype in this subset of cell lines future work should validate this further. Despite this, as part of a larger study (section 3.8), the cell lines used in this project were explored using Lamin A/C, a marker of nuclear envelope ageing, where it was shown that there was no change in the shape of the nuclear envelope between iAstrocytes and donor fibroblast in both the control and sporadic lines (Bell et al., 2024). Additionally, levels of expression of TERF2, LAMA3, and RANBP17 between fibroblasts and iAstrocytes remained unchanged, highlighting that the cell lines used in this project have not returned to their stem cell phase during the reprogramming stages for each line across cell type (Bell et al., 2024).

3.7. Conclusion

The overall aim of this chapter was to characterise the direct conversion of fibroblasts to iAstrocytes from control individuals and individuals living with AD. The confirmation of $EAAT2^+$ and $GFAP^+$ astrocytes highlights the functionality of the differentiated astrocytes in culture. This, coupled with positive staining for CD44 and Vimentin highlights a consistent and homogenous astrocyte culture population. Therefore, highlighting the relevancy of the using direct conversion to generate human-derived astrocytes to study Aβ-astrocyte interactions.

3.8. Additional Chapter Information

The results of this chapter were part of a larger study of which the author of this thesis was listed as second author: Bell, S. M., **Wareing, H**., Capriglia, F., Hughes, R., Barnes, K., Hamshaw, A., Adair, L., Shaw, A., Olejnik, A., De, S., New, E., Shaw, P. J., De Marco, M., Venneri, A., Blackburn, D. J., Ferraiuolo, L., & Mortiboys, H. (2024). Increasing hexokinase 1 expression improves mitochondrial and glycolytic functional deficits seen in sporadic

Alzheimer's disease astrocytes. *Molecular psychiatry*, https://doi.org/10.1038/s41380-024-02746-8. As part of this study, the following cell lines listed in this thesis were characterised: Control 1, Control 2, AD 1, and AD 2. Cell lines (Control 3 and AD 3) were stained in the same capacity, but were not used in the wider study but were used in the assays completed in this thesis.

Chapter 4. Evaluating the Uptake of Aβ Isoforms in iAstrocytes

4.1. Chapter Introduction

Following the confirmation of homogeneous populations of iAstrocytes (Chapter 3, pp., 57-73), the next step in this thesis was to evaluate the uptake of Aβ species in both control and AD iAstrocytes. The accumulation of Aβ aggregates into plaques within the brain of AD patients is a key pathological hallmark of the disease. Both experimental and clinical data have suggested that an imbalance between the production and clearance of Aβ is a key driver of pathology in AD (Yousif Saleh et al., 2024). Efficient Aβ clearance is critical for maintaining brain homeostasis, as impaired removal is associated with toxic accumulation and disease progression (Espay et al., 2023). Among cell-mediated clearance, glial cells - such as microglia and astrocytes - play a pivotal role in clearing toxins and debris, including Aβ, in the brain (Lee and Landreth, 2010). However, astrocytes, central to maintaining brain homeostasis, also actively contribute to Aβ clearance, though the exact molecular mechanisms remain largely unknown (Giusti et al., 2024).

During the production of Aβ, cleavage of the amyloid precursor protein produces a heterogeneous population of peptides, prone to misfolding and aggregation, with Aβ40 and Aβ42 being the most abundant (Baek and Lee, 2024). The aggregation of Aβ is a highly complex and dynamic process involving the transition from monomeric peptides into oligomers (Chen et al., 2017). These oligomers aggregate further into protofibrils and fibrils and eventually form extracellular plaques. In addition, throughout Alzheimer's disease (AD) progression, the ratio to Aβ40: Aβ42 in the cerebrospinal fluid (CSF) decreases, reflecting the deposition of Aβ42 into plaques (Andersson et al., 2025; Hansson et al., 2019). The relative uptake of Aβ40 and Aβ42 aggregates and preferential uptake of oligomeric compared to fibrillar species in astrocytes remains unclear. Additionally, whether different Aβ40: Aβ42 ratios influence astrocytic Aβ uptake remains mostly unexplored. Understanding how astrocytes interact with different Aβ isoforms and aggregation states is essential for elucidating their role in Aβ clearance and its implications in AD pathology.

In order to investigate Aβ uptake, iAstrocytes were treated with different isoforms and aggregation states of Aβ, and the uptake was measured by immunofluorescence (Sections 2.2.6 and 2.2.9.). This chapter describes the development of an experimental system

designed to simulate Aβ species aggregation and uptake in iAstrocytes. Finally, the potential mechanisms for clearance and downstream pathways activated by Aβ are briefly discussed.

4.2. Hypothesis, Aims, and Objectives

4.2.1. Hypothesis

In AD, there is a reduction in the clearance of Aβ, believed to be from an imbalance between the production and removal of Aβ. Astrocytes which have a key role in the internalistion of Aβ are dysregulated.

Hypothesis: There will be less uptake of Aβ in iAstrocytes derived from individuals living with AD than in controls.

4.2.2. Aims

This chapter aimed to elucidate how astrocytes process different proportions of Aβ40 and Aβ42, shedding light on whether there is preferential uptake of either peptide, and how changes in their ratio impact the clearance efficiency. Given that the Aβ42 to Aβ40 ratio has been correlated with disease progression rates, understanding how these isoforms interplay with astrocytes holds potential significance in comprehending the underlying mechanisms of AD pathology.

4.2.3. Objectives

1. Establish a system to mimic Aβ aggregation, including in vitro Aβ aggregate preparation and characterisation of their identity using single-aggregate imaging.

2. Quantify the uptake of Aβ in iAstrocytes, comparing the role of Aβ40 and Aβ42 isoforms, as well as oligomeric and fibrillar forms, and varying Aβ40: Aβ42 ratios to evaluate potential differences in uptake efficiency.

4.3. Results

4.3.1. Thioflavin T based Aβ Aggregation and Characterisation of Species at the Single-aggregate Level

The first step was to generate distinct populations of Aβ species: Aβ40 (10:0), Aβ40; Aβ42 (9:1), Aβ40; Aβ42 (7:3), and Aβ42 (0:10). Briefly, monomeric Aβ40, Aβ42, and their mixtures (7:3 and 9:1) (50 μM), were diluted in PBS and incubated at 37°C (Section 2.2.9). Thioflavin T (ThT) fluorescence kinetics, a widely used method for Aβ aggregation and monitoring, was employed to track *in vitro* aggregate formation (Xue et al., 2017) (Figure 17). Importantly, ThT does not alter Aβ aggregation kinetics significantly or influence the properties of the aggregates formed (Benilova et al., 2014). A time point-based isolation of Aβ aggregates was used to generate oligomers and fibrils for uptake experiments (Section 2.2.9, Table 10). For oligomeric Aβ species, samples were collected at the end of the lag phase, a time point previously shown to contain enriched oligomeric species (Niu et al., 2024). Although the mid-aggregation phase contains a higher proportion of oligomers, it also includes significant protofibril and fibrillar structures (Xue et al., 2017). The end of the lag phase was selected as the optimal time point to minimise fibril contamination and maximise the enrichment of oligomers.

Conversely, for fibrillar Aβ species, samples were collected at the plateau phase of aggregation, which has been shown to consist of mature fibrils predominantly (Rusakov et al., 2024). To characterise oligomeric and fibrillar Aβ species formed during aggregation, Total Internal Reflection Fluorescence (TIRF) Microscopy was used (Section 2.2.13). TIRF allowed the visualisation of single aggregates and confirmed the presence of oligomers and fibrils (Figure 18, A and B). The co-aggregation of Aβ40 and Aβ42 fibrils was also confirmed using TIRF (Figure 18, C), whereby the fluorophores conjugated with antibodies were excited by an evanescent wave from the bottom of the coverslip (Mattheyses et al., 2010). The evanescent wave in TIRF allows for observing fluorescent molecules for long periods before photobleaching (Yang et al., 2021). Additionally, TIRF allows for a better-resolved image and lower background signal compared to conventional methods.

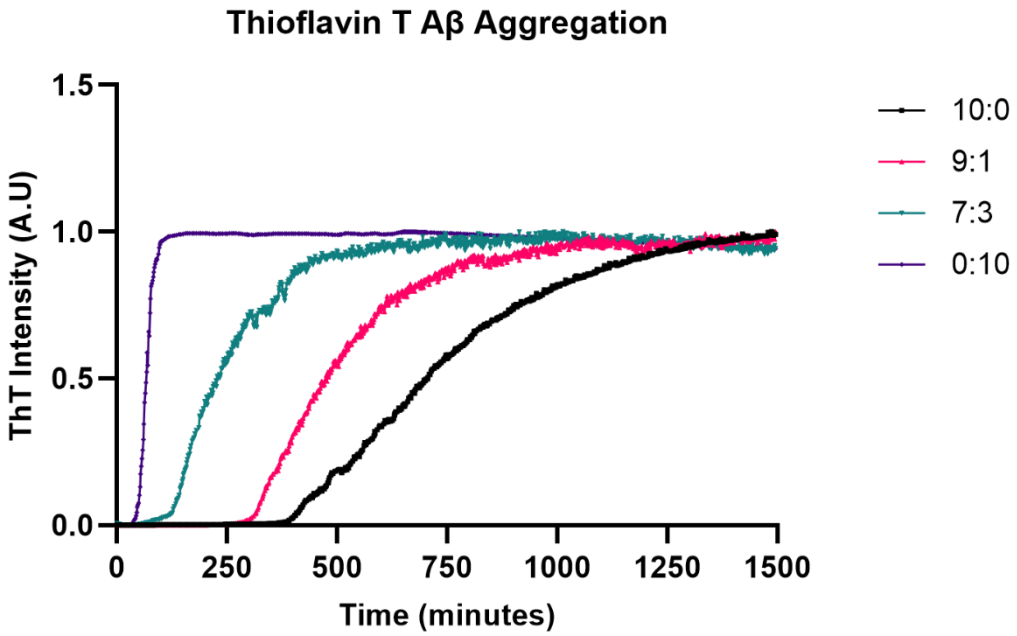

Figure 17. Thioflavin T (ThT) based Aβ aggregation curve. *The aggregation of Aβ40 (10:0) (black), Aβ40: Aβ42 (9:1) (pink), Aβ40: Aβ42 (7:3) (green), and Aβ42 (0:10) (purple) (50 μM diluted in PBS, 37°C). Aggregation monitored by ThT intensity (A.U.) against Time (minutes), ThT = excitation; 450 nm, emission; 482 nm. Each aggregation curve represents the average of 3 repeats.*

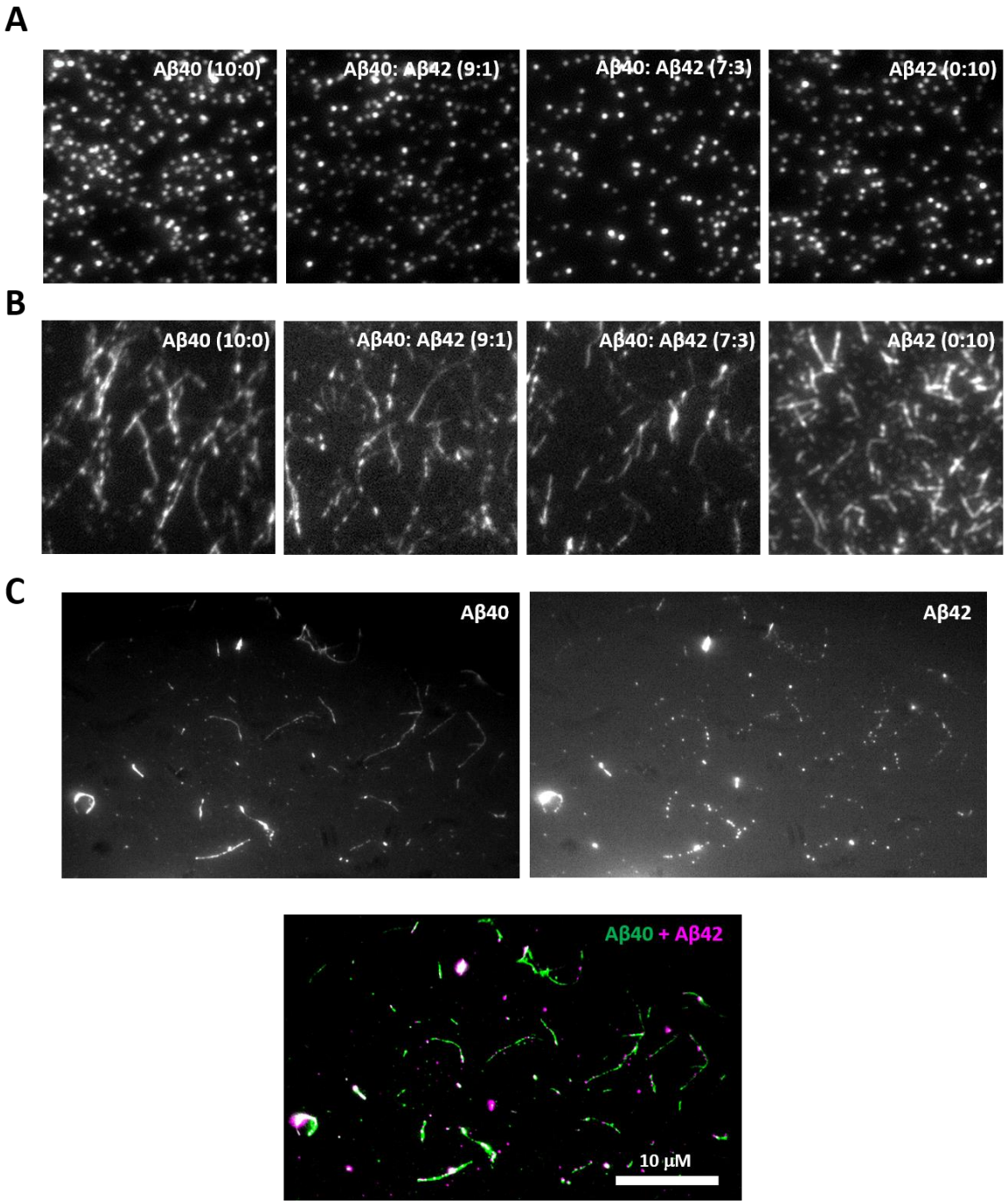

Figure 18. Total Internal Reflection Fluorescence (TIRF) microscopy images of Aβ species. A. *representative TIRF images of oligomeric Aβ (2.5 μM) aggregates; Aβ40 (10:0), Aβ40: Aβ42 (9:1), Aβ40: Aβ42 (7:3), and Aβ42 (0:10) (6E10-647 nm)**. B.*** *Representative TIRF images of fibrillar Aβ aggregates; Aβ40 (10:0), Aβ40: Aβ42 (9:1), Aβ40: Aβ42 (7:3), and Aβ42 (0:10) (6E10-647 nm)**. C.*** *Aβ40 and Aβ42 co-aggregate during fibril formation. Aβ40 (Anti-40-488 nm), Aβ42 (Anti-42-637 nm)* and merged.

4.3.2. Uptake of Aβ in iAstrocytes

To evaluate and compare the uptake of different Aβ isoforms, the Aβ-mediated treatment assay was used (Section 2.2.9). Briefly, on day 7 of differentiation, iAstrocytes were treated with Aβ before being fixed for immunocytochemistry as described in section 2.2.6. Initially, treatment periods of 1, 24, and 48 hours were compared (Figure 19). However, the longer treatment of Aβ42 (24 and 48 hours) resulted in non-detectable iAstrocytes (Figure 19). Therefore, quantitative image analysis of immunocytochemistry (section 2.3.2) would have been inaccurate, and subsequently, 24 and 48 hours were not used. In contrast, Aβ40-treated astrocytes exhibited no detectable Aβ40 spots after 24 and 48 hours, indicating that Aβ40 underwent significant degradation over time, making quantification unreliable. Given these findings, the time point of 1 hour was chosen as the optimal condition, allowing for reliable detection of cells and quantification of Aβ uptake.

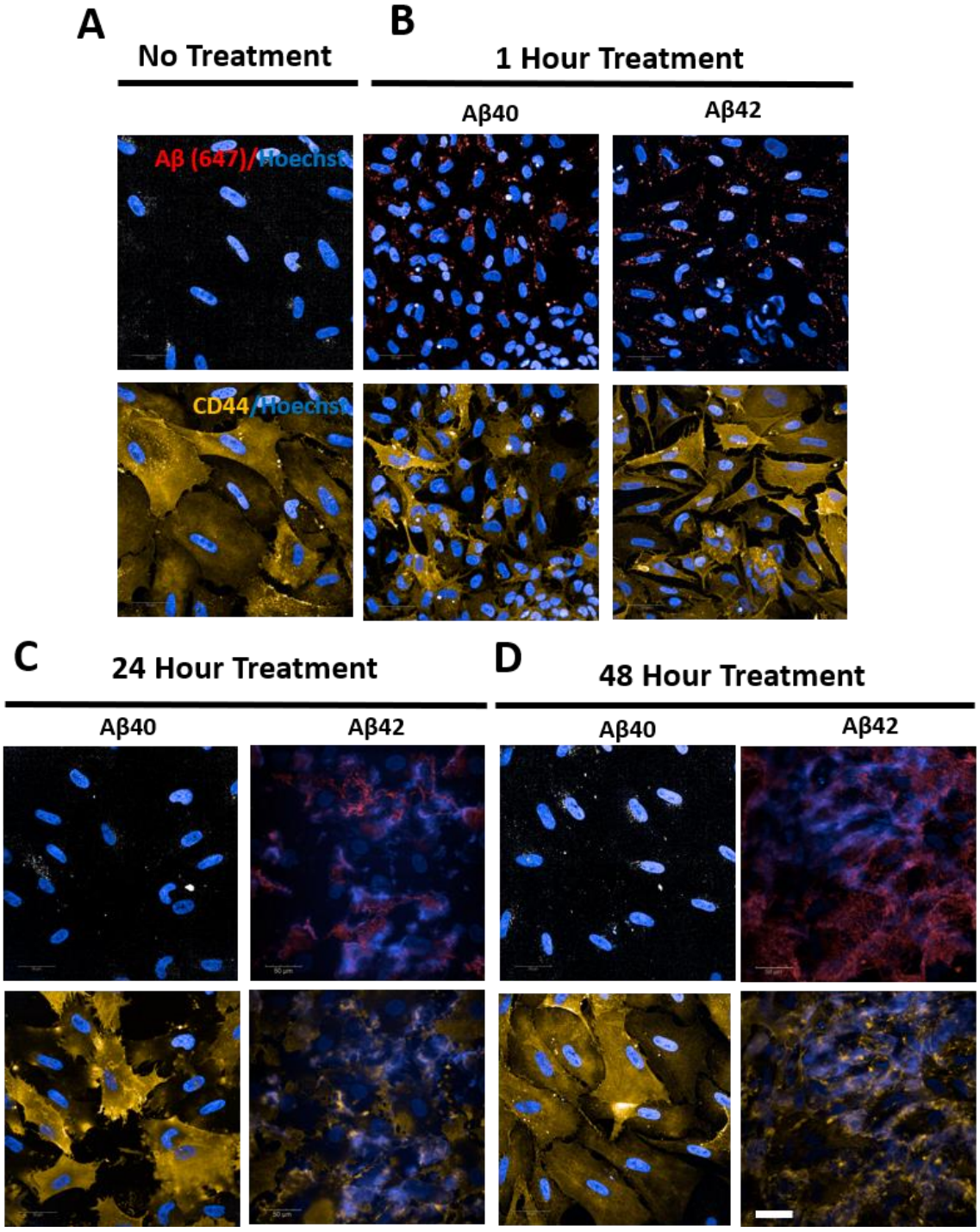

Figure 19. Illustrations of iAstrocytes after Aβ (2.5 μM) treatment using immunocytochemistry. ***A.*** *Representative images of no Aβ treatment.* ***B.*** *Representative images of Aβ40 and Aβ42 after 1 hour's treatment.* ***C.*** *Representative images of Aβ40 and Aβ42 after 24 hours treatment* ***D.*** *Representative images of Aβ40 and Aβ42 after 48 hours treatment. Images show Aβ stained with 6E10-Alexa 647 nm (red), Astrocytes stained with CD44 (yellow), and Hoechst (blue). Scale bar (50μm).*

4.3.2.1. The Uptake of Aβ in Control iAstrocytes

This section aimed to investigate the extent of uptake by Control iAstrocytes comparing different Aβ isoforms in both oligomeric and fibrillar forms (Figures 20, A and). All Aβ aggregate types were taken up by iAstrocytes (Figures 21 and 22), with a statistically significantly higher uptake of Aβ42 (0:10) oligomers than Aβ40 (10:0) and Aβ40: Aβ42 (9:1) (Kruskal-Wallis, H = 17.32, p-values = 0.0015 and 0.0029, respectively). There was no statistically significant difference between the other groups (Figure 20, A, S6). In the fibrillar group, there was no statistically significant difference in uptake between isoforms (Figure 20, B).

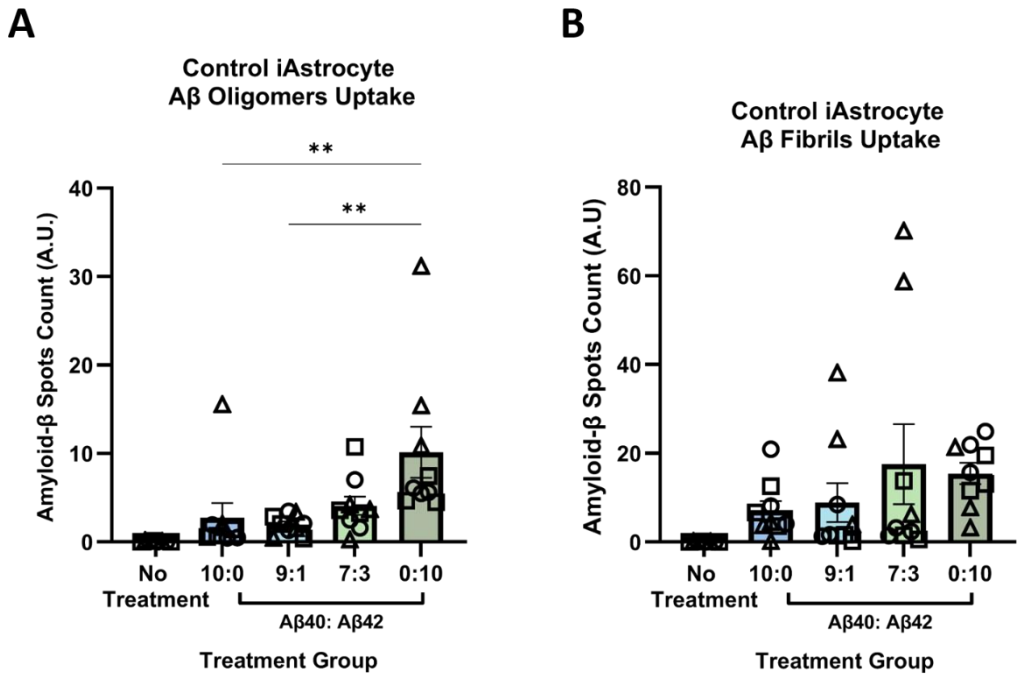

Figure 20. The uptake of Aβ in control iAstrocytes after 1-hour (2.5 μM) treatment. (A) *Aβ42 oligomers are taken up more than Aβ40 and Aβ40: Aβ42 (9:1) but not Aβ40: Aβ42 (7:3) in control iAstrocytes. (**B**) Aβ fibrils are not specifically taken up in control iAstrocytes. For iAstrocytes, each data point represents 3 technical repeats averaged into 1 biological repeat per line (total cell lines = 3). Data is visualised as mean ± S.D. Statistical analysis was completed using Kruskal-Wallis (**A**: H = 17.32, p-value = 0.0006) and **B**: H = 5.539, p-value = 0.1364). For oligomer post hoc analysis a Dunn's multiple comparisons test was performed. Post hoc analysis was not completed for fibrils due to overall Kruskal-Wallis displaying as non-significant. Where there are no statistical lines = non-significant (ns), * p-value = <0.05, ** p-value = <0.01, *** p-value = <0.001*, and **** *p-value = <0.0001.*

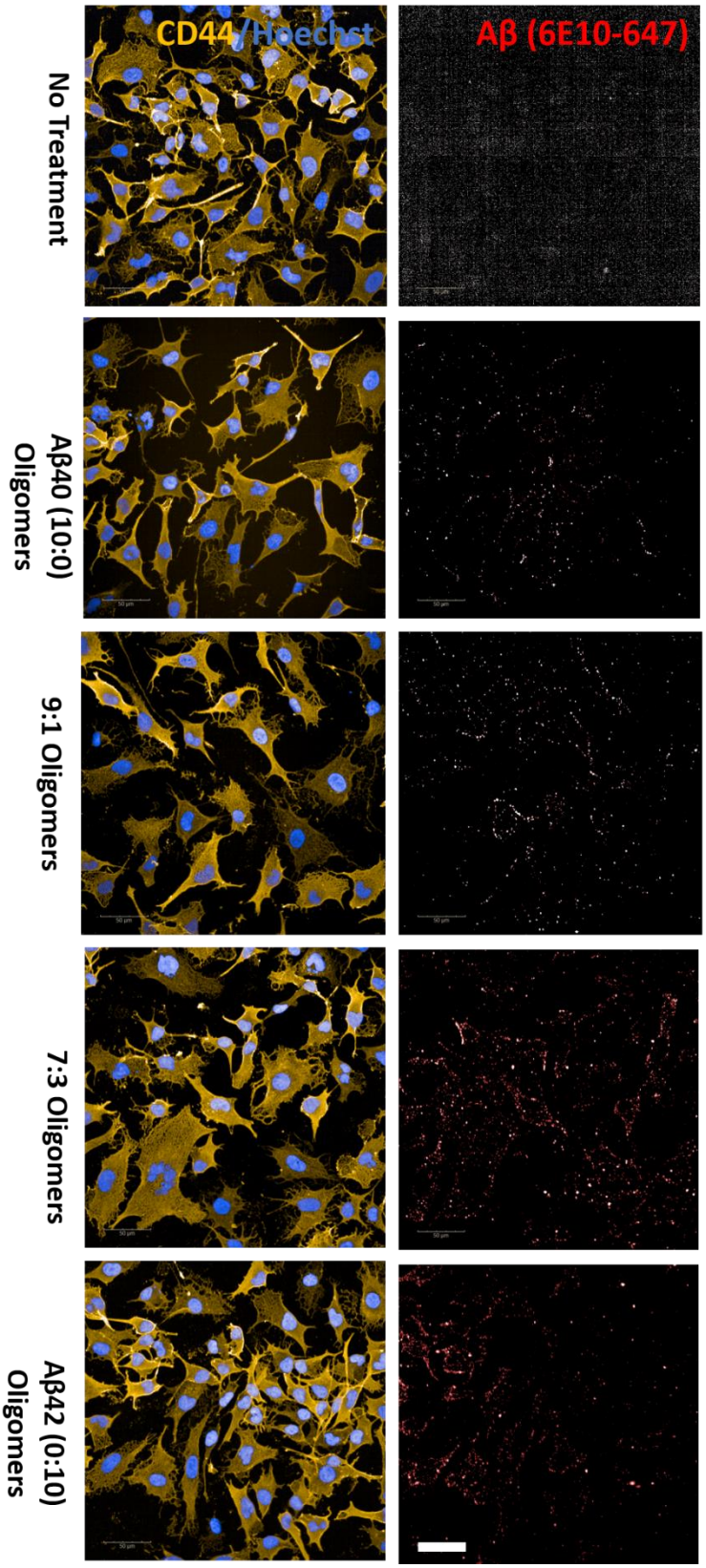

Figure 21. Illustrations of control iAstrocytes after Aβ (2.5 μM) oligomers treatment using immunocytochemistry. *CD44 (yellow), Hoechst (blue), and Aβ (6E10-Alexa 647 nm, red). Scale bar (50 μm).*

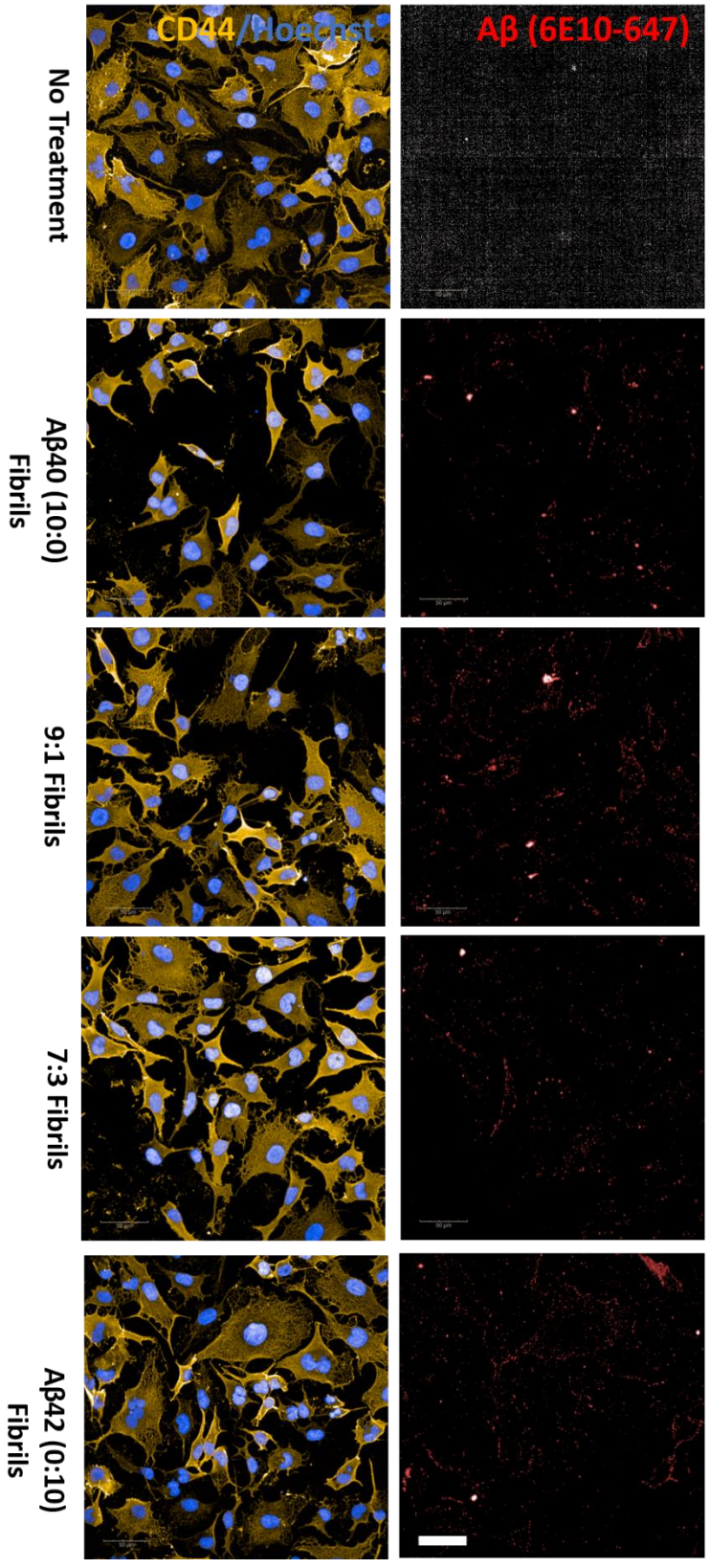

Figure 22. Illustrations of control iAstrocytes after Aβ (2.5 μM) fibrils treatment using immunocytochemistry. *CD44 (yellow), Hoechst (blue), and Aβ (6E10-Alexa 647 nm, red). Scale bar (50 μm).*

4.3.2.2. The Uptake of Aβ in AD iAstrocytes

As for AD iAstrocytes, Aβ42 (0:10) oligomer uptake was significantly higher than Aβ40: Aβ42 (9:1) and Aβ40: Aβ42 (7:3) (ANOVA, F= 8.214, p-values = 0.001 and 0.0007) (Figure 23, A). Though there was a trend of higher uptake of Aβ40 compared to Aβ40: Aβ42 (7:3) and Aβ40: Aβ42 (9:1), there was no statistically significant difference between the groups (S7). In the fibrillar group, though there was a trend to increased uptake as the ratio to Aβ42 to Aβ40, it was not statistically different (Kruskal-Wallis, H = 0.0572, Figure 23, B).

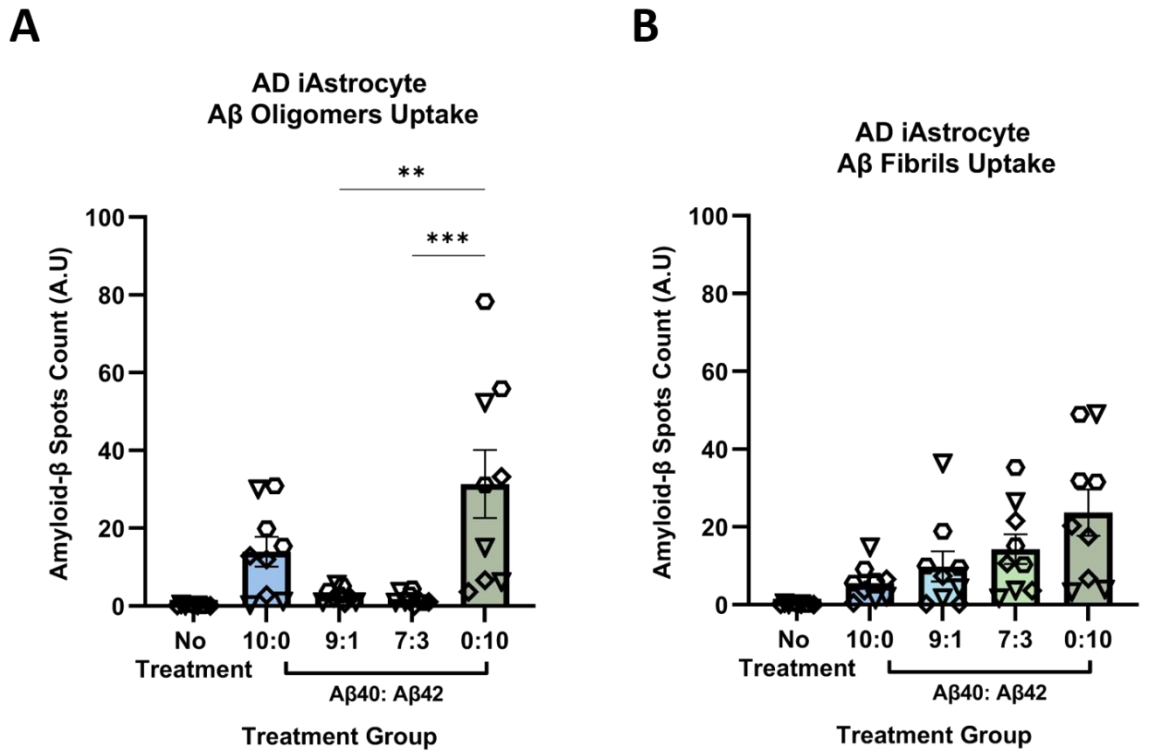

Figure 23. The uptake of Aβ in AD iAstrocytes after 1-hour (2.5 μM) treatment. A. *Aβ42 oligomers are up-taken more than Aβ40: Aβ42 (9:1 and 7:3), and no treatment but not Aβ40 (10:0).* ***B.*** *Aβ fibrils are not specifically up-taken in control iAstrocytes. For iAstrocytes, each data point represents 3 technical repeats averaged into 1 biological repeat per line (total cell lines = 3). Data is visualised as mean ± S.D. Statistical analysis was completed using ANOVA (**A**; F= 8.214, p-value = 0.0003). For oligomer post hoc analysis a Tukey's multiple comparison test was performed. Post hoc analysis was not completed for fibrils due to overall Kruskal-Wallis displaying as non-significant. Where there are no statistical lines = non-significant (ns), * p-value = <0.05, ** p-value = <0.01, *** p-value = <0.001, and **** p-value = <0.0001.*

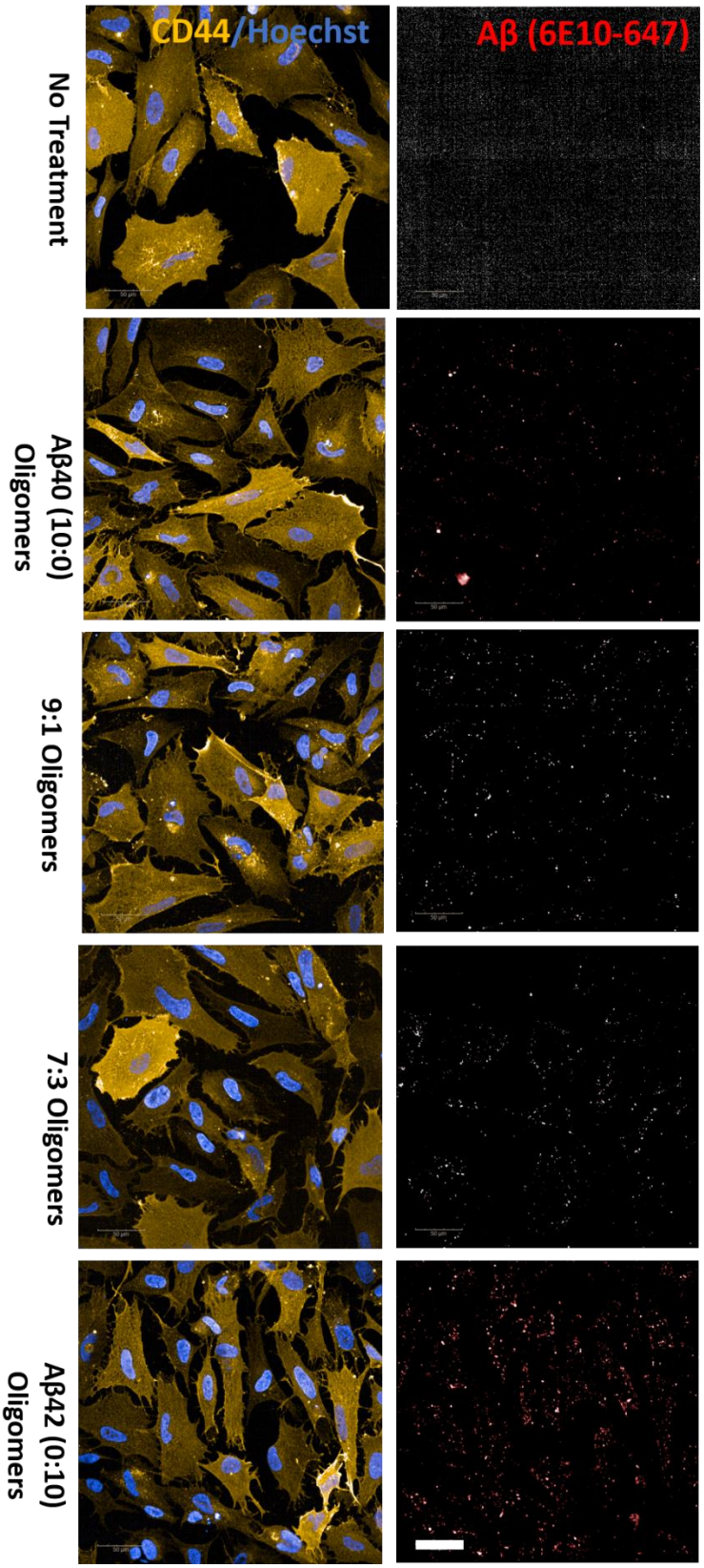

Figure 24. Illustrations of AD iAstrocytes after Aβ (2.5 μM) oligomers treatment using immunocytochemistry. *CD44 (yellow), Hoechst (blue), and Aβ (6E10-Alexa 647 nm, red). Scale bar (50 μm).*

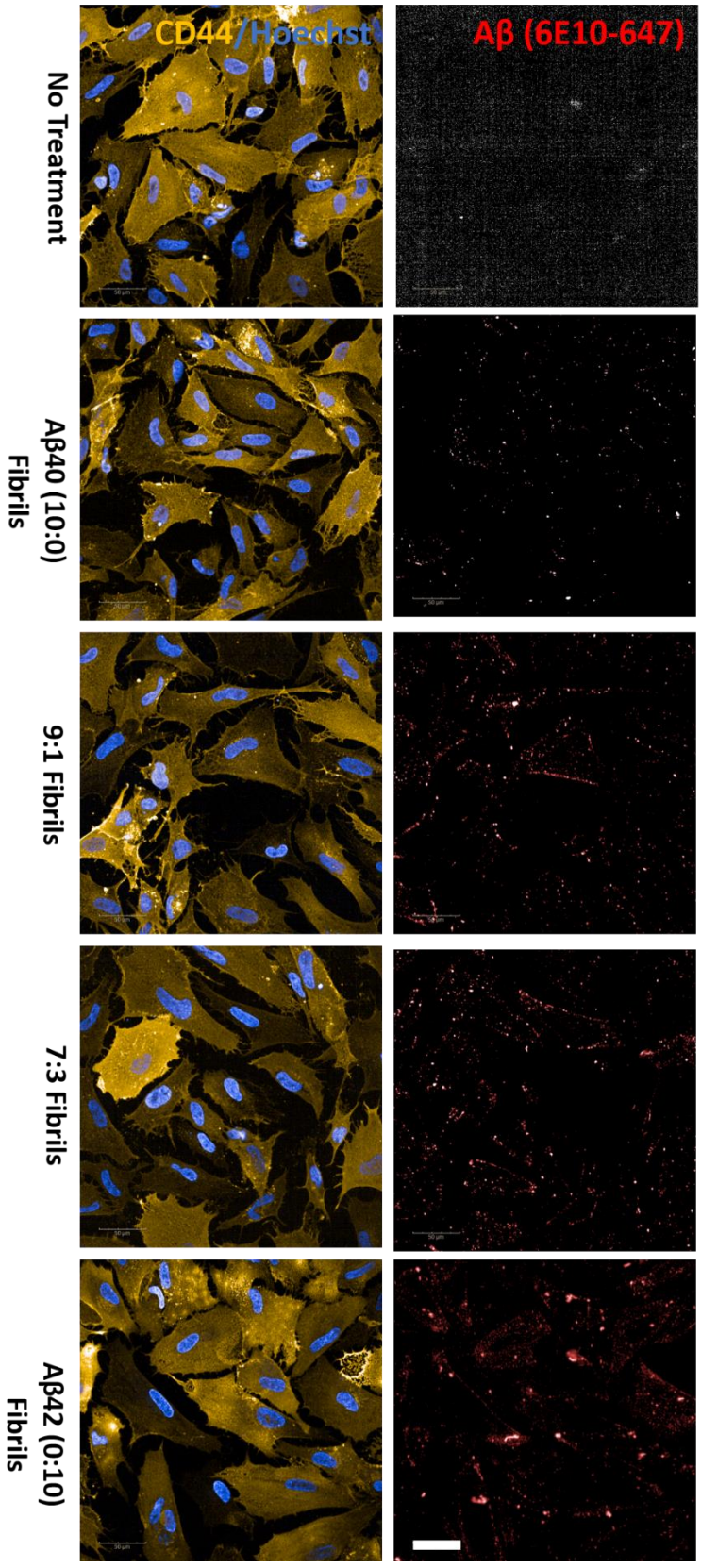

Figure 25. Illustrations of AD iAstrocytes after Aβ (2.5 μM) fibrils treatment using immunocytochemistry. *CD44 (yellow), Hoechst (blue), and Aβ (6E10-Alexa 647 nm, red). Scale bar (50 μm).*

4.4. Discussion

4.4.1. Establishing a system for mimicking Aβ Uptake

To better understand the uptake of Aβ isoforms and different aggregation states, a robust system that closely mimicked Aβ aggregate species was required. Aβ aggregation is a highly complex and dynamic process involving the transition of monomeric Aβ peptides into soluble oligomers, which further assemble into insoluble fibrils and ultimately form amyloid plaques. Although the mechanisms of Aβ aggregation in the human brain remain largely unknown, *in vitro* aggregation assays using recombinant protein have enabled the rate of amyloid aggregation to be modelled kinetically in a controlled and reproducible manner. A sigmoidal reaction course follows this process in three distinct phases: lag, exponential rise, and stationary plateau phase (or saturation) (Soto and Pritzkow, 2018).

In kinetically modelled Aβ aggregation, a slow and thermodynamically unfavourable lag phase is followed by a rapid exponential rise. Finally, the reaction rate declines due to the declining soluble species at the stationary phase (Knowles et al., 2014) (Figure 17). The lag phase represents a slow, thermodynamically unfavourable stage, where monomeric Aβ peptides gradually accumulate, interact, and begin to misfold (Niu et al., 2024). During this, primary nuclei form, a process that occurs at a low rate due to the thermodynamic barrier associated with nucleation (Arosio et al., 2015). Although inefficient, primary nucleation provides the foundation for further aggregation, leading to the formation of small and unstable Aβ oligomers. Once these initial nuclei form, aggregation enters the exponential phase, where elongation and secondary nucleation mechanisms drive the rapid conversion of monomers into higher-order aggregation.

In humans, monomeric Aβ is cleaved from APP and released into the extracellular space, where it can become misfolded, unstable, and prone to aggregation to attain structural stability (Kumar et al., 2016; Ueno et al., 2014). Once aggregation is initiated and the elongation phase begins, the depletion of monomeric species characterises it as they transition into higher-order structures (Cremades and Dobson, 2018). This phase progresses rapidly, initially marked by the formation and accumulation of oligomers, followed by the assembly of protofibrils, ultimately leading to mature fibril formation. Towards the end of the elongation phase, aggregation slows as the reaction reaches the stationary phase,

where soluble Aβ species are depleted, and fibrils dominate the aggregate population (Niu et al., 2024). Throughout the aggregation process, Aβ undergoes significant structural rearrangements. However, Aβ is a largely intrinsically disordered protein, and common methods to determine the structure of Aβ have proven difficult (Chen et al., 2017). Despite this, studies have shown that Aβ monomers are undefined coil-like structures that consist of a-helixes (Yang et al., 2022a). As aggregation progresses, these α-helical regions begin to fold into a secondary structures consisting of β-sheets commonly believed to be oligomers. As aggregation continues, the β-sheets are further arranged into more stable cross-β sheets, a core characteristic of Aβ fibrils (Niu et al., 2024). It is the exploitation of the formation of β-sheets during aggregation which allowed for the establishment of mimicking aggregation in this study.

ThT is a fluorescent dye with a high affinity for β-sheets and is used to monitor aggregation kinetics in real-time for Aβ and other peptides such as alpha-synuclein, Tau, and TDP-43 (Xue et al., 2017). As oligomeric species begin to form, indicated by detectable β-sheets at the end of the lag phase into the elongation phase, the intensity of ThT increases (Figure 26, T1). As aggregation progresses further, ThT intensity plateaus, marking the transition to the stationary phase, where the reaction slows as soluble monomers are depleted and fibrillar aggregates dominate (Figure 26, T2) (Rusakov et al., 2024). Given the complexity of Aβ aggregation dynamics, specific time points were selected to isolate different aggregate species. Oligomers were collected at the end of the lag phase; a time point previously shown to contain a higher proportion of soluble oligomers. However, small protofibril species may also be present. While mid-aggregation time points contain even higher oligomer content, they also include a larger fraction of fibrillar species, making the end of the lag phase the optimal time point for enriching oligomeric Aβ species. For fibrils, samples were taken at the plateau phase of aggregation, a stage previously confirmed to contain mature, stable fibrils.

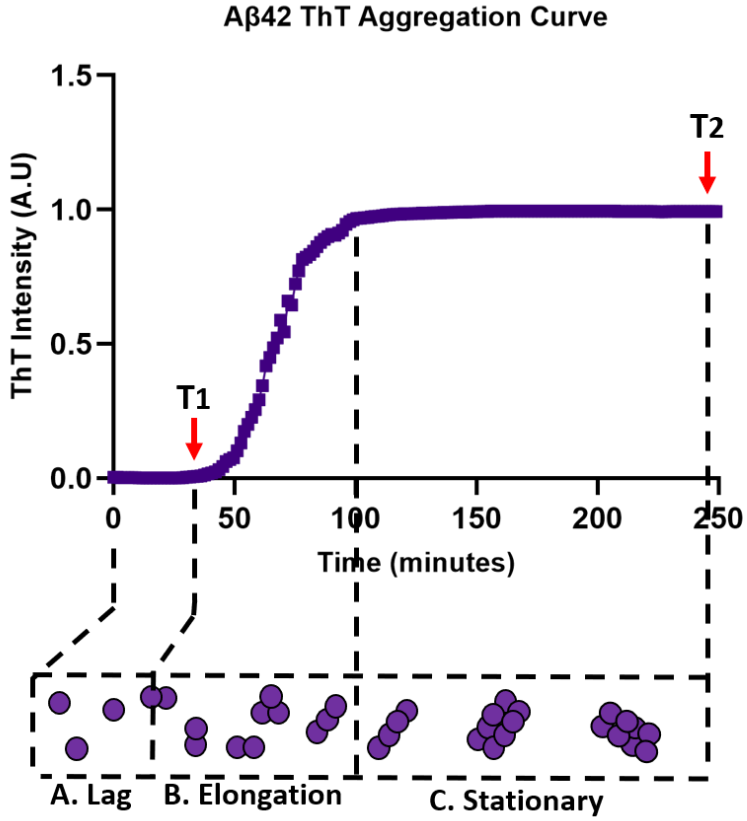

Figure 26. In vitro kinetic model of Aβ aggregation visual explanation using Aβ42. *The rate of Aβ is modelled kinetically in a sigmoidal reaction course in three distinct phases: lag, exponential, and stationary using Thioflavin T (ThT) intensity (A.U.) (excitation = 450 nm, emission = 482nm).* ***A****. Lag phase where monomeric Aβ peptides begin to accumulate for stability. As oligomeric species begin to form, indicated by detectable β-sheets at the end of the lag phase into the elongation phase, the intensity of ThT begins to increase (T1)* ***B.*** *The elongation phase is represented by a depletion of monomeric species and an increased concentration of oligomers, protofibrils and fibrillar species.* ***C****. The intensity of ThT begins to plateau, indicating the rate of the reaction declining as a result of the decline in soluble species and the formation of insoluble fibrils (T2). Aβ42 (0:10) (50 μM) aggregation curve is shown in this figure. Sample points for oligomers (T1) and fibrils (T2) sampling are shown.*

The results from the ThT aggregation assay show that Aβ42 (0:10) aggregates at a faster rate than Aβ40 (10:0) (Figure 17). Aβ40 is a 40-residue peptide compared to Aβ42, which has 42 residues. These two additional amino acids at the C-terminus are believed to be contributing factors to the difference in the aggregation rate of Aβ42. Firstly, Aβ42 has a higher hydrophobicity than Aβ40, making Aβ42 more prone to aggregation (Lin et al., 2019). The C terminus has a reduced entropy, meaning that Aβ42 requires less energy to aggregate due to the rigidity, which promotes β-sheet formation (Phan and Schmit, 2022; Yan and Wang, 2006). As a result, Aβ42 monomers are more likely to aggregate into soluble oligomers, which have a fast aggregation rate (Vadukul et al., 2020). Furthermore, the end C-terminus of Aβ42 has been shown to act as a site that facilitates the seeding of more aggregation and produces an increased oligomer population (Mei et al., 2022). Oligomers then interact with receptors and inhibit neurotransmitter release in the neurones of mice in the hippocampus (Mei et al., 2022).

In addition to Aβ42 exhibiting a faster aggregation rate, the aggregation assay indicates that increasing the proportion of Aβ42 accelerates the overall aggregation process (Figure 17). It is important to note that it is widely debated if Aβ42 speeds up the aggregation rate or if Aβ40 slows down the aggregation rate. Earlier studies have shown that the aggregation rate is affected and is determined by increasing Aβ42 ratios that speed up aggregation (Kuperstein et al., 2010). Interestingly, the changes in Aβ40: Aβ42 had a significant impact on the neurotoxicity of aggregates produced both *in vitro* and *in vivo*, with increased Aβ42: Aβ40 ratios driving acute synaptic dysregulation (Kuperstein et al., 2010).

The results of the ThT assay in this body of work highlight that in terms of aggregation mechanisms, Aβ42 and Aβ40 influence each other during aggregation (Figure 17). One reason studying Aβ peptide interaction during its coaggregation is difficult is its intricate structure, which is hypothesised to be intrinsically unstructured and unstable. Therefore, standard crystallisation methods to stabilise it are not easy (Chen et al., 2017). Studies have shown that though the kinetics are affected by the presence of each peptide, fibrils formed during aggregation have distinct homogenous populations (Cukalevski et al., 2015). Instead, Aβ40 and Aβ42 interact during the primary nucleation stage, whereby oligomeric species are formed but separate at the fibrillar stages (Cukalevski et al., 2015). However, studies have shown that Aβ40 and Aβ42 interact to form mixed aggregates both at the oligomeric and fibrillar stages (Gu and Guo, 2021; Gu and Guo, 2013).

Furthermore, it has been highlighted that Aβ40 has an inhibitory effect on Aβ42 fibril formation, which is counteracted by increasing Aβ42 ratios (Jan et al., 2008). Others have shown that Aβ40 fibrils act as seeds and promote Aβ42 aggregation (Tran et al., 2017). The opposing results between studies highlight the complex nature of Aβ40: Aβ42 aggregation. The notion that Aβ40 and Aβ42 interact during aggregation is supported by the TIRF imaging in this chapter, which shows that Aβ40 and Aβ42 fibrils co-aggregate together (Figure 18, C). This, coupled with the rate of aggregation being influenced by the ratio of Aβ40: Aβ42 suggest that these peptides do interact with one another. However, for the scope of this thesis, further investigation into the molecular basis of their interaction was not pursued. Instead, ThT aggregation curves were used to define aggregate species, which were then characterised using high-resolution imaging techniques to gain insights into individual Aβ species, aggregates were further visualized using TIRF microscopy-based single-molecule imaging. TIRF microscopy was employed to detect individual aggregates in the coverslip surface, whereby oligomeric species sampled at the end of the phase represent typical oligomer structures with smaller spherical compact clusters (Figure 18, A). Fibrils sampled at the stationary phase, compared to oligomers, are larger and have an extended chain structure (Schmit et al., 2011; Ahmed et al., 2010) (Figure 18, B). However, the use of TIRF and ThT kinetics for characterisation of Aβ species is restricted as it gives limited information about the structural aspects of the aggregate species themselves. For example, in Figure 16, B, the Aβ40 are long fibrils, whilst the Aβ42 fibrils appear to be more punctuated, driving implications of what species were present within the samples. To overcome this limitation, future work should focus on more characterisation of the different Aβ species through methods such as Transmission Electron Microscopy, Cryo-electron Microscopy, Nuclear Magnetic Resonance Spectroscopy, and Atomic Force Microscopy, which provide high-resolution qualitative information for different Aβ structures (Matuszyk et al., 2022). On the other hand, circular dichroism (CD) is often used in the analysis of the tertiary structure of Aβ (Bruggink et al., 2012). Similar to ThT, it utilises the formation of β-sheets formed during aggregation, and has been shown to correspond with ThT kinetics, and therefore would have been a good complementary method to confirm further oligomeric and fibrillar species used in this thesis.

4.4.2. The Uptake of Aβ in iAstrocytes

The next objective in the chapter was to determine the extent of the uptake of Aβ40 and Aβ42 isoforms in varying ratios using human iAstrocytes. Previously, the uptake of specific species of Aβ (Aβ40 and Aβ42), and isoform (oligomers and fibrils) remains largely unexplored in human-derived astrocytes. In this study, iAstrocytes, in both control and AD lines, Aβ is taken up regardless of species or ratio. In control lines, when iAstrocytes were treated with Aβ oligomers, Aβ42 (10:0) were up taken significantly more than both Aβ40 (10:0) and Aβ40: Aβ42 (9:1), but not Aβ40: Aβ42 (7:3), suggesting a preferentially uptake to Aβ42 (10:0) oligomers. However, there was no trend or significant difference in the uptake of Aβ fibrils, suggesting that there is no strong preferential uptake of Aβ species in control astrocytes. In AD patient-derived models, when iAstrocytes were treated with Aβ oligomers, Aβ42 (0:10) was taken up significantly more than both Aβ40: Aβ42 9:1 and 7:3, but not Aβ40 oligomers. On the other hand, Aβ40 was not taken up significantly more than Aβ40: Aβ42 9:1 and 7:3, indicating that Aβ42 oligomers are preferentially taken up by AD astrocytes. After the treatment of Aβ fibrils, there was an overall trend that the uptake also increased as the ratio to Aβ42: Aβ40 was increased. However, this was not statistically significant, indicating that similar to control iAstrocytes, Aβ fibrils are not preferentially taken up compared to each other. Interestingly, a common trend in both control and AD iAstrocytes is that Aβ42 oligomers are taken up more readily overall than the other species. This is an interesting and unexpected finding as Aβ42 is the main component of plaques, despite Aβ40 being 10 times more abundant (Gu and Guo, 2013). Aβ is produced and removed continuously in the brain, and it is hypothesised that a chronic imbalance between production and clearance leads to cells becoming overloaded and dysfunctional (Behl, 2024; Abanto et al., 2024; Hampel et al., 2021; Tarasoff-Conway et al., 2015b; Saido and Leissring, 2012). To optimise this assay, a higher concentration of Aβ could evaluate if an overload of Aβ would cause a substantial difference in the uptake. However, *in vivo*, concentrations of Aβ have shown to be picomolar compared to the 2.5 μM concentrations used in this study. Therefore, increasing the concentration of Aβ in this case would be less reflective of AD physiological conditions. The results in this study show the acute internalisation of Aβ after 1-hour treatment; therefore, chronic treatment of Aβ over different time points may have helped to elude differences, particularly in the uptake of Aβ42 fibrils, which may have

decreased over time. However, when the astrocytes were treated for 24 and 48 hours with Aβ42, they could not be analysed due to prominent cell death (Figure 19). This further highlights the toxicity of Aβ42 and the need for optimising the chronic treatment of Aβ in this context. Future experiments would be interesting to compare different time points of post-treatment aggregate build-up in iAstrocytes.

It is also important to note that large variability is seen between cell lines when evaluating the uptake of Aβ. One limitation of human-derived models is the large heterogeneity between individuals, leading to inherent variability (Reddin et al., 2023). The variability between cell lines highlights the complex nature of the populations, which may be affected differently during disease influenced by a magnitude of genetic and environmental differences. This study used 3 lines per group, and the sample size may have influenced the results. For example, when evaluating the uptake of Aβ in blood monocytes, a sample size of 13 control and AD patients was required to show that AD patients had reduced uptake (Chen et al., 2020). Therefore, the increased sample size in this study may have helped with variability and eluded the uptake of Aβ in iAstrocytes.

Next, one of the key roles of astrocytes in the brain is to regulate brain homeostasis and clear debris and toxins from the brain. Aβ is considered pathological, and in particular, Aβ42 is regarded as the most toxic form (Phillips, 2019; Song et al., 2022; Vadukul et al., 2020). As a result, the iAstrocytes preferentially uptake Aβ42 as a protective mechanism to reduce extracellular Aβ burden, preventing neighbouring neuronal damage, and regulate homeostasis and maintain healthy balance (Giusti et al., 2024; Ries and Sastre, 2016a). Though the uptake, clearance, and degradation of Aβ in astrocytes is beneficial to cells initially, the uptake of aggregates has been shown to have toxic effects. Firstly, Aβ aggregates are readily internalised by astrocytes but are not effectively degraded for up to 10 weeks in iPSC cell culture (Konstantinidis et al., 2023a). Furthermore, in the co-culture of astrocytes and cortical neurones, astrocytes rapidly phagocytosed Aβ42 but do not readily degrade it (Sollvander et al., 2016). As a result, astrocytes exhibited severe lysosomal dysfunction and micro-vesicles containing Aβ, which induced apoptosis on the neurones (Sollvander et al., 2016). Others have shown that exposure to Aβ42 but not Aβ40 induces a reduced metabolism response in astrocytes, such as reduced glucose uptake, glycolysis, and increased oxidative stress (Allaman et al., 2010).

Furthermore, Aβ42 oligomers' internalisation has been linked to receptor-mediated

toxicity, protein synthesis impairment, and membrane dysfunction (Vadukul et al., 2020; Maina et al., 2018; Sengupta et al., 2016). This is particularly interesting as the Aβ42 oligomers were significantly taken up in this study in AD astrocytes (Figure 20 and 23, A). Given that AD and control astrocytes significantly took up Aβ42 oligomers in this study, it remains an open question, whether this increased uptake contributes to increased astrocyte dysfunction in AD. Next, astrocytes have been proposed to have several clearance and degradation pathways of Aβ pathways. Therefore, the next logical step was to investigate the mechanisms of Aβ clearance and astrocyte degradation to determine whether these processes differ between control and AD lines.

4.4.3. Clearance and Degradation of Aβ by Astrocytes

There have been multiple proposed pathways associated with *A*β degradation and clearance. This includes but not limited to membrane-associated Aβ, which is targeted by an extensive network known as the protein quality control (PQC) system. The PQC system consists of molecular chaperones, lysosomes, proteases, and endosomes, which degrade and remove proteins via the ubiquitin-proteasome system or the autophagy autophagy-lysosome system, respectively (Xin et al., 2018). Alternatively, soluble extracellular Aβ can be degraded through cellular uptake by cell surface enzymatic pathways (Baranello et al., 2015). For example, Neprilysin is an enzyme that functions to breakdown of proteins and in particular, has been shown to metabolise Aβ (Kim et al., 2023a; Davis et al., 2021; Vodovar et al., 2015).

In healthy individuals, Neprilysin has a role in the degradation of Aβ in both the CSF and deposits in the brain alongside other proteases such as ACE, ECE-1, and IDE, but Neprilysin was most effective (Vodovar et al., 2015). Earlier studies have shown that the expression of Neprilysin was lower in high plaque areas of AD brains (Caccamo et al., 2005; Yasojima et al., 2001). In APP transgenic mice, reduced Neprilysin function is associated with the toxicity of Aβ oligomers, which induce dysfunctional synaptic plasticity in neurones and promote plaque formation (Watamura et al., 2024). Neprilysin is highly expressed in astrocytes (Yamamoto et al., 2022), which was confirmed in this study through immunocytochemistry staining (S1). Interestingly, the localisation of the positive Neprilysin staining mimics the location of the Golgi apparatus (S1). Neprilysin is synthesised in the Golgi apparatus but is transported to the membrane to act as a peptidase secreted into the extracellular space to

break down proteins (Baranello et al., 2015). Secreted Neprilysin has been shown to degrade Aβ monomers and aggregates (Rofo et al., 2022). The ICC staining was carried out on iAstrocytes in quiescent conditions. Therefore, the localisation of Neprilysin in the iAstrocytes not being at the membrane may be because it is not being synthesised due to lack of stimulus. Future experiments should examine Neprilysin expression and localisation following Aβ treatment and its co-localisation with the Golgi apparatus to determine whether astrocyte-mediated clearance mechanisms are altered in AD. Furthermore, the lack of Neprilysin at the membrane has other implications for the cell model used in this thesis. Whilst the direct programming method has several advantages, it raises questions of the functional aspect of iAstrocytes that may not be fully recapitulated after direct conversion. Previous studies have shown that directly reprogrammed cells can have an immature or incomplete functional maturation (Qian and Srivastava, 2013). For example, directly converted neurones have been shown to express neuronal markers and marked neuronal electrophysiology, but fail to form stable synaptic networks (Qian and Srivastava, 2013). As a result, future work to further validate the functional properties of iAstrocytes in an important future step.

Next, besides enzymatic pathways, as part of astrocytes regulation of clearance, they utilise receptor-mediated endocytosis and phagocytosis (Ries and Sastre, 2016b). For example, low-density lipoprotein receptor-related protein 1 (LRP1) is an endocytic/signalling receptor on the cell surface of cells which binds to over 40 ligands and proteins (Zhou et al., 2024; Shinohara et al., 2017). When activated, LRP1 produces vesicles which surround the ligand or protein, resulting in the internalisation into the cell (Chen et al., 2022). In the hippocampus, entorhinal cortex, and cerebellum, the expression of LRP1 is high in neurones, areas which are affected in AD (Shinohara et al., 2017). Additionally, LRP1 is expressed in astrocytes and microglia due to their role in clearing debris from the brain. In the context of AD, LRP1 is a major receptor for apolipoprotein E (APOE), a protein which regulates cholesterol and fats. The APOE gene has several alleles, including APOE2, APOE3, and APOE4, with APOE4 being one of the strongest genetic risk factors for AD (Shinohara et al., 2017). As LRP1, APOE, and Aβ have all been shown to interact (Tachibana et al., 2019), one next step in this thesis was to investigate the expression of LRP1 in astrocytes.

Similarly, another receptor of interest was the triggering receptor expressed on myeloid cells 2 (TREM2). TREM2 plays an important role in the phagocytosis of debris such as Aβ

(Deczkowska et al., 2020). In microglia, TREM2 dysfunction of TREM2 prevents the clearance of Aβ deposits in the brain and increases neuronal damage (Huang et al., 2023). It has been described that loss-of-function gene variants in TREM2 are another associated risk factor for AD (Kiianitsa et al., 2024). TREM2 has also been documented to be expressed in astrocytes, similar to LRP1; the next step was to investigate TREM2 expression in astrocytes. The ICC staining for LRP1 and TREM2 was completed on the same plate. As part of the analysis, secondary antibodies were used to control for non-specific background noise. During this experiment, the Alexa FluorTM was non-specifically bound to the nucleus regions of the cells (S2, S3, S4, and S5). Therefore, the specific binding of LRP1 and TREM2 could not be entirely determined.

4.5. Conclusions

By establishing a system for mimicking Aβ aggregation, the results of this chapter show that control and AD astrocytes have a substantially preferential uptake of Aβ42 oligomer aggregates. The overall results in this chapter have added novel knowledge of how astrocytes in both healthy individuals and individuals with AD uptake different Aβ aggregate species, and show that astrocytes are involved with the cellular uptake of Aβ. In this chapter, a robust and optimised model was established to systematically study Aβ uptake in iAstrocytes, enabling a quantitative comparison of different Aβ isoforms (Aβ40 vs Aβ42) and aggregation states (oligomers vs fibrils). Using multiple patient-derived and control iAstrocyte lines provided insights into the dynamics of Aβ internalisation. The findings demonstrate that control and AD iAstrocytes efficiently internalise Aβ aggregates, regardless of species or aggregation state. However, key differences emerged in how these astrocytes processed Aβ. Control and AD iAstrocytes exhibited a strong preference for Aβ42 oligomers, but no isoform or aggregation state for fibrils, suggesting that astrocytes internalise Aβ fibrils through a non-selective mechanism. Since impaired Aβ clearance is a hallmark of sporadic AD, these results suggest that the underlying issue may not be solely due to reduced Aβ uptake but rather a complex interplay of multiple factors. The preferential internalisation of Aβ42 species may reflect a compensatory clearance mechanism. In contrast, internalisation could contribute to cellular stress and dysfunction,

to exacerbated disease pathology. Overall, this chapter establishes a novel model to study Aβ aggregation, and provides a valuable framework for future research into astrocyte-mediated Aβ uptake.

Chapter 5. The Induction of Pro-inflammatory Markers in iAstrocytes after Aβ Treatment

5.1. Chapter Overview

In the previous chapter, the uptake of different Aβ40 and Aβ42 isoforms, as well as oligomeric and fibrillar forms, were evaluated (Chapter 4, pp., 74-99). In addition, it was assessed how varying Aβ40: Aβ42 ratios influence astrocytic uptake. One unexplored aspect is how different Aβ aggregates induce neuroinflammatory responses due to interaction with astrocytes. The next step was to evaluate how different Aβ species interact with astrocytes to drive inflammatory responses via pro-inflammatory cytokines/chemokines; MCP-1, IL-1β, IL6, and TNF-α, and changes in expression of GFAP, CD44, and Vimentin. Identifying specific induction of pro-inflammatory markers as a result of Aβ species will be essential for deciphering the role of glial dysfunction in AD progression. This chapter discusses the induction of pro-inflammatory markers and potentially downstream pathways associated with them.

5.2. Introduction

As a general definition, inflammation is a natural defence mechanism in both the peripheral and central nervous systems (CNS). It can be initiated in response to various stimuli such as injury, illness, or stress. Inflammation in the CNS (neuroinflammation) aids in protecting, repairing, and removing pathogens, debris, or toxins in the brain. Microglia and astrocytes, the resident glial cells, have a critical role in regulating neuroinflammation (DiSabato et al., 2016). Neuroinflammation is considered to be a pathological hallmark of neurodegenerative conditions such as PD, ALS, and AD (Botella Lucena and Heneka, 2024; Tansey et al., 2022; Komine and Yamanaka, 2015). In recent years, studies have found that the activation of glial cells is an early sign of AD, preceding the histopathological and pathological features that can be detected in the brain (Botella Lucena and Heneka, 2024). As part of the activation process, astrocytes undergo several morphological, transcriptional, and physiological changes and are referred to as reactive astrocytes (Singh, 2022). Reactive astrocytes exert changes in cell morphology, including increased size, extended branching, and elongation

(Singh, 2022; Cheng et al., 2019). Morphological changes in astrocytes are accompanied by the increased expression of GFAP, Vimentin, and CD44, common markers of reactive astrocytes (Bradford et al., 2024; Konstantinidis et al., 2023a; Smit et al., 2021). Notably, reactive astrocytes are associated with elevated production of pro-inflammatory markers: cytokines and chemokines (Chen et al., 2024).

5.2.1. Cytokines and Chemokines as Pro-inflammatory Markers

Cytokines and chemokines are cell signalling molecules that provide cells with the ability to communicate and induce multicellular responses to stimuli (Botella Lucena and Heneka, 2024). In particular, Tumor Necrosis Factor-α (TNF-α), Interleukin-1-β (IL-1β), Interleukin-6 (IL6), and monocyte chemoattractant protein 1 (MCP1) upregulation are closely associated with AD (Liu et al., 2023). TNF-α, IL-1β, IL6, and MCP1 are major markers that regulate the human body's inflammatory response (Liu et al., 2023; Gonzalez Caldito, 2023). They are produced by several cells of the innate immune system: macrophages, T cells, NK cells, and neutrophils. They are also made in non-immune cells such as neurons, microglial, and astrocytes. Pro-inflammatory markers are essential in responding to infection, injury, or tissue damage. For example, in the brain, IL-1β plays a role in regulating synaptic activity and plasticity (Tsai, 2017). Studies have shown that in mice, it is readily expressed in the hippocampus, a region important for memory and learning, one of the areas affected in the early stages of AD (Takemiya et al., 2017).

The presence of elevated pro-inflammatory markers has been observed in both the early and late stages of AD, highlighting their critical role in disease progression (Deng et al., 2024; Wang et al., 2023; Chai et al., 2023). While TNF-α, IL-1β, IL6, and MCP1 are well-known inflammatory markers elevated in AD, their interplay with different aggregated Aβ species remains incompletely understood. Given that astrocytes have a key role in inflammation and are the most abundant type of glial cell, constituting approximately 40% of the mammalian brain (Zhou et al., 2019), their response to Aβ is crucial for understanding AD pathology. Since neuroinflammation often precedes amyloid plaque formation, understanding how different Aβ species - such as Aβ40, Aβ42, and their mixtures - trigger astrocyte inflammatory responses are essential for identifying early intervention targets. By studying how these Aβ species influence astrocytic reactivity, this chapter aims to clarify the molecular connections between Aβ aggregation, uptake, and neuroinflammation.

5.2. Hypothesis, Aims, and Objectives

5.2.1 Hypothesis

Astrocytes can become reactive to stressors such as Aβ as part of the inflammatory response and upregulate the expression and secretion of pro-inflammatory markers. In AD, pro-inflammatory chemokines and cytokines, TNF-α, IL-1β, IL6, and MCP1, are increased.

Hypothesis 1: The secretion of pro-inflammatory markers from both control and AD lines will be Aβ isoform dependent.

Hypothesis 2: There will be elevated pro-inflammatory markers in AD iAstrocytes compared to controls.

Hypothesis 3: The treatment of Aβ will result in increased expression of GFAP, Vimentin, and CD44 in both control and AD lines.

5.2.2. Aims

This chapter aimed to evaluate the induction of pro-inflammatory markers after the uptake of varying Amyloid-β aggregates in control and sporadic AD iAstrocytes. Identifying which Aβ compositions and aggregated states are the most potent in inducing astrocytic inflammation will aid in uncovering Aβ species that contribute to the positive feedback cycle between protein aggregation, clearance impairment, and inflammation. This will provide insights into key mechanisms that exacerbate AD pathology and may inform therapeutic strategies to break this cycle.

5.2.3. Objectives

1. Measure and evaluate the secretion of pro-inflammatory markers, TNF-α, IL-1β, IL6, and MCP1 after treatment with Aβ aggregates of varying species and ratios.

2. Assess whether patient-derived iAstrocytes exhibit a heightened inflammatory response compared to control iAstrocytes by measuring and comparing the secretion of TNF-α, IL-1β, IL6, and MCP1 in response to Aβ treatment.

3. Investigate the expression of GFAP, Vimentin, and CD44 in response to Aβ uptake, shedding light on how astrocytes respond to different Aβ species at the molecular level.

5.3. Results

This chapter aimed to evaluate the induction of pro-inflammatory markers after the uptake of varying Amyloid-β aggregates in control and sporadic AD iAstrocytes. Aβ species were derived from methods described in section 2.2.9. Post-treatment with Aβ (section 2.2.9), the iAstrocyte culture media was collected, and levels (pg/mL) of MCP-1, IL-1β, IL6 and TNF-α were measured by ELISA (section 2.2.10). This assay was completed in conjunction with results in Chapter 4, showing the direct link between uptake and pro-inflammatory markers. The differences in expression of GFAP, Vimentin, and CD44 were assessed by immunocytochemistry (section 2.2.6).

5.3.1. The Induction of Pro-Inflammatory Markers

5.3.1.2. The Induction of TNF-α in Control iAstrocytes after Treatment with Aβ

Oligomers

Control iAstrocytes showed a statistically significant increase in TNF-α after Aβ oligomer treatment (One-way ANOVA, Figure 27, A: F = 167.6, p-value = <0.0001). Compared to no Aβ treatment, Aβ40 (10:0), Aβ40: Aβ42 (9:1), Aβ40: Aβ42 (7:3), and Aβ42 (0:10) resulted in significant induction of TNF-α (p-values: <0.0001, <0.0001, <0.0001, and <0.0001), respectively. As the ratio of Aβ42: Aβ40 (7:3 and 0:10) increases, there is a significant rise in TNF-α compared to lower ratios (9:1 and 10:0) (p-values: <0.0001, 0.0003, <0.0001 and <0.0001). However, there was no significant difference between the Aβ40 and Aβ40: Aβ42 (9:1) (>0.9999).

Fibrils

Similarly, after the treatment with Aβ fibrils, there was a significant secretion of TNF-α (One-way ANOVA, Figure 27, B: F = 56.12, p-value = <0.0001). All Aβ treatment groups —Aβ40 (10:0), Aβ40: Aβ42 (9:1), Aβ40: Aβ42 (7:3), and Aβ42 (0:10) — induced higher TNF-α than the no-treatment group (p-values: <0.0001, <0.0001, <0.0001, and <0.0001). Aβ42 (0:10) resulted in statistically significant higher TNF-a than Aβ40 (10:0) and Aβ40: Aβ42 (9:1), but

not Aβ40: Aβ42 (7:3) (p-values; <0.0001, <0.0001, and 0.309). However, there was no difference between Aβ40 (10:0) and Aβ40: Aβ42 (9:1), whilst Aβ40: Aβ42 (7:3) drove a higher TNF-a than Aβ40: Aβ42 (9:1) (p-values; >0.9999 and <0.0001). Suggesting that higher Aβ42 concentrations are needed to drive more TNF-α secretion from iAstrocytes.

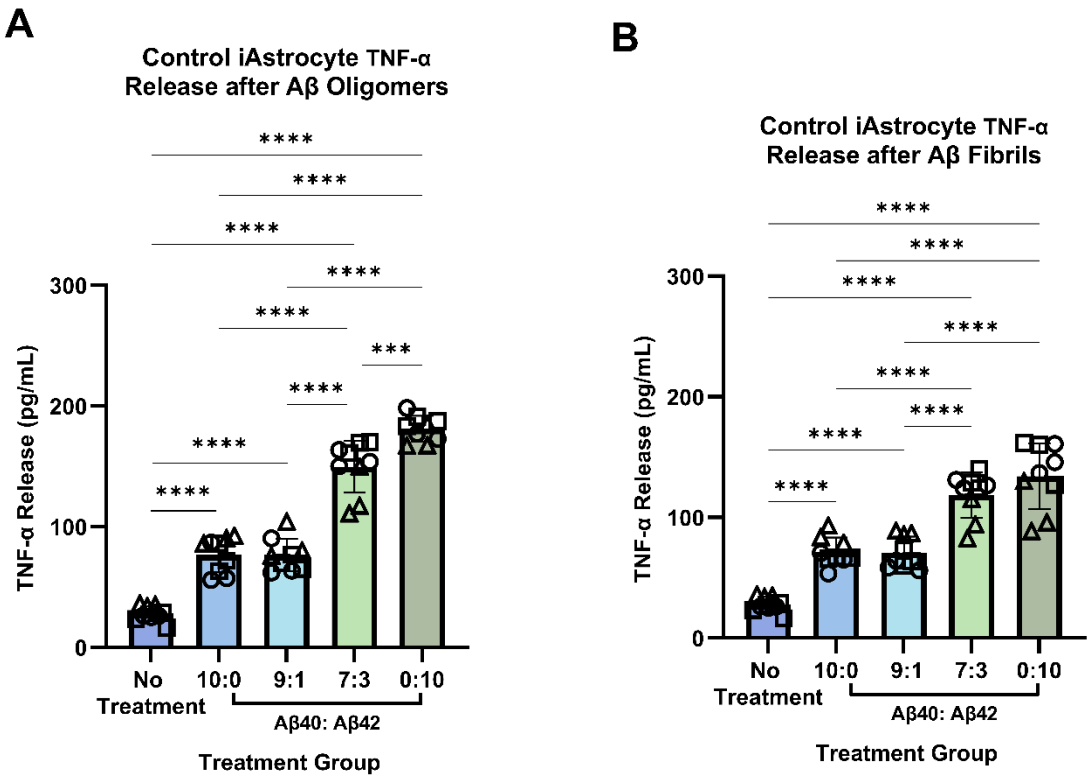

Figure 27. *The induction of TNF-α in control iAstrocytes after treatment with Aβ. Aβ oligomers (**A**) and Fibrils (**B**) result in the induction of TNF-α in control iAstrocytes, and isoform-specific differences in Aβ. For iAstrocytes, each data point represents 3 technical repeats averaged into 1 biological repeat per line (total cell lines = 3 per group). Data is visualised as mean ± S.D. Statistical analysis was completed using ANOVA (A; F = 167.6, p-value = <0.0001 and B; F = 56.12, p-value = <0.0001). Post-hoc analyses were completed using Tukey's multiple comparison and can be found in Tables 11 and 12. Where there are no statistical lines = non-significant (ns), * p-value = <0.05, ** p-value = <0.01, *** p-value = <0.001, and **** p-value = <0.0001.*

5.3.1.3. The Induction of TNF-α in AD iAstrocytes after Treatment with Aβ

Oligomers

The next objective was to compare the amount of TNF-α produced by AD iAstrocytes when treated with different oligomeric forms of Aβ. There were statistically significant increases in TNF-α (Welch's ANOVA, Figure 28, W = 187.5, p-value = <0.0001). All forms of oligomeric Aβ resulted in a significant increase of TNF-α compared to no treatment (p-values = <0.0001, <0.0001, <0.0001, and <0.0001), respectively. Aβ42 (0:10) resulted in higher induction than Aβ40 (10:0), Aβ40: Aβ42 (9:1), but not Aβ40: Aβ42 (7:3) (p-values = <0.0001, <0.0001, and 0.0766). Furthermore, Aβ40: Aβ42 (7:3) resulted in higher induction of TNF-α than Aβ40 (10:0) and Aβ40: Aβ42 (9:1) (p-values = <0.0001 and <0.0001). Finally, when comparing Aβ40: Aβ42 (9:1) and Aβ40 (10:0), there was no significant increase in TNF-α induction (p-value = 0.5857).

Fibrils

The study further evaluated TNF-α secretion in AD iAstrocytes after treatment with Aβ fibrils. Aβ40 (10:0), Aβ40: Aβ42 (9:1), Aβ40: Aβ42 (7:3), and Aβ42 (0:10) resulted in significant TNF-α induction compared to the untreated group (Welch's ANOVA, Figure 28, B; W = 64.66, p-values: <0.0001, <0.0001, <0.0001, and <0.0001, respectively). However, unlike the oligomeric Aβ species, no significant differences in TNF-α secretion were detected between the Aβ fibril isoforms, except for Aβ42 (0:10) compared to Aβ40 (10:0) and Aβ40: Aβ42 (9:1) (Table 14). These results suggest that while Aβ fibrils contribute to TNF-α induction, their impact is composition-dependent on oligomeric species and Aβ42, highlighting the more significant pro-inflammatory potential of soluble Aβ species and Aβ42 isoforms.

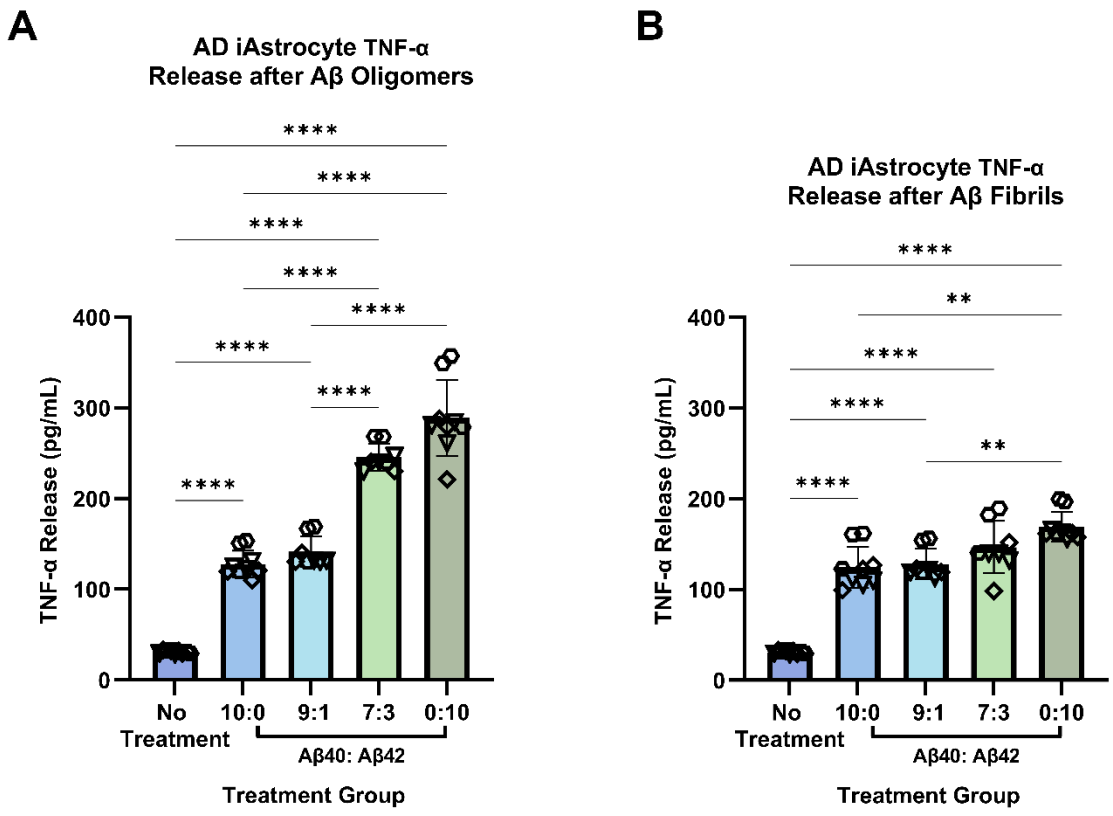

Figure 28. *The induction of TNF-α in AD iAstrocytes after treatment with Aβ oligomers (**A**) and Fibrils **(B**) see the secretion of TNF-α in control iAstrocytes, and isoform-specific differences in Aβ in oligomers and fibrils. For iAstrocytes, each data point represents 3 technical repeats averaged into 1 biological repeat per line (total cell lines = 3 per group). Data is visualised as mean ± S.D. Statistical analysis was completed using Welch's ANOVA (A; W= F = 187.5, p-value = <0.0001 and B; W = 64.66, p-value = <0.0001). Post-hoc analyses were completed using Dunnett's T3 multiple comparisons test comparison and can be found in Tables 13 and 14. Where there are no statistical lines = non-significant (ns), * p-value = <0.05, ** p-value = <0.01, *** p-value = <0.001, and **** p-value = <0.0001.*

5.3.1.4. The Induction of TNF-α in Control and AD iAstrocytes after Treatment with Aβ

Next, differences in TNF-α induction between control and AD iAstrocytes following treatment with Aβ oligomers and fibrils were examined by re-graphing the data presented in the previous sections (5.3.1 and 5.3.2). Following oligomeric treatment of Aβ40 (10:0), Aβ40: Aβ42 (9:1), Aβ40: Aβ42 (7:3), and Aβ42 (0:10), there was a statistically higher secretion of TNF-α in AD iAstrocytes than control (Figure 29, B-E, p-values = <0.0001, <0.0001, <0.0001, and <0.0001), suggesting a heightened inflammatory response in AD astrocytes. In addition, the fibrillar Aβ group exhibited a significant TNF-α induction observed in AD iAstrocytes after treatment with Aβ40 (10:0), Aβ40: Aβ42 (9:1), Aβ40: Aβ42 (7:3), and Aβ42 (0:10) (Figure 29, F-I: p-values = <0.0001, <0.0001, 0.0267 and 0.0044). These results indicate that both Aβ oligomers and fibrils are more potent inducers of TNF-α in AD astrocytes compared to control iAstrocytes.

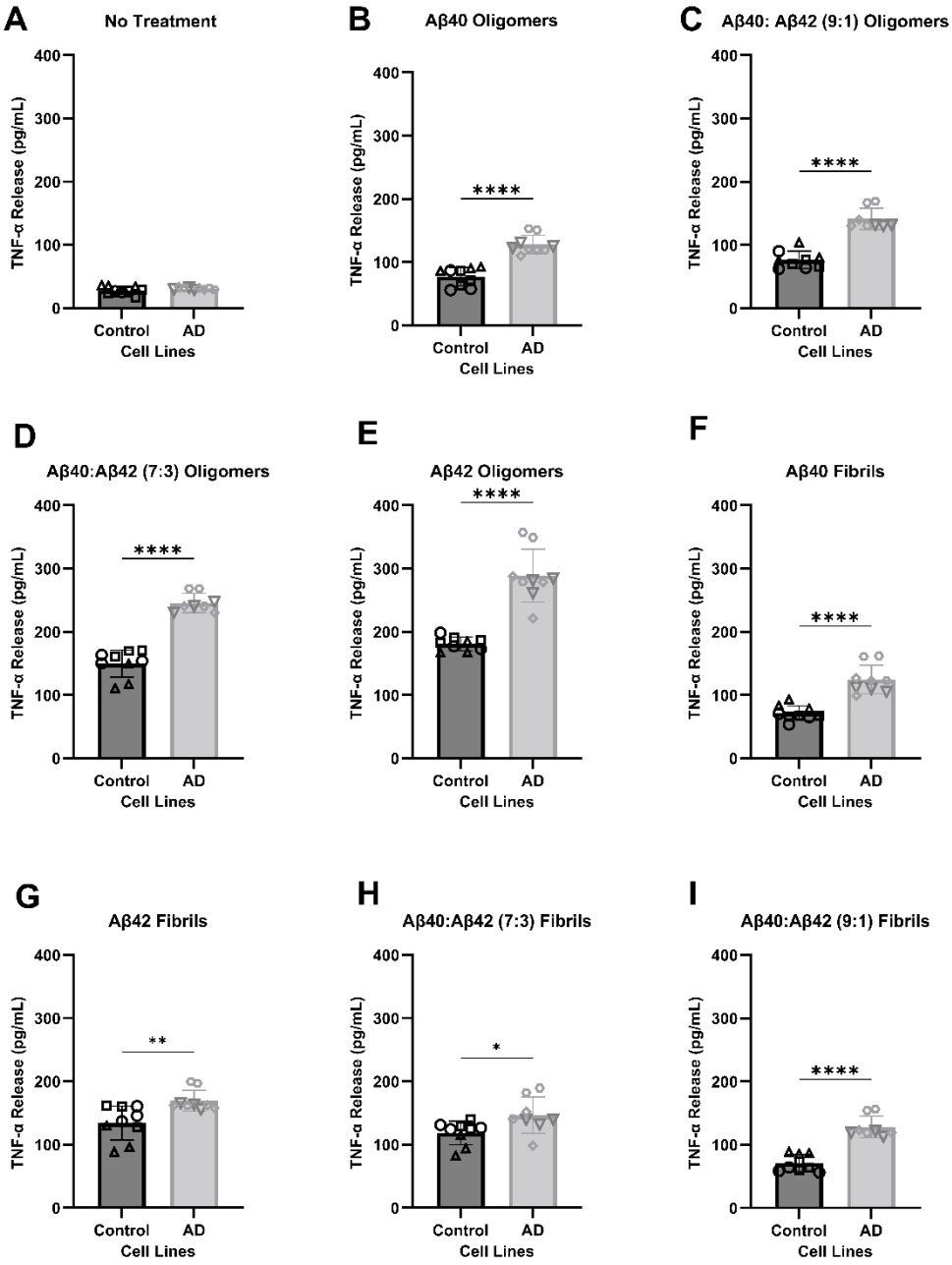

Figure 29. The induction of TNF-α in control and AD iAstrocytes after treatment with Aβ. *No treatment (**A**), Aβ oligomers (**B-E**) and Fibrils (**F-I**). For iAstrocytes, each data point represents 3 technical repeats averaged into 1 biological repeat per line (total cell lines = 3 per group). Data is visualised as mean ± S.D. Statistical analysis was completed using parametric unpaired t test, or non-parametric Mann-Whitney U test dependent on Shapiro-Wilk normality. Where there are no statistical lines = non-significant (ns), * p-value = <0.05, ** p-value = <0.01, *** p-value = <0.001, and **** p-value = <0.0001.*

5.3.1.5. The Induction of MCP1 in Control iAstrocytes after Treatment with Aβ

Oligomers

When evaluating MCP1, there was a statistically larger release after Aβ oligomer treatment (One-way ANOVA, Figure 30, A: F = 171.9, p-value = < 0.0001). Compared to no treatment, all species of Aβ resulted in significant induction of MCP1 (p-values = <0.0001, <0.0001, <0.0001, and <0.0001), respectively. When comparing isoforms, Aβ42 (0:10) resulted in higher secretion than all other isoforms (p-values = <0.0001, <0.0001, and <0.0001). Furthermore, Aβ40: Aβ42 (7:3) resulted in higher induction of MCP1 than Aβ40 (10:0) and Aβ40: Aβ42 (9:1) (p-values = <0.0001 and <0.0001). Lower Aβ42 ratios did not markedly influence MCP1 induction in control iAstrocytes (p-value = 0.8806).

Fibrils

Similar to oligomer treatment, there was a statistically higher release of MCP1 after fibrillar Aβ treatment (Welch's ANOVA, Figure 30, B: W = 90.55, p-value = <0.0001). Aβ40 (10:0), Aβ40: Aβ42 (9:1), Aβ40: Aβ42 (7:3), and Aβ42 (0:10) resulted in significant induction of MCP1 compared to no treatment (Figure p-values; <0.0001, 0.0006, <0.0001, and <0.0001), respectively. Additionally, Aβ42 (0:10) and Aβ40: Aβ42 (7:3) resulted in higher induction than Aβ40 (10:0) (p-values = <0.0002 and 0.0072). However, comparisons between other Aβ fibril isoforms showed no other significant differences (Table 12), suggesting that while Aβ42 fibrils can drive MCP1 secretion, the effect is less pronounced and variable than oligomeric forms.

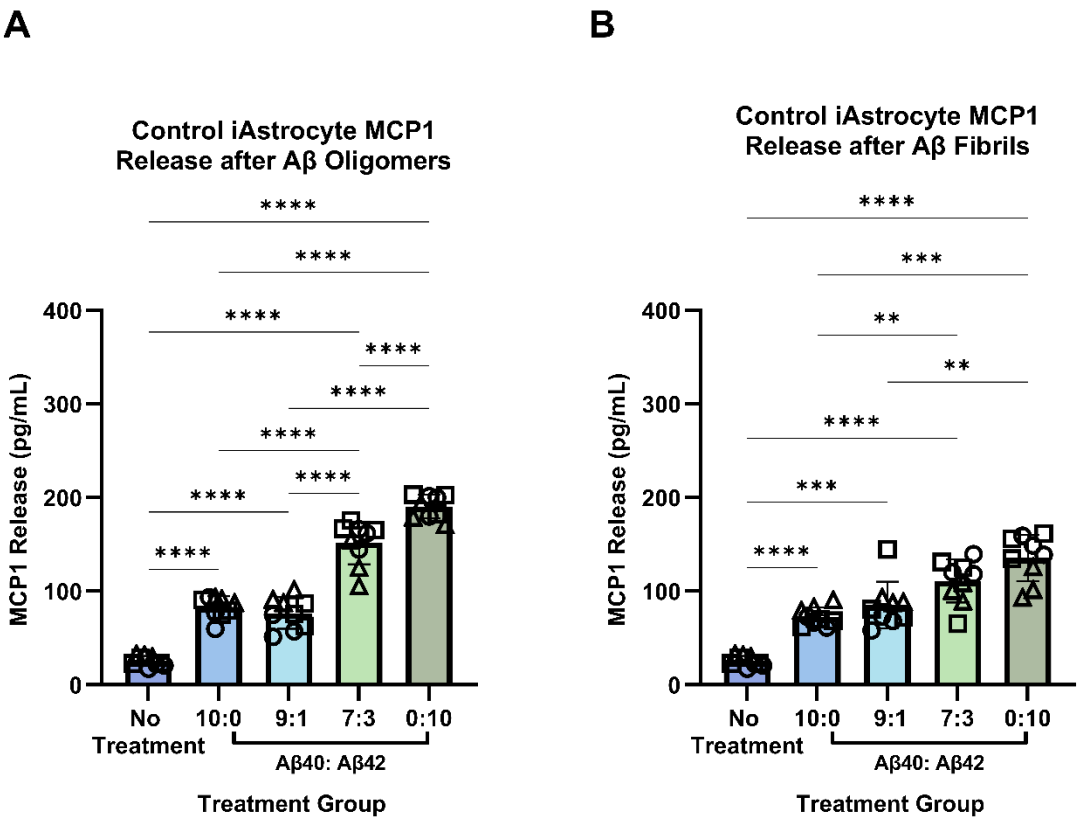

Figure 30. The induction of MCP1 in control iAstrocytes after treatment with Aβ. *Aβ oligomers (**A**) and Fibrils (**B**) result in the induction of MCP1 in control iAstrocytes, and isoform-specific differences in Aβ. For iAstrocytes, each data point represents 3 technical repeats averaged into 1 biological repeat per line (total cell lines = 3 per group). Data is visualised as mean ± S.D. Statistical analysis was completed using One-way ANOVA (**A**; W = 171.9, p-value = <0.0001) and Welch's ANOVA (**B**; W = 90.55, p-value = 0.0001). Post-hoc analyses were completed using Tukey's multiple comparison and Dunnett's T3 multiple comparisons test comparison, and can be found in Tables 11 and 12. Where there are no statistical lines = non-significant (ns), * p-value = <0.05, ** p-value = <0.01, *** p-value = <0.001, and **** p-value = <0.0001.*

5.3.1.6. The Induction of MCP1 in AD iAstrocytes after Treatment with Aβ

Oligomers

The aim was to compare the extent of MCP1 induction from AD iAstrocytes after treatment with Aβ isoforms in oligomeric form, which revealed a statistically higher induction of MCP1 (Welch's ANOVA, Figure 31, A: W = 139.5, p-value = <0.0001). Aβ40 (10:0), Aβ40: Aβ42 (9:1), Aβ40: Aβ42 (7:3), and Aβ42 (0:10) resulted in significant induction of MCP1 compared to no treatment (p-values = <0.0001, <0.0001, <0.0001, and <0.0001), respectively. Both Aβ42 (0:10) and Aβ40: Aβ42 (7:3) resulted in higher induction of MCP1 than lower ratios; Aβ40 (10:0) and Aβ40: Aβ42 (9:1) (p-values = <0.0001, <0.0001, <0.0001 and <0.0001). However, the other groups had no significant differences (Table 13).

Fibrils

Next, MCP1 release was statistically higher after treating iAstrocytes with Aβ fibrils (Welch's ANOVA, Figure 31, B: W = 64.66, p-value = <0.0001). Compared to no treatment, Aβ40 (10:0), Aβ40: Aβ42 (9:1), Aβ40: Aβ42 (7:3), Aβ42 (0:10), resulted in significant induction of MCP1 (p-values = <0.0001, <0.0001, <0.0001, and <0.0001), respectively. However, no statistically significant differences were observed between the Aβ fibril isoforms. These results suggest that while fibrillar Aβ induces MCP1 secretion, the response is less dependent on Aβ composition than oligomeric species in AD iAstrocytes (Table 14).

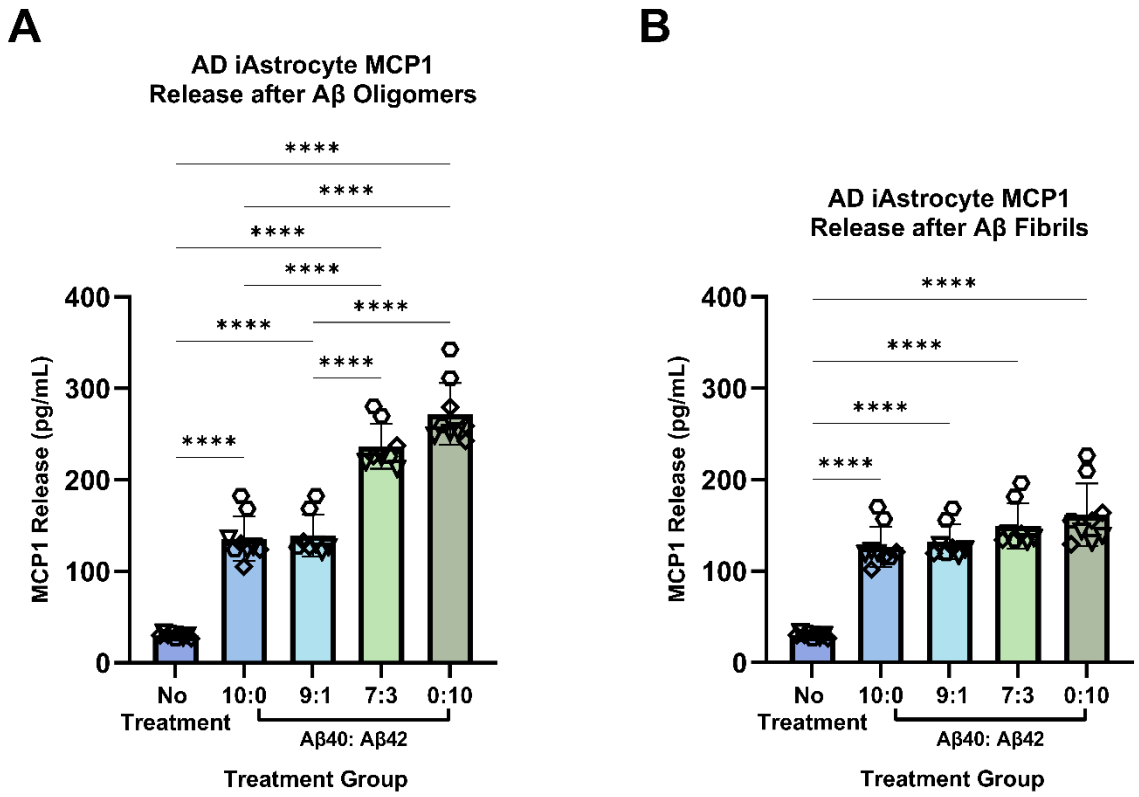

Figure 31. The induction of MCP1 in AD iAstrocytes after treatment with Aβ. *Aβ oligomers (**A**) and Fibrils (**B**) result in the induction of MCP1 in AD iAstrocytes, and isoform specific differences in Aβ. For iAstrocytes, each data point represents 3 technical repeats averaged into 1 biological repeat per line (total cell lines = 3 per group). Data is visualised as mean ± S.D. Statistical analysis was completed using Welch's ANOVA (A; W = 139.5, p-value = <0.0001 and B; W = 64.66, p-value = <0.0001). Post-hoc analyses were completed using Dunnett's T3 multiple comparisons test comparison, and can be found in Tables 13 and 14. Where there are no statistical lines = non-significant (ns), * p-value = <0.05, ** p-value = <0.01, *** p-value = <0.001, and **** p-value = <0.0001.*

5.3.1.7. The Induction of MCP1 in Control and AD iAstrocytes after Treatment with Aβ

Differences in MCP1 induction after Aβ oligomers and fibrils were examined between control and AD iAstrocytes (Table 15). Oligomeric Aβ40 (10:0), Aβ40: Aβ42 (9:1), Aβ40: Aβ42 (7:3), and Aβ42 (0:10) oligomers resulted in higher MCP1 induction in AD iAstrocytes when compared to control iAstrocytes (Figure 32, B-E: p-values = <0.0001, <0.0001, <0.0001, and <0.0001), respectively. These results suggest that AD iAstrocytes have higher MCP1 induction than controls after Aβ treatment. In fibrils, Aβ40 (10:0), Aβ40: Aβ42 (7:3), and Aβ40: Aβ42 (9:1) significantly increased MCP1 induction in AD iAstrocytes (Figure 32, F, H and I: p-values = <0.0001, 0.0022 and 0.0009). However, there were no statistically significant differences for no treatment and Aβ42 (0:10) (Figure 32, A and H: p-values = 0.0875 and 0.0819), respectively. These findings show that Aβ oligomers trigger a more substantial MCP1 production than fibrils when comparing AD and control iAstrocytes.

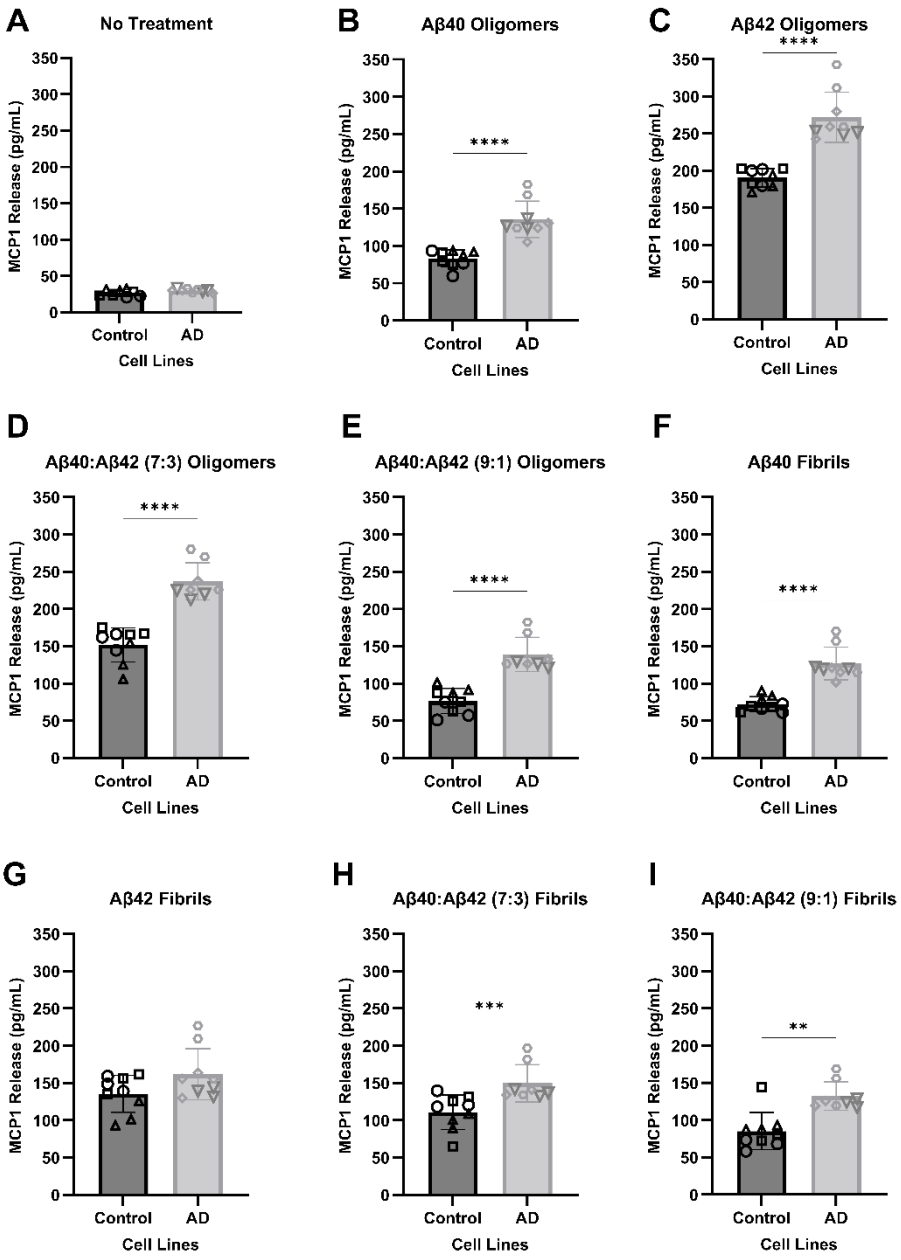

Figure 32. The induction of MCP1 in control and AD iAstrocytes after treatment with Aβ. *No treatment (**A**), Aβ oligomers (**B-E**) and Fibrils (**F-I**). For iAstrocytes, each data point represents 3 technical repeats averaged into 1 biological repeat per line (total cell lines = 3 per group). Data is visualised as mean ± S.D. Statistical analysis was completed using unpaired t-test or Mann-Whitney Test dependent on Shapiro-Wilk normality. Where there are no statistical lines = non-significant (ns), * p-value = <0.05, ** p-value = <0.01, *** p-value = <0.001, and **** p-value = <0.0001.*

5.3.1.8. The Induction of IL6 in Control iAstrocytes after Treatment with Aβ

Oligomers

In control iAstrocytes, IL6 was released statistically significantly more after Aβ oligomers (One-way ANOVA, Figure 33, A: F = 158.6, p-value = <0.0001). Compared to no treatment, all species of Aβ resulted in significantly higher IL6 (p-values = <0.0001, <0.0001, <0.0001, and <0.0001), respectively. Aβ42 (0:10) resulted in higher induction than Aβ40 (10:0). Aβ40: Aβ42 (9:1), and Aβ40: Aβ42 (7:3) (p-values = <0.0001, <0.0001, and <0.0001). Furthermore, Aβ40: Aβ42 (7:3) resulted in higher induction of IL6 than Aβ40 (10:0) and Aβ40: Aβ42 (9:1) (p-values = <0.0001 and <0.0001). Finally, when comparing Aβ40: Aβ42 (9:1) and Aβ40 (10:0) there was not a significant increase IL6 induction (p-value = 0.8063).

Fibrils

As a result of fibril treatment, there was a statistically significantly more extensive IL6 induction after (Welch's ANOVA, Figure 33, B: WF = 87.69, p-value = <0.0001). All Aβ isoforms resulted in a significant induction of IL6 compared to no treatment, but although there was a trend towards an increase (p-values = 0.0001, 0.0004, <0.0001 and <0.0001), respectively. As the ratio of Aβ42: Aβ40 (7:3 and 0:10) increases, there is a significant rise in IL6 compared to lower ratios (9:1 and 10:0) (p-values = 0.3092, 0.4982, 0.0002, and 0.0004. However, despite a trend in the increases of IL6, there was no statistically higher release for Aβ42 (0:10) compared to Aβ42: Aβ40 (7:3) (p-value = 0.0223), or between Aβ40 (10:0) and Aβ42: Aβ40 (9:1) (p-value = >0.9999).

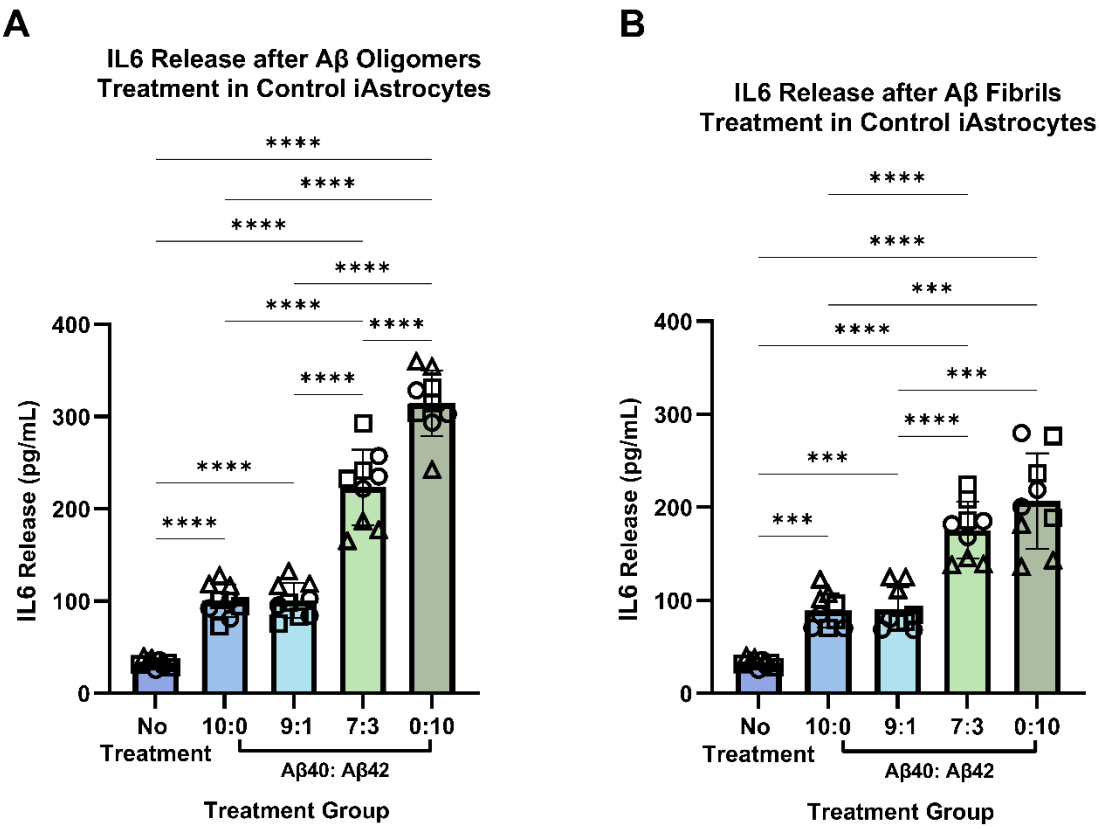

Figure 33. The induction of IL6 in control iAstrocytes after treatment with Aβ*. Aβ oligomers (**A**) and Fibrils (**B**) result in the induction of IL6 in Control iAstrocytes, and isoform-specific differences in Aβ. For iAstrocytes, each data point represents 3 technical repeats averaged into 1 biological repeat per line (total cell lines = 3 per group). Data is visualised as mean ± S.D. Statistical analysis was completed using One-way ANOVA (A; F = 158.6, p-value = <0.0001) and Welch's ANOVA (B; F= 87.69, p-value = 0.0001). Post-hoc analyses were completed using Tukey's multiple comparison or Dunnett's T3 multiple comparisons test comparison and can be found in Tables 11 and 12. Where there are no statistical lines = non-significant (ns), * p-value = <0.05, ** p-value = <0.01, *** p-value = <0.001, and **** p-value = <0.0001.*

5.3.1.9. The Induction of IL6 in AD iAstrocytes after Treatment with Aβ

Oligomers

When evaluating IL6 in AD iAstrocytes, there was a statistically significant difference in IL6 induction after oligomer treatment (Welch's ANOVA, Figure 34, A: W = 203.0, p-value = <0.0001). All groups, Aβ40 (10:0), Aβ40: Aβ42 (9:1), Aβ40: Aβ42 (7:3), and Aβ42 (0:10), resulted in significant induction of IL6 compared to no treatment (p-values = <0.0001, <0.0001, <0.0001, and <0.0001), respectively. Aβ42 (0:10) resulted in higher induction than Aβ40 (10:0), Aβ40: Aβ42 (9:1), and Aβ40: Aβ42 (7:3) (p-values = <0.0001, <0.0001, and 0.0148). Furthermore, Aβ40: Aβ42 (7:3) resulted in higher induction of IL6 than Aβ40 (10:0) and Aβ40: Aβ42 (9:1) (p-values = <0.0001 and <0.0001). Finally, when comparing Aβ40: Aβ42 (9:1) and Aβ40 (10:0) there was not a significant increase in IL6 induction (p-value = 0.9321). These results suggest that an increasing Aβ ratio contributes to a larger IL6 secretion.

Fibrils

The study further evaluated IL6 secretion in AD iAstrocytes after treatment with Aβ fibrils, revealing a statistically significant difference in IL6 induction (Welch's ANOVA, Figure 34, B: W = 87.79 p-value = <0.0001). All forms of fibrillar Aβ resulted in a significant increase of IL6 compared to no treatment (p-values = <0.0001, <0.0001, <0.0001, and <0.0001), respectively. Aβ42 (0:10) resulted in more IL6 induction than Aβ40 (10:0), Aβ40: Aβ42 (9:1) and Aβ40: Aβ42 (7:3) (p-values = 0.0004, 0.0001 and 0.0136). However, no statistical differences were found between the other Aβ isoforms (Table 14). These results suggest that fibrils can drive IL6 secretion, but the effect is less pronounced and variable than oligomeric forms.

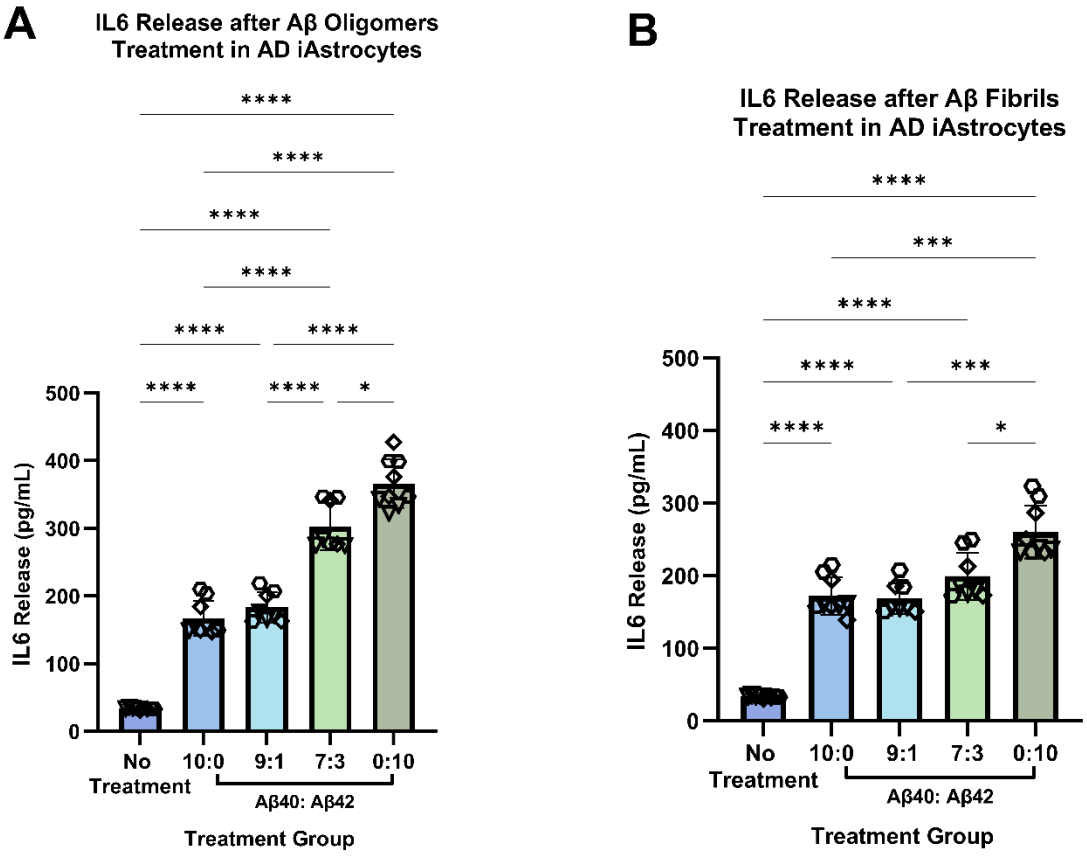

Figure 34. The induction of IL6 in AD iAstrocytes after treatment with Aβ. *Aβ oligomers (**A**) and Fibrils (**B**) result in the induction of IL6 in AD iAstrocytes, and isoform-specific differences in Aβ. For iAstrocytes, each data point represents 3 technical repeats averaged into 1 biological repeat per line (total cell lines = 3 per group). Data is visualised as mean ± S.D. Statistical analysis was completed using Welch's ANOVA (**A**; W = 203.0, p-value = <0.0001 and **B**; W = 87.79, p-value = <0.0001). Post-hoc analyses were completed using or Dunnett's T3 multiple comparisons test and can be found in Tables 13 and 14. Where there are no statistical lines = non-significant (ns), * p-value = <0.05, ** p-value = <0.01, *** p-value = <0.001, and **** p-value = <0.0001.*

5.3.1.10. The Induction of IL6 in Control and AD iAstrocytes after Treatment with Aβ

Next, the differences in IL6 secretion after Aβ oligomer and fibril treatment were compared in control and AD iAstrocytes (Figure 35, Table 15). In oligomers, Aβ40 (10:0), Aβ40: Aβ42 (9:1), Aβ40: Aβ42 (7:3), and Aβ42 (0:10) resulted in higher IL6 induction in AD iAstrocytes (p-values = <0.0001, <0.0001, 0.0014, and 0.0075), respectively. In fibrils, Aβ40 (10:0), Aβ40: Aβ42 (9:1) and Aβ42 (0:10) resulted in significantly higher IL6 induction in AD iAstrocytes (p-values = <0.0001, <0.0001, and 0.0294). However, there were no statistically significant differences in no treatment and Aβ40: Aβ42 (7:3) (p-values = 0.6845 and 0.2653, respectively. The findings show that Aβ oligomers and fibrils treatment triggers a more substantial IL6 production in AD iAstrocytes than control iAstrocytes.

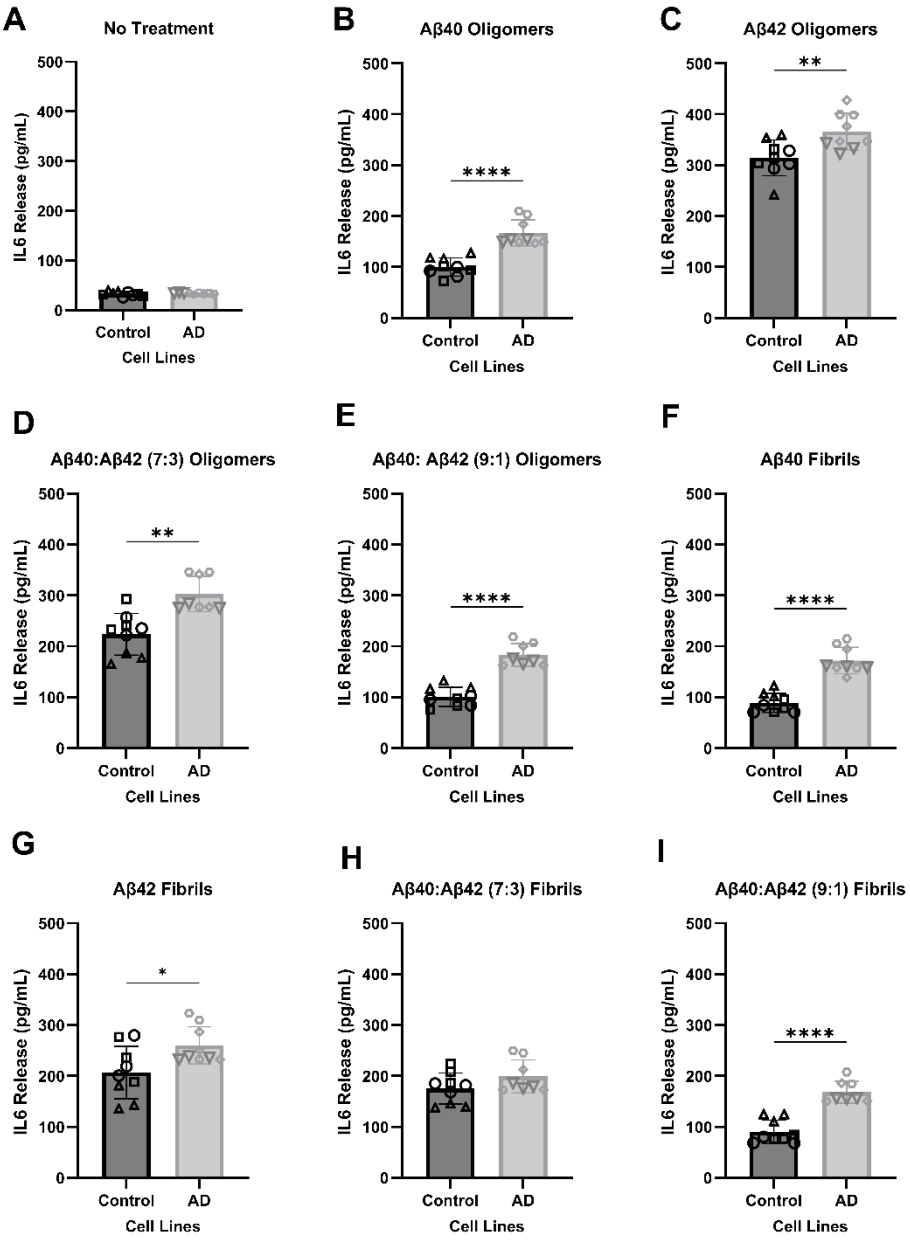

Figure 35. The induction of IL6 in control and AD iAstrocytes after treatment with Aβ. *No treatment (**A**), Aβ oligomers (**B-E**) and Fibrils (**F-I**). For iAstrocytes, each data point represents 3 technical repeats averaged into 1 biological repeat per line (total cell lines = 3 per group). Data is visualised as mean ± S.D. Statistical analysis was completed using unpaired t-test or Mann-Whitney Test dependent on Shapiro-Wilk normality. Where there are no statistical lines = non-significant (ns), * p-value = <0.05, ** p-value = <0.01, *** p-value = <0.001, and **** p-value = <0.0001.*

5.3.1.11. The Induction of IL-1β in Control iAstrocytes after Treatment with Aβ

Oligomers

Control iAstrocytes showed a statistically significant increase in IL-1β upon exposure to Aβ oligomers (One-way ANOVA, Figure 36, A: F = 138.5, p-value = <0.0001) with all Aβ isoforms inducing IL-1β secretion compared to no treatment (Table 11). When comparing isoforms, Aβ42 (0:10) fibrils induced IL-1β statistically more than all other isoforms (p-values = <0.0001, <0.0001, and <0.0001). Furthermore, Aβ40: Aβ42 (7:3) resulted in higher induction of IL-1β than Aβ40 (10:0) and Aβ40: Aβ42 (9:1) (p-value = <0.0001 and <0.0001). Finally, when comparing Aβ40: Aβ42 (9:1) and Aβ40 (10:0), there was no significant increase in IL-1β induction (p-value = 0.9971), indicating that a lower Aβ42 ratio does not have a major influence on IL-1β secretion in iAstrocytes.

Fibrils

Similarly, in response to Aβ fibrils, there was significant induction of IL-1β (One-way ANOVA, Figure 36, B: F = 46.12, p-value = <0.0001). As the ratio of Aβ42: Aβ40 increases, there is a statistically significant release of IL-1β compared to no treatment (Table). However, there was no trend in difference between Aβ40 (10:0) and Aβ40: Aβ42 (9:1) for higher IL-1β induction (p-value = >0.9999). Highlighting that higher Aβ42 levels are key drivers of IL-1β in control iAstrocytes. Between isoforms, Aβ42 (0:10) was higher than Aβ40: Aβ42 (9:1) and Aβ40 (10:0) (p-values = <0.0001 and <0.0001). However, no statistical differences were seen between the other Aβ isoforms (Table 12). These results suggest that whilst Aβ42 fibrils can drive IL-1β secretion, the effect is less pronounced and variable than oligomeric forms.

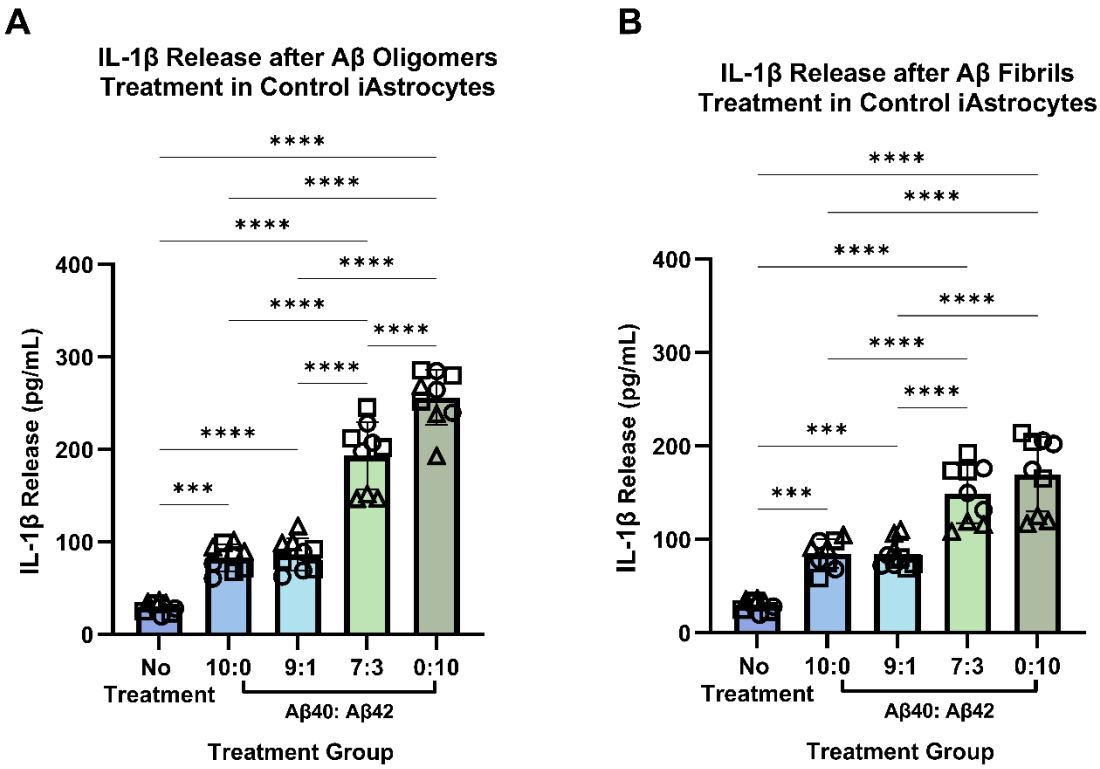

Figure 36. ***The induction of IL-1β in control iAstrocytes after treatment with Aβ.*** *Aβ oligomers (**A**) and Fibrils (**B**) result in the induction of IL-1β in Control iAstrocytes, and isoform-specific differences in Aβ). For iAstrocytes, each data point represents 3 technical repeats averaged into 1 biological repeat per line (total cell lines = 3 per group). Data is visualised as mean ± S.D. Statistical analysis was completed using ANOVA (**A**; F= 138.5, p-value = <0.0001 and **B**; F= 46.12, p-value = <0.0001). Post-hoc analyses were completed using Tukey's multiple comparison and can be found in Tables 11 and 12. Where there are no statistical lines = non-significant (ns), * p-value = <0.05, ** p-value = <0.01, *** p-value = <0.001, and **** p-value = <0.0001.*

5.3.1.12. The Induction of IL-1β in AD iAstrocytes after Treatment with Aβ

Oligomers

The aim was to compare the extent of IL-1β induction from AD iAstrocytes after treatment with Aβ isoforms in oligomeric form, which revealed a statistically higher secretion of IL-1β in oligomer treatment (Welch's ANOVA, Figure 37, A: W = 179.7, p-value = <0.0001). Aβ40 (10:0), Aβ40: Aβ42 (9:1), Aβ40: Aβ42 (7:3), and Aβ42 (0:10) resulted in release of IL-1β compared to no treatment (p-values = <0.0001, <0.0001, <0.0001, and <0.0001), respectively. Both Aβ42 (0:10) and Aβ40: Aβ42 (7:3) resulted in higher induction than Aβ40 (10:0) and Aβ40: Aβ42 (9:1) (p-values = <0.0001. <0.0001, <0.0001 and <0.0001). There were no statistically significant differences between the other isoforms (Table 13).

Fibrils

As a result of fibril treatment, there was a statistically significantly larger IL-1β release in AD iAstrocytes (Welch's ANOVA, Figure 37, B: W = 61.80, p-value = <0.0001). All fibrillar Aβ isoforms resulted in significant induction of IL-1β compared to no treatment (p-values = <0.0001, <0.0001, <0.0001, and <0.0001), respectively. Aβ42 (0:10) resulted in significantly more IL-1β induction than Aβ40: Aβ42 (9:1) and Aβ40 (10:0) (p-values = 0.002 and 0.0045). However, no statistical differences were found between the Aβ isoforms (Table 14). These results suggest that while Aβ fibrils contribute to IL-1β induction, their impact is less composition-dependent than oligomers, highlighting the greater pro-inflammatory potential of soluble Aβ species.

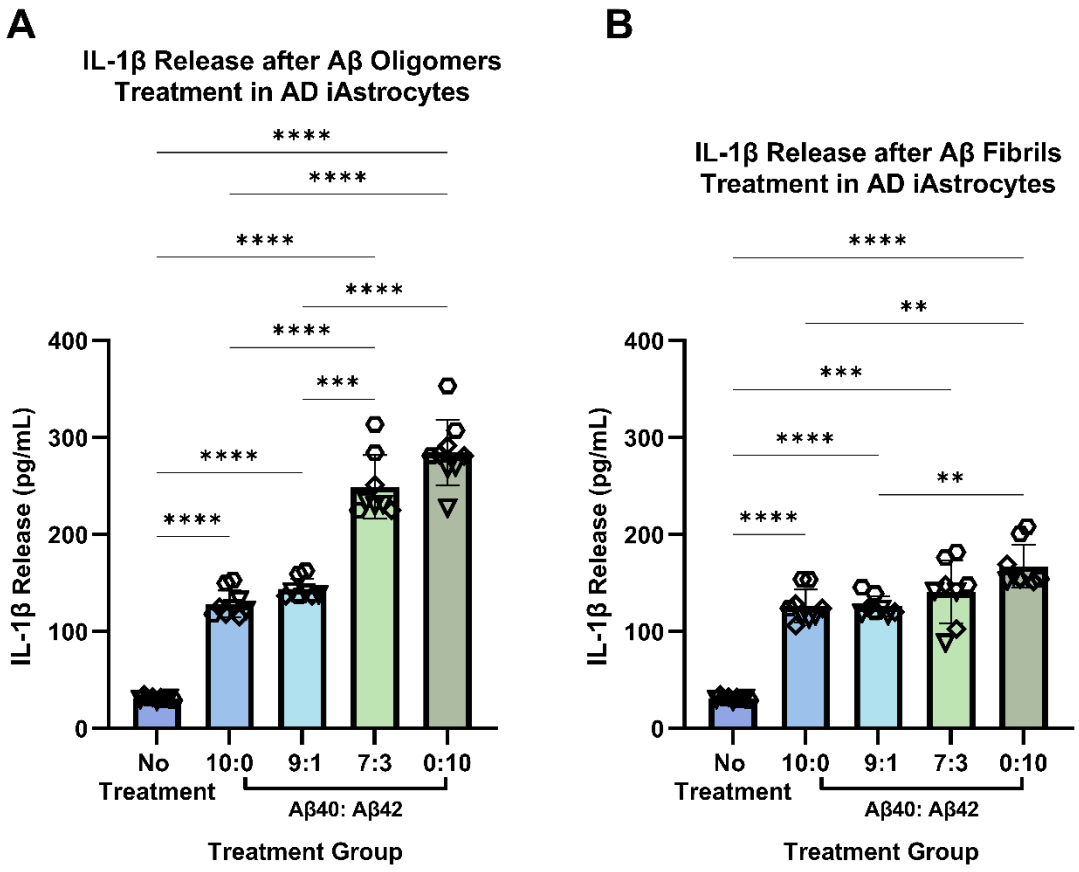

Figure 37. The Induction of IL-1β in AD iAstrocytes after Treatment with Aβ*. Aβ oligomers (**A**) and Fibrils (**B**) result in the induction of IL-1β in AD iAstrocytes, and isoform-specific differences in Aβ. For iAstrocytes, each data point represents 3 technical repeats averaged into 1 biological repeat per line (total cell lines = 3 per group). Data is visualised as mean ± S.D. Statistical analysis was completed using Welch's ANOVA (**A**; W = 179.7, p-value = <0.0001 and **B**; W = 61.80, p-value = 0.0001). Post-hoc analyses were completed using Dunnett's T3 multiple comparisons test and can be found in Tables 13 and 14. Where there are no statistical lines = non-significant (ns), * p-value = <0.05, ** p-value = <0.01, *** p-value = <0.001, and **** p-value = <0.0001.*

5.3.1.13. The Induction of IL-1β in Control and AD iAstrocytes after Treatment with Aβ

Next, the difference between control and AD iAstrocytes IL-1β induction was examined following Aβ oligomer and fibril treatment (Figure 38). Aβ40 (10:0), Aβ40: Aβ42 (9:1) and Aβ40: Aβ42 (7:3) resulted in significantly more IL-1β induction in AD iAstrocytes (p-values = <0.0001, <0.0001, and 0.0048). Though there was a trend in increase, there was not substantially more IL-1β induction after Aβ42 (0:10) treatment (p-value = 0.0780). There were also no significant differences in no-treatment cytokine expression (p-value = 0.6069). In fibrils, Aβ40 (10:0) and Aβ40: Aβ42 (9:1) resulted in significantly higher IL-1β induction in AD iAstrocytes (p-values = <0.0001 and <0.0001). However, there were no statistically significant differences in Aβ40: Aβ42 (7:3) and Aβ42 (0:10) (p-values = 0.6152 and 0.6495).

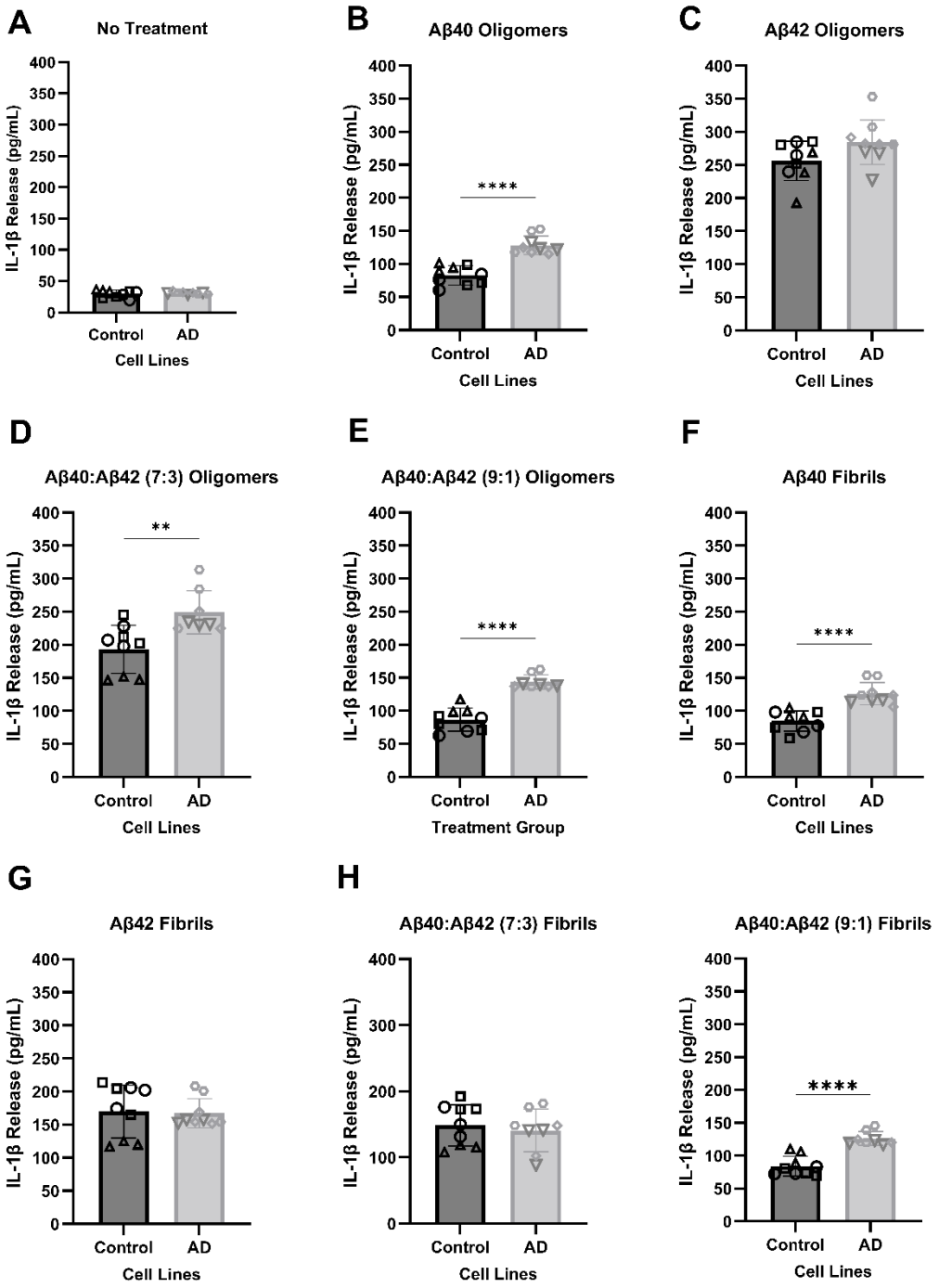

Figure 38. The induction of IL-1β in control and AD iAstrocytes after treatment with Aβ. *No treatment (**A**), Aβ oligomers (**B-E**) and Fibrils (**F-I**). For iAstrocytes, each data point represents 3 technical repeats averaged into 1 biological repeat per line (total cell lines = 3 per group). Data is visualised as mean ± S.D. Statistical analysis was completed using unpaired t-test or Mann-Whitney Test dependent on Shapiro-Wilk normality. Where there are no statistical lines = non-significant (ns), * p-value = <0.05, ** p-value = <0.01, *** p-value = <0.001, and **** p-value = <0.0001.*

5.3.1.14. Summary of Cytokine and Chemokine Release in Control and AD iAstrocytes

***Table 11**. Summary TNF-α, MCP1, IL6, and IL-1β release after Aβ oligomers treatment in control iAstrocytes.*

	TNF-α	MCP1	IL6	IL-1β
No Treatment vs. 10:0	**** (<0.0001)	**** (<0.0001)	**** (<0.0001)	*** (0.0002)
No Treatment vs. 9:1	**** (<0.0001)	**** (<0.0001)	**** (<0.0001)	**** (<0.0001)
No Treatment vs. 7:3	**** (<0.0001)	**** (<0.0001)	**** (<0.0001)	**** (<0.0001)
No Treatment vs. 0:10	**** (<0.0001)	**** (<0.0001)	**** (<0.0001)	**** (<0.0001)
10:0 vs. 9:1	ns (>0.9999)	ns (0.8806)	ns (>0.9999)	ns (0.9971)
10:0 vs. 7:3	**** (<0.0001)	**** (<0.0001)	**** (<0.0001)	**** (<0.0001)
10:0 vs. 0:10	**** (<0.0001)	**** (<0.0001)	**** (<0.0001)	**** (<0.0001)
9:1 vs. 7:3	**** (<0.0001)	**** (<0.0001)	**** (<0.0001)	**** (<0.0001)
9:1 vs. 0:10	**** (<0.0001)	**** (<0.0001)	**** (<0.0001)	**** (<0.0001)
7:3 vs. 0:10	*** (0.0003	**** (<0.0001)	**** (<0.0001)	**** (<0.0001)

Table 12. *Summary TNF-α, MCP1, IL6, and IL-1β release after Aβ fibrils treatment in control iAstrocytes.*

	TNF-α	MCP1	IL6	IL-1β
No Treatment vs. 10:0	**** (<0.0001)	**** (<0.0001)	*** (0.0001)	*** (0.0003)
No Treatment vs. 9:1	**** (<0.0001)	*** (0.0006)	*** (0.0004)	*** (0.0003)
No Treatment vs. 7:3	**** (<0.0001)	**** (<0.0001)	**** (<0.0001)	**** (<0.0001)
No Treatment vs. 0:10	**** (<0.0001)	**** (<0.0001)	**** (<0.0001)	**** (<0.0001)
10:0 vs. 9:1	ns (>0.9999)	ns (0.7991)	ns (>0.9999)	ns (>0.9999)
10:0 vs. 7:3	**** (<0.0001)	** (0.0072)	**** (<0.0001)	**** (<0.0001)
10:0 vs. 0:10	**** (<0.0001)	*** (0.0002)	*** (0.0007)	**** (<0.0001)
9:1 vs. 7:3	**** (<0.0001)	ns (0.2806)	**** (<0.0001)	**** (<0.0001)
9:1 vs. 0:10	**** (<0.0001)	** (0.0052)	*** (0.0007)	**** (<0.0001)
7:3 vs. 0:10	ns (0.309)	ns (0.32)	ns (0.7)	ns (0.3924)

Table 13. *Summary TNF-α, MCP1, IL6, and IL-1β release after Aβ oligomers treatment in AD iAstrocytes.*

	TNF-α	MCP1	IL6	IL-1β
No Treatment vs. 10:0	**** (<0.0001)	**** (<0.0001)	**** (<0.0001)	**** (<0.0001)
No Treatment vs. 9:1	**** (<0.0001)	**** (<0.0001)	**** (<0.0001)	**** (<0.0001)
No Treatment vs. 7:3	**** (<0.0001)	**** (<0.0001)	**** (<0.0001)	**** (<0.0001)
No Treatment vs. 0:10	**** (<0.0001)	**** (<0.0001)	**** (<0.0001)	**** (<0.0001)
10:0 vs. 9:1	ns (0.5857)	ns (>0.9999)	ns (0.8063)	ns (0.1726)
10:0 vs. 7:3	**** (<0.0001)	**** (<0.0001)	**** (<0.0001)	**** (<0.0001)
10:0 vs. 0:10	**** (<0.0001)	**** (<0.0001)	**** (<0.0001)	**** (<0.0001)
9:1 vs. 7:3	**** (<0.0001)	**** (<0.0001)	**** (<0.0001)	*** (<0.0002)
9:1 vs. 0:10	**** (<0.0001)	**** (<0.0001)	**** (<0.0001)	**** (<0.0001)
7:3 vs. 0:10	ns (0.1236)	ns (0.209)	ns (0.0197)	ns (0.3182)

Table 14. *Summary TNF-α, MCP1, IL6, and IL-1β release after Aβ fibrils treatment in AD iAstrocytes.*

	TNF-α	MCP1	IL6	IL-1β
No Treatment vs. 10:0	**** (<0.0001)	**** (<0.0001)	**** (<0.0001)	**** (<0.0001)
No Treatment vs. 9:1	**** (<0.0001)	**** (<0.0001)	**** (<0.0001)	**** (<0.0001)
No Treatment vs. 7:3	**** (<0.0001)	**** (<0.0001)	**** (<0.0001)	*** (0.0002)
No Treatment vs. 0:10	**** (<0.0001)	**** (<0.0001)	**** (<0.0001)	**** (<0.0001)
10:0 vs. 9:1	ns (>0.9999)	ns (0.9997)	ns (>0.9999)	ns (>0.9999)
10:0 vs. 7:3	ns (0.5952)	ns (0.4322)	ns (0.4982)	ns (0.9165)
10:0 vs. 0:10	** (0.0023)	ns (0.1778)	*** (0.0004)	** (0.0045)
9:1 vs. 7:3	ns (0.7111)	ns (0.7075)	ns (0.3092)	ns (0.8796)
9:1 vs. 0:10	** (0.0014)	ns (0.3212)	*** (0.0002)	** (0.0028)
7:3 vs. 0:10	ns (0.4698)	ns (0.9904)	* (0.0223)	ns (0.4727)

***Table 15**. Summary TNF-α, MCP1, IL6, and IL-1β release for AD vs Control iAstrocytes.*

	TNF-α	MCP1	IL6	IL-1β
No Treatment	ns (0.2325)	ns (0.0875)	ns (0.6845)	ns (0.6069)
Aβ40 Oligomers	**** (<0.0001)	**** (<0.0001)	**** (<0.0001)	**** (<0.0001)
Aβ40: Aβ42 (9:1) Oligomers	**** (<0.0001)	**** (<0.0001)	**** (<0.0001)	**** (<0.0001)
Aβ40: Aβ42 (7:3) Oligomers	**** (<0.0001)	**** (<0.0001)	** (0.0014)	** (0.0048)
Aβ42 Oligomers	**** (<0.0001)	**** (<0.0001)	** (0.0075)	ns (0.0780)
Aβ40 Fibrils	**** (<0.0001)	**** (<0.0001)	**** (<0.0001)	**** (<0.0001)
Aβ40: Aβ42 (9:1) Fibrils	**** (<0.0001)	** (0.0022)	**** (<0.0001)	**** (<0.0001)
Aβ40: Aβ42 (7:3) Fibrils	* (0.0267)	*** (0.0009)	ns (0.2653)	ns (0.6152)
Aβ42 Fibrils	** (0.0044)	ns (0.0819)	* (0.0294)	ns (0.6495)

5.3.2. Expression of GFAP, Vimentin, and CD44 Post Aβ Treatment

Immunocytochemistry investigated if Aβ treatment differentially activates the expression of GFAP, Vimentin, and CD44 in iAstrocytes. The analysis focused on three key aspects: the percentage of positively stained cells, the intensity of staining, and the total cellular area occupied by the stained marker.

5.3.2.1. Control Astrocytes

For this analysis, one control iAstrocyte line (Control 2) was examined due to assay time constraints (n = 3 biological replicates). After each split into a different passage and experimental assay was classed as a biological repeat. Each biological repeat was an average of 3 technical repeats.

5.3.2.2. Glial Fibrillary Acidic Protein (GFAP)

Immunocytochemical staining was performed to assess the effect of Aβ treatment on GFAP expression (Figure 39, A). Analysis of GFAP in iAstrocytes showed high and consistent GFAP expression across all Aβ treatment groups, with no significant changes in GFAP positivity following exposure to different Aβ species (Figure 40, A). The percentage of $GFAP^{+ve}$ cells remained high in all five groups with no treatment, Aβ40 oligomers, Aβ42 oligomers, Aβ40 fibrils, and Aβ42 fibrils % mean (n=3 of control 2) of 99.83%, 99.83%, 99.85%, 99.78, and 99.81%, respectively. These findings indicate that iAstrocytes maintain GFAP expression regardless of Aβ treatment, confirming the presence of a stable $GFAP^{+ve}$ astrocyte population.

Next, the extent of GFAP intensity after treatment with Aβ was investigated. The data showed high variability between treatment groups and revealed no significant differences in GFAP intensity across conditions (One-way ANOVA, Figure 40, D: F= 2.558, p-value = 0.8996). Finally, the total GFAP+ area per cell was analysed to assess potential changes in astrocyte morphology after Aβ exposure. Although there was a trend that Aβ40 and Aβ42 oligomers increased the $GFAP^{+ve}$ area, there were no statistically significant differences (One-way ANOVA, Figure 40, G: F= 0.5305, p-value = 0.7165). These results suggest that

while astrocytes maintain GFAP expression following Aβ treatment, neither Aβ aggregation state nor isoform composition significantly alters GFAP intensity or cellular morphology under these experimental conditions.

5.3.2.3. Vimentin

Like GFAP, vimentin expression was visualised and analysed to assess potential changes following Aβ treatment (Figures 39 and 40). Immunocytochemical analysis of the % of positive cells revealed a high proportion and consistent vimentin expression in all treatment conditions (Figure 40, B). The percentage of Vimentin^{+ve} cells was high in all five groups with no treatment, Aβ40 oligomers, Aβ42 oligomers, Aβ40 fibrils, and Aβ42 fibrils % mean (n=3 of control 2) of 99.94%, 99.97%, 99.93%, 99.96, and 99.96%, respectively. These findings suggest that vimentin expression is maintained regardless of Aβ isoform or aggregation state, indicating the persistence of a stable Vimentin^{+ve} iAstrocyte population across conditions. The intensity of vimentin staining was quantified to investigate potential changes in Vimentin expression levels further after Aβ treatment. Although there was a trend towards increased vimentin intensity after Aβ40 oligomers, Aβ42 oligomers, and Aβ42 fibrils, it was not statistically significant (One-way ANOVA, Figure 40, E: F= 0.3190, p-value = 0.8590). Finally, the difference in the morphology based on the vimentin area was investigated. Though there was a trend that Aβ40/Aβ42 oligomers and Aβ42 fibrils increased area, it was not statistically different (One-way ANOVA, Figure 40, H: F= 1.339, p-value = 0.3212). These results suggest that similar to GFAP, Aβ treatment does not significantly alter vimentin expression levels or astrocyte morphology despite minor non-significant trends.

5.3.2.4. CD44

Immunocytochemical staining was performed to evaluate potential changes in CD44 expression following Aβ treatment, and the percentage of CD44-positive cells (CD44^{+ve}), staining intensity, and total CD44 area were analysed (Figures 39 and 40). The percentage of

CD44^{+ve} cells was high in all five groups with no treatment, Aβ40 oligomers, Aβ42 oligomers, Aβ40 fibrils, and Aβ42 fibrils % mean (n=3 of control 2) of 99.50%, 99.74%, 99.63%, 99.32%, and 99.53%, respectively (Figure 40, C). These results indicate a positive population of CD44^{+ve} iAstrocytes regardless of Aβ treatment group. Next, the intensity of CD44 staining was analysed to determine whether Aβ treatment influenced CD44 expression levels. Though there was a trend towards increased CD44 after Aβ40 oligomers, Aβ40 fibrils, and Aβ42 fibrils, there was not a statistically different intensity of CD44 (One-way ANOVA, Figure 40, E: F= 0.3923, p-value = 0.8097). Additionally, the total CD44^{+ve} area per cell was measured to assess whether astrocyte morphology or CD44 expression patterns changed following Aβ exposure showing a non-statistical difference (One-way ANOVA, Figure 40, I: F= 0.7037, p-value = 0.6072). These findings suggest that similar to GFAP and Vimentin, CD44 expression remains largely unchanged following Aβ treatment, despite minor, non-significant trends in intensity and area expansion observed in specific Aβ-treated groups.

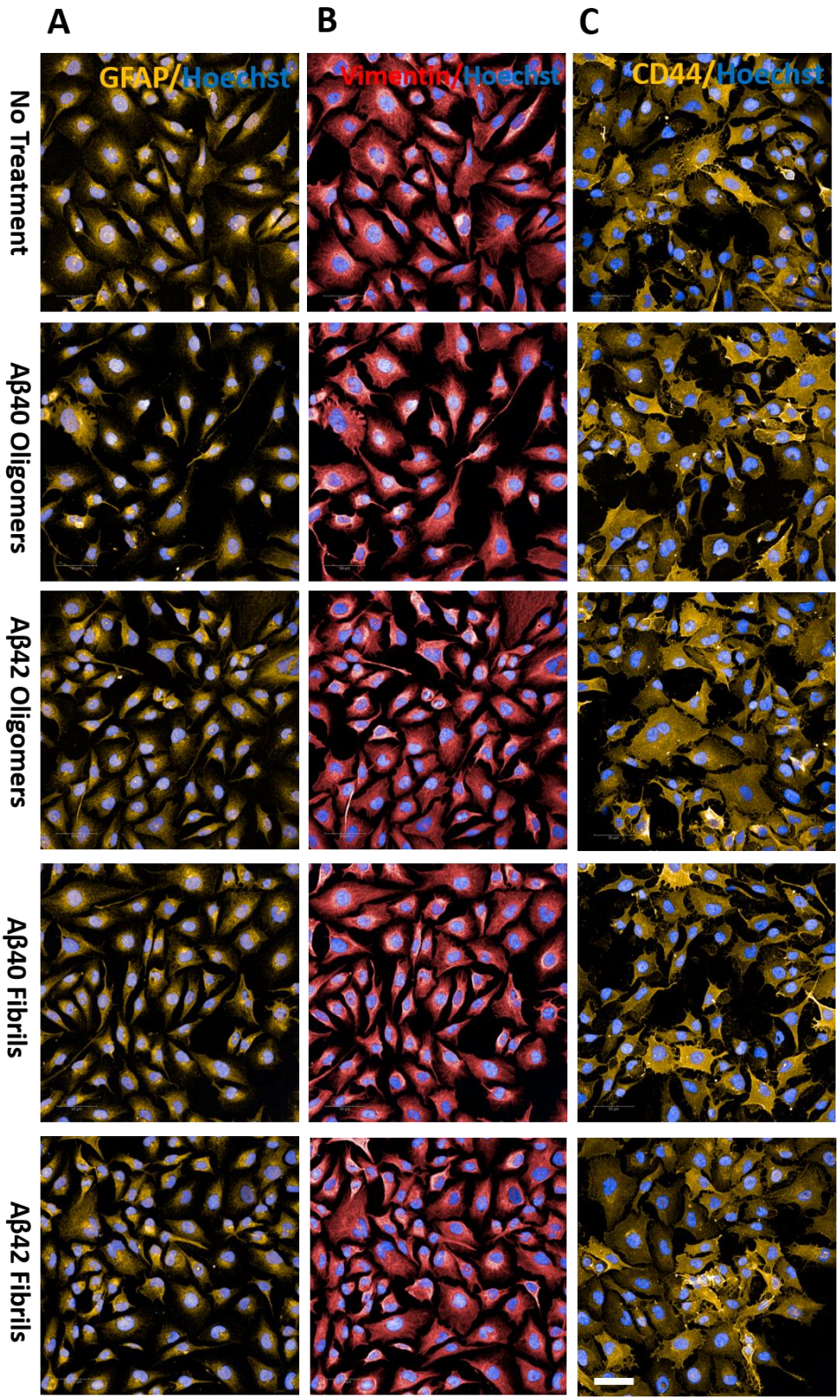

Figure 39. ***Illustrations of control iAstrocytes after Aβ (2.5 μM) treatment using immunocytochemistry. A.*** *Representative GFAP (**A**), Vimentin (**B**), and CD44 (**C**) after no treatment, Aβ40 oligomers, Aβ42 oligomers, Aβ40 fibrils, and Aβ42 fibrils. Scale bar (50 μm).*

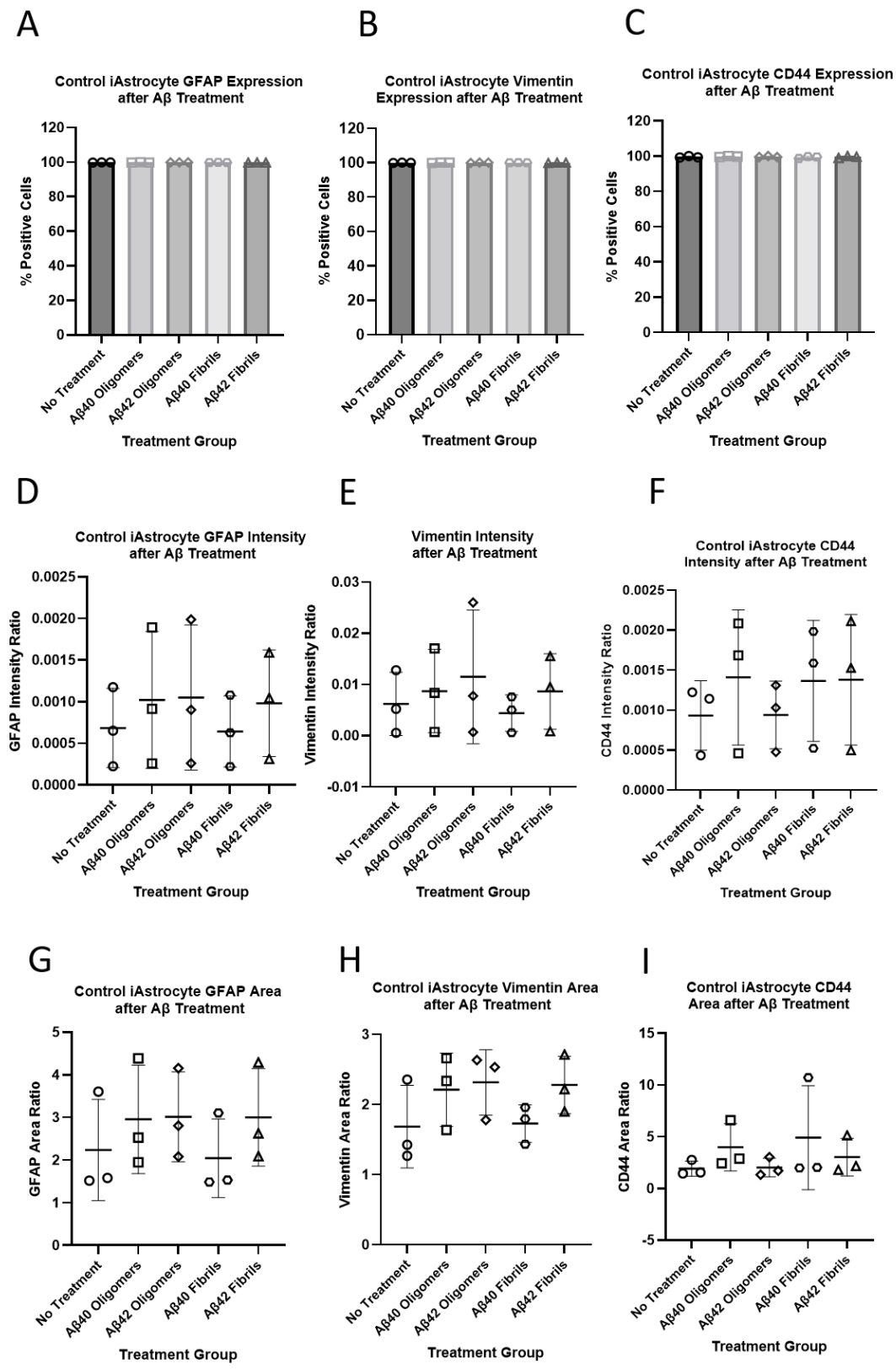

Figure 40. Quantification of GFAP, Vimentin and CD44 expression in control iAstrocytes. *The percentage of cells with positive staining for GFAP (**A**), Vimentin (**B**), and CD44 (**C**) after treatment with Aβ. **D.** Aβ species do not cause a significant difference in GFAP intensity (F=*

2.558, p-value = 0.8996). ***E.*** *Aβ species do not cause a significant difference in Vimentin intensity (F= 0.3190, p-value = 0.8590).* ***F.*** *Aβ species do not cause a significant difference in CD44 intensity (F= 0.3923, p-value = 0.8097).* ***G.*** *Aβ species do not cause a significant difference in the GFAP+ area (F= 0.5305, p-value = 0.7165).* ***H.*** *Aβ species do not cause a significant difference in the Vimentin+ area. F= 1.339, p-value = 0.3212).* ***I.*** *Aβ species do not cause a significant difference in the Vimentin+ area (F= 0.7037, p-value = 0.6072). All statistical analyses were completed using one-way ANOVA. Post-hoc analysis was not completed because the overall ANOVAs were displayed as non-significant. Data is visualised as mean ± S.D. Biological repeats (n=3) of one control line (control 2) were averaged from 3 technical repeats. For intensity after Aβ treatment, results were normalised total intensity/cell area/total cell count to create an intensity ratio. For intensity after Aβ treatment, results were normalised total area/total cell count.*

5.3.2.5. AD Astrocytes

In the following sections, one sporadic line (AD 2) was analysed due to assay time constraints. CD44 and Vimentin (n=3) and GFAP (n=1). After each split into a different passage and experimental assay was classed as a biological repeat. Each biological repeat was an average of 3 technical repeats.

5.3.2.6. Glial Fibrillary Acidic Protein (GFAP)

The results in the following section are preliminary; no statistical analysis was done because it is one repeat. Immunocytochemical staining was performed to assess the effect of Aβ treatment on GFAP expression (Figure 41, A). The percentage of GFAP-positive ($GFAP^{+ve}$) cells, staining intensity, and total GFAP area were analysed. The results showed high and consistent GFAP expression across all Aβ treatment groups, with no significant changes in GFAP positivity following exposure to different Aβ species (Figure 42, A). The percentage of $GFAP^{+ve}$ cells was high in all five groups with no treatment, Aβ40 oligomers, Aβ42 oligomers, Aβ40 fibrils, and Aβ42 fibrils of 99.52%, 99.54%, 99.61%, 99.73%, and 99.35%, respectively. These findings indicate that iAstrocytes maintain GFAP expression regardless of Aβ treatment, confirming the presence of a stable $GFAP^{+ve}$ astrocyte population. The results of this section can be supported by $GFAP^{+ve}$ staining during characterisation (Chapter 3, section 3.5.2). Next, the extent of GFAP intensity after treatment with Aβ was investigated. The preliminary data shows that Aβ42 fibrils increase GFAP intensity but not in the other groups (Figure 42, D). Finally, the difference in $GFAP^{+ve}$ area after Aβ treatment was investigated. The preliminary data suggests a trend towards a decrease in area in Aβ40 oligomers but not in the other groups (Figure 42, G).

5.3.2.7. Vimentin

Like GFAP, vimentin expression was visualised and analysed to assess potential changes following Aβ treatment (Figures 41, B and 42). Immunocytochemical analysis of the % of positive cells revealed a high proportion and consistent vimentin expression in all treatment conditions (Figure 42, B). The percentage of $Vimentin^{+ve}$ cells was high in all five groups with no treatment, Aβ40 oligomers, Aβ42 oligomers, Aβ40 fibrils, and Aβ42 fibrils % mean (n=3 of AD 2) of 99.95%, 99.95%, 99.96%, 100%, and 99.95%, respectively. These findings suggest

that vimentin expression is maintained regardless of Aβ isoform or aggregation state, indicating the persistence of a stable Vimentin^{+ve} iAstrocyte population across conditions. The intensity of vimentin staining was quantified to further investigate potential changes in Vimentin expression levels. Though there was a trend towards decreased Aβ42 oligomers and Aβ40 fibrils, there was no statistical difference in intensity (One-way ANOVA, Figure 42, E: F= 0.3969, p-value = 0.8065). Finally, there were no statistically significant differences in morphology of the iAstrocytes after Aβ treatment based on Vimentin (One-way ANOVA, Figure 42, H: F= 0.05522, p-value = 0.9934).

5.3.2.8. CD44

Immunocytochemical staining was performed to evaluate potential changes in CD44 expression following Aβ treatment, and the percentage of CD44-positive cells (CD44+ve), staining intensity, and total CD44 area were analysed (Figures 41 and 42). The percentage of CD44^{+ve} cells was high in all five groups with no treatment, Aβ40 oligomers, Aβ42 oligomers, Aβ40 fibrils, and Aβ42 fibrils % mean (n=3 of AD 2) of 99.21%, 99.43%, 99.44%, 99.67%, and 99.98%, respectively (Figure 42, C). These results indicate a positive population of CD44^{+ve} iAstrocytes regardless of the Aβ treatment group. Next, the intensity of CD44 staining was analysed to determine whether Aβ treatment influenced CD44 expression levels. There was a trend towards decreased CD44 intensity after Aβ40 oligomers, Aβ40 fibrils, and Aβ42 fibrils; it was not statistically significant (One-way ANOVA, Figure 42, F: F= 1.707, p-value = 0.2245). When evaluating the CD44^{+ve} area, there were no statistically different morphological changes following Aβ treatment (One-way ANOVA, Figure 42, I: F= 0.0032, p-value = 0.9978). Suggesting suggest that similar to Vimentin, CD44 expression remains following Aβ treatment in iAstrocytes remains mostly unchanged.

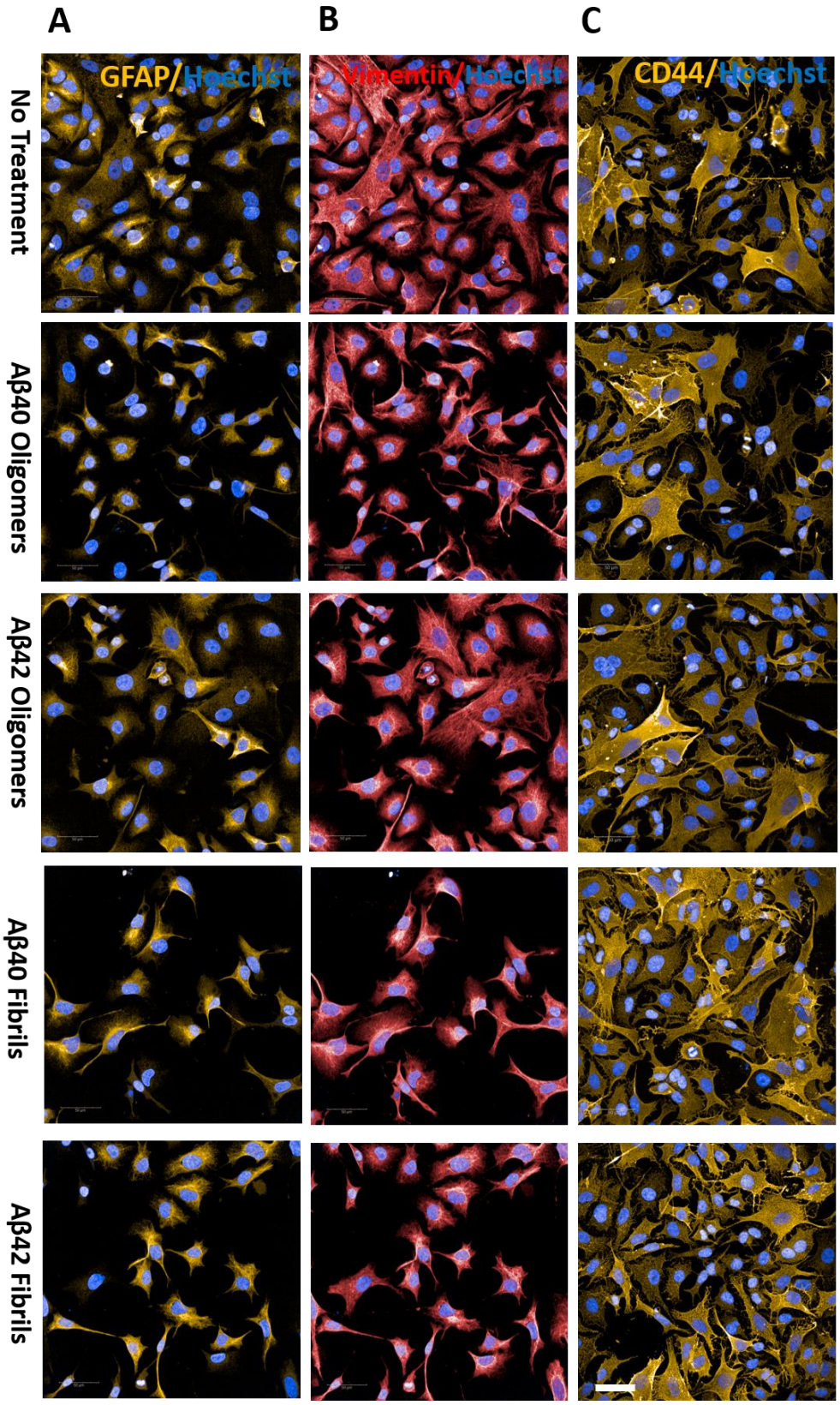

***Figure 41**. **Illustrations of AD iAstrocytes after Aβ (2.5 μM) treatment using immunocytochemistry. A.** Representative GFAP (**A**), Vimentin (**B**), and CD44 (**C**) after no treatment, Aβ40 oligomers, Aβ42 oligomers, Aβ40 fibrils, and Aβ42 fibrils. Scale bar (50 μm).*

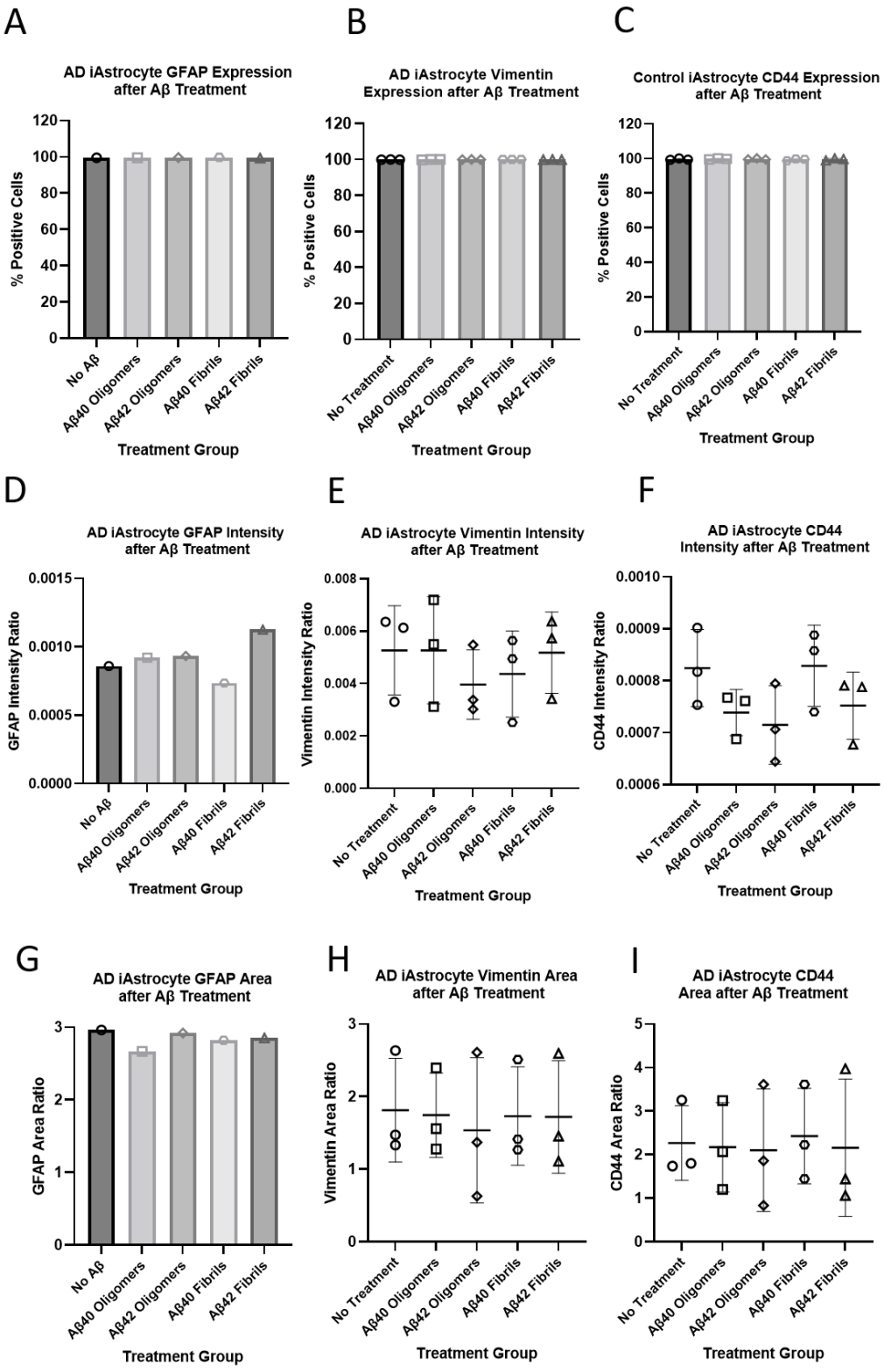

Figure 42. Quantification of GFAP, Vimentin and CD44 expression in AD iAstrocytes. *The percentage of cells with positive staining for GFAP (preliminary) (**A**), Vimentin (**B**), and CD44 (**C**) after treatment with Aβ. Preliminary GFAP intensity (**D**) and GFAP area (**G**). Statistical analysis was not completed (n=1). **E.** Aβ species do not cause a significant difference in Vimentin intensity*

(F= F= 0.3969, p-value = 0.8065). ***F.*** *Aβ species do not cause a significant difference in CD44 intensity (F= 1.707, p-value = 0.2245).* ***H.*** *Aβ species do not cause a significant difference in the Vimentin+ area (F= 0.05522, p-value = 0.9934).* ***I.*** *Aβ species do not cause a significant difference in CD44+ area (F= 0.0032, p-value = 0.9978). All statistical analyses were completed using one-way ANOVA. Post-hoc analysis was not completed because the overall ANOVAs were displayed as non-significant. Data is visualised as mean ± S.D. Biological repeats (n=3) of one AD line (AD 2) were averaged from 3 technical repeats for Vimentin and CD44. For intensity after Aβ treatment, results were normalised total intensity/cell area/total cell count to create an intensity ratio. For intensity after Aβ treatment, results were normalised total area/total cell count.*

5.4. Discussion

5.4.1. Overview

This chapter aimed to investigate the induction of pro-inflammatory markers in iAstrocytes in response to different Aβ aggregate species and compositions. Previously, the release of pro-inflammatory markers after the uptake of specific species of Aβ in different ratios, and isoform (oligomers and fibrils) remains largely unexplored in human-derived astrocytes. The results highlight that both control and AD iAstrocytes exhibit increased secretion of pro-inflammatory cytokines, TNF-α, IL6, and IL-1β, and chemokine, MCP1, in response to Aβ treatment. This outcome was expected, as astrocytes have a pivotal role in maintaining homeostasis in the brain and responding to environmental cues. Under normal physiological conditions, astrocytes survey and respond to physical and chemical signals within their surroundings. However, during Aβ deposition and propagation, aggregated Aβ can activate acute or chronic responses in the astrocytes, as indicated by the excessive secretion of pro-inflammatory markers (Deng et al., 2024). Interestingly, when comparing the induction of pro-inflammatory markers after the treatment of Aβ, key patterns in both AD and control groups emerge, suggesting potential differences in astrocytic reactivity and inflammatory responses between the two groups. Firstly, AD lines had a heightened secretion of pro-inflammatory markers compared to control lines, particularly in response to oligomeric species, and at lower Aβ40: Aβ42 fibril ratios (10:0 and 9:1). Finally, in iAstrocytes, Aβ42 aggregates are a key driver of pro-inflammatory cytokines and chemokine induction.

5.4.2. Astrocytes derived from individuals with AD have an amplified induction of pro-inflammatory markers after the treatment of Aβ

At baseline, or no Aβ treatment, there was no difference in cytokine levels between control and AD astrocytes. This suggests that Aβ exposure is the key trigger for inflammation rather than intrinsic differences in resting cytokine levels. However, distinct differences emerged following Aβ oligomer treatment. Upon treatment with Aβ oligomers, Aβ40 (10:0), Aβ40: Aβ42 (9:1), and Aβ40: Aβ42 (7:3) induced higher TNF-α, MCP1, IL-1β, and IL6 secretion in AD astrocytes compared to control iAstrocytes. Similarly, Aβ42 (0:10) led to increased TNF-α, MCP1, and IL6 secretion in AD astrocytes compared to controls, though IL-1β levels did not

differ significantly. Similarly, when analysing Aβ fibril treatments, specific patterns of pro-inflammatory marker induction were observed based on the Aβ species and ratio. Aβ40 and Aβ40: Aβ42 (9:1) fibril treatment resulted in a higher pro-inflammatory cytokine induction than control across all measured cytokines. These results align with previous findings and add the knowledge of pro-inflammatory markers from human derived astrocytes showing that individuals with AD have elevated levels of pro-inflammatory markers, TNF-α, IL6, IL-1β and MCP1 (Meraz-Rios et al., 2013). Previous studies have also shown that AD patients' cerebrospinal fluid levels of pro-inflammatory markers are elevated (Taipa et al., 2019; Chen et al., 2018; Jiang et al., 2011). Furthermore, in post-mortem tissue, heightened pro-inflammatory markers are associated with brain regions affected by AD pathology, such as the mid-temporal cortex, hippocampus, and entorhinal cortex (Chai et al., 2023; Wood et al., 2015). Earlier studies have shown in transgenic mouse models that overexpress APP, a key presenilin gene in producing Aβ, and known familial AD risk factor, cytokine levels were dependent on Aβ levels (Patel et al., 2005). Elevated pro-inflammatory markers have been closely associated with astrocytes and after exposure to Aβ (Gonzalez-Reyes et al., 2017). With changes in the Aβ ratio in fibrils, distinct patterns of pro-inflammatory markers were observed between AD and control. When analysing the fibrillar species, Aβ42 fibrils exhibited the highest potency in inducing pro-inflammatory markers. However, despite their strong inflammatory response, there was no significant difference in cytokine induction between AD and control astrocytes for MCP1 and IL-1β, but did cause higher TNF-α and IL6. Furthermore, Aβ40: Aβ42 (7:3) fibrils resulted in higher TNF-α and MCP1 secretion in AD astrocytes but did not significantly affect IL6 or IL-1β compared to control. Suggesting that fibrils have more of selective activation of astrocytes in this context. Although both control and AD iAstrocytes exhibit an increased secretion of cytokines and chemokines, AD exhibited a heightened induction of pro-inflammatory markers overall compared to control astrocytes, particularly with oligomer treatment. Suggesting that oligomeric Aβ species are more potent in triggering astrocyte-associated inflammation, potentially due to their higher solubility, reactivity, or ability to engage astrocyte receptors (Tolar et al., 2021).

In summary, both Aβ oligomers and fibrils induced significant pro-inflammatory cytokine and chemokine secretion in iAstrocytes, with astrocytic cytokine and chemokine release depending on Aβ species, conformation, and ratio, with AD-derived astrocytes displaying heightened sensitivity.

5.4.3. iAstrocytes have a selective response to the induction of pro-inflammatory markers after the treatment of Aβ

As previously discussed, treatment with Aβ oligomers resulted in a significantly higher induction of pro-inflammatory markers in AD astrocytes than control astrocytes. Aβ oligomers are closely related to AD pathogenesis *in vitro*, *in vivo*, animal models and individuals with AD (Madhu and Mukhopadhyay, 2021). This is due to their soluble nature, allowing them to move in the intracellular space and interact with multiple receptors on the cell membrane to induce extracellular and intracellular toxicity to trigger downstream AD-associated pathways. Aβ oligomers have been linked to neuroinflammation, oxidative stress, mitochondria damage, tau hyperphosphorylation, membrane permeabilisation, and calcium dysregulation (Azargoonjahromi, 2024). Furthermore, Aβ oligomers have been associated with synaptic dysfunction, neuronal degeneration, DNA damage, and, ultimately, neuronal death associated with AD. In mice, the concentration of Aβ oligomers is correlated with the severity of neurotoxicity (DaRocha-Souto et al., 2011).

When treated with Aβ oligomers and fibrils, AD and control astrocytes secreted TNF-α, MCP1, IL-1β, and IL6 across all Aβ ratios. However, when analysing different Aβ ratios compositions, composition-dependent responses occur in both control and AD lines. When comparing Aβ40 (10:0) and Aβ40 (9:1) there were markedly no significant increase TNF-α, MCP1, IL6, and IL-1β. Suggesting a composition-dependent response, where specific Aβ ratios influence astrocytic cytokine secretion patterns. This distinction is crucial, as it highlights differences in how astrocytes respond to different Aβ species and suggests that Aβ-induced inflammation may vary depending on the aggregation state of the peptide. This chapter demonstrates that control and AD astrocytes secrete pro-inflammatory markers in response to Aβ exposure, reinforcing that pro-inflammatory signalling is critical to astrocyte-mediated responses to amyloid pathology. Pro-inflammatory markers play a vital role in cell communication, which can activate or be activated by pathways that have downstream effects related to cellular function, inflammation, and AD (Chen et al., 2024).

Firstly, TNF-α, IL6, IL-1β and MCP1 have all been implicated in activating the mitogen-activated protein kinase (MAPK) pathways (Sabio and Davis, 2014; Kim and Choi, 2010). The MAPK pathway is a highly conserved signalling cascade that regulates essential cellular

functions, including cell growth, apoptosis, proliferation, metabolism, inflammation, and stress responses. In Tg2576 mice where APP is overexpressed, Aβ has been shown to upregulate the MAPK pathway via the nicotinic acetylcholine receptors (a7 nAChR) in the hippocampus (Dineley et al., 2001). Whereby Tg2576 mice with elevated a7 nAChR failed to complete the Morris water maze test, which measures spatial learning and memory (Dineley et al., 2001). Suggesting the link between Aβ and nAChRs in AD pathology. In cell culture and rat cortex, Aβ has been shown to activate the MAPK-associated P38K and JNK pathway in astrocytes (Saha et al., 2020). P38K and JNK are stress-activated protein kinases which have been shown to induce the production of TNF-α, IL6, and IL-1β (Saha et al., 2020; Cuenda and Rousseau, 2007). Besides the MAPK pathways, the JAK-STAT pathway regulates gene expression and cell activation for several functions, including immune system function, tissue repair, cell proliferation, and apoptosis (O'Shea et al., 2015). It has also been shown to activate cytokine production in response to stress (Hu et al., 2021). The JAK-STAT pathway functions by a specific cytokine binding to receptors on the cell membrane, triggering the Janus kinase enzyme (JAK) enzyme to phosphorylate the STAT protein (Xue et al., 2023). In response, the STAT translocates to the nucleus, regulating gene expression. IL6, IL-1β, and TNF-α have been shown to stimulate the JAK-STAT pathway, which in turn activates the production of MCP1 as a downstream target (Hu et al., 2023; Huang et al., 2022; Hu et al., 2021). MCP1 is increased in both AD and control, regardless of Aβ ratio and species, compared to no treatment of Aβ. As MCP1 is consistently upregulated, this could be potentially due to its role as a chemokine immune signalling molecule in response to Aβ and pro-inflammatory markers; TNF-α, IL6, and IL-1β. MCP1 is predominantly secreted from glial cells, and elevated levels have been found in AD patients' plasma and CSF (Westin et al., 2012). In this study, the AD astrocytes had significantly higher MCP1 induction after Aβ treatment all ratios. In transgenic mouse models of AD (APP/PSEN1, and Tg2576), a decrease in MCP1 expression increased the levels of soluble Aβ in the brain (Zuena et al., 2019). Suggesting a link between MCP1 and Aβ clearance. MCP1 has also been located in the senile plaques of AD patients (Zuena et al., 2019). Highlighting an important relationship between Aβ and MCP1.

Another pathway which TNF-α, IL6, IL-1β, and MCP1 have been associated with is the nuclear factor kappa (NF-kB) pathway (Yu et al., 2020; Rex et al., 2019). The NF-kB pathway is a complex, highly regulated signalling cascade which has a pivotal role in the inflammatory

and immune response. Though NF-kB is found in both glial cells and neurones, toll-like receptors, which are predominantly found in glial cells, activate the Nf-kB pathway (Li et al., 2021; Kaltschmidt et al., 2005). The activation of the NF-kB pathway leads to the expression of pro-inflammatory markers, including TNF-α, IL6, IL-1β, and MCP1. In the context of AD, Aβ oligomers, in particular, have been shown to activate the NF-kB pathway in neurones and glial cells and induce the expression of pro-apoptotic genes (Snow and Albensi, 2016). For example, Aβ40 activated several NF-kB regulatory genes in primary neurones, promoting dysregulation and cell death (Valerio et al., 2006). Interestingly, studies have shown that in the cerebral cortex of AD patients, NF-kB levels correlate with the APP-cleaving enzymes BACE1 and β-secretase (Sun et al., 2022). Others have shown that the activation of the NF-kB pathway leads to the increased accumulation of Aβ42 and increased cytokines and chemokine production as a result (Kaur et al., 2019). The NF-kB pathway dysregulation is associated with the overexpression of pro-inflammatory cytokines, leading to a cycle of elevated inflammatory response (Sun et al., 2022). This prolonged or chronic inflammatory response is a key hallmark of AD (Botella Lucena and Heneka, 2024).

5.4.4. Dual Role of Inflammation in AD and Associated Neurodegeneration

Although inflammation is widely regarded as a pathological feature of AD and other neurodegenerative diseases, it also has potential neuroprotective functions (DiSabato et al., 2016). For example, IL6 has been shown to promote neuronal survival and regeneration of synapses after injury (Yang et al., 2012). On the other hand, TNF-α can modulate synaptic plasticity in neurones which is essential for learning and memory (Park and Bowers, 2010). In astrocytes, MCP1 has been shown to be neuroprotective against excitotoxicity, whilst TNF-α aids calcium and glutamate regulation (Wang et al., 2023; Gonzalez Caldito, 2023).

Despite the observed increase in pro-inflammatory marker secretion following Aβ treatment, this study did not evaluate the induction of anti-inflammatory markers, which are also key players in neuroimmune homeostasis. In CSF and plasma of AD patients, anti-inflammatory cytokines such as IL-1ra, IL-33, and IL-10 are elevated (Chen et al., 2024). During disease progression, IL-2, IL-3, IL-33, and IL-33 increase, potentially protecting against neuroinflammation (Brosseron et al., 2014). Other anti-inflammatory cytokines included IL-4, IL-10, and TGF-β (Gonzalez Caldito, 2023). Many pro-inflammatory markers

have anti-inflammatory markers of the same family. For example, IL-1β and IL-33 belong to the IL-1 family and are often induced simultaneously (Chen et al., 2024). The diverging pathway of function may arise due to the complex nature of pathways, which are activated from cytokines and result in a variation of signalling pathways.

Given that AD astrocytes overall had higher induction of pro-inflammatory markers than control in this study, it is possible that control astrocytes may have a greater ability to upregulate anti-inflammatory responses, thereby maintaining a more balanced inflammatory state. It would also be interesting to measure the secretion of anti-inflammatory markers as a result of Aβ treatment as a future research point, as this could provide further insights into the regulatory mechanisms that govern the inflammatory balance in astrocytes and their role in AD progression.

5.4.5. Aβ42 is a Key Driver of the Induction of Pro-inflammatory Markers in iAstrocytes

In control and AD iAstrocytes, increased ratios of Aβ42 (Aβ42 alone or Aβ40: Aβ42 (7:3)) result in significantly increased cytokine secretion compared to lower ratios of Aβ40 (Aβ40 alone or Aβ40: Aβ42 (9:1)) oligomers in all cytokines. This is also supported by the results that with increasing Aβ42, there are significantly higher cytokines and chemokines across all groups besides Aβ40 (10:0) vs Aβ40: Aβ42 (9:1), or Aβ40: Aβ42 (7:3) vs Aβ42 (0:10) (Summary Table) in control iAstrocytes. In both control and AD astrocytes, Aβ42 (0:10) and Aβ40: Aβ42 (7:3) induced the secretion of IL-1β compared to Aβ40 (10:0) and Aβ40; Aβ42 (9:1). Highlighting that Aβ42 is a key regulator of the induction of pro-inflammatory markers in iAstrocytes. One note is that when control iAstrocytes were treated with Aβ oligomers, there was a trend to higher taken up as the ratio the Aβ42: Aβ40 was increased. As a result, Aβ42 (10:0) aggregates were taken up significantly more than both Aβ40 (10:0) and Aβ40: Aβ42 (9:1), but not Aβ40: Aβ42 (7:3), suggesting a preferentially uptake to Aβ42 (10:0) oligomers. In AD patient-derived models, when iAstrocytes were treated with Aβ oligomers, Aβ42 (0:10) was taken up significantly more than both Aβ40: Aβ42 9:1 and 7:3, but not Aβ40 oligomers. Therefore, the release of cytokines and chemokines during increased Aβ42: Aβ40 ratios may be as a result of the internalisation of Aβ itself. Therefore, the increased uptake of Aβ42 may correlate with the secretion of cytokines and chemokines, and future analyse should focus on normalising the release to uptake of Aβ species. Despite this, the hypothesis

that Aβ42 is more toxic than Aβ40 is widely accepted, and several studies have highlighted its greater toxicity (Song et al., 2022; Phillips, 2019; Chang and Chen, 2014; Hayden and Teplow, 2013; Kuperstein et al., 2010). There was not a significant difference in cytokine secretion between Aβ40 (10:0) and Aβ40: Aβ42 (9:1), suggesting that lower Aβ42 concentrations do not strongly induce pro-inflammatory cytokines in both control and AD cell lines. These results highlight an important link between increased Aβ42 compared to Aβ40 in the induction of pro-inflammatory markers.

Aβ40 is the more abundant isoform in the human brain and is found at levels ~10 times higher than Aβ42 in the healthy brain (Dorey et al., 2015). However, despite its lower concentration, Aβ42 is the predominant component of amyloid plaques, particularly in the frontal cortex and hippocampus, the brain regions most affected by AD. Over the course of disease progression, the Aβ40: Aβ42 ratio in the CSF increases, reflecting the selective deposition of Aβ42 into plaques, a well-established biomarker of AD pathology (Hansson et al., 2019). While CSF measures Aβ in the brain fluid, Aβ positron emission tomography (Aβ PET) measures widespread aggregate deposition of plaques in the brain (Lowe et al., 2024). A decreased Aβ40: Aβ42 ratio is associated with an increase in Aβ plaques in the brain, of which Aβ42 is the main component (Yang et al., 2022b; Gu and Guo, 2013). The change in Aβ accumulation is found in the earlier stages of AD and before detectable levels of cognitive decline (Hampel et al., 2021). Other studies have shown that the inflammatory response is an early characteristic of AD (Chen et al., 2024; Botella Lucena and Heneka, 2024). The findings from this study demonstrate that an increased Aβ42 ratio strongly induces pro-inflammatory cytokine secretion in astrocytes, reinforcing the link between Aβ42 accumulation and neuroinflammation. The results of this chapter highlight an important connection between Aβ42 and cytokine production in astrocytes, with Aβ42-rich oligomers acting as key drivers of pro-inflammatory marker induction. Given that Aβ42 accumulation and inflammation both precede cognitive decline in AD, these findings suggest that targeting Aβ42-mediated astrocyte activation could be a viable strategy for modulating early neuroinflammatory responses in AD.

5.4.6. Expression of GFAP, Vimentin, and CD44 in Astrocytes post Aβ Treatment

As part of the morphological changes, astrocytes exhibit an increased expression of immunoreactivity markers such as GFAP, Vimentin, and CD44 (Konstantinidis et al., 2023a; Smit et al., 2021). Additionally, astrocytes undergo hypertrophy including increased cell body size and branching (Kumar et al., 2023). Therefore, as CD44, GFAP, and Vimentin were analysed as reactivity markers after the treatment of Aβ. The results of this study showed that although the astrocytes had positive staining for all reactivity markers, there were no statistical differences in both the intensity and the area of the cells. Though, there were trends of Aβ40 oligomers and Aβ42 oligomers increasing CD44, GFAP, and Vimentin in control iAstrocytes. A trend of increased area of GFAP and Vimentin accompanied this. However, there was no clear upregulation of markers. In AD, preliminary data of GFAP also suggests no trends in the intensity of area changes. A main hypothesis for these results is due to the small sample size of cell lines (1 control, 1 AD line, n=3). In the case of AD GFAP staining, this was carried out n=1. Furthermore, there is a large variability between the repeats, and future work should look to complete the repeats with more cell lines.

5.5. Conclusions

This chapter provides new key insights into the role of Aβ aggregation state and composition in driving astrocyte-mediated inflammation. The findings demonstrate that Aβ42 is a primary driver of pro-inflammatory cytokine induction in both control and AD iAstrocytes, with higher Aβ42 ratios (Aβ42 alone or Aβ40: Aβ42 (7:3) inducing significantly more TNF-α, IL6, IL-1β, and MCP1 secretion compared to lower Aβ42 compositions. This response was particularly pronounced in AD astrocytes, suggesting that AD-derived astrocytes are primed or reactive, making them more susceptible to Aβ-induced inflammatory signalling. While Aβ oligomers were the most potent inducers of pro-inflammatory markers, Aβ42 fibrils selectively increased secretion of specific pro-inflammatory markers, reinforcing that different Aβ conformations contribute distinctly to astrocyte reactivity. The results also suggest a composition-dependent response, where lower Aβ42 ratios (pure Aβ40 or Aβ40: Aβ42 (9:1) did not strongly induce inflammation, while higher Aβ42 ratios had a more robust effect. These findings align with the widely accepted notion that Aβ42 is more neurotoxic than Aβ40, largely due to its greater

aggregation propensity and ability to trigger cellular stress pathways. In healthy individuals, Aβ40 is ~10 times more abundant than Aβ42; however, in AD, Aβ42 preferentially deposits into plaques, a hallmark of disease pathology. Over time, the Aβ42: Aβ40 ratio progressively increases in the AD brain, marking one of the earliest dysfunctions observed in the disease. This imbalance disrupts Aβ clearance, impairs synaptic function, and exacerbates neuroinflammation, contributing to the early pathology of AD. Since neuroinflammation and Aβ dysregulation emerge early in AD, these findings further support the hypothesis that Aβ42-induced astrocyte activation plays a key role in a self-sustaining inflammatory feedback loop.

Altogether, this chapter highlights how different Aβ compositions influences astrocyte function and provides valuable insights into the link between Aβ aggregation and inflammation. These results indicate that targeting Aβ42-mediated astrocyte activation could be a potential therapeutic strategy to modulate early neuroinflammatory responses in AD. Future research should explore how astrocytic pro-inflammatory responses interact with anti-inflammatory pathways to determine whether a dysregulated immune balance contributes to AD pathogenesis.

Chapter 6. Chronic Inflammation and Aβ Uptake in iAstrocytes

6. Chapter Overview

Following the induction of pro-inflammatory markers post Aβ uptake in iAstrocytes (Chapter 5, pp., 101-147), the next step was to investigate if chronic inflammation influences the uptake of Aβ species in both control and sporadic AD iAstrocytes. To address this, iAstrocytes were treated with high (100ng/mL) or low (10ng/mL) doses of cytokine mixtures for 24 hours pre-Aβ treatment, and the uptake was measured by immunofluorescence (Sections 2.2.6 and 2.2.11.). This chapter explores how prolonged treatment of pro-inflammatory markers impacts astrocytes and their ability to uptake Aβ—overall, shedding light on the interplay between neuroinflammation and Aβ internalisation mechanism in AD progression.

6.1. Introduction

Neuroinflammation is a key regulatory process in the peripheral and central nervous systems (CNS), acting as a protective response to injury, illness, or stress. Inflammation protects neural tissue, repair damage, and clears away pathogens, cellular debris, and toxins from the brain. Astrocytes are essential in controlling and modulating neuroinflammatory processes, including the clearance of Aβ in the brain, associated with the inflammatory response. While acute neuroinflammation benefits pathogen defence and tissue repair, prolonged or chronic neuroinflammation has emerged as a key driver of AD pathology (Kinney et al., 2018). Evidence from postmortem AD brains and preclinical studies indicates that persistent inflammation is a hallmark of disease progression (Novoa et al., 2022; Knezevic and Mizrahi, 2018; Gomez-Nicola and Boche, 2015; Sudduth et al., 2013).

Astrocyte activation is often seen as a protective mechanism, as it has been associated with enhanced Aβ clearance (Novoa et al., 2022). However, prolonged inflammation exacerbates both Aβ and Tau pathology, key hallmarks of AD (Kinney et al., 2018). In particular, studies have shown that pro-inflammatory markers influence the uptake of Aβ, altering glia-mediated clearance capacity (Botella Lucena and Heneka, 2024). Prolonged elevated levels of pro-inflammatory markers have been linked to a vicious cycle of aggregation and inflammation, where inflammation enhances Aβ production and

aggregation, and aggregated Aβ further sustains inflammatory responses (Whiten et al., 2020).

Beyond Aβ aggregation and inflammation, inflammation-induced astrocyte activation can alter extracellular vesicle composition, modify lipid metabolism, and compromise blood-brain barrier integrity, all of which facilitate the spread of toxic Aβ species throughout the brain (Singh, 2022; Kim et al., 2022; Gharbi et al., 2020). Given the elevation of pro-inflammatory markers after Aβ uptake in both control and AD iAstrocytes (Chapter 5, pp., 101-149), it is crucial to determine whether AD-derived astrocytes are more susceptible to inflammation than control astrocytes. Previous findings suggest that AD astrocytes exist in a reactivity continuum, which may make them more sensitive to inflammatory stimuli (Sarkar and Biswas, 2021; Linnerbauer et al., 2020). As a result, this could potentially impair Aβ internalisation, leading to increased accumulation of toxic Aβ species and exacerbating disease progression. In contrast, if control and AD iAstrocytes respond similarly to prolonged cytokine exposure, this would suggest that chronic inflammation disrupts Aβ clearance pathways in astrocytes universally, regardless of the disease state. Therefore, it is critical to begin understanding how prolonged inflammation influences astrocyte-mediated Aβ uptake. Overall, this chapter will provide insights into the dynamic interplay between neuroinflammation, protein uptake, and disease progression in AD.

6.2. Hypothesis, Aims, and Objectives

6.2.1. Hypothesis

Chronic inflammation is a hallmark of AD, along with impaired Aβ clearance in the brain. Astrocytes have a pivotal role in both Aβ clearance and inflammation.

Hypothesis 1: Prolonged treatment of pro-inflammatory cytokines will alter the uptake of Aβ species by iAstrocytes, specifically AD iAstrocytes.

6.2.2. Aims

This chapter aimed to investigate if chronic inflammation affected the uptake of Aβ species in both control and AD iAstrocytes. It sought to identify if there are differences in Aβ40 and Aβ42: oligomers or fibrils, uptake after prolonged cytokine treatment. Given the pivotal role in AD pathology, understanding how chronic inflammation may influence the build-up of Aβ in the brain is critical. This chapter aimed to determine whether AD iAstrocytes exhibit heightened susceptibility to chronic inflammation, potentially exacerbating Aβ aggregation, neurotoxicity, and neurodegeneration.

6.2.3. Objectives

1. Quantify the differential uptake of Aβ40 and Aβ42 (oligomers and fibrils) in iAstrocytes after 24-hour cytokine treatment, assessing uptake in a dose-dependent manner.

2. Determine whether chronic cytokine exposure differentially affects Aβ uptake in control versus AD iAstrocytes, evaluating if AD-derived iAstrocytes are more vulnerable to prolonged inflammatory conditions.

6.3. Results

6.3.1. Uptake of Aβ in Control iAstrocytes after Prolonged Cytokine Treatment

In order to assess the effect of chronic inflammation of Aβ, the cytokine exposure assay was utilised (Section 2.2.11). Briefly, iAstrocytes were treated with a mixture of cytokines for 24 hours at a low (10 ng/mL) and high dose (100 ng/mL). After 24 hours, iAstrocytes were then treated with Aβ (2.5 μM) for 1 hour before being fixed for immunocytochemistry as described in section (sections 2.2.6. and 2.2.9) (Figures 44, 45, 46, and 47). In control iAstrocytes, the uptake after low dose cytokines remained largely unchanged, though there was a trend towards less uptake after high cytokine treatment (Figure 43, A).

However, there were no significant differences for Aβ40 oligomers (One-way ANOVA, Figure 43, A: $F = 0.8442$, p-value = 0.4753), Aβ42 oligomers (One-way ANOVA, Figure 43, B: $F = 1.176$, p-value = 0.3709), Aβ40 fibrils (One-way ANOVA, Figure 43, C: $F = 1.305$, p-value = 0.336), and Aβ42 fibrils (One-way ANOVA, Figure 43, D: $F = 2.655$, p-value = 0.149). Despite this non-significant decrease, after high cytokine treatment, there was a decrease of 56.07%, 74.53%, 63.16%, and 68.10% of Aβ40 oligomers, Aβ42 oligomers, Aβ40 fibrils, and Aβ42 fibrils, respectively (Figure 43, E-H). The lack of differences may stem from the large variability seen in the pure Aβ groups, which is also reflected in changes in standard deviation (S8). Highlighting a decreased variation in Aβ uptake when treated with cytokines.

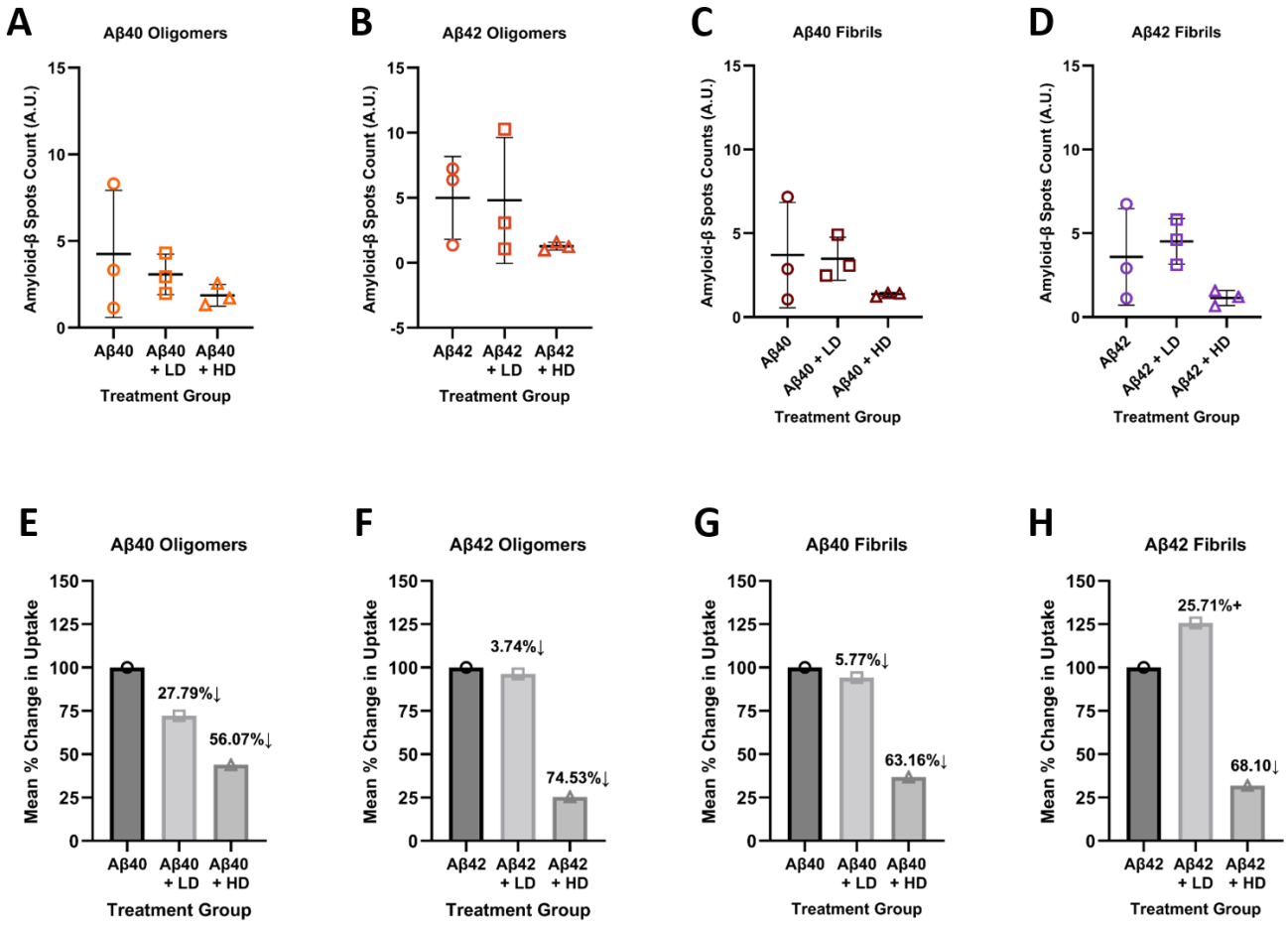

Figure 43. The uptake of Aβ in control iAstrocytes after 24-hour cytokine treatment and 1-hour Aβ (2.5 μM) treatment. A. *The uptake of Aβ40 oligomers is not significantly reduced after cytokine treatment (F = 0.8442, p-value = 0.4753).* ***B.*** *The uptake of Aβ42 oligomers is not significantly reduced after cytokine treatment (F = 1.176, p-value = 0.3709).* ***C.*** *The uptake of Aβ40 fibrils is not significantly reduced after cytokine treatment (F = 1.305, p-value = 0.336)* ***D.*** *The uptake of Aβ42 fibrils is not significantly reduced after cytokine treatment (F = 2.655, p-value = 0.149). LD = low dose (10 ng/mL). HD = high dose (100 ng/mL). For iAstrocytes (n=1), each data point represents 3 technical repeats averaged into 1 biological repeat of one cell line. Data is visualised as mean ± S.D. All statistical analysis was completed using one-way ANOVA. Post hoc analysis was not completed due to overall ANOVA displaying as non-significant. Where there are no statistical lines = non-significant (ns), * p-value = <0.05, ** p-value = <0.01, *** p-value = <0.001, and **** p-value = <0.0001.* ***E.*** *Average mean percentage in decrease of Aβ40 oligomers.* ***F.*** *Average mean percentage in decrease of Aβ42 oligomers.* ***G.*** *Average mean percentage in decrease of Aβ40 fibrils.* ***H.*** *Average mean percentage in decrease of Aβ42 fibrils.*

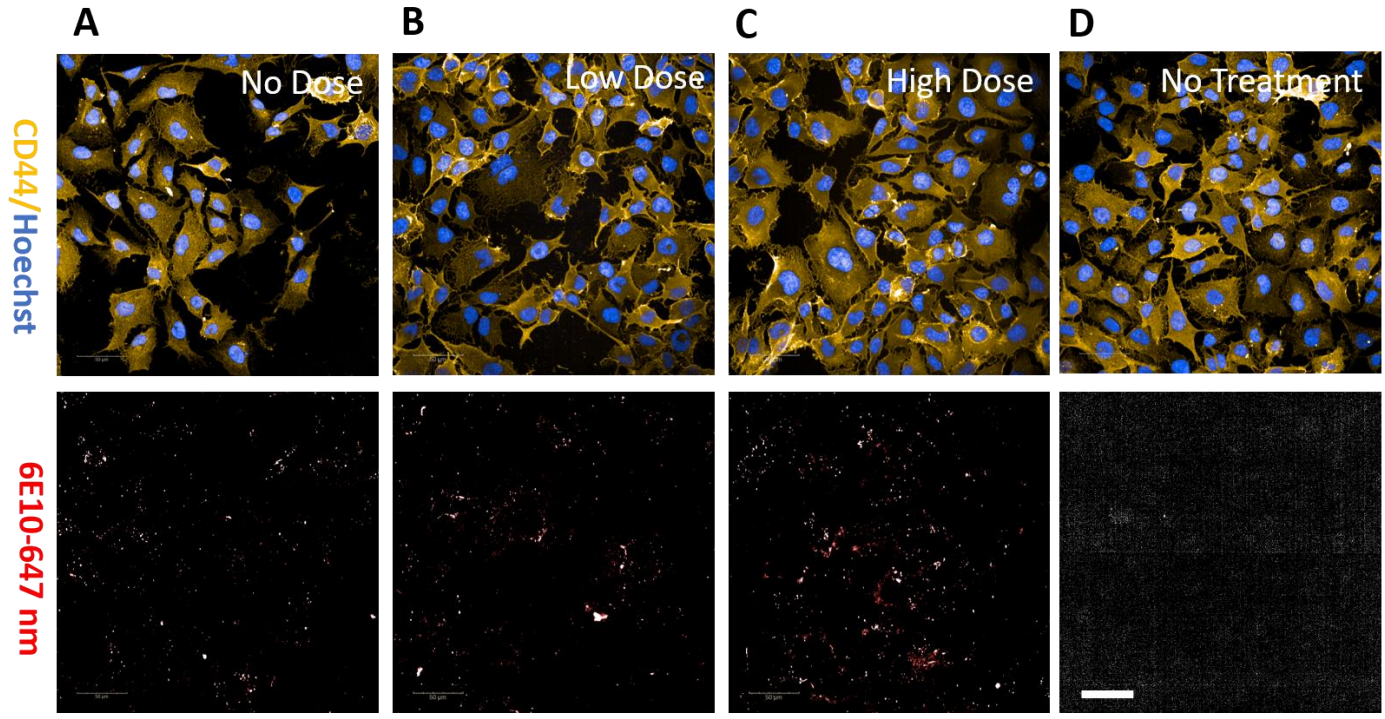

Figure 44. Illustrations of control iAstrocytes after Aβ40 (2.5 μM) oligomers treatment using immunocytochemistry. A. *No dose cytokines* ***B.*** *Low dose cytokines (10 ng/mL).* ***C.*** *High dose cytokines (100 ng/mL).* ***D.*** *No treatment. CD44 (yellow), Hoechst (blue), and Aβ (6E10-647 nm, red). Scale bar (50 μm).*

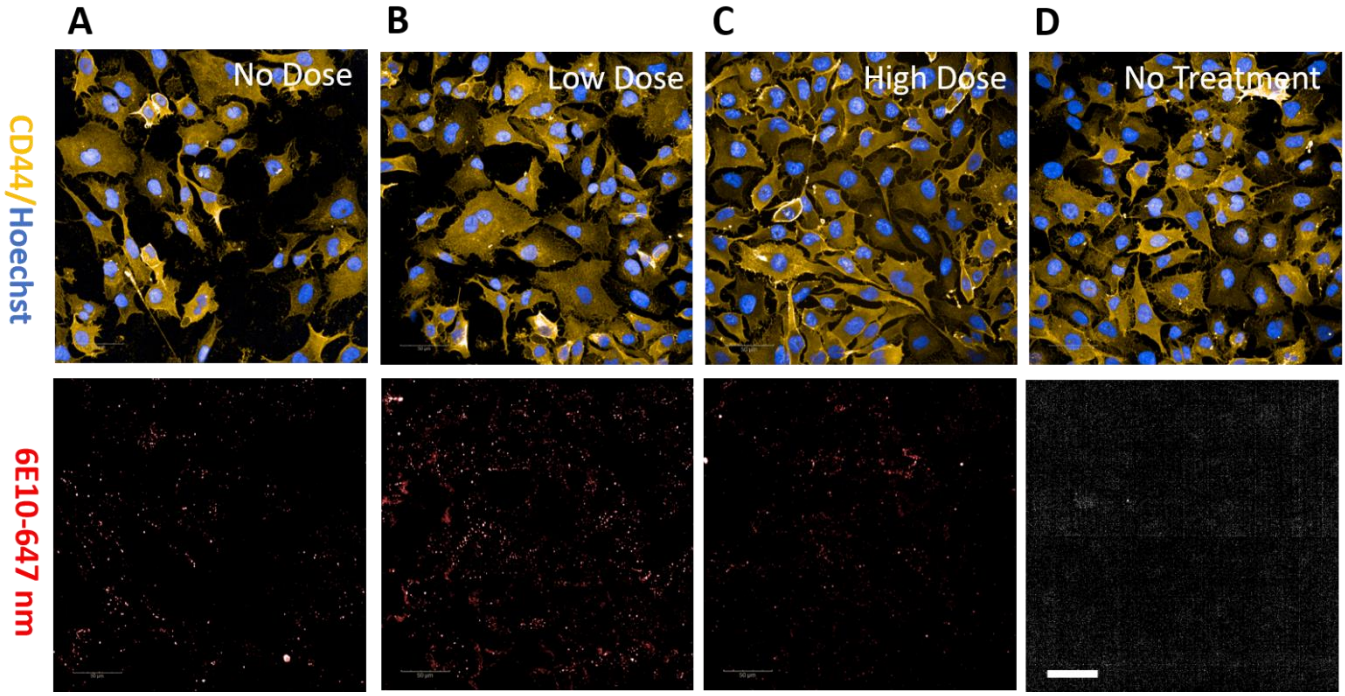

Figure 45. Illustrations of control iAstrocytes after Aβ42 (2.5 μM) oligomers treatment using immunocytochemistry. A. *No dose cytokines* ***B.*** *Low dose cytokines (10 ng/mL).* ***C.*** *High dose cytokines (100 ng/ mL).* ***D.*** *No treatment. CD44 (yellow), Hoechst (blue), and Aβ (6E10-647 nm, red). Scale bar (50 μm).*

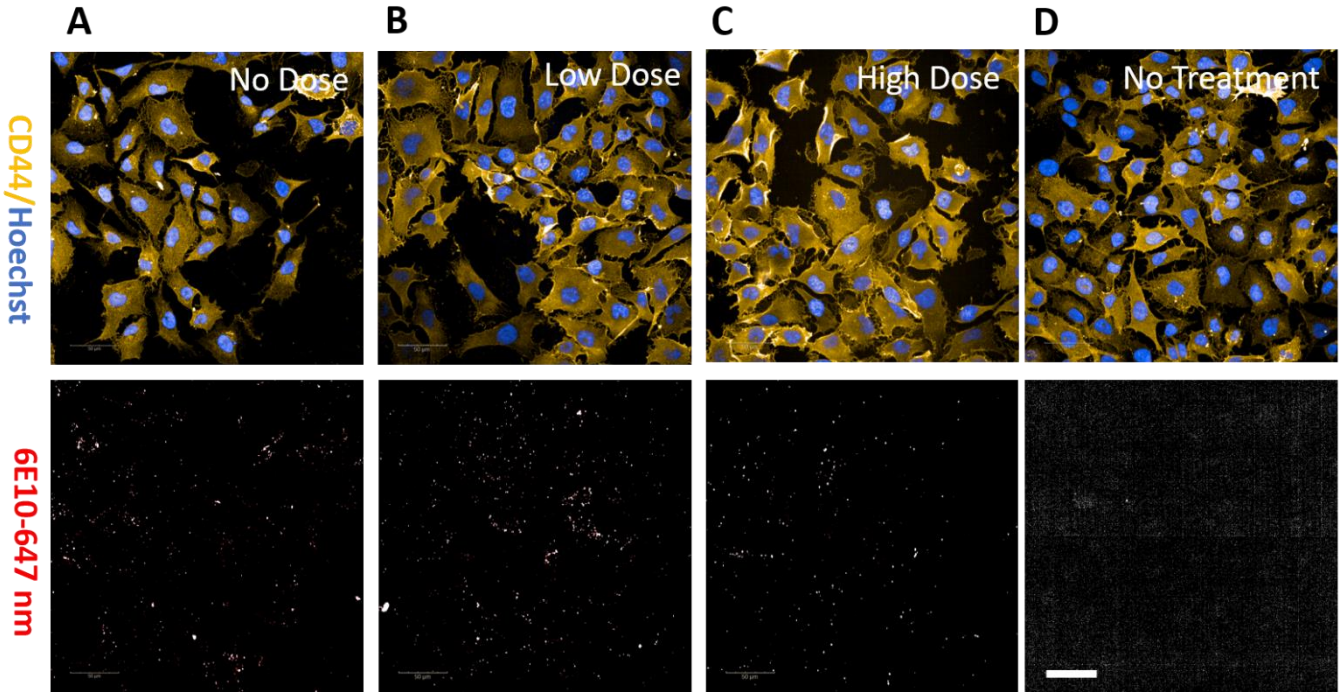

***Figure 46**. Illustrations of control iAstrocytes after Aβ40 (2.5 μM) fibrils treatment using immunocytochemistry. **A.** No dose cytokines **B.** Low dose cytokines (10 ng/mL). **C.** High dose cytokines (100 ng/ mL). **D.** No treatment. CD44 (yellow), Hoechst (blue), and Aβ (6E10-647 nm, red). Scale bar (50 μm).*

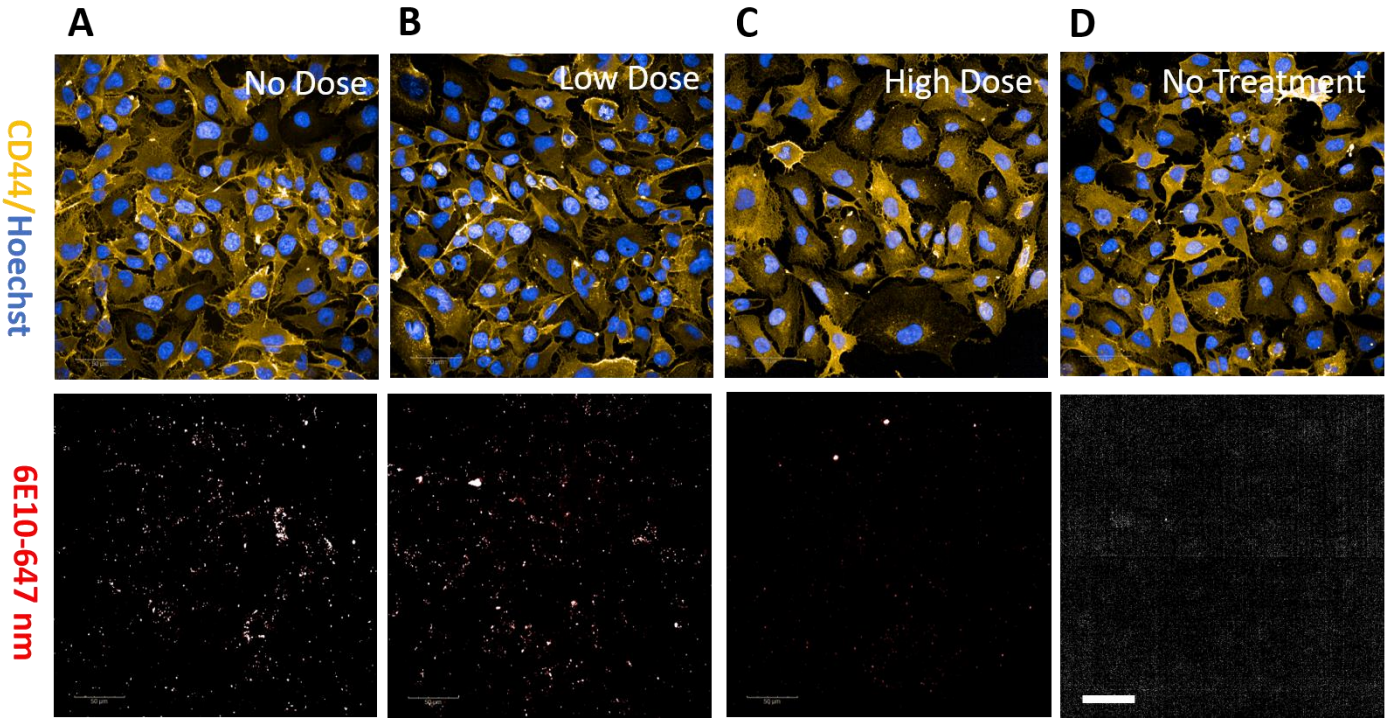

Figure 47. Illustrations of control iAstrocytes after Aβ40 (2.5 μM) fibrils treatment using immunocytochemistry. ***A.*** *No dose cytokines* ***B.*** *Low dose cytokines (10 ng/mL).* ***C.*** *High dose cytokines (100 ng/ mL).* ***D.*** *No treatment. CD44 (yellow), Hoechst (blue), and Aβ (6E10-647 nm, red). Scale bar (50 μm).*

6.3.2. Uptake of Aβ in AD iAstrocytes after Prolonged Cytokine Treatment

Similarly, to assess the impact of chronic inflammation on Aβ uptake in AD iAstrocytes, Aβ aggregates were visualised and quantified using immunocytochemistry (Figures 49, 50, 51, and 52). In contrast to control, in AD iAstrocytes, there was a statistically significant decrease in the uptake of Aβ40 oligomers (One-way ANOVA, Figure 48, A: $F = 8.683$, p-value = 0.0169), Aβ42 oligomers (One-way ANOVA, Figure 48, B: $F = 32.53$, p-value = 0.0006), Aβ40 fibrils (Figure 48, C: $F = 6.931$, p-value = 0.0276), and Aβ42 fibrils (One-way ANOVA, Figure 48, D: $F = 9.648$, p-value = 0.0133). This decrease was prominent after the treatment of low-dose cytokines for Aβ40 oligomers, Aβ42 oligomers, Aβ40 fibrils, and Aβ42 fibrils (p-values = 0.0227, 0.0012, 0.388, and 0.0171), respectively.

Similarly, the treatment of high cytokines significantly reduced the uptake of Aβ40 oligomers, Aβ42 oligomers, Aβ40 fibrils, and Aβ42 fibrils (p-values = 0.0307, 0.0009, 0.0442, and 0.0265). However, when comparing the low and high doses, there was no statistically significant difference in the uptake of Aβ isoforms (Figure 48, A-D). These results are supported by the differences in mean percentage, whereby low dose before high dose has a large effect on uptake (Figure 48, E-H). These results highlight that prolonged inflammatory signalling in AD astrocytes, regardless of cytokine dose used in this experimental design, impairs their ability to internalise Aβ, irrespective of its isoforms or aggregation state. This compromised uptake mechanism could potentially lead to further accumulation of toxic Aβ species in the brain, exacerbating disease progression and neurodegeneration in AD.

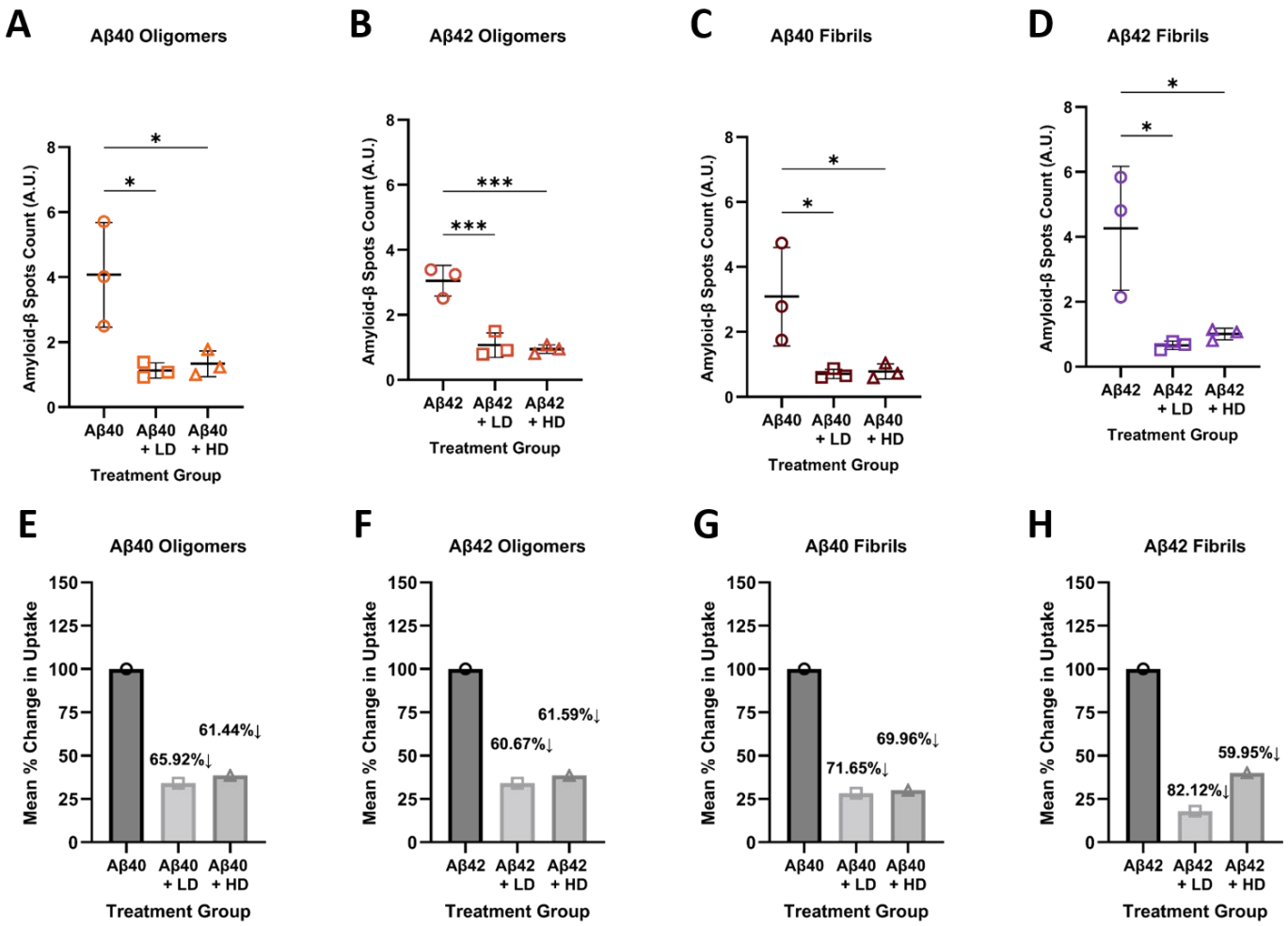

Figure 48. The uptake of Aβ in AD iAstrocytes after 24-hour cytokine treatment and 1-hour Aβ (2.5 μM) treatment. ***A.*** *The uptake of Aβ40 oligomers is significantly reduced after cytokine treatment at both high and low dose, but not between cytokine groups (ANOVA, F = 8.683, p-value = 0.0169).* ***B.*** *The uptake of Aβ42 oligomers is significantly reduced after cytokine treatment at both high and low dose, but not between cytokine groups (ANOVA, F = 32.53, p-value = 0.0006).* ***C.*** *The uptake of Aβ40 fibrils is significantly reduced after cytokine treatment at both high and low dose, but not between cytokine groups (ANOVA, F = 6.931, p-value = 0.0276).* ***D.*** *The uptake of Aβ42 fibrils is significantly reduced after cytokine treatment at both high and low dose, but not between cytokine groups (ANOVA, F = 9.648, p-value = 0.0133). LD = low dose (10 ng/mL). HD = high dose (100 ng/mL). For iAstrocytes (n=1), each data point represents 3 technical repeats averaged into 1 biological repeat of one cell line. Data is visualised as mean ± S.D. Statistical analysis was completed using ANOVA. Post-hoc analyses were completed using Tukey's multiple comparison and can be found in S9. Where there are no statistical lines = non-significant (ns), * p-value = <0.05, ** p-value = <0.01, *** p-value = <0.001, and **** p-value = <0.0001.* ***E.*** *Average mean percentage in decrease of Aβ40 oligomers.* ***F.*** *Average mean percentage in decrease of Aβ42 oligomers.* ***G.*** *Average mean percentage in decrease of Aβ40 fibrils.* ***H.*** *Average mean percentage in decrease of Aβ42 fibrils.*

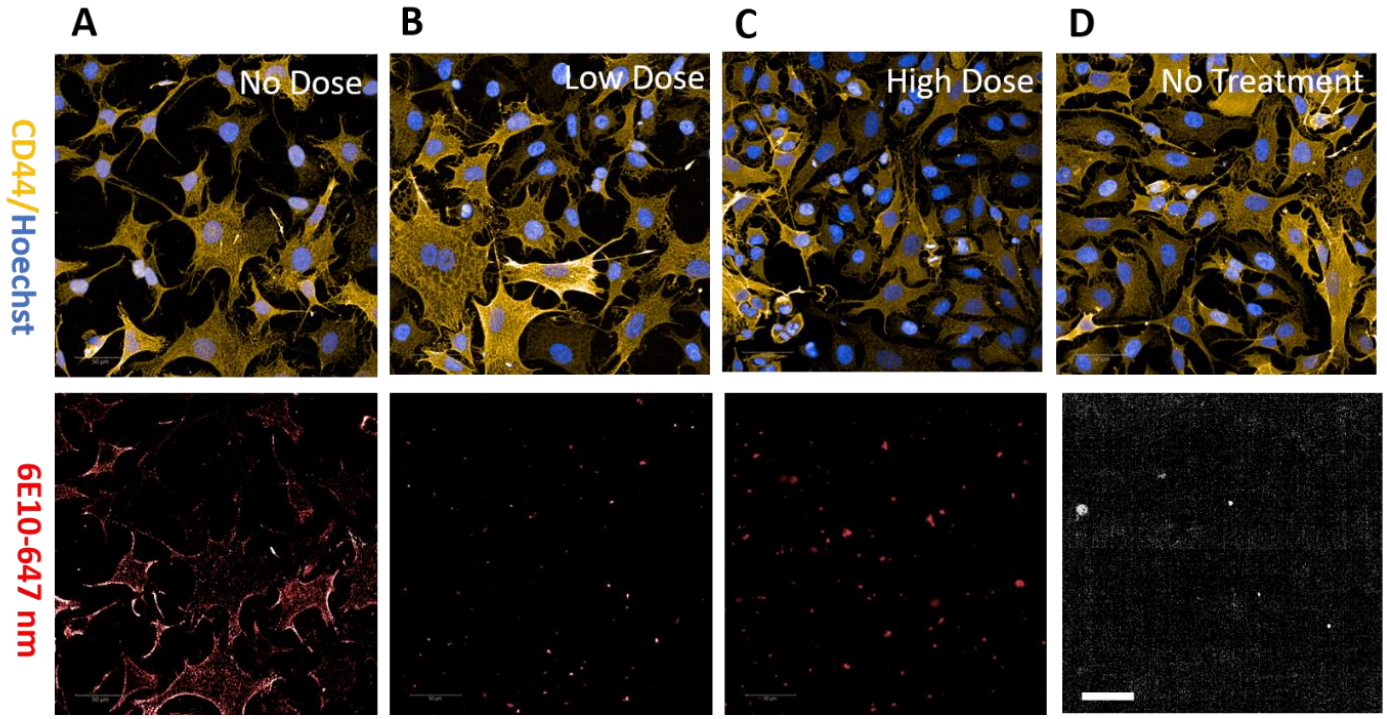

Figure 49. Illustrations of AD iAstrocytes after Aβ40 (2.5 μM) oligomers treatment using immunocytochemistry. A. *No dose cytokines* ***B.*** *Low dose cytokines (10 ng/mL).* ***C.*** *High dose cytokines (100 ng/mL).* ***D.*** *No treatment. CD44 (yellow), Hoechst (blue), and Aβ (6E10-647 nm, red). Scale bar (50 μm).*

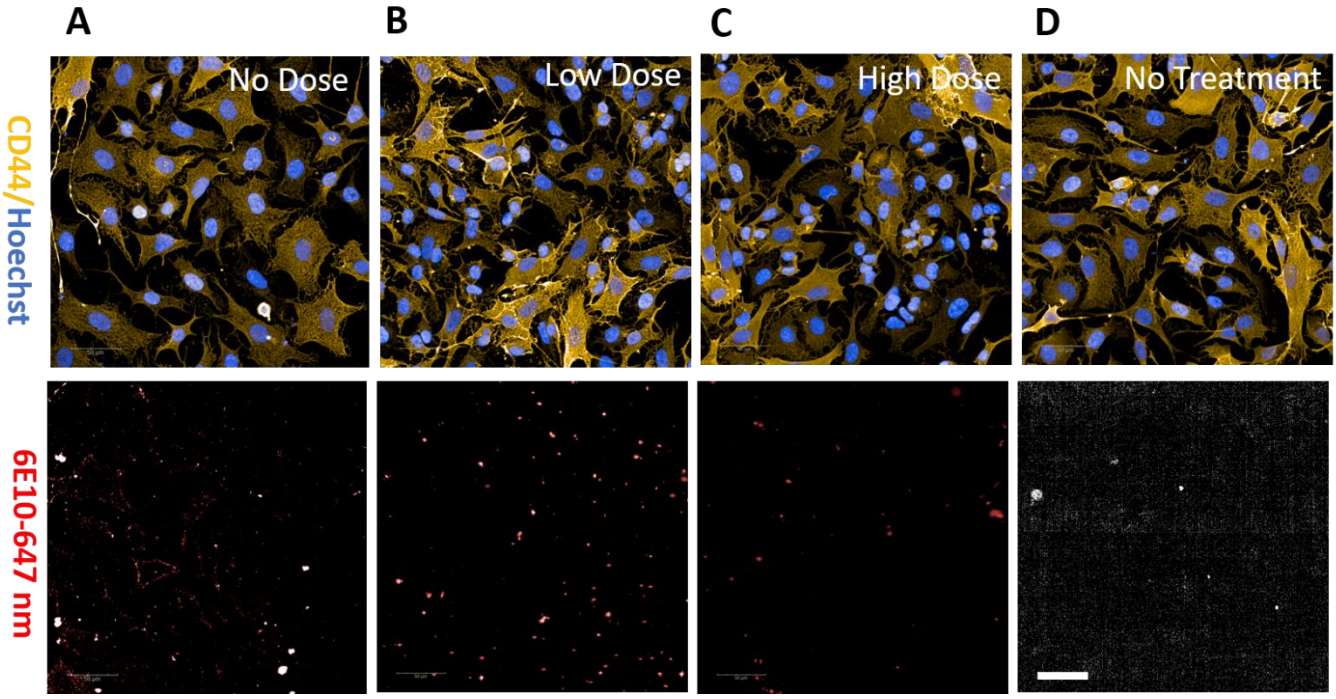

***Figure 50**. Illustrations of AD iAstrocytes after Aβ42 (2.5 μM) oligomers treatment using immunocytochemistry. **A.** No dose cytokines **B.** Low dose cytokines (10 ng/mL). **C.** High dose cytokines (100 ng/mL). **D.** No treatment. CD44 (yellow), Hoechst (blue), and Aβ (6E10-647 nm, red). Scale bar (50 μm).*

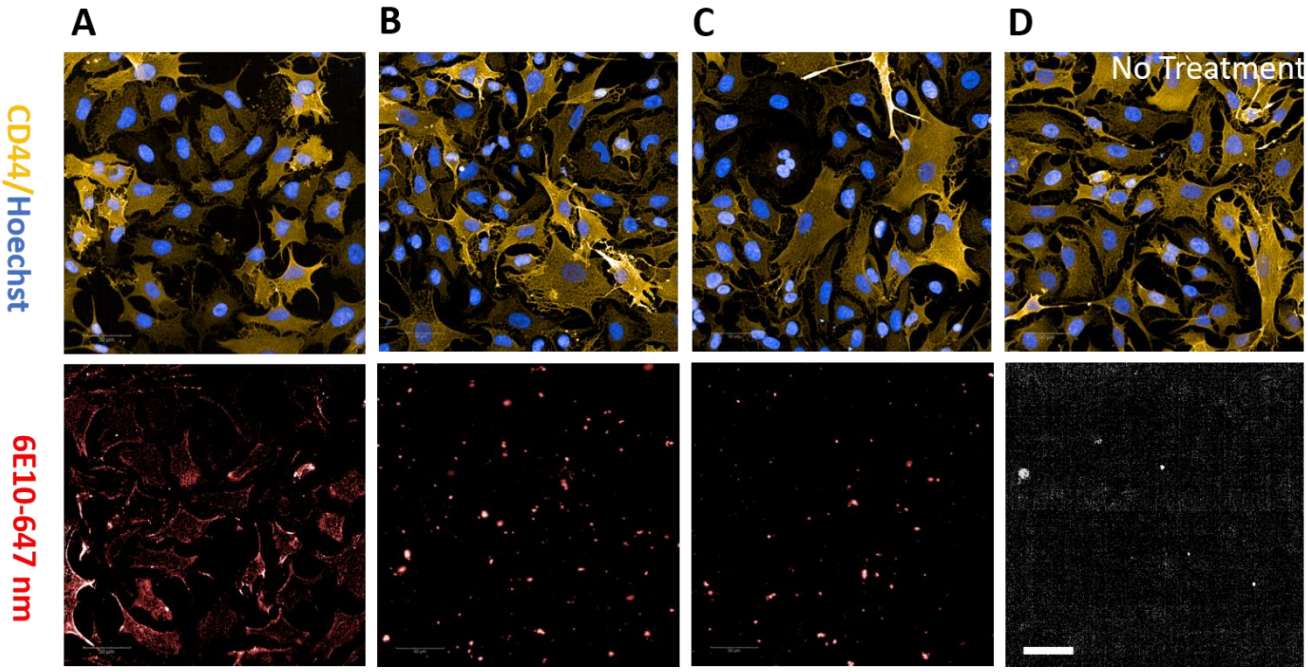

Figure 51. Illustrations of AD iAstrocytes after Aβ40 (2.5 μM) fibrils treatment using immunocytochemistry. A. *No dose cytokines* ***B.*** *Low dose cytokines (10 ng/mL).* ***C.*** *High dose cytokines (100 ng/ mL).* ***D.*** *No treatment. CD44 (yellow), Hoechst (blue), and Aβ (6E10-647 nm, red). Scale bar (50 μm).*

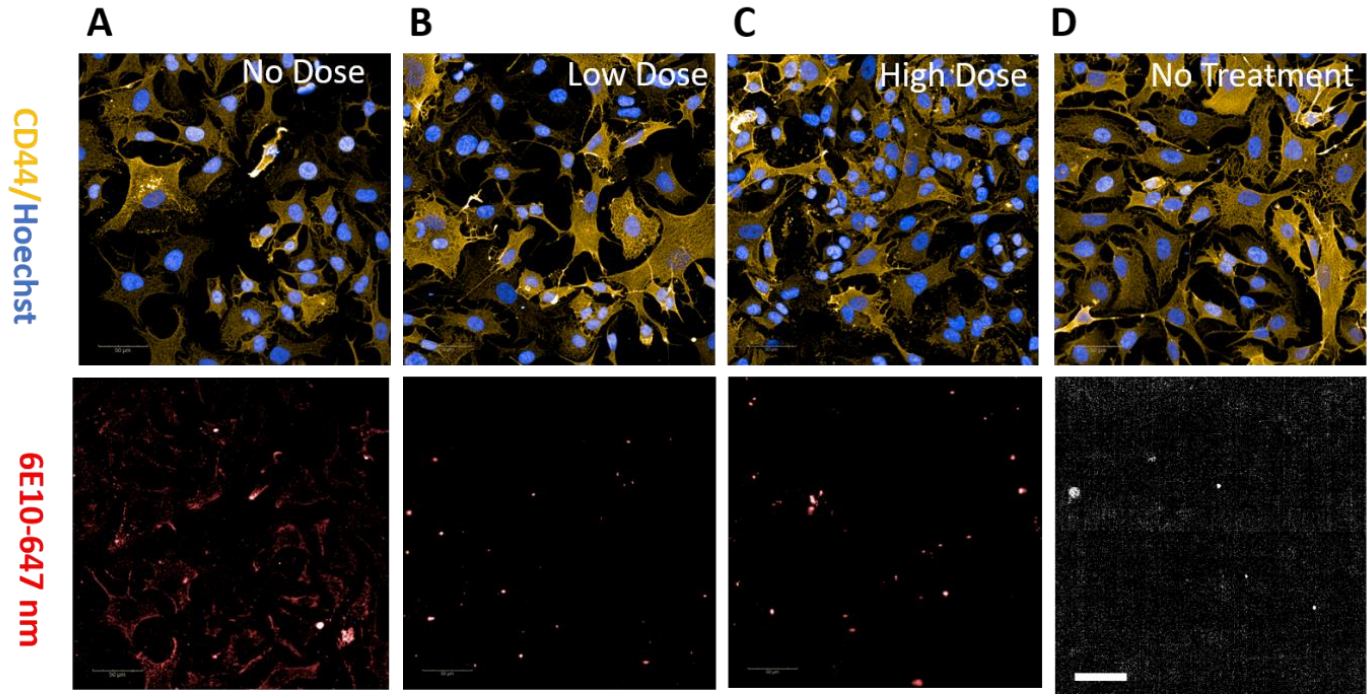

Figure 52. Illustrations of AD iAstrocytes after Aβ42 (2.5 μM) fibrils treatment using immunocytochemistry. *__A.__ No dose cytokines __B.__ Low dose cytokines (10 ng/mL). __C.__ High dose cytokines (100 ng/ mL). __D.__ No treatment. CD44 (yellow), Hoechst (blue), and Aβ (6E10-647 nm, red). Scale bar (50 μm).*

6.4. Discussion

6.4.2. Prolonged Treatment of Cytokines Reduces Aβ Uptake in iAstrocytes

This chapter aimed to investigate whether prolonged cytokine exposure alters the uptake of Aβ40/Aβ42 oligomers or fibrils. The overall results of this chapter show that in both control and AD patient-derived iAstrocytes, the uptake of Aβ is reduced regardless of isoform or aggregation state. However, in control iAstrocytes, this trend was not statistically significant despite a profound reduction, particularly in the high-dose treatment. In contrast, in AD iAstrocytes, there is a significant reduction in the uptake of Aβ at both low and high-dose cytokines. This reduction is irrespective of Aβ40 and Aβ42 and aggregate species. Despite this, there is no significant difference between uptake at low and high doses. These results support current literature that prolonged pro-inflammatory cytokines affect Aβ uptake in astrocytes.

Cytokines are widely recognised to play a dual role in AD pathology. While they are initially protective by activating immune cells such as microglia and astrocytes to enhance Aβ clearance, the prolonged presence has been shown to have pathological effects. Previous studies have highlighted that in response to being exposed to chronic pro-inflammatory cytokines, the phagocytosis of Aβ is significantly reduced in microglia, leading to an increase in Aβ deposits in the brain (Wang et al., 2015; Heneka et al., 2015). In particular, TNF-α, IL-1β, and IL6 have all been linked to reduced uptake and degradation of Aβ in microglia (Lawrence et al., 2023). Given the similarities in astrocytic and microglial Aβ handling, it is likely that prolonged exposure to these cytokines also disrupts astrocytic Aβ clearance mechanisms, as observed in this study.

Several other proposed mechanisms of Aβ clearance include enzymes, molecular chaperones, lysosomes, proteases, and endosomes expressed on the surface or internally by astrocytes that degrade and remove Aβ (Xin et al., 2018). However, the specific mechanisms by which chronic cytokine exposure alters Aβ clearance pathways in astrocytes were not explored in this study. Other studies have shown that overexposure to cytokines has been shown to downregulate receptors on astrocytes that are necessary for Aβ binding and uptake (Zhang et al., 2023c). Furthermore, prolonged inflammatory signals can dysregulate the internalisation of Aβ through phagocytosis (Lee and Landreth, 2010). *In vitro* and *in situ*

studies have shown that reactive astrocytes reduce Aβ deposits by phagocytosis (Singh, 2022). When exposed to TNF-α and IL-1β, both microglia and astrocytes have been shown to have suppressed phagocytic activity to engulf Aβ aggregates (Novoa et al., 2022). Therefore, future would be interesting to look into the effect of pro-inflammatory markers on potential Aβ clearance pathways in the iAstrocytes used in this thesis.

A defining feature of neuroinflammation is the transition of astrocytes into two main reactive phenotypes: neuroprotective (A2) and neurotoxic (A1) (Liddelow et al., 2017). The prolonged exposure to pro-inflammatory cytokines, such as IL-1β, TNF-α, and IL6, shifts astrocytes towards an A1-like reactive state, which is characterised by reduced Aβ clearance, increased neurotoxicity, and impaired neuronal synaptic support (Goshi et al., 2025). However, conflicting evidence challenges the notion that inflammatory activation universally drives astrocytes toward a neurotoxic state. Some studies suggest that co-stimulation with IL-1β and TNF-α induces an inflammatory reactive phenotype, yet these astrocytes retain neuroprotective functions despite their activation (Hyvarinen et al., 2019).

These opposite results complicate the view that neuroinflammation is solely detrimental. Instead, it suggests that reactive astrocytes exist on a spectrum where their functional role is context-dependent. In addition, they highlight the dynamic and complex nature of astrocyte reactivity, which depends on the specific inflammatory mediators, the duration and intensity of cytokine exposure, and the stage of the disease. In the short term, inflammation may be protective by enhancing Aβ clearance and neuronal support. In contrast, prolonged reactivity may disrupt the regulation of Aβ degradation and sustain neurotoxicity.

Understanding this delicate balance is crucial for deciphering the role of astrocyte-mediated inflammation in Alzheimer's disease pathogenesis, particularly in determining whether prolonged neuroinflammatory signalling is a cause or consequence of impaired Aβ clearance. In particular, AD is now widely regarded as a multifactorial disease involving a complex interplay of inflammation, Aβ accumulation, and cellular dysfunction. Therefore, it is critical to investigate how cytokine-driven changes in astrocyte function contribute to disease progression. Though the results in this chapter show that prolonged cytokines treatment at both low and high doses reduces Aβ uptake, it is important to note that the results are taken from three biological repeats of one cell line in each group. Therefore, future work should aim to replicate these experiments across multiple iAstrocyte lines to

enhance statistical power and generalisability. Expanding this analysis will provide a clearer understanding of the broader impact of chronic inflammation on astrocyte-mediated Aβ uptake in AD. Finally, one important limitation of this study is that prolonged inflammation does not affect Aβ uptake in isolation, and has been shown to have a widespread impact on astrocyte function. By measuring the uptake of Aβ alone, it does not indicate the global effect on both control and AD astrocytes. Therefore, an optimisation of this assay should include experiments that measure overall cell health. For example, Gamma-H2AX (γH2AX) phosphorylation which is an early detector of DNA damage responses to the repair of DNA double-strand breaks (Prabhu et al., 2024). Additionally, using the cell proliferation and viability MTT test will give a direct measurement of mitochondrial and metabolic activity of astrocytes (Garg et al., 2018). Furthermore, membrane integrity assays such as lactate dehydrogenase (LDH) release from the cells will give an indication of cellular damage and death (Cox et al., 2021). Together, these assays will provide a more comprehensive outlook on the role of prolonged inflammation on cell health.

6.5. Conclusions

The findings in this chapter demonstrate that astrocytes play a direct role in Aβ uptake and that prolonged exposure to pro-inflammatory environments modulates their ability to clear Aβ. In control iAstrocytes, cytokine treatment led to a non-significant reduction in Aβ uptake, whereas in AD-derived iAstrocytes, both low and high doses of cytokines significantly impaired Aβ uptake. Overall, the results suggest that prolonged inflammation compromises astrocyte-mediated Aβ uptake, potentially contributing to increased Aβ accumulation and thus Aβ-mediated neurodegeneration and disease progression. These results support the overall hypothesis (section 7.2), that elevated levels of pro-inflammatory markers are associated with a feedback cycle. Where Aβ production and aggregation lead to inflammation, inflammation enhances Aβ aggregation, and aggregated Aβ further sustains inflammatory responses, leading to cellular dysfunctions observed in AD.

Chapter 7. Main Discussions and Conclusions

7.1. Overview

In this final chapter, the following sections will combine the results of the previous chapters and discuss how fit into / impact the overall field of AD. In addition, the main limitations and future work are also discussed, along with the final conclusions to the body of work presented in this thesis.

7.2. Astrocytes Contribute to a Positive-Inflammatory Feedback Loop Associated to Alzheimer's Disease

Astrocytes are pivotal in the uptake and clearance of Aβ in the brain as part of the inflammatory response to maintain homeostasis (Montoliu-Gaya et al., 2018; Thal, 2012). Alongside microglia, astrocytes are often positioned around Aβ deposits in the brain and have been hypothesised to protect surrounding cells, such as neurones, from Aβ toxicity and promote cell survival, and maintain brain homeostasis (Beretta et al., 2024). Furthermore, reactive astrocytes with a high Aβ load are commonly found in the brains of individuals with AD (Sollvander et al., 2016), highlighting the importance of astrocytes in Aβ clearance and neuronal health. Astrocytes become reactive as part of the inflammatory response and undergo several morphological and functional changes, including the increased secretion of pro-inflammatory markers, such as cytokines and chemokines (Deng et al., 2024). In this thesis, the treatment of different Aβ isoforms resulted in the increased secretion of pro-inflammatory cytokines, TNF-α, IL6, and IL-1β, and chemokine, MCP1. This response was observed in both control and AD iAstrocytes, all six lines used in this study. However, astrocytes derived from AD patients had an amplified induction of pro-inflammatory markers after treatment with Aβ40 and Aβ42 (oligomers and fibrils) compared to control lines.

These results align with the observation that all of these pro-inflammatory markers are shown to increase in individuals with AD than cognitively healthy individuals. Though, a few studies have argued that pro-inflammatory markers have a beneficial effect (Wang et al., 2023; Gonzalez Caldito, 2023; Yang et al., 2012; Park and Bowers, 2010), most of the studies indicate that the secretion of TNF-α, IL6, IL-1β, and MCP1 are closely associated with the

activation and dysregulation of cell signalling pathways, including apoptosis, proliferation, metabolism, and inflammation (Liu et al., 2023; Zhou et al., 2019; Kaur et al., 2019; DiSabato et al., 2016). Furthermore, when astrocytes were activated with TNF-α and other pro-inflammatory cytokines, IL1α and C1q, this led to other brain cells such as neuronal and oligodendrocyte death (Zheng and Wang, 2025). In this study, the prolonged treatment with cytokines reduced the uptake of Aβ40 and Aβ42 (both oligomers and fibrils) in control and AD iAstrocytes. However, this uptake was significantly reduced in AD iAstrocytes only. The chronic treatment of cytokines reduces the ability of astrocytes to internalise Aβ, enhancing the build-up of insoluble deposits and, ultimately, plaque formation. Increased Aβ aggregates could induce more cytokines and chemokines release, creating a higher pro-inflammatory environment and inducing downstream neuronal dysregulation, more Aβ production and degeneration (Zhu et al., 2024). Altogether, this leads to a harmful cycle commonly observed in AD, where less clearance increases Aβ aggregation, inducing more inflammation and neurotoxicity, thus creating a feedback loop (Figure 52). This hypothesis is supported by the enhanced presence of markers of inflammation, such as reactive astrocytes and cytokines, situated in brain regions with high Aβ and Tau neurofibrillary tangles (NFTs), pathological hallmarks of AD (Domingues et al., 2017). This result also supports the observed results that a sustained inflammatory state is a critical early feature of AD (Botella Lucena and Heneka, 2024).

Morphological changes such as hypertrophy and increased vimentin, GFAP, and CD44 expression are other astrocyte reactivity markers (Zhang et al., 2023d). However, in this study, no statistically significant differences were found in the mean percentage of cells expressing vimentin, GFAP, and CD44, or their expression level after Aβ40 and Aβ42 (oligomer and fibril) treatment. These results were consistent in both control and AD iAstrocytes, for both lines. A previous study reported that levels of CD44 expression are significantly higher in individuals with AD (Pinner et al., 2017). GFAP is also a key biomarker for AD, with correlations to disease progression, including Aβ and Tau deposition (Leipp et al., 2024). Although increased expression of GFAP, Vimentin, and CD44 has been linked to Aβ and AD – in this study perhaps a lack of increased expression of these markers in iAstrocytes is due to an already high basal state expression before treatment of Aβ. Therefore, changes in these markers might not be sensitive to Aβ alone. However, a group of studies in animal models reports opposite findings, where the double-knockdown of both

GFAP and Vimentin in *APP/PS1* mice leads to increased Aβ plaque and neuronal dysfunction (Kraft et al., 2013). It is important to note that the prolonged treatment of cytokines and the expression of GFAP, Vimentin, and CD44 were carried out in a small sample size of cell lines. In the case of GFAP, n=1 (one biological repeat of one line) was carried out in the AD iAstrocytes. Therefore, increasing the sample size in this experiment is an important future step to enhance the reproducibility of these results further.

An unexplored avenue in this study is Aβ production by astrocytes and how this may influence uptake and inflammatory responses. Aβ is derived from the cleavage of the amyloid precursor protein (APP) by β and γ-secretase (Huang and Liu, 2020). TNF-α, IL6, and IL-1β can stimulate APP processing in astrocytes through the upregulation of β and γ-secretase (Zhang et al., 2023d; Alasmari et al., 2018). The processing of APP increases the production of Aβ aggregates, which are prone to aggregation and misfolding (Alasmari et al., 2018; Domingues et al., 2017; Rubio-Perez and Morillas-Ruiz, 2012). It has been hypothesised that an imbalance between production and clearance leads to the pathology associated with AD (Saido and Leissring, 2012; Tarasoff-Conway et al., 2015). In this study, the induction of pro-inflammatory markers after Aβ treatment could have induced Aβ production, further adding to the pathological cascade to induce more cytokine and chemokine release, which dysregulates astrocytic function and uptake. However, this requires further investigation of Aβ production and subsequent cytokine release in astrocytes and how this mechanism contributes to the feedback loop (Figure 52). Additionally, it is also important to note that the pathology associated with AD involves several other cell types.

Firstly, the resident macrophages, microglia, are one of the core cells of the brain's scavenger and immune defence cells. Like astrocytes, microglia play an essential role in homeostasis through cell-to-cell signalling, neuronal support, removing debris such as Aβ, and inflammation (Deng et al., 2024). Dysregulation in these microglial cell mechanisms has been closely associated with AD (Prater et al., 2023; Miao et al., 2023; Leng and Edison, 2021). Astrocytes and microglia work in close association, coordinate, and influence each other’s function in the human brain (Garland et al., 2022). In the context of Aβ, early studies have shown that in co-cultures of microglia and astrocytes, astrocytes have been shown to reduce microglial-mediated degradation (Sokolowski and Mandell, 2011). This mechanism is not fully understood, but it has been hypothesised that the production of cytokines from

astrocytes may negatively impact microglia degradation of Aβ (Sokolowski and Mandell, 2011). Conversely, as part of microglia's role in inflammation, microglia also secrete pro-inflammatory markers. Pro-inflammatory markers have been linked to increased Aβ production and the secretion of cytokines in astrocytes (Wu and Eisel, 2023; Di Benedetto et al., 2022; Liddelow et al., 2017). Impaired astrocyte functions also increased the microglia number surrounding Aβ plaques in transgenic mice (Wegiel et al., 2001). Together, these studies highlight the importance of the relationship between microglia and astrocytes and the potential mechanism to propagate a positive-inflammatory feedback loop further during AD. Besides microglia, neurones are another crucial cell type in AD.

The gradual and progressive neuronal dysregulation and death throughout the brain, leading to brain atrophy and, ultimately, memory loss, are the core and prominent characteristics of AD. Neurones are associated with both Aβ plaques, which are positioned extracellularly, and intracellular NFTs (Zheng and Wang, 2025). Neurones are susceptible to changes in homeostasis, which are primarily regulated by astrocytes and microglia (Wu and Eisel, 2023). Persistent exposure to pro-inflammatory cytokines leads to the disruption of neuronal function, reduction of plasticity and synaptic dysfunction, and ultimately, neurodegeneration commonly observed in AD (Heneka et al., 2015). It has also been shown that the neurones can also release pro-inflammatory cytokines like glial cells under stress. This secretion of inflammatory signals from neurones can lead to further astrocyte activation due to their role in protection, therefore adding to the feedback loop. Notably, neurones are the major source of Aβ production, which has been shown to increase during neuroinflammation (Zhang et al., 2023b; Wang et al., 2021). Exposure of TNF-α has been shown to increase Aβ production and aggregation in neurones (Whiten et al., 2020). It has been reported that an increase in the Aβ load, which is not effectively cleared by astrocytes, contributes to the build-up of Aβ, downstream toxicity, and subsequent neuronal death. The complex nature of Aβ build-up, clearance, and inflammatory pathways that are mediated by several cell types in the brain that interact together highlights the main limitation of this body of work.

Though the results in this body of work highlight a novel understanding of different Aβ isoforms uptake and subsequent specific cytokine/chemokine release by human-derived iAstrocytes, future work should aim to include the investigation of microglia and neurones in this context. For example, co-cultures of astrocytes, microglia, and neurones to see how the

interactions between these cells may influence the feedback loop and their role in Aβ uptake and subsequent pro-inflammatory release. However, in the context of the direct conversion model used in this thesis, the iNPCs are tripotent (Meyer et al., 2014). As a result, the iNPCs can only be differentiated into astrocytes, oligodendrocytes, and neurones. Therefore, other means of model systems, such as iPSCs, would need to be utilised to investigate microglia.

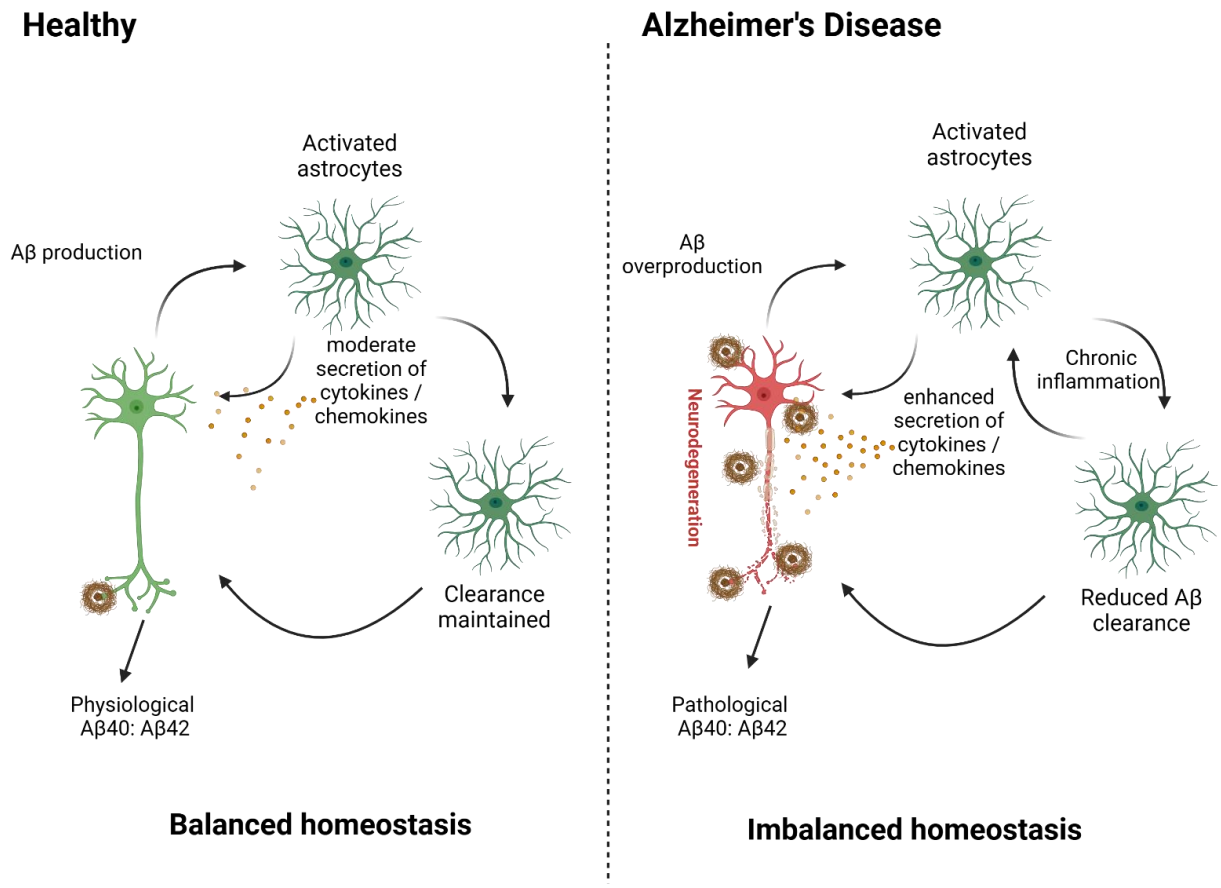

Figure 53. Illustrative diagram summarising the feedback loop. *In the healthy brain Aβ clearance is maintained by activated astrocytes to keep a physiological Aβ40: Aβ42 deposition. In AD, chronic inflammatory states shift astrocytes from an Aβ-clearing phenotype to one with less clearance. Less clearance further activates astrocytes, creating a higher inflammatory environment and inducing downstream neuronal dysregulation and degeneration. Leading to a harmful cycle where less clearance increases Aβ production and aggregation, inducing further activation of astrocytes, increasing the release of pro-inflammatory markers, reduced clearance and further neurodegeneration.*

7.3. Different Aβ40 and Aβ42 Isoforms Influence Aggregation and Subsequent Pro-Inflammatory Response in iAstrocytes

In this study, higher Aβ42 ratios (Aβ42 alone or Aβ40: Aβ42 (7:3) induced significantly more TNF-α, IL6, IL-1β, and MCP1 compared to Aβ40: Aβ42 (9:1) and Aβ40 in control and AD iAstrocytes. In AD astrocytes, this response was particularly pronounced. Together, these results are interesting as the Aβ42: Aβ40 ratio in the CSF decreases throughout disease progression, reflecting the relatively enhanced deposition of Aβ42 into plaques, a well-established biomarker of AD pathology (Hansson et al., 2019). The findings from this study demonstrate that Aβ42 strongly induces a pro-inflammatory cytokine secretion in astrocytes, reinforcing the link between Aβ42 and neuroinflammation. This is interesting as both changes in Aβ deposition alongside inflammation are an early biomarker of AD (Chen et al., 2024; Botella Lucena and Heneka, 2024).

Interestingly, Aβ42 oligomers were taken up significantly more than Aβ40 and Aβ40: Aβ42 (9:1) in control iAstrocytes. Similarly, Aβ42 oligomers were taken up more than Aβ40: Aβ42 (9:1) and Aβ40: Aβ42 (9:1), but not Aβ40 oligomers. In fibrils, there was a trend of more uptake of Aβ with increasing Aβ42: Aβ40 ratio, however, there was no statistical difference in the uptake of Aβ. Together, these results suggest that although both control and AD astrocytes uptake Aβ, in response, secrete pro-inflammatory markers, the AD lines may be more susceptible to Aβ42 and, therefore, have an increased induction of cytokines/chemokines after the internalisation of Aβ, providing insights into inflammatory responses in AD astrocytes. The findings in this thesis further substantiate this conclusion, revealing no substantial increase in pro-inflammatory markers across the fibrillar group for Aβ species. However, Aβ fibrils stimulate a more selectively inflammatory response, specifically at higher Aβ42: Aβ40 ratios, reinforcing that different Aβ conformations contribute distinctly to astrocyte reactivity. However, Aβ oligomers were the most potent inducers of pro-inflammatory markers, and in particular, an increased ratio of Aβ42 (e.g., Aβ42 alone or Aβ40: Aβ42 (7:3) resulted in significantly increased cytokine secretion when compared to Aβ40: Aβ42 (10:0 and 9:1) oligomers in all cytokines—suggesting that Aβ42 oligomers drive a heightened and more universal response inflammatory in AD iAstrocytes. However, it is important to note that no further analysis besides TIRF and ThT kinetics were used to characterise the aggregates, therefore, restricting information about the overall

composition of the different Aβ species. Despite this, the results in this study are in line with current literature which indicates that oligomers are more potent.

Aβ42 oligomers have been shown to induce neuronal synaptic loss and death, disrupt ion channels, mitochondrial dysfunction, and oxidative stress (Meng et al., 2024; Bigi et al., 2024; Azargoonjahromi, 2024; Tolar et al., 2021). Furthermore, Aβ42 aggregates are shown to stimulates Tau seeding and cellular uptake of Tau in primary mouse neurones and human neuroblastoma cells (Shin et al., 2019). Aβ42 oligomers have been shown to interrupt cell-to-cell signalling and trigger a cascade of inflammatory responses (Zhang et al., 2022). The toxicity of oligomers has been linked to their heterogeneous, transient, and soluble nature, allowing them to spread easily throughout the brain. Coupled with this, the rate of Aβ42 aggregation to form higher order aggregates is the fastest, as a result of higher hydrophobicity, reduced entropy, and two extra residues at the C-terminus, which acts as a nucleation site for enhanced aggregation to increase more aggregate species (Phan and Schmit, 2022; Mei et al., 2022; Lin et al., 2019).

In addition, several studies have shown that Aβ42 is more toxic than Aβ40 (Song et al., 2022; Phillips, 2019; Chang and Chen, 2014; Hayden and Teplow, 2013; Kuperstein et al., 2010). Even Aβ40 has been implicated to have some protective properties in Tg2575 mice (overexpressing APP), and increased Aβ40 reduced Aβ42 deposition by up to 60% (Kim et al., 2007). Next, during Aβ production, cleavage of APP by β and γ-secretase is non-specific and therefore produces a heterogenous population of Amyloid-β isoforms from 1-42, with Aβ40 and Aβ42 residues being the most abundant (Murphy and LeVine, 2010). In Drosophila melanogaster, changes in eye organisation are a standard method for determining toxic phenotypes. Aβ38 and Aβ40 were not only not toxic, but also shown a protective effect when expressed dose-dependently with Aβ42 (Moore et al., 2018). In non-transgenic mice, Aβ38 and Aβ40 did not induce locomotor dysregulation, a core regulator of cognitive function in mice when compared to Aβ42 (Moore et al., 2018). Interestingly, Aβ38 and Aβ40 are associated with a reduced risk of AD progression (Schneider et al., 2025; Cullen et al., 2022). As an extension of the work in this thesis, it would be interesting to investigate the uptake of Aβ38 and its role in the induction of pro-inflammatory markers as a potential protective mechanism. In neuronal cell culture, a lower Aβ40: Aβ42 ratio drives acute synaptic regulation and apoptosis (Kuperstein et al., 2010). Furthermore, the Aβ40: Aβ42 (Aβ42 alone and 7:3) exhibited neurotoxicity, but Aβ40: Aβ42 (9:1 and Aβ40 alone) did not

exhibit neurotoxicity during neuronal cell viability assays (Kuperstein et al., 2010). In this study, the results suggest a composition-dependent response, where lower Aβ42 ratios (Aβ40 alone or Aβ40: Aβ42 (9:1) did not strongly induce pro-inflammatory markers, while higher Aβ42 ratios had a more robust effect. These findings align with the hypothesis that Aβ42 is more toxic than Aβ40, and in the case of astrocytes, Aβ42 results in more activation. Another limitation of the work in this thesis is that no cellular toxicity or survival assays were completed during the uptake and secretion of pro-inflammatory markers to elucidate the effects of Aβ species and compositions on astrocytes. Despite this, other studies have shown that mouse astrocytes activated by mixtures of Aβ and cytokines (TNF-α, IL-1α, and C1q) activated pathways associated with ageing and AD (LaRocca et al., 2021a; Liddelow et al., 2017).

Potentially due to the faster rate of formation and higher toxicity of Aβ42, the preferential up take of Aβ42 aggregates serves as a protective mechanism against neighbouring cells, such as neurones, from damage, reducing extracellular Aβ accumulation, and helping to maintain brain homeostasis (Giusti et al., 2024; Ries and Sastre, 2016b). In astrocytes, preferential internalisation of Aβ42 species may reflect a compensatory clearance mechanism. On the other hand, it also contributes to cellular stress and dysfunction to exacerbate disease pathology. For example, the higher release of pro-inflammatory markers in response to Aβ42 aggregates leads to more activation and a heightened inflammatory environment. This, coupled with the reduced uptake of both Aβ40 and Aβ42 (oligomers and fibrils) after prolonged cytokine treatment, supports the hypothesis that AD astrocytes are more susceptible to Aβ-induced inflammatory responses. When treated with prolonged cytokines, there is no trend in differences between isoform uptake with decreases in Aβ40 and Aβ42 (oligomers and fibrils), even at low dosages. However, it is necessary to point out that the effect of cytokines on Aβ40: Aβ42 (7:3 and 9:1) uptake in iAstrocytes was not studied due to time constraints, so the question of how the ratio of Aβ40: Aβ42 remains open in this context. Despite this, the results of this thesis and previous studies suggest that patient-derived astrocytes are more susceptible to inflammation and are already compromised; therefore, when treated with cytokines, the uptake of Aβ is universally affected. Altogether, these results also complement the feedback loop hypothesis, as mentioned in the previous section.

7.4. Overall Conclusions

In conclusion, this thesis successfully characterised and confirmed a homogeneous population of iAstrocytes, enabling a human-derived model to study Aβ uptake by astrocytes and associated pro-inflammatory responses. By implementing a system to prepare different Aβ aggregates based on their isoform and aggregation state, the findings contribute to a novel understanding of how astrocytes uptake different Aβ aggregate species and their role in Aβ clearance. The overall results in this thesis provide key insights into the role of different Aβ species and aggregate forms that trigger astrocyte-mediated secretion of pro-inflammatory markers. It highlights the importance of understanding how different Aβ compositions influence astrocyte-mediated uptake and provides valuable mechanistic insights into the link between Aβ aggregation and inflammation. Furthermore, prolonged treatment of pro-inflammatory markers, mimicking a chronic inflammation environment, is linked to a disruption of Aβ up take, regardless of their isoform and aggregation state, which may contribute to a feedback cycle of impaired astrocyte function and exacerbated neuroinflammation, leading to the enhanced Aβ plaque deposition and the early pathology of AD. Overall, this thesis was able to gain a better understanding of the interplay between astrocytes and Aβ aggregates during uptake and neuroinflammation in a human-derived model both in healthy and AD conditions.

References

Abanto, J.*, et al.* (2024). 'Increases in amyloid-beta42 slow cognitive and clinical decline in alzheimer's disease trials', *Brain,* 147(10)**,** pp. 3513-3521.

Ahmed, M.*, et al.* (2010). 'Structural conversion of neurotoxic amyloid-beta(1-42) oligomers to fibrils', *Nat Struct Mol Biol,* 17(5)**,** pp. 561-7.

Akdemir, E. S.*, et al.* (2020). 'Astrocytogenesis: Where, when, and how', *F1000Res,* 9(pp. 233.

Akhtar, A.*, et al.* (2022). 'Preclinical models for alzheimer's disease: Past, present, and future approaches', *ACS Omega,* 7(51)**,** pp. 47504-47517.

Alasmari, F.*, et al.* (2018). 'Neuroinflammatory cytokines induce amyloid beta neurotoxicity through modulating amyloid precursor protein levels/metabolism', *Biomed Res Int,* 2018(pp. 3087475.

Allaman, I.*, et al.* (2010). 'Amyloid-beta aggregates cause alterations of astrocytic metabolic phenotype: Impact on neuronal viability', *J Neurosci,* 30(9)**,** pp. 3326-38.

Allen, S. P.*, et al.* (2014). 'Superoxide dismutase 1 mutation in a cellular model of amyotrophic lateral sclerosis shifts energy generation from oxidative phosphorylation to glycolysis', *Neurobiol Aging,* 35(6)**,** pp. 1499-509.

Almeida, Z. L.*, et al.* (2025). 'Morphological and molecular profiling of amyloid-beta species in alzheimer's pathogenesis', *Mol Neurobiol,* 62(4)**,** pp. 4391-4419.

Alzheimer's Research UK. 2025. *Types of dementia* [Online]. Available: https://www.alzheimersresearchuk.org/dementia-information/types-of-dementia/ [Accessed 06/03/2025].

Alzheimer's Society. 2025. *Facts for the media about dementia* [Online]. Available: https://www.alzheimers.org.uk/about-us/news-and-media/facts-media [Accessed].

Andersson, E.*, et al.* (2025). 'Soluble cerebral abeta protofibrils link abeta plaque pathology to changes in csf abeta(42)/abeta(40) ratios, neurofilament light and tau in alzheimer's disease model mice', *Nat Aging,* 5(3)**,** pp. 366-375.

Araki, T.*, et al.* (2021). 'The effects of microglia- and astrocyte-derived factors on neurogenesis in health and disease', *Eur J Neurosci,* 54(5)**,** pp. 5880-5901.

Arosio, P.*, et al.* (2015). 'On the lag phase in amyloid fibril formation', *Phys Chem Chem Phys,* 17(12)**,** pp. 7606-18.

Ashe, K. H. (2020). 'The biogenesis and biology of amyloid beta oligomers in the brain', *Alzheimers Dement,* 16(11)**,** pp. 1561-1567.

Ashique, S*., et al.* (2024). 'Aducanumab in alzheimer's disease: A critical update', *Curr Med Chem,* 31(31)**,** pp. 5004-5026.

Au, W. H*., et al.* (2024). 'Activation of the keap1/nrf2 pathway suppresses mitochondrial dysfunction, oxidative stress, and motor phenotypes in c9orf72 als/ftd models', *Life Sci Alliance,* 7(9)**,** pp. e202402853-202402870.

Azargoonjahromi, A. (2024). 'The duality of amyloid-beta: Its role in normal and alzheimer's disease states', *Mol Brain,* 17(1)**,** pp. 44-68.

Baek, Y. & Lee, M. (2024). 'Exploring the complexity of amyloid-beta fibrils: Structural polymorphisms and molecular interactions', *Biochem Soc Trans,* 52(4)**,** pp. 1631-1646.

Bali, J*., et al.* (2012). 'Role of genes linked to sporadic alzheimer's disease risk in the production of beta-amyloid peptides', *Proc Natl Acad Sci U S A,* 109(38)**,** pp. 15307-15311.

Barage, S. H. & Sonawane, K. D. (2015). 'Amyloid cascade hypothesis: Pathogenesis and therapeutic strategies in alzheimer's disease', *Neuropeptides,* 52(1)**,** pp. 1-18.

Baranello, R. J*., et al.* (2015). 'Amyloid-beta protein clearance and degradation (abcd) pathways and their role in alzheimer's disease', *Curr Alzheimer Res,* 12(1)**,** pp. 32-46.

Basu, A. & Tiwari, V. K. (2021). 'Epigenetic reprogramming of cell identity: Lessons from development for regenerative medicine', *Clin Epigenetics,* 13(1)**,** pp. 144.

Bateman, R. J*., et al.* (2012). 'Clinical and biomarker changes in dominantly inherited alzheimer's disease', *N Engl J Med,* 367(9)**,** pp. 795-804.

Behl, C. (2024). 'In 2024, the amyloid-cascade-hypothesis still remains a working hypothesis, no less but certainly no more', *Front Aging Neurosci,* 16(1459224)**,** pp. no pagination.

Bell, S. M*., et al.* (2018). 'Ursodeoxycholic acid improves mitochondrial function and redistributes drp1 in fibroblasts from patients with either sporadic or familial alzheimer's disease', *J Mol Biol,* 430(21)**,** pp. 3942-3953.

Bell, S. M*., et al.* (2024). 'Increasing hexokinase 1 expression improves mitochondrial and glycolytic functional deficits seen in sporadic alzheimer's disease astrocytes', *Mol Psychiatry,* 30(pp. 1369-1382.

Bellaver, B.*, et al.* (2023). 'Astrocyte reactivity influences amyloid-beta effects on tau pathology in preclinical alzheimer's disease', *Nat Med,* 29(7)**,** pp. 1775-1781.

Benilova, I.*, et al.* (2014). 'The alzheimer disease protective mutation a2t modulates kinetic and thermodynamic properties of amyloid-beta (abeta) aggregation', *J Biol Chem,* 289(45)**,** pp. 30977-89.

Beretta, C.*, et al.* (2024). 'Amyloid-beta deposits in human astrocytes contain truncated and highly resistant proteoforms', *Mol Cell Neurosci,* 128(pp. 103916.

Bernal, A. & Arranz, L. (2018). 'Nestin-expressing progenitor cells: Function, identity and therapeutic implications', *Cell Mol Life Sci,* 75(12)**,** pp. 2177-2195.

Bharadwaj, P.*, et al.* (2018). 'Role of the cell membrane interface in modulating production and uptake of alzheimer's beta amyloid protein', *Biochim Biophys Acta Biomembr,* 1860(9)**,** pp. 1639-1651.

Bhat, R.*, et al.* (2012). 'Astrocyte senescence as a component of alzheimer's disease', *PLoS One,* 7(9)**,** pp. e45069-45079.

Bigi, A.*, et al.* (2024). 'A single-domain antibody detects and neutralises toxic abeta(42) oligomers in the alzheimer's disease csf', *Alzheimers Res Ther,* 16(1)**,** pp. 13.

Bishop, G. M. & Robinson, S. R. (2004). 'Physiological roles of amyloid-beta and implications for its removal in alzheimer's disease', *Drugs Aging,* 21(10)**,** pp. 621-30.

Botella Lucena, P. & Heneka, M. T. (2024). 'Inflammatory aspects of alzheimer's disease', *Acta Neuropathol,* 148(1)**,** pp. 31-53.

Bouwman, F. H.*, et al.* (2022). 'Clinical application of csf biomarkers for alzheimer's disease: From rationale to ratios', *Alzheimers Dement (Amst),* 14(1)**,** pp. e12314-26.

Bradford, B. M.*, et al.* (2024). 'Cell adhesion molecule cd44 is dispensable for reactive astrocyte activation during prion disease', *Sci Rep,* 14(1)**,** pp. 13749-13761.

Bradl, M. & Lassmann, H. (2010). 'Oligodendrocytes: Biology and pathology', *Acta Neuropathol,* 119(1)**,** pp. 37-53.

Brandebura, A. N.*, et al.* (2023). 'Astrocyte contribution to dysfunction, risk and progression in neurodegenerative disorders', *Nat Rev Neurosci,* 24(1)**,** pp. 23-39.

Breijyeh, Z. & Karaman, R. (2020). 'Comprehensive review on alzheimer's disease: Causes and treatment', *Molecules,* 25(24)**,** pp. 5789-5815.

Brosseron, F.*, et al.* (2014). 'Body fluid cytokine levels in mild cognitive impairment and alzheimer's disease: A comparative overview', *Mol Neurobiol,* 50(2)**,** pp. 534-44.

Bruggink, K. A.*, et al.* (2012). 'Methods for analysis of amyloid-beta aggregates', *J Alzheimers Dis,* 28(4)**,** pp. 735-58.

Burda, J. E. & Sofroniew, M. V. (2014). 'Reactive gliosis and the multicellular response to cns damage and disease', *Neuron,* 81(2)**,** pp. 229-48.

Caballero, M. A. A.*, et al.* (2020). 'Age-dependent amyloid deposition is associated with white matter alterations in cognitively normal adults during the adult life span', *Alzheimers Dement,* 16(4)**,** pp. 651-661.

Caccamo, A.*, et al.* (2005). 'Age- and region-dependent alterations in abeta-degrading enzymes: Implications for abeta-induced disorders', *Neurobiol Aging,* 26(5)**,** pp. 645-54.

Cai, H.*, et al.* (2023a). 'Plasma biomarkers predict alzheimer's disease before clinical onset in chinese cohorts', *Nat Commun,* 14(1)**,** pp. 6747-57.

Cai, W.*, et al.* (2023b). 'Physiological roles of beta-amyloid in regulating synaptic function: Implications for ad pathophysiology', *Neurosci Bull,* 39(8)**,** pp. 1289-1308.

Cai, W.*, et al.* (2023c). 'The amyloid-beta clearance: From molecular targets to glial and neural cells', *Biomolecules,* 13(2)**,** pp. 313-333.

Cavieres-Lepe, J. & Stuardo, N. (2021). 'Amyloid beta clearance is disrupted by depletion of low-density lipoprotein receptor-related protein 4 (lrp4) in astrocytes', *J Neurosci,* 41(17)**,** pp. 3749-3751.

Cerneckis, J.*, et al.* (2024). 'Induced pluripotent stem cells (ipscs): Molecular mechanisms of induction and applications', *Signal Transduct Target Ther,* 9(1)**,** pp. 112-138.

Chai, Y. L.*, et al.* (2023). 'Inflammatory panel cytokines are elevated in the neocortex of late-stage alzheimer's disease but not lewy body dementias', *J Neuroinflammation,* 20(1)**,** pp. 111-123.

Chang, Y. J. & Chen, Y. R. (2014). 'The coexistence of an equal amount of alzheimer's amyloid-beta 40 and 42 forms structurally stable and toxic oligomers through a distinct pathway', *FEBS J,* 281(11)**,** pp. 2674-87.

Chen, G. F.*, et al.* (2017). 'Amyloid beta: Structure, biology and structure-based therapeutic development', *Acta Pharmacol Sin,* 38(9)**,** pp. 1205-1235.

Chen, K.*, et al.* (2022). 'Lrp1 is a neuronal receptor for alpha-synuclein uptake and spread', *Mol Neurodegener,* 17(1)**,** pp. 57.

Chen, S. H.*, et al.* (2020). 'Amyloid-beta uptake by blood monocytes is reduced with ageing and alzheimer's disease', *Transl Psychiatry,* 10(1)**,** pp. 423.

Chen, X.*, et al.* (2018). 'Cerebrospinal fluid inflammatory cytokine aberrations in alzheimer's disease, parkinson's disease and amyotrophic lateral sclerosis: A systematic review and meta-analysis', *Front Immunol,* 9(19)**,** pp. 2122-2133.

Chen, Y. & Yu, Y. (2023). 'Tau and neuroinflammation in alzheimer's disease: Interplay mechanisms and clinical translation', *J Neuroinflammation,* 20(1)**,** pp. 165.

Chen, Y. X.*, et al.* (2021). 'Diagnosis and treatment for mild cognitive impairment: A systematic review of clinical practice guidelines and consensus statements', *Front Neurol,* 27(8)**,** pp. e719849-e719861.

Chen, Z.*, et al.* (2024). 'Roles of cytokines in alzheimer's disease', *Int J Mol Sci,* 25(11)**,** pp. 5803-5818.

Cheng, X.*, et al.* (2019). 'Morphological and functional alterations of astrocytes responding to traumatic brain injury', *J Integr Neurosci,* 18(2)**,** pp. 203-215.

Chun, H.*, et al.* (2020). 'Severe reactive astrocytes precipitate pathological hallmarks of alzheimer's disease via h(2)o(2)(-) production', *Nat Neurosci,* 23(12)**,** pp. 1555-1566.

Cline, E. N.*, et al.* (2018). 'The amyloid-beta oligomer hypothesis: Beginning of the third decade', *J Alzheimers Dis,* 64(s1)**,** pp. S567-S610.

Cohen, S. I.*, et al.* (2013). 'Proliferation of amyloid-beta42 aggregates occurs through a secondary nucleation mechanism', *Proc Natl Acad Sci U S A,* 110(24)**,** pp. 9758-9763.

Costantini, E.*, et al.* (2018). 'The role of immunosenescence in neurodegenerative diseases', *Mediators Inflamm***,** pp. 6039171-83.

Cox, M. C.*, et al.* (2021). 'Application of ldh assay for therapeutic efficacy evaluation of ex vivo tumor models', *Sci Rep,* 11(1)**,** pp. 18571.

Cozza, M.*, et al.* (2023). 'Exploring cerebral amyloid angiopathy: Insights into pathogenesis, diagnosis, and treatment', *J Neurol Sci,* 454(pp. 120866-75.

Creese, B.*, et al.* (2019). 'Mild behavioral impairment as a marker of cognitive decline in cognitively normal older adults', *Am J Geriatr Psychiatry,* 27(8)**,** pp. 823-834.

Cremades, N. & Dobson, C. M. (2018). 'The contribution of biophysical and structural studies of protein self-assembly to the design of therapeutic strategies for amyloid diseases', *Neurobiol Dis,* 109(Pt B)**,** pp. 178-190.

Cuenda, A. & Rousseau, S. (2007). 'P38 map-kinases pathway regulation, function and role in human diseases', *Biochim Biophys Acta,* 1773(8)**,** pp. 1358-75.

Cukalevski, R.*, et al.* (2015). 'The abeta40 and abeta42 peptides self-assemble into separate homomolecular fibrils in binary mixtures but cross-react during primary nucleation', *Chem Sci,* 6(7)**,** pp. 4215-4233.

Cullen, N.*, et al.* (2022). 'Association of csf abeta(38) levels with risk of alzheimer disease-related decline', *Neurology,* 98(9)**,** pp. e958-e967.

Dai, D. L.*, et al.* (2023). 'Human alzheimer's disease reactive astrocytes exhibit a loss of homeostastic gene expression', *Acta Neuropathol Commun,* 11(1)**,** pp. 127-146.

DaRocha-Souto, B.*, et al.* (2011). 'Brain oligomeric beta-amyloid but not total amyloid plaque burden correlates with neuronal loss and astrocyte inflammatory response in amyloid precursor protein/tau transgenic mice', *J Neuropathol Exp Neurol,* 70(5)**,** pp. 360-376.

Davis, N.*, et al.* (2021). 'Pharmacological ablation of astrocytes reduces abeta degradation and synaptic connectivity in an ex vivo model of alzheimer's disease', *J Neuroinflammation,* 18(1)**,** pp. 73.

De Strooper, B. & Karran, E. (2016). 'The cellular phase of alzheimer's disease', *Cell,* 164(4)**,** pp. 603-615.

Deczkowska, A.*, et al.* (2020). 'The physiology, pathology, and potential therapeutic applications of the trem2 signaling pathway', *Cell,* 181(6)**,** pp. 1207-1217.

Deng, Q.*, et al.* (2024). 'Microglia and astrocytes in alzheimer's disease: Significance and summary of recent advances', *Aging Dis,* 15(4)**,** pp. 1537-1564.

Di Benedetto, G.*, et al.* (2022). 'Role of microglia and astrocytes in alzheimer's disease: From neuroinflammation to ca(2+) homeostasis dysregulation', *Cells,* 11(17)**,** pp. 2728.

Dineley, K. T.*, et al.* (2001). 'Beta-amyloid activates the mitogen-activated protein kinase cascade via hippocampal alpha7 nicotinic acetylcholine receptors: In vitro and in vivo mechanisms related to alzheimer's disease', *J Neurosci,* 21(12)**,** pp. 4125-33.

DiSabato, D. J.*, et al.* (2016). 'Neuroinflammation: The devil is in the details', *J Neurochem,* 139(2)**,** pp. 136-153.

Domingues, C.*, et al.* (2017). 'Impact of cytokines and chemokines on alzheimer's disease neuropathological hallmarks', *Curr Alzheimer Res,* 14(8)**,** pp. 870-882.

Dorey, A.*, et al.* (2015). 'Cerebrospinal fluid abeta40 improves the interpretation of abeta42 concentration for diagnosing alzheimer's disease', *Front Neurol,* 6(pp. 247-254.

Drummond, E. & Wisniewski, T. (2017). 'Alzheimer's disease: Experimental models and reality', *Acta Neuropathol,* 133(2)**,** pp. 155-175.

Espay, A. J.*, et al.* (2023). 'The proteinopenia hypothesis: Loss of abeta(42) and the onset of alzheimer's disease', *Ageing Res Rev,* 92(102112)**,** pp. no pagination.

Farhy-Tselnicker, I. & Allen, N. J. (2018). 'Astrocytes, neurons, synapses: A tripartite view on cortical circuit development', *Neural Dev,* 13(1)**,** pp. 7.

Ferraiuolo, L.*, et al.* (2016). 'Oligodendrocytes contribute to motor neuron death in als via sod1-dependent mechanism', *Proc Natl Acad Sci U S A,* 113(42)**,** pp. E6496-E6505.

Flagmeier, P.*, et al.* (2020). 'Direct measurement of lipid membrane disruption connects kinetics and toxicity of abeta42 aggregation', *Nat Struct Mol Biol,* 27(10)**,** pp. 886-891.

Frost, G. R. & Li, Y. M. (2017). 'The role of astrocytes in amyloid production and alzheimer's disease', *Open Biol,* 7(12)**,** pp. 170228-170242.

Fu, Z.*, et al.* (2025). 'Human induced neural progenitor cells generated from three-dimensional aggregate-based culture significantly improve post-stroke recovery in tmcao mice', *Stem Cell Res Ther,* 16(1)**,** pp. 312.

Gabande-Rodriguez, E.*, et al.* (2020). 'Microglial phagocytosis in aging and alzheimer's disease', *J Neurosci Res,* 98(2)**,** pp. 284-298.

Garg, S.*, et al.* (2018). 'Integration of conventional cell viability assays for reliable and reproducible read-outs: Experimental evidence', *BMC Res Notes,* 11(1)**,** pp. 403.

Garland, E. F.*, et al.* (2022). 'Microglia and astrocyte function and communication: What do we know in humans?', *Front Neurosci,* 16(pp. 824888.

Gatto, N.*, et al.* (2021). 'Directly converted astrocytes retain the ageing features of the donor fibroblasts and elucidate the astrocytic contribution to human cns health and disease', *Aging Cell,* 20(1)**,** pp. e13281-e13301.

Gharbi, T.*, et al.* (2020). 'The function of astrocyte mediated extracellular vesicles in central nervous system diseases', *Front Cell Dev Biol,* 8(pp. 568889.

Giovannoni, F. & Quintana, F. J. (2020). 'The role of astrocytes in cns inflammation', *Trends Immunol,* 41(9)**,** pp. 805-819.

Giusti, V.*, et al.* (2024). 'Brain clearance of protein aggregates: A close-up on astrocytes', *Mol Neurodegener,* 19(5)**,** pp. 1-18.

Gomez-Nicola, D. & Boche, D. (2015). 'Post-mortem analysis of neuroinflammatory changes in human alzheimer's disease', *Alzheimers Res Ther,* 7(1)**,** pp. 42.

Gonzalez-Reyes, R. E.*, et al.* (2017). 'Involvement of astrocytes in alzheimer's disease from a neuroinflammatory and oxidative stress perspective', *Front Mol Neurosci,* 10(427)**,** pp.

Gonzalez Caldito, N. (2023). 'Role of tumor necrosis factor-alpha in the central nervous system: A focus on autoimmune disorders', *Front Immunol,* 14(pp. 1213448.

Goshi, N.*, et al.* (2025). 'Direct effects of prolonged tnf-alpha and il-6 exposure on neural activity in human ipsc-derived neuron-astrocyte co-cultures', *Front Cell Neurosci,* 19(pp. 1512591.

Gotz, J.*, et al.* (2018). 'Rodent models for alzheimer disease', *Nat Rev Neurosci,* 19(10)**,** pp. 583-598.

Gradisnik, L. & Velnar, T. (2023). 'Astrocytes in the central nervous system and their functions in health and disease: A review', *World J Clin Cases,* 11(15)**,** pp. 3385-3394.

Gu, L. & Guo, Z. (2013). 'Alzheimer's abeta42 and abeta40 peptides form interlaced amyloid fibrils', *J Neurochem,* 126(3)**,** pp. 305-11.

Gu, L. & Guo, Z. (2021). 'Alzheimer's abeta42 and abeta40 form mixed oligomers with direct molecular interactions', *Biochem Biophys Res Commun,* 534(pp. 292-296.

Habchi, J.*, et al.* (2018). 'Cholesterol catalyses abeta42 aggregation through a heterogeneous nucleation pathway in the presence of lipid membranes', *Nat Chem,* 10(6)**,** pp. 673-683.

Habib, N.*, et al.* (2020). 'Disease-associated astrocytes in alzheimer's disease and aging', *Nat Neurosci,* 23(6)**,** pp. 701-706.

Hammond, T. R.*, et al.* (2019). 'Immune signaling in neurodegeneration', *Immunity,* 50(4)**,** pp. 955-974.

Hampel, H.*, et al.* (2021). 'The amyloid-beta pathway in alzheimer's disease', *Mol Psychiatry,* 26(10)**,** pp. 5481-5503.

Hansson, O.*, et al.* (2019). 'Advantages and disadvantages of the use of the csf amyloid beta (abeta) 42/40 ratio in the diagnosis of alzheimer's disease', *Alzheimers Res Ther,* 11(1)**,** pp. 34-49.

Hayden, E. Y. & Teplow, D. B. (2013). 'Amyloid beta-protein oligomers and alzheimer's disease', *Alzheimers Res Ther,* 5(6)**,** pp. 60-71.

Heneka, M. T.*, et al.* (2015). 'Neuroinflammation in alzheimer's disease', *Lancet Neurol,* 14(4)**,** pp. 388-405.

Hong, S.*, et al.* (2016). 'Complement and microglia mediate early synapse loss in alzheimer mouse models', *Science,* 352(6286)**,** pp. 712-716.

Hu, Q.*, et al.* (2023). 'Jak/stat pathway: Extracellular signals, diseases, immunity, and therapeutic regimens', *Front Bioeng Biotechnol,* 11(pp. 1110765.

Hu, X.*, et al.* (2021). 'The jak/stat signaling pathway: From bench to clinic', *Signal Transduct Target Ther,* 6(1)**,** pp. 402-35.

Huang, B.*, et al.* (2022). 'The role of il-6/jak2/stat3 signaling pathway in cancers', *Front Oncol,* 12(pp. 1023177.

Huang, W.*, et al.* (2023). 'The role of trem2 in alzheimer's disease: From the perspective of tau', *Front Cell Dev Biol,* 11(pp. 1280257-66.

Huang, Y. R. & Liu, R. T. (2020). 'The toxicity and polymorphism of beta-amyloid oligomers', *Int J Mol Sci,* 21(12)**,** pp. 4477-4495.

Hyvarinen, T.*, et al.* (2019). 'Co-stimulation with il-1beta and tnf-alpha induces an inflammatory reactive astrocyte phenotype with neurosupportive characteristics in a human pluripotent stem cell model system', *Sci Rep,* 9(1)**,** pp. 16944.

Iqbal, K.*, et al.* (2013). 'Animal models of the sporadic form of alzheimer's disease: Focus on the disease and not just the lesions', *J Alzheimers Dis,* 37(3)**,** pp. 469-74.

Jack, C. R., Jr.*, et al.* (2024). 'Revised criteria for the diagnosis and staging of alzheimer's disease', *Nat Med,* 30(8)**,** pp. 2121-2124.

Jack, C. R., Jr.*, et al.* (2018). 'Nia-aa research framework: Toward a biological definition of alzheimer's disease', *Alzheimers Dement,* 14(4)**,** pp. 535-562.

Jan, A.*, et al.* (2008). 'The ratio of monomeric to aggregated forms of abeta40 and abeta42 is an important determinant of amyloid-beta aggregation, fibrillogenesis, and toxicity', *J Biol Chem,* 283(42)**,** pp. 28176-89.

Jansen, W. J.*, et al.* (2022). 'Prevalence estimates of amyloid abnormality across the alzheimer disease clinical spectrum', *JAMA Neurol,* 79(3)**,** pp. 228-243.

Jeong, H.*, et al.* (2022). 'Physiological roles of monomeric amyloid-beta and implications for alzheimer's disease therapeutics', *Exp Neurobiol,* 31(2)**,** pp. 65-88.

Jia, J.*, et al.* (2024). 'Biomarker changes during 20 years preceding alzheimer's disease', *N Engl J Med,* 390(8)**,** pp. 712-722.

Jiang, H.*, et al.* (2011). 'Elevated csf levels of tace activity and soluble tnf receptors in subjects with mild cognitive impairment and patients with alzheimer's disease', *Mol Neurodegener,* 6(pp. 69-77.

Johansson, L.*, et al.* (2024). 'Amyloid beta 1-40 and 1-42 fibril ratios and maturation level cause conformational differences with minimal impact on autophagy and cytotoxicity', *J Neurochem,* 168(9)**,** pp. 3308-3322.

Jones, R. S.*, et al.* (2013). 'Amyloid-beta-induced astrocytic phagocytosis is mediated by cd36, cd47 and rage', *J Neuroimmune Pharmacol,* 8(1)**,** pp. 301-11.

Jurga, A. M.*, et al.* (2021). 'Beyond the gfap-astrocyte protein markers in the brain', *Biomolecules,* 11(9)**,** pp. 1361-1389.

Kaltschmidt, B.*, et al.* (2005). 'Signaling via nf-kappab in the nervous system', *Biochim Biophys Acta,* 1745(3)**,** pp. 287-99.

Kamphuis, W.*, et al.* (2015). 'Gfap and vimentin deficiency alters gene expression in astrocytes and microglia in wild-type mice and changes the transcriptional response of reactive glia in mouse model for alzheimer's disease', *Glia,* 63(6)**,** pp. 1036-56.

Kano, M.*, et al.* (2020). 'Reduced astrocytic reactivity in human brains and midbrain organoids with prkn mutations', *NPJ Parkinsons Dis,* 6(1)**,** pp. 33-42.

Kato, D.*, et al.* (2022). 'Comparative studies for amyloid beta degradation: "Neprilysin vs insulysin", "monomeric vs aggregate", and "whole abeta(40) vs its peptide fragments"', *Biochem Biophys Rep,* 30(pp. 101268-101279.

Kaur, D.*, et al.* (2019). 'Activation of microglia and astrocytes: A roadway to neuroinflammation and alzheimer's disease', *Inflammopharmacology,* 27(4)**,** pp. 663-677.

Khakh, B. S. & Sofroniew, M. V. (2015). 'Diversity of astrocyte functions and phenotypes in neural circuits', *Nat Neurosci,* 18(7)**,** pp. 942-952.

Khodadadei, F.*, et al.* (2022). 'The effect of a1 and a2 reactive astrocyte expression on hydrocephalus shunt failure', *Fluids Barriers CNS,* 19(1)**,** pp. 78.

Kiianitsa, K.*, et al.* (2024). 'Trem2 variants that cause early dementia and increase alzheimer's disease risk affect gene splicing', *Brain,* 147(7)**,** pp. 2368-2383.

Kim, E.*, et al.* (2023a). 'Irisin reduces amyloid-beta by inducing the release of neprilysin from astrocytes following downregulation of erk-stat3 signaling', *Neuron,* 111(22)**,** pp. 3619-3633 e8.

Kim, E. K. & Choi, E. J. (2010). 'Pathological roles of mapk signaling pathways in human diseases', *Biochim Biophys Acta,* 1802(4)**,** pp. 396-405.

Kim, H.*, et al.* (2022). 'Reactive astrocytes transduce inflammation in a blood-brain barrier model through a tnf-stat3 signaling axis and secretion of alpha 1-antichymotrypsin', *Nat Commun,* 13(1)**,** pp. 6581.

Kim, J.*, et al.* (2007). 'Abeta40 inhibits amyloid deposition in vivo', *J Neurosci,* 27(3)**,** pp. 627-33.

Kim, K. Y.*, et al.* (2023b). 'Gfap as a potential biomarker for alzheimer's disease: A systematic review and meta-analysis', *Cells,* 12(9)**,** pp. 1309.

Kim, S.*, et al.* (2024). 'Astrocytic autophagy plasticity modulates abeta clearance and cognitive function in alzheimer's disease', *Mol Neurodegener,* 19(1)**,** pp. 55-81.

Kinney, J. W.*, et al.* (2018). 'Inflammation as a central mechanism in alzheimer's disease', *Alzheimers Dement (N Y),* 4(pp. 575-590.

Knezevic, D. & Mizrahi, R. (2018). 'Molecular imaging of neuroinflammation in alzheimer's disease and mild cognitive impairment', *Prog Neuropsychopharmacol Biol Psychiatry,* 80(Pt B)**,** pp. 123-131.

Knowles, T. P.*, et al.* (2014). 'The amyloid state and its association with protein misfolding diseases', *Nat Rev Mol Cell Biol,* 15(6)**,** pp. 384-96.

Komine, O. & Yamanaka, K. (2015). 'Neuroinflammation in motor neuron disease', *Nagoya J Med Sci,* 77(4)**,** pp. 537-49.

Konstantinidis, E.*, et al.* (2023a). 'Long-term effects of amyloid-beta deposits in human ipsc-derived astrocytes', *Mol Cell Neurosci,* 125(pp. 103839.

Konstantinidis, E.*, et al.* (2023b). 'Intracellular deposits of amyloid-beta influence the ability of human ipsc-derived astrocytes to support neuronal function', *J Neuroinflammation,* 20(1)**,** pp. 3-20.

Kovacs, G. (2019). 'Molecular pathology of neurodegenerative diseases: Principles and practice', *J Clin Pathol,* 72(11)**,** pp. 725-735.

Kraft, A. W.*, et al.* (2013). 'Attenuating astrocyte activation accelerates plaque pathogenesis in app/ps1 mice', *FASEB J,* 27(1)**,** pp. 187-98.

Krencik, R.*, et al.* (2011). 'Specification of transplantable astroglial subtypes from human pluripotent stem cells', *Nat Biotechnol,* 29(6)**,** pp. 528-534.

Kumar, A.*, et al.* (2023). 'Reactive astrogliosis: A friend or foe in the pathogenesis of alzheimer's disease', *J Neurochem,* 164(3)**,** pp. 309-324.

Kumar, V.*, et al.* (2016). 'Protein aggregation and neurodegenerative diseases: From theory to therapy', *Eur J Med Chem,* 124(29)**,** pp. 1105-1120.

Kundel, F.*, et al.* (2018). 'Shedding light on aberrant interactions - a review of modern tools for studying protein aggregates', *FEBS J,* 285(19)**,** pp. 3604-3630.

Kuperstein, I.*, et al.* (2010). 'Neurotoxicity of alzheimer's disease abeta peptides is induced by small changes in the abeta42 to abeta40 ratio', *EMBO J,* 29(19)**,** pp. 3408-20.

LaRocca, T. J.*, et al.* (2021a). 'Amyloid beta acts synergistically as a pro-inflammatory cytokine', *Neurobiol Dis,* 159(pp. 105493.

LaRocca, T. J.*, et al.* (2021b). 'Amyloid beta acts synergistically as a pro-inflammatory cytokine', *Neurobiol Dis,* 159(pp. 105493-105512.

Lawrence, J. M.*, et al.* (2023). 'Roles of neuropathology-associated reactive astrocytes: A systematic review', *Acta Neuropathol Commun,* 11(1)**,** pp. 42.

Lee, C. Y. & Landreth, G. E. (2010). 'The role of microglia in amyloid clearance from the ad brain', *J Neural Transm (Vienna),* 117(8)**,** pp. 949-60.

Leipp, F.*, et al.* (2024). 'Glial fibrillary acidic protein in alzheimer's disease: A narrative review', *Brain Commun,* 6(6)**,** pp. fcae396.

Lemoine, M. (2021). 'The evolution of the hallmarks of aging', *Front Genet,* 12(pp. 693071-693025.

Leng, F. & Edison, P. (2021). 'Neuroinflammation and microglial activation in alzheimer disease: Where do we go from here?', *Nat Rev Neurol,* 17(3)**,** pp. 157-172.

Li, H.*, et al.* (2024). 'The role and mechanism of abeta clearance dysfunction in the glymphatic system in alzheimer's disease comorbidity', *Front Neurol,* 15(pp. 1474439-1474449.

Li, L.*, et al.* (2021). 'Role of astroglial toll-like receptors (tlrs) in central nervous system infections, injury and neurodegenerative diseases', *Brain Behav Immun,* 91(740)**,** pp. 740-755.

Li, W.*, et al.* (2025). 'The ldl receptor-related protein 1: Mechanisms and roles in promoting abeta efflux transporter in alzheimer's disease', *Biochem Pharmacol,* 231(pp. 116643.

Liddelow, S. A.*, et al.* (2017). 'Neurotoxic reactive astrocytes are induced by activated microglia', *Nature,* 541(7638)**,** pp. 481-487.

Lin, Y.*, et al.* (2019). 'Characterizing the structural and thermodynamic properties of abeta42 and abeta40', *Biochem Biophys Res Commun,* 510(3)**,** pp. 442-448.

Linnerbauer, M.*, et al.* (2020). 'Astrocyte crosstalk in cns inflammation', *Neuron,* 108(4)**,** pp. 608-622.

Liu, E.*, et al.* (2024a). 'Updates in alzheimer's disease: From basic research to diagnosis and therapies', *Transl Neurodegener,* 13(1)**,** pp. 45-94.

Liu, Y.*, et al.* (2023). 'Neuroimmune mechanisms underlying alzheimer's disease: Insights into central and peripheral immune cell crosstalk', *Ageing Res Rev,* 84(pp. 101831.

Liu, Y.*, et al.* (2024b). 'The interaction between ageing and alzheimer's disease: Insights from the hallmarks of ageing', *Transl Neurodegener,* 13(1)**,** pp. 7-39.

Livingston, G.*, et al.* (2020). 'Dementia prevention, intervention, and care: 2020 report of the lancet commission', *Lancet,* 396(10248)**,** pp. 413-446.

Long, J. M. & Holtzman, D. M. (2019). 'Alzheimer disease: An update on pathobiology and treatment strategies', *Cell,* 179(2)**,** pp. 312-339.

Lowe, V. J.*, et al.* (2024). 'Amyloid pet detects the deposition of brain abeta earlier than csf fluid biomarkers', *Alzheimers Dement,* 20(11)**,** pp. 8097-8112.

Madhu, P. & Mukhopadhyay, S. (2021). 'Distinct types of amyloid-beta oligomers displaying diverse neurotoxicity mechanisms in alzheimer's disease', *J Cell Biochem,* 122(11)**,** pp. 1594-1608.

Maina, M. B.*, et al.* (2018). 'The involvement of abeta42 and tau in nucleolar and protein synthesis machinery dysfunction', *Front Cell Neurosci,* 12(pp. 220.

Mattheyses, A. L.*, et al.* (2010). 'Imaging with total internal reflection fluorescence microscopy for the cell biologist', *J Cell Sci,* 123(Pt 21)**,** pp. 3621-3628.

Mattsson, N.*, et al.* (2018). 'Prevalence of the apolipoprotein e epsilon4 allele in amyloid beta positive subjects across the spectrum of alzheimer's disease', *Alzheimers Dement,* 14(7)**,** pp. 913-924.

Matuszyk, M. M.*, et al.* (2022). 'Biological and methodological complexities of beta-amyloid peptide: Implications for alzheimer's disease research', *J Neurochem,* 160(4)**,** pp. 434-453.

Mayne, K.*, et al.* (2020). 'Aging and neurodegenerative disease: Is the adaptive immune system a friend or foe?', *Front Aging Neurosci,* 12(pp. 572090.

McKean, N. E.*, et al.* (2021). 'A review of the current mammalian models of alzheimer's disease and challenges that need to be overcome', *Int J Mol Sci,* 22(23)**,** pp.

McKhann, G. M.*, et al.* (2011). 'The diagnosis of dementia due to alzheimer's disease: Recommendations from the national institute on aging-alzheimer's association workgroups on diagnostic guidelines for alzheimer's disease', *Alzheimers Dement,* 7(3)**,** pp. 263-9.

McKinney, C. E. (2017). 'Using induced pluripotent stem cells derived neurons to model brain diseases', *Neural Regen Res,* 12(7)**,** pp. 1062-1067.

Mei, C.*, et al.* (2024). 'Advances of therapy for alzheimer's disease: An updated review', *Brain-X,* 2(3)**,** pp. e68-e84.

Mei, J.*, et al.* (2022). 'Toxicity mechanism of abeta42 oligomer in the binding between the gaba(b)r1a sushi1 domain and amyloid precursor protein 9mer: A mechanism like substitution reaction', *ACS Chem Neurosci,* 13(13)**,** pp. 2048-2059.

Meng, X.*, et al.* (2024). 'Neurotoxic beta-amyloid oligomers cause mitochondrial dysfunction-the trigger for panoptosis in neurons', *Front Aging Neurosci,* 16(pp. 1400544.

Meraz-Rios, M. A.*, et al.* (2013). 'Inflammatory process in alzheimer's disease', *Front Integr Neurosci,* 7(13)**,** pp. 59-74.

Mertens, J.*, et al.* (2015). 'Directly reprogrammed human neurons retain aging-associated transcriptomic signatures and reveal age-related nucleocytoplasmic defects', *Cell Stem Cell,* 17(6)**,** pp. 705-718.

Meyer, K.*, et al.* (2014). 'Direct conversion of patient fibroblasts demonstrates non-cell autonomous toxicity of astrocytes to motor neurons in familial and sporadic als', *Proc Natl Acad Sci U S A,* 111(2)**,** pp. 829-32.

Miao, J.*, et al.* (2023). 'Microglia in alzheimer's disease: Pathogenesis, mechanisms, and therapeutic potentials', *Front Aging Neurosci,* 15(pp. 1201982.

Middeldorp, J. & Hol, E. M. (2011). 'Gfap in health and disease', *Prog Neurobiol,* 93(3)**,** pp. 421-43.

Monterey, M. D*., et al.* (2021). 'The many faces of astrocytes in alzheimer's disease', *Front Neurol,* 12(pp. 619626.

Montoliu-Gaya, L*., et al.* (2018). 'Abeta-oligomer uptake and the resulting inflammatory response in adult human astrocytes are precluded by an anti-abeta single chain variable fragment in combination with an apoe mimetic peptide', *Mol Cell Neurosci,* 89(pp. 49-59.

Moore, B. D*., et al.* (2018). 'Short abeta peptides attenuate abeta42 toxicity in vivo', *J Exp Med,* 215(1)**,** pp. 283-301.

Moretto, G*., et al.* (1993). 'Cd44 expression in human astrocytes and oligodendrocytes in culture', *J Neuropathol Exp Neurol,* 52(4)**,** pp. 419-423.

Mormino, E. C. & Papp, K. V. (2018). 'Amyloid accumulation and cognitive decline in clinically normal older individuals: Implications for aging and early alzheimer's disease', *J Alzheimers Dis,* 64(s1)**,** pp. S633-S646.

Mroczko, B*., et al.* (2018). 'Amyloid beta oligomers (abetaos) in alzheimer's disease', *J Neural Transm (Vienna),* 125(2)**,** pp. 177-191.

Mukhopadhyay, S. & Banerjee, D. (2021). 'A primer on the evolution of aducanumab: The first antibody approved for treatment of alzheimer's disease', *J Alzheimers Dis,* 83(4)**,** pp. 1537-1552.

Murphy, M. P. & LeVine, H. (2010). 'Alzheimer's disease and the amyloid-beta peptide', *J Alzheimers Dis,* 19(1)**,** pp. 311-23.

Nazere, K*., et al.* (2022). 'Amyloid beta is internalized via macropinocytosis, an hspg- and lipid raft-dependent and rac1-mediated process', *Front Mol Neurosci,* 15(pp. 804702-804713.

Nelson, P. T*., et al.* (2012). 'Correlation of alzheimer disease neuropathologic changes with cognitive status: A review of the literature', *J Neuropathol Exp Neurol,* 71(5)**,** pp. 362-381.

Nguyen, H. D*., et al.* (2024). 'Molecular mechanisms implicated in protein changes in the alzheimer's disease human hippocampus', *Mech Ageing Dev,* 219(111930)**,** pp.

Nhan, H. S*., et al.* (2015). 'The multifaceted nature of amyloid precursor protein and its proteolytic fragments: Friends and foes', *Acta Neuropathol,* 129(1)**,** pp. 1-19.

NHS UK. 2024. *Diagnosis alzheimer's disease* [Online]. Available: https://www.nhs.uk/conditions/alzheimers-disease/diagnosis/#:~:text=Mental%20ability%20tests,related%20to%20vision%20(visuospatial%20abilities) [Accessed 06/03/2025].

Niemantsverdriet, E.*, et al.* (2017). 'Alzheimer's disease csf biomarkers: Clinical indications and rational use', *Acta Neurol Belg,* 117(3)**,** pp. 591-602.

Niu, Z.*, et al.* (2024). 'Aggregation mechanisms and molecular structures of amyloid-beta in alzheimer's disease', *Chemistry,* 30(48)**,** pp. e202400277.

Novoa, C.*, et al.* (2022). 'Inflammation context in alzheimer's disease, a relationship intricate to define', *Biol Res,* 55(1)**,** pp. 39.

O'Shea, J. J.*, et al.* (2015). 'The jak-stat pathway: Impact on human disease and therapeutic intervention', *Annu Rev Med,* 66(pp. 311-28.

Office for National Statistics. 2024. *Death registration summary statistics, england and wales: 2023* [Online]. Available: https://www.ons.gov.uk/peoplepopulationandcommunity/birthsdeathsandmarriages/deaths/bulletins/deathregistrationsummarystatisticsenglandandwales/2023 [Accessed].

Omole, A. E. & Fakoya, A. O. J. (2018). 'Ten years of progress and promise of induced pluripotent stem cells: Historical origins, characteristics, mechanisms, limitations, and potential applications', *PeerJ,* 6(pp. e4370-e4417.

Ozcelikay-Akyildiz, G.*, et al.* (2024). 'The evaluation of clinical applications for the detection of the alzheimer's disease biomarker gfap', *Crit Rev Anal Chem***,** pp. 1-12.

Parisi, I. & Collinson, J. M. (2012). 'Regulation of merkel cell development by pax6', *Int J Dev Biol,* 56(5)**,** pp. 341-350.

Park, K. M. & Bowers, W. J. (2010). 'Tumor necrosis factor-alpha mediated signaling in neuronal homeostasis and dysfunction', *Cell Signal,* 22(7)**,** pp. 977-83.

Patani, R.*, et al.* (2023). 'Functional roles of reactive astrocytes in neuroinflammation and neurodegeneration', *Nat Rev Neurol,* 19(7)**,** pp. 395-409.

Patel, N. S.*, et al.* (2005). 'Inflammatory cytokine levels correlate with amyloid load in transgenic mouse models of alzheimer's disease', *J Neuroinflammation,* 2(1)**,** pp. 9.

Paterson, R. W.*, et al.* (2018). 'Cerebrospinal fluid in the differential diagnosis of alzheimer's disease: Clinical utility of an extended panel of biomarkers in a specialist cognitive clinic', *Alzheimers Res Ther,* 10(1)**,** pp. 32-43.

Pereira, J. B.*, et al.* (2021). 'Plasma gfap is an early marker of amyloid-beta but not tau pathology in alzheimer's disease', *Brain,* 144(11)**,** pp. 3505-3516.

Phan, T. M. & Schmit, J. D. (2022). 'Conformational entropy limits the transition from nucleation to elongation in amyloid aggregation', *Biophys J,* 121(15)**,** pp. 2931-2939.

Phatnani, H. & Maniatis, T. (2015). 'Astrocytes in neurodegenerative disease', *Cold Spring Harb Perspect Biol,* 7(6)**,** pp.

Phillips, J. C. (2019). 'Why abeta42 is much more toxic than abeta40', *ACS Chem Neurosci,* 10(6)**,** pp. 2843-2847.

Pilla, E.*, et al.* (2017). 'Coping with protein quality control failure', *Annu Rev Cell Dev Biol,* 33(pp. 439-465.

Pinner, E.*, et al.* (2017). 'Cd44 splice variants as potential players in alzheimer's disease pathology', *J Alzheimers Dis,* 58(4)**,** pp. 1137-1149.

Plant, C.*, et al.* (2010). 'Automated detection of brain atrophy patterns based on mri for the prediction of alzheimer's disease', *Neuroimage,* 50(1)**,** pp. 162-74.

Prabhu, K. S.*, et al.* (2024). 'H2ax: A key player in DNA damage response and a promising target for cancer therapy', *Biomed Pharmacother,* 175(pp. 116663.

Prado, M. A. & Baron, G. (2012). 'Seeding plaques in alzheimer's disease', *J Neurochem,* 120(5)**,** pp. 641-3.

Prater, K. E.*, et al.* (2023). 'Human microglia show unique transcriptional changes in alzheimer's disease', *Nat Aging,* 3(7)**,** pp. 894-907.

Preman, P.*, et al.* (2021). 'Astrocytes in alzheimer's disease: Pathological significance and molecular pathways', *Cells,* 10(3)**,** pp. 540-559.

Purushotham, S. S. & Buskila, Y. (2023). 'Astrocytic modulation of neuronal signalling', *Front Netw Physiol,* 3(pp. 1205544.

Qian, L. & Srivastava, D. (2013). 'Direct cardiac reprogramming: From developmental biology to cardiac regeneration', *Circ Res,* 113(7)**,** pp. 915-21.

Rabbito, A.*, et al.* (2020). 'Biochemical markers in alzheimer's disease', *Int J Mol Sci,* 21(6)**,** pp. 1989-2000.

Rajani, R. M.*, et al.* (2024). 'Selective suppression of oligodendrocyte-derived amyloid beta rescues neuronal dysfunction in alzheimer's disease', *PLoS Biol,* 22(7)**,** pp. e3002727.

Rao, P.*, et al.* (2015). 'Designing novel nanoformulations targeting glutamate transporter excitatory amino acid transporter 2: Implications in treating drug addiction', *J Pers Nanomed,* 1(1)**,** pp. 3-9.

Reddin, I. G.*, et al.* (2023). 'Large inherent variability in data derived from highly standardised cell culture experiments', *Pharmacol Res,* 188(pp. 106671.

Rex, J.*, et al.* (2019). 'Il-1beta and tnfalpha differentially influence nf-kappab activity and fasl-induced apoptosis in primary murine hepatocytes during lps-induced inflammation', *Front Physiol,* 10(117)**,** pp. no pagination.

Ricciarelli, R. & Fedele, E. (2017). 'The amyloid cascade hypothesis in alzheimer's disease: It's time to change our mind', *Curr Neuropharmacol,* 15(6)**,** pp. 926-935.

Ries, M. & Sastre, M. (2016a). 'Mechanisms of abeta clearance and degradation by glial cells', *Front Aging Neurosci,* 8(pp. 160-169.

Ries, M. & Sastre, M. (2016b). 'Mechanisms of abeta clearance and degradation by glial cells', *Front Aging Neurosci,* 8(160)**,** pp.

Rofo, F.*, et al.* (2022). 'Blood-brain barrier penetrating neprilysin degrades monomeric amyloid-beta in a mouse model of alzheimer's disease', *Alzheimers Res Ther,* 14(1)**,** pp. 180.

Romanazzo, S.*, et al.* (2020). 'Targeting cell plasticity for regeneration: From in vitro to in vivo reprogramming', *Adv Drug Deliv Rev,* 161-162(pp. 124-144.

Ross, C. A. & Poirier, M. A. (2004). 'Protein aggregation and neurodegenerative disease', *Nat Med,* 10(pp. 10-17.

Ross, J. A. & Dodel, R. (2025). 'Preclinical csf proteomic changes: A milestone in biomarker detection for autosomal dominant alzheimer's disease', *Signal Transduct Target Ther,* 10(1)**,** pp. 16-19.

Rubio-Perez, J. M. & Morillas-Ruiz, J. M. (2012). 'A review: Inflammatory process in alzheimer's disease, role of cytokines', *ScientificWorldJournal,* 2012(pp. 756357.

Rusakov, K.*, et al.* (2024). 'Thioflavin t horizontal line a reporter of microviscosity in protein aggregation process: The study case of alpha-synuclein', *J Phys Chem Lett,* 15(25)**,** pp. 6685-6690.

Sabio, G. & Davis, R. J. (2014). 'Tnf and map kinase signalling pathways', *Semin Immunol,* 26(3)**,** pp. 237-45.

Saha, P*., et al.* (2020). 'P38k and jnk pathways are induced by amyloid-beta in astrocyte: Implication of mapk pathways in astrogliosis in alzheimer's disease', *Mol Cell Neurosci,* 108(pp. 103551.

Saido, T. & Leissring, M. A. (2012). 'Proteolytic degradation of amyloid beta-protein', *Cold Spring Harb Perspect Med,* 2(6)**,** pp. a006379.

Sakurai, K. & Osumi, N. (2008). 'The neurogenesis-controlling factor, pax6, inhibits proliferation and promotes maturation in murine astrocytes', *J Neurosci,* 28(18)**,** pp. 4604-12.

Sami, N*., et al.* (2017). 'Protein aggregation, misfolding and consequential human neurodegenerative diseases', *Int J Neurosci,* 127(11)**,** pp. 1047-1057.

Sarkar, S. & Biswas, S. C. (2021). 'Astrocyte subtype-specific approach to alzheimer's disease treatment', *Neurochem Int,* 145(pp. 104956.

Scheltens, P*., et al.* (2021). 'Alzheimer's disease', *Lancet,* 397(10284)**,** pp. 1577-1590.

Schmit, J. D*., et al.* (2011). 'What drives amyloid molecules to assemble into oligomers and fibrils?', *Biophys J,* 100(2)**,** pp. 450-8.

Schneider, L. S*., et al.* (2025). 'Linking higher amyloid beta 1-38 (abeta(1-38)) levels to reduced alzheimer's disease progression risk', *Alzheimers Dement,* 21(2)**,** pp. e14545.

Schwartzentruber, A*., et al.* (2020). 'Oxidative switch drives mitophagy defects in dopaminergic parkin mutant patient neurons', *Sci Rep,* 10(1)**,** pp. 15485-15499.

Sengupta, U*., et al.* (2016). 'The role of amyloid-beta oligomers in toxicity, propagation, and immunotherapy', *EBioMedicine,* 6(pp. 42-49.

Serrano-Pozo, A*., et al.* (2024). 'Astrocyte transcriptomic changes along the spatiotemporal progression of alzheimer's disease', *Nat Neurosci,* 27(12)**,** pp. 2384-2400.

Sharma, A*., et al.* (2019). 'Divergent roles of astrocytic versus neuronal eaat2 deficiency on cognition and overlap with aging and alzheimer's molecular signatures', *Proc Natl Acad Sci U S A,* 116(43)**,** pp. 21800-21811.

Shi, Y*., et al.* (2017). 'Induced pluripotent stem cell technology: A decade of progress', *Nat Rev Drug Discov,* 16(2)**,** pp. 115-130.

Shin, W. S.*, et al.* (2019). 'Amyloid beta-protein oligomers promote the uptake of tau fibril seeds potentiating intracellular tau aggregation', *Alzheimers Res Ther,* 11(1)**,** pp. 86.

Shinohara, M.*, et al.* (2017). 'Role of lrp1 in the pathogenesis of alzheimer's disease: Evidence from clinical and preclinical studies', *J Lipid Res,* 58(7)**,** pp. 1267-1281.

Singh, D. (2022). 'Astrocytic and microglial cells as the modulators of neuroinflammation in alzheimer's disease', *J Neuroinflammation,* 19(1)**,** pp. 206.

Smit, T.*, et al.* (2021). 'Reactive astrocytes as treatment targets in alzheimer's disease-systematic review of studies using the appsweps1de9 mouse model', *Glia,* 69(8)**,** pp. 1852-1881.

Snow, W. M. & Albensi, B. C. (2016). 'Neuronal gene targets of nf-kappab and their dysregulation in alzheimer's disease', *Front Mol Neurosci,* 9(pp. 118.

Sokolowski, J. D. & Mandell, J. W. (2011). 'Phagocytic clearance in neurodegeneration', *Am J Pathol,* 178(4)**,** pp. 1416-28.

Sollvander, S.*, et al.* (2016). 'Accumulation of amyloid-beta by astrocytes result in enlarged endosomes and microvesicle-induced apoptosis of neurons', *Mol Neurodegener,* 11(1)**,** pp. 38.

Song, C.*, et al.* (2022). 'Conformational essentials responsible for neurotoxicity of abeta42 aggregates revealed by antibodies against oligomeric abeta42', *Molecules,* 27(19)**,** pp. 6751-6763.

Sosna, J.*, et al.* (2018). 'Early long-term administration of the csf1r inhibitor plx3397 ablates microglia and reduces accumulation of intraneuronal amyloid, neuritic plaque deposition and pre-fibrillar oligomers in 5xfad mouse model of alzheimer's disease', *Mol Neurodegener,* 13(1)**,** pp. 11.

Soto, C. & Pritzkow, S. (2018). 'Protein misfolding, aggregation, and conformational strains in neurodegenerative diseases', *Nat Neurosci,* 21(10)**,** pp. 1332-1340.

Strelnikova, P. A.*, et al.* (2025). 'Blood plasma proteomic markers of alzheimer's disease, current status and application prospects', *Expert Rev Proteomics,* 22(1)**,** pp. 11-18.

Sudduth, T. L.*, et al.* (2013). 'Neuroinflammatory phenotype in early alzheimer's disease', *Neurobiol Aging,* 34(4)**,** pp. 1051-9.

Sun, E.*, et al.* (2022). 'The pivotal role of nf-kb in the pathogenesis and therapeutics of alzheimer's disease', *Int J Mol Sci,* 23(16)**,** pp. 8972.

Suzuki, S.*, et al.* (2010). 'The neural stem/progenitor cell marker nestin is expressed in proliferative endothelial cells, but not in mature vasculature', *J Histochem Cytochem,* 58(8)**,** pp. 721-730.

Tachibana, M.*, et al.* (2019). 'Apoe4-mediated amyloid-beta pathology depends on its neuronal receptor lrp1', *J Clin Invest,* 129(3)**,** pp. 1272-1277.

Taipa, R.*, et al.* (2019). 'Proinflammatory and anti-inflammatory cytokines in the csf of patients with alzheimer's disease and their correlation with cognitive decline', *Neurobiol Aging,* 76(pp. 125-132.

Takahashi, K.*, et al.* (2015). 'Glutamate transporter eaat2: Regulation, function, and potential as a therapeutic target for neurological and psychiatric disease', *Cell Mol Life Sci,* 72(18)**,** pp. 3489-3506.

Takahashi, K.*, et al.* (2007). 'Induction of pluripotent stem cells from adult human fibroblasts by defined factors', *Cell,* 131(5)**,** pp. 861-72.

Takahashi, K. & Yamanaka, S. (2006). 'Induction of pluripotent stem cells from mouse embryonic and adult fibroblast cultures by defined factors', *Cell,* 126(4)**,** pp. 663-676.

Takemiya, T.*, et al.* (2017). 'Brain interleukin-1 facilitates learning of a water maze spatial memory task in young mice', *Front Behav Neurosci,* 11(202)**,** pp. no pagination.

Tansey, M. G.*, et al.* (2022). 'Inflammation and immune dysfunction in parkinson disease', *Nat Rev Immunol,* 22(11)**,** pp. 657-673.

Tarasoff-Conway, J. M.*, et al.* (2015a). 'Clearance systems in the brain-implications for alzheimer disease', *Nat Rev Neurol,* 11(8)**,** pp. 457-470.

Tarasoff-Conway, J. M.*, et al.* (2015b). 'Clearance systems in the brain-implications for alzheimer disease', *Nat Rev Neurol,* 11(8)**,** pp. 457-70.

Thakurela, S.*, et al.* (2016). 'Mapping gene regulatory circuitry of pax6 during neurogenesis', *Cell Discov,* 2(pp. 15045-15067.

Thal, D. R. (2012). 'The role of astrocytes in amyloid beta-protein toxicity and clearance', *Exp Neurol,* 236(1)**,** pp. 1-5.

Tian, Y.*, et al.* (2025). 'The p3 peptides (abeta(17-40/42)) rapidly form amyloid fibrils that cross-seed with full-length abeta', *Nat Commun,* 16(1)**,** pp. 2040-2053.

Todd, A. C. & Hardingham, G. E. (2020). 'The regulation of astrocytic glutamate transporters in health and neurodegenerative diseases', *Int J Mol Sci,* 21(24)**,** pp. 9607-9637.

Tolar, M.*, et al.* (2021). 'Neurotoxic soluble amyloid oligomers drive alzheimer's pathogenesis and represent a clinically validated target for slowing disease progression', *Int J Mol Sci,* 22(12)**,** pp. 6355.

Tran, J.*, et al.* (2017). 'Cross-seeding between abeta40 and abeta42 in alzheimer's disease', *FEBS Lett,* 591(1)**,** pp. 177-185.

Tsai, S. J. (2017). 'Effects of interleukin-1beta polymorphisms on brain function and behavior in healthy and psychiatric disease conditions', *Cytokine Growth Factor Rev,* 37(pp. 89-97.

Turnquist, C.*, et al.* (2016). 'P53 isoforms regulate astrocyte-mediated neuroprotection and neurodegeneration', *Cell Death Differ,* 23(9)**,** pp. 1515-28.

Uddin, M. S.*, et al.* (2020). 'Revisiting the amyloid cascade hypothesis: From anti-abeta therapeutics to auspicious new ways for alzheimer's disease', *Int J Mol Sci,* 21(16)**,** pp. 5858-5892.

Ueno, M.*, et al.* (2014). 'Clearance of beta-amyloid in the brain', *Curr Med Chem,* 21(35)**,** pp. 4085-90.

Ullah, R. & Lee, E. J. (2023). 'Advances in amyloid-beta clearance in the brain and periphery: Implications for neurodegenerative diseases', *Exp Neurobiol,* 32(4)**,** pp. 216-246.

Vadukul, D. M.*, et al.* (2020). 'Internalisation and toxicity of amyloid-beta 1-42 are influenced by its conformation and assembly state rather than size', *FEBS Lett,* 594(21)**,** pp. 3490-3503.

Valerio, A.*, et al.* (2006). 'Nf-kappab pathway: A target for preventing beta-amyloid (abeta)-induced neuronal damage and abeta42 production', *Eur J Neurosci,* 23(7)**,** pp. 1711-20.

van der Lee, S. J.*, et al.* (2018). 'The effect of apoe and other common genetic variants on the onset of alzheimer's disease and dementia: A community-based cohort study', *Lancet Neurol,* 17(5)**,** pp. 434-444.

Vaz, I. M.*, et al.* (2021). 'Chromosomal aberrations after induced pluripotent stem cells reprogramming', *Genet Mol Biol,* 44(3)**,** pp. e20200147-20200154.

Villemagne, V. L.*, et al.* (2011). 'Longitudinal assessment of abeta and cognition in aging and alzheimer disease', *Ann Neurol,* 69(1)**,** pp. 181-92.

Vodovar, N.*, et al.* (2015). 'Neprilysin, cardiovascular, and alzheimer's diseases: The therapeutic split?', *Eur Heart J,* 36(15)**,** pp. 902-5.

Wang, B.*, et al.* (2017). 'Decreased complexity in alzheimer's disease: Resting-state fmri evidence of brain entropy mapping', *Front Aging Neurosci,* 9(pp. 378-389.

Wang, H.*, et al.* (2021). 'Regulation of beta-amyloid production in neurons by astrocyte-derived cholesterol', *Proc Natl Acad Sci U S A,* 118(33)**,** pp. e2102191118.

Wang, T.*, et al.* (2023). 'Mcp-1 levels in astrocyte-derived exosomes are changed in preclinical stage of alzheimer's disease', *Front Neurol,* 14(pp. 1119298.

Wang, W. Y.*, et al.* (2015). 'Role of pro-inflammatory cytokines released from microglia in alzheimer's disease', *Ann Transl Med,* 3(10)**,** pp. 136.

Wang, Y.*, et al.* (2022). 'Cd44 deficiency represses neuroinflammation and rescues dopaminergic neurons in a mouse model of parkinson's disease', *Pharmacol Res,* 177(pp. 106133.

Watamura, N.*, et al.* (2024). 'The dopaminergic system promotes neprilysin-mediated degradation of amyloid-beta in the brain', *Sci Signal,* 17(848)**,** pp. eadk1822.

Wegiel, J.*, et al.* (2001). 'The role of microglial cells and astrocytes in fibrillar plaque evolution in transgenic app(sw) mice', *Neurobiol Aging,* 22(1)**,** pp. 49-61.

Weller, R. O.*, et al.* (2008). 'Perivascular drainage of amyloid-beta peptides from the brain and its failure in cerebral amyloid angiopathy and alzheimer's disease', *Brain Pathol,* 18(2)**,** pp. 253-66.

Westin, K.*, et al.* (2012). 'Ccl2 is associated with a faster rate of cognitive decline during early stages of alzheimer's disease', *PLoS One,* 7(1)**,** pp. e30525.

Wharton, S. B.*, et al.* (2019). 'Epidemiological pathology of abeta deposition in the ageing brain in cfas: Addition of multiple abeta-derived measures does not improve dementia assessment using logistic regression and machine learning approaches', *Acta Neuropathol Commun,* 7(1)**,** pp. 198-210.

Whiten, D. R.*, et al.* (2020). 'Tumour necrosis factor induces increased production of extracellular amyloid-beta- and alpha-synuclein-containing aggregates by human alzheimer's disease neurons', *Brain Commun,* 2(2)**,** pp. fcaa146.

Wildsmith, K. R.*, et al.* (2013). 'Evidence for impaired amyloid beta clearance in alzheimer's disease', *Alzheimers Res Ther,* 5(4)**,** pp. 33.

Wood, L. B.*, et al.* (2015). 'Identification of neurotoxic cytokines by profiling alzheimer's disease tissues and neuron culture viability screening', *Sci Rep,* 5(pp. 16622-16635.

Wu, Y. & Eisel, U. L. M. (2023). 'Microglia-astrocyte communication in alzheimer's disease', *J Alzheimers Dis,* 95(3)**,** pp. 785-803.

Xin, S. H.*, et al.* (2018). 'Clearance of amyloid beta and tau in alzheimer's disease: From mechanisms to therapy', *Neurotox Res,* 34(3)**,** pp. 733-748.

Xu, L.*, et al.* (2018). 'Effect of leukocyte inhibitory factor on neuron differentiation from human induced pluripotent stem cell-derived neural precursor cells', *Int J Mol Med,* 41(4)**,** pp. 2037-2049.

Xue, C.*, et al.* (2017). 'Thioflavin t as an amyloid dye: Fibril quantification, optimal concentration and effect on aggregation', *R Soc Open Sci,* 4(1)**,** pp. 160696-160708.

Xue, C.*, et al.* (2023). 'Evolving cognition of the jak-stat signaling pathway: Autoimmune disorders and cancer', *Signal Transduct Target Ther,* 8(1)**,** pp. 204-228.

Yadav, K.*, et al.* (2019). 'Protein misfolding diseases and therapeutic approaches', *Curr Protein Pept Sci,* 20(12)**,** pp. 1226-1245.

Yamamoto, N.*, et al.* (2022). 'Poly(i:C) promotes neurotoxic amyloid beta accumulation through reduced degradation by decreasing neprilysin protein levels in astrocytes', *J Neurochem,* 163(6)**,** pp. 517-530.

Yan, Y. & Wang, C. (2006). 'Abeta42 is more rigid than abeta40 at the c terminus: Implications for abeta aggregation and toxicity', *J Mol Biol,* 364(5)**,** pp. 853-62.

Yang, H.*, et al.* (2022a). 'Based on molecular structures: Amyloid-beta generation, clearance, toxicity and therapeutic strategies', *Front Mol Neurosci,* 15(pp. 927530.

Yang, J.*, et al.* (2021). 'Single molecule characterization of amyloid oligomers', *Molecules,* 26(4)**,** pp. 948-968.

Yang, P.*, et al.* (2012). 'Il-6 promotes regeneration and functional recovery after cortical spinal tract injury by reactivating intrinsic growth program of neurons and enhancing synapse formation', *Exp Neurol,* 236(1)**,** pp. 19-27.

Yang, Y.*, et al.* (2022b). 'Cryo-em structures of amyloid-beta 42 filaments from human brains', *Science,* 375(6577)**,** pp. 167-172.

Yang, Z. & Wang, K. K. (2015). 'Glial fibrillary acidic protein: From intermediate filament assembly and gliosis to neurobiomarker', *Trends Neurosci,* 38(6)**,** pp. 364-74.

Yasojima, K.*, et al.* (2001). 'Reduced neprilysin in high plaque areas of alzheimer brain: A possible relationship to deficient degradation of beta-amyloid peptide', *Neurosci Lett,* 297(2)**,** pp. 97-100.

Yokoyama, M.*, et al.* (2022). 'Mouse models of alzheimer's disease', *Front Mol Neurosci,* 15(pp. 912995.

Yoon, S. S. & Jo, S. A. (2012). 'Mechanisms of amyloid-beta peptide clearance: Potential therapeutic targets for alzheimer's disease', *Biomol Ther (Seoul),* 20(3)**,** pp. 245-55.

Yousif Saleh, S.*, et al.* (2024). 'Investigation of amyloid-beta peptide production and clearance pathways in different stages of alzheimer's disease', *Acta Neurobiol Exp (Wars),* 84(3)**,** pp. 288-295.

Yu, H.*, et al.* (2020). 'Targeting nf-kappab pathway for the therapy of diseases: Mechanism and clinical study', *Signal Transduct Target Ther,* 5(1)**,** pp. 209-231.

Yu, J.*, et al.* (2007). 'Induced pluripotent stem cell lines derived from human somatic cells', *Science,* 318(5858)**,** pp. 1917-20.

Yuan, J. & Ofengeim, D. (2024). 'A guide to cell death pathways', *Nat Rev Mol Cell Biol,* 25(5)**,** pp. 379-395.

Zhang, H.*, et al.* (2022). 'Role of abeta in alzheimer's-related synaptic dysfunction', *Front Cell Dev Biol,* 10(pp. 964075.

Zhang, H.*, et al.* (2023a). 'Cellular response to beta-amyloid neurotoxicity in alzheimer's disease and implications in new therapeutics', *Animal Model Exp Med,* 6(1)**,** pp. 3-9.

Zhang, M.*, et al.* (2018). 'Highly efficient methods to obtain homogeneous dorsal neural progenitor cells from human and mouse embryonic stem cells and induced pluripotent stem cells', *Stem Cell Res Ther,* 9(1)**,** pp. 67-80.

Zhang, T.*, et al.* (2019). 'Human neural stem cells reinforce hippocampal synaptic network and rescue cognitive deficits in a mouse model of alzheimer's disease', *Stem Cell Reports,* 13(6)**,** pp. 1022-1037.

Zhang, W.*, et al.* (2023b). 'Role of neuroinflammation in neurodegeneration development', *Signal Transduct Target Ther,* 8(1)**,** pp. 267.

Zhang, X. X.*, et al.* (2021). 'The epidemiology of alzheimer's disease modifiable risk factors and prevention', *J Prev Alzheimers Dis,* 8(3)**,** pp. 313-321.

Zhang, Y.*, et al.* (2023c). 'Amyloid beta-based therapy for alzheimer's disease: Challenges, successes and future', *Signal Transduct Target Ther,* 8(1)**,** pp. 248.

Zhang, Y.*, et al.* (2023d). 'Amyloid beta-based therapy for alzheimer's disease: Challenges, successes and future', *Signal Transduct Target Ther,* 8(1)**,** pp. 248-274.

Zhao, H.*, et al.* (2021). 'Inflammation and tumor progression: Signaling pathways and targeted intervention', *Signal Transduct Target Ther,* 6(1)**,** pp. 263.

Zheng, Q. & Wang, X. (2025). 'Alzheimer's disease: Insights into pathology, molecular mechanisms, and therapy', *Protein Cell,* 16(2)**,** pp. 83-120.

Zhong, C.*, et al.* (2022). 'Tumorigenicity risk of ipscs in vivo: Nip it in the bud', *Precis Clin Med,* 5(1)**,** pp. pbac004.

Zhou, B.*, et al.* (2019). 'Astrocyte morphology: Diversity, plasticity, and role in neurological diseases', *CNS Neurosci Ther,* 25(6)**,** pp. 665-673.

Zhou, J.*, et al.* (2024). 'Astrocytic lrp1 enables mitochondria transfer to neurons and mitigates brain ischemic stroke by suppressing arf1 lactylation', *Cell Metab,* 36(9)**,** pp. 2054-2068 e14.

Zhou, S.*, et al.* (2016). 'Neurosphere based differentiation of human ipsc improves astrocyte differentiation', *Stem Cells Int,* 2016(pp. 4937689.

Zhou, Y.*, et al.* (2015). 'An astrocyte regenerative response from vimentin-containing cells in the spinal cord of amyotrophic lateral sclerosis's disease-like transgenic (g93a sod1) mice', *Neurodegener Dis,* 15(1)**,** pp. 1-12.

Zhu, J.*, et al.* (2024). 'Cellular senescence in alzheimer's disease: From physiology to pathology', *Transl Neurodegener,* 13(1)**,** pp. 55-78.

Zuena, A. R.*, et al.* (2019). 'Chemokines in alzheimer's disease: New insights into prokineticins, chemokine-like proteins', *Front Pharmacol,* 10(622)**,** pp. no pagination.

Zukowska, J.*, et al.* (2024). 'Molecular basis of selective amyloid-beta degrading enzymes in alzheimer's disease', *FEBS J,* 291(14)**,** pp. 2999-3029.

Appendix: Supplementary Data

The following figure was taken with permission from thesis submitted by Chris Ryan Ratnathurai in fulfilment of for the degree of Master of Science in Translational Neuroscience, the University of Sheffield. Supervisor of project Dr Simon Bell, who was the project manager and academic supervisor. As part of this project, I acted as co-supervisor in the laboratory, carrying out the ICC staining protocol, image and data analysis alongside Ryan. The data used from Ryan's thesis into this thesis has been used as a proof on concept to support discussion argument in Chapter four, Section 4.4.3.

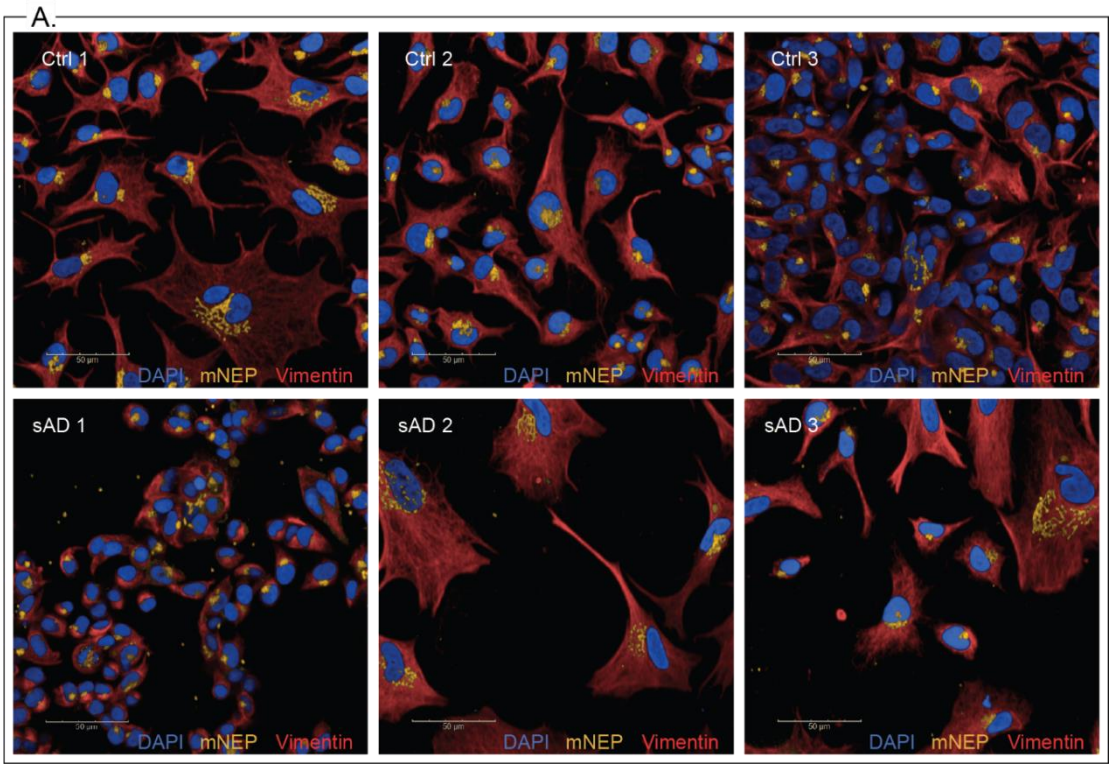

S1. *Representative images of Control and AD astrocytes showing Vimentin (red), Neprilysin (yellow), and Hoechst (DAPI, blue) in Control and AD astrocytes by immunocytochemistry. Scale bar (50 µm).*

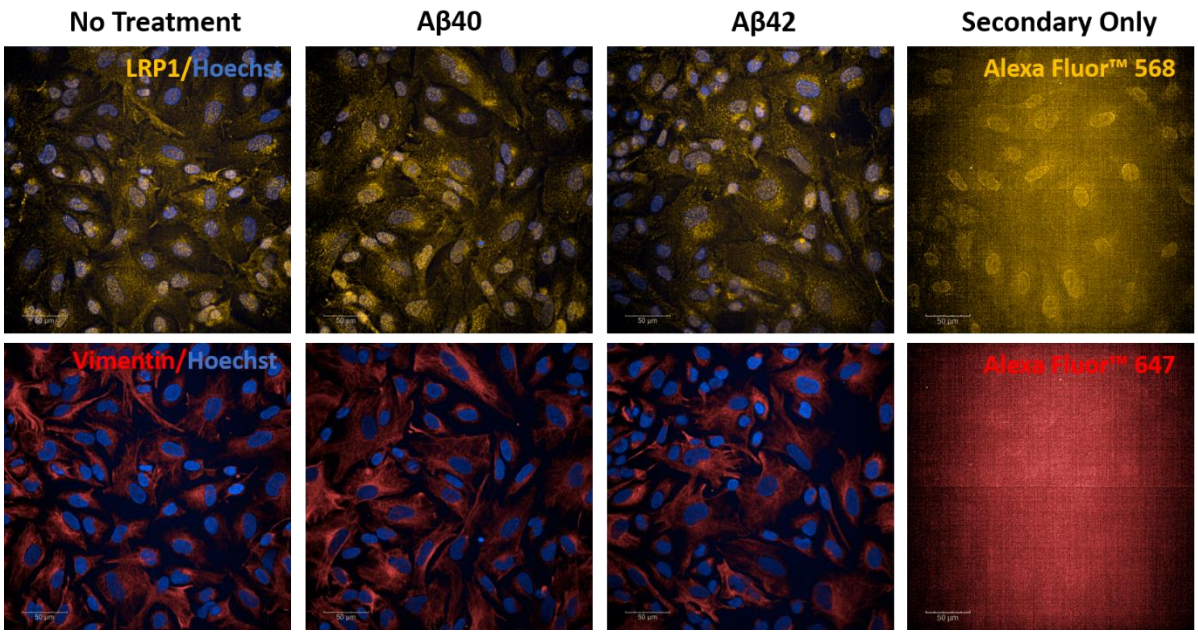

S2. *Representative immunocytochemistry images of AD (1) astrocytes for LRP1 (yellow), Vimentin (red), Hoechst (blue) after No treatment, Aβ40, Aβ42, and secondary antibody (Alexa Fluor™ 568 and Alexa Fluor™ 647). Scale bar (50 µm) (n=1).*

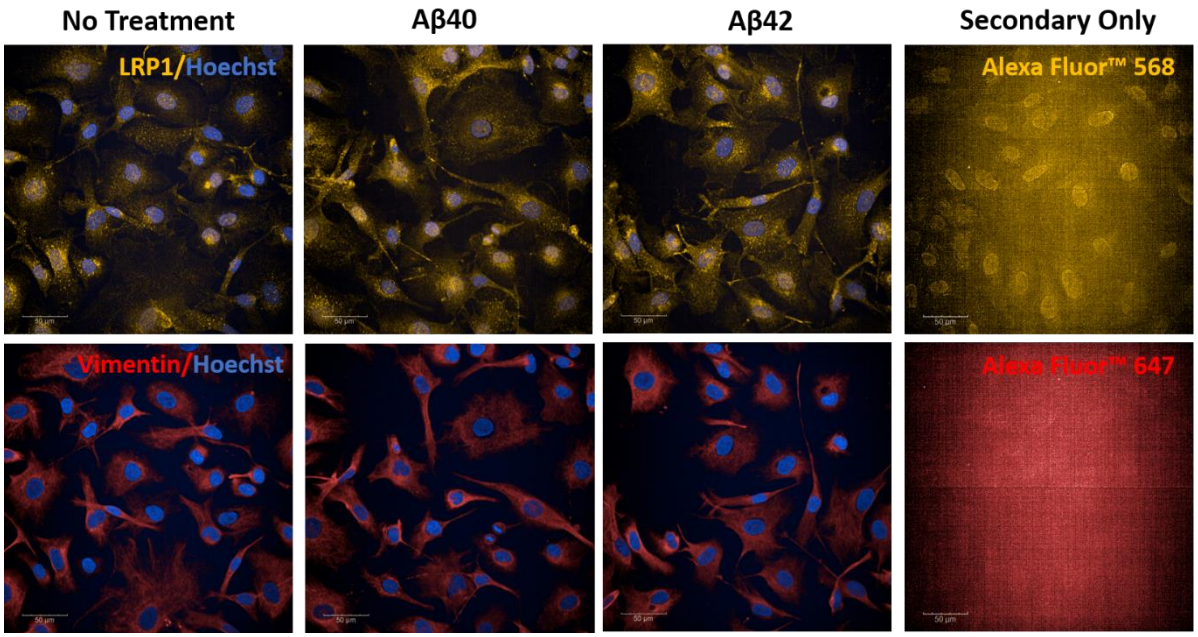

S3*. Representative immunocytochemistry images of Control (1) astrocytes for LRP1 (yellow), Vimentin (red), Hoechst (blue) after no treatment, Aβ40, Aβ42, and secondary antibody (Alexa Fluor™ 568 and Alexa Fluor™ 647). Scale bar (50 µm) (n=1).*

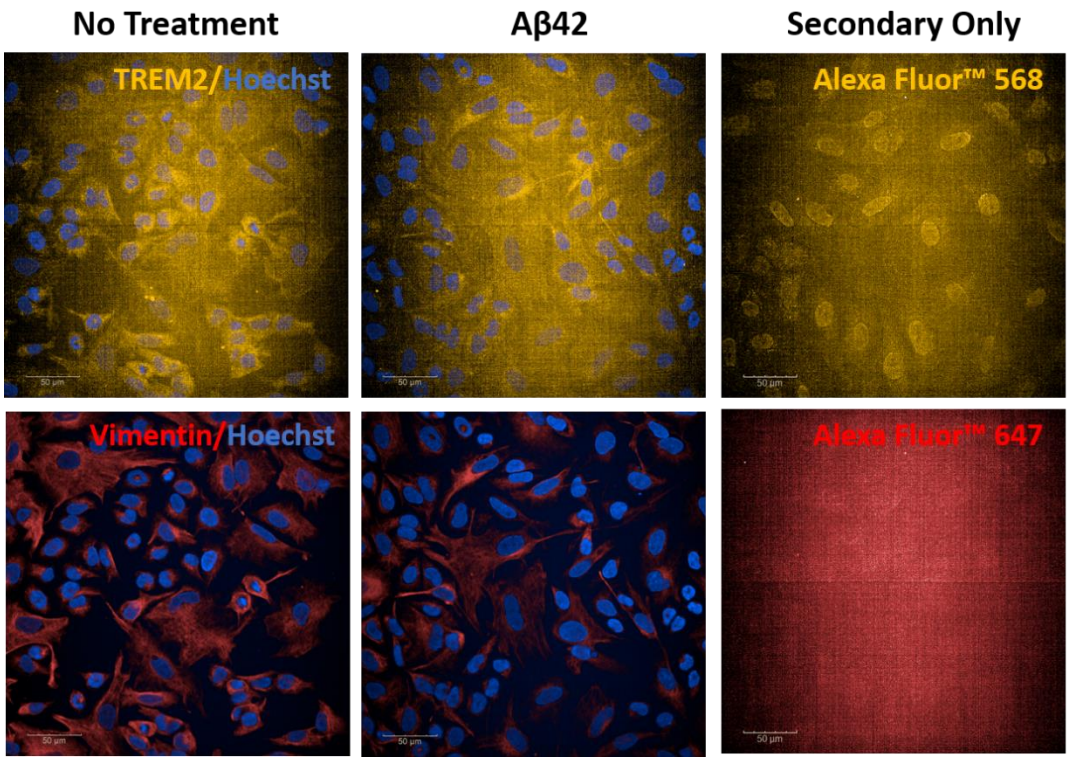

***S4**. Representative immunocytochemistry images of AD (1) astrocytes for TREM2 (yellow), Vimentin (red), Hoechst (blue) after no treatment, Aβ42, and secondary antibody (Alexa Fluor™ 568 and Alexa Fluor™ 647). Scale bar (50 µm) (n=1). Images not collected for Aβ40 due to no detectable cells in well.*

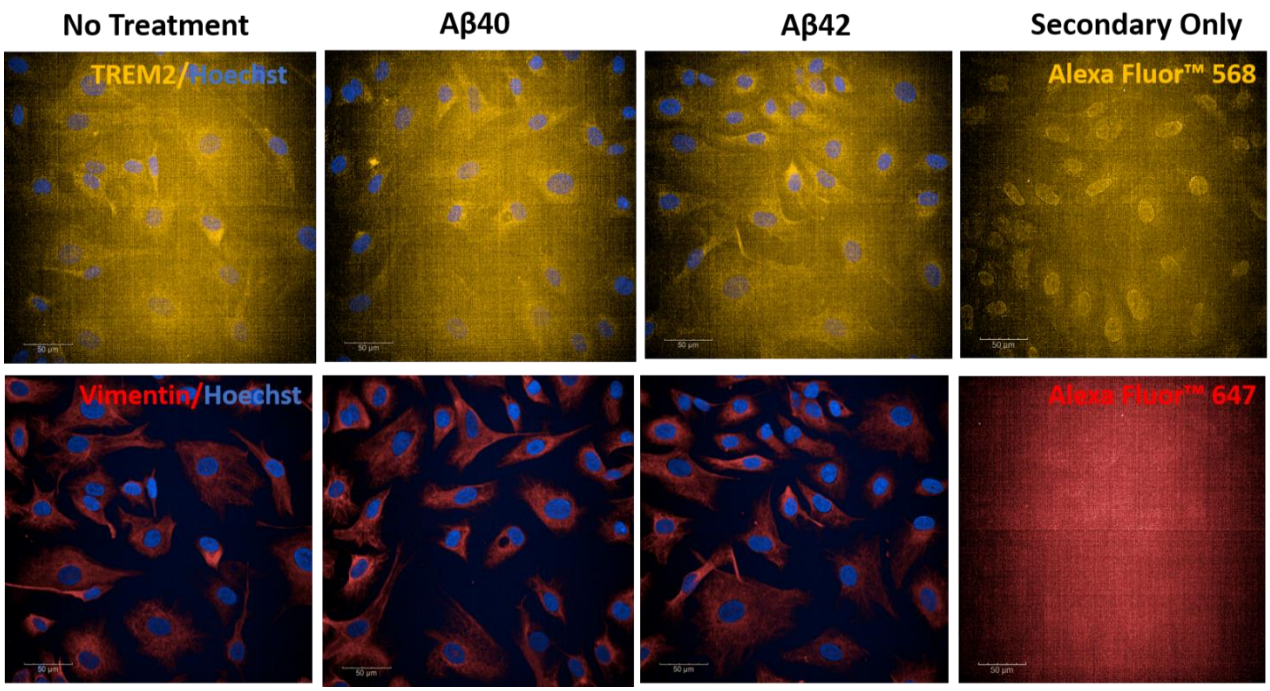

S5. *Representative immunocytochemistry images of Control (1) astrocytes for TREM2 (yellow), Vimentin (red), Hoechst (blue) after no treatment, Aβ40, Aβ42, and secondary antibody (Alexa Fluor™ 568 and Alexa Fluor™ 647). Scale bar (50 µm) (n=1).*

S6. ***The Uptake of Aβ Oligomers in Control iAstrocytes after 1-hour treatment Kruskal-Wallis Test.*** *Dunn's multiple comparisons test, summary and p-value are shown.*

Dunn's multiple comparisons test	Summary	Adjusted P Value
10:0 vs. 9:1	ns	>0.9999
10:0 vs. 7:3	ns	0.5869
10:0 vs. 0:10	**	0.0015
9:1 vs. 7:3	ns	0.8388
9:1 vs. 0:10	**	0.0029
7:3 vs. 0:10	ns	0.2644

S7. The Uptake of Aβ Oligomers in AD iAstrocytes after 1-hour treatment ANOVA Test. *Tukey's multiple comparisons test, summary and p-value are shown. s*

Tukey's multiple comparisons test	Summary	Adjusted P Value
10:0 vs. 9:1	ns	0.3638
10:0 vs. 7:3	ns	0.3003
10:0 vs. 0:10	ns	0.0683
9:1 vs. 7:3	ns	0.9992
9:1 vs. 0:10	**	0.001
7:3 vs. 0:10	***	0.0007

S8. The uptake of Aβ in control iAstrocytes after 24-hour cytokine treatment and 1-hour Aβ (2.5 μM) treatment standard deviation. *Treatment group and standard deviation is shown. Low dose (LD) and high dose (HD).*

Treatment Group	Standard Deviation
Aβ40 Oligomers	3.67
Aβ40 Oligomers + LD	1.18
Aβ40 Oligomers + HD	0.62
Aβ42 Oligomers	3.18
Aβ42 Oligomers + LD	4.84
Aβ42 Oligomers + HD	0.3
Aβ40 Fibrils	3.14
Aβ40 Fibrils + LD	1.27
Aβ40 Fibrils + HD	0.12
Aβ42 Fibrils	2.87
Aβ42 Fibrils + LD	1.35
Aβ42 Fibrils + HD	0.45

S9. The uptake of Aβ in AD iAstrocytes after 24-hour cytokine treatment and 1-hour Aβ (2.5 μM) treatment ANOVA. Tukey's multiple comparisons test, summary and p-value are shown. Low dose (LD) and high dose (HD).

Tukey's multiple comparisons test	Summary	Adjusted P Value
Aβ40 Oligomers vs. Aβ40 Oligomers + LD	*	0.0227
Aβ40 Oligomers vs. Aβ40 Oligomers + HD	*	0.0307
Aβ40 Oligomers + LD vs. Aβ40 Oligomers + HD	ns	0.9633
Aβ42 Oligomers vs. Aβ42 Oligomers + LD	*	0.0012
Aβ42 Oligomers vs. Aβ42 Oligomers + HD	***	0.0009
Aβ42 Oligomers + LD vs. Aβ42 Oligomers + HD	ns	0.9091
Aβ40 Fibrils vs. Aβ40 Fibrils + LD	*	0.0388
Aβ40 Fibrils vs. Aβ40 Fibrils + HD	*	0.0442
Aβ40 Fibrils + LD vs. Aβ40 Fibrils + HD	ns	0.9937
Aβ42 Fibrils vs. Aβ42 Fibrils + LD	*	0.0171
Aβ42 Fibrils vs. Aβ42 Fibrils + HD	*	0.0265
Aβ42 Fibrils + LD vs. Aβ42 Fibrils + HD	ns	0.9223

S10. The uptake of Aβ in AD iAstrocytes after 24-hour cytokine treatment and 1-hour Aβ (2.5 μM) treatment standard deviation*. Treatment group and standard deviation is shown.* Low dose (LD) and high dose (HD).

Treatment Group	Standard Deviation
Aβ40 Oligomers	1.61
Aβ40 Oligomers + LD	0.23
Aβ40 Oligomers + HD	0.39
Aβ42 Oligomers	0.47
Aβ42 Oligomers + LD	0.37
Aβ42 Oligomers + HD	0.13
Aβ40 Fibrils	1.52
Aβ40 Fibrils + LD	0.14
Aβ40 Fibrils + HD	0.23
Aβ42 Fibrils	1.91
Aβ42 Fibrils + LD	0.2
Aβ42 Fibrils + HD	0.18

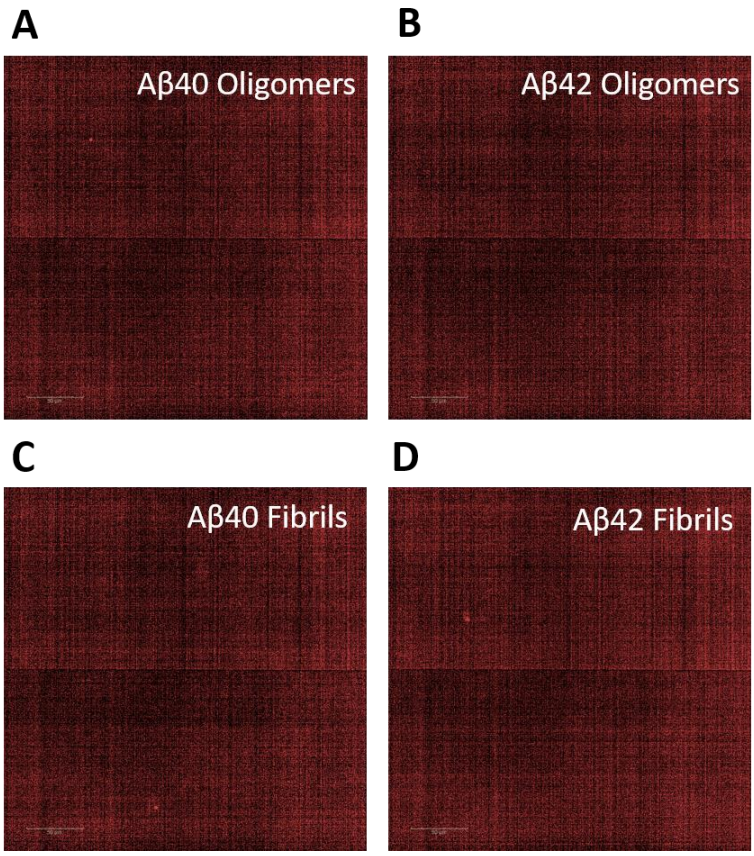

S11. *Representative Immunocytochemistry images of (**A**) Aβ40 Oligomers, (**B**) Aβ42 Oligomers, (**C**) Aβ42 Oligomers, and (**D**) Aβ40 Fibrils with no cells present. Stained with 6E10-647 nm. Scale bar (50µm).*